University of Alberta

River ice breakup forecasting using artificial neural networks and fuzzy logic systems

by

Liming Zhao

A thesis submitted to the Faculty of Graduate Studies and Research
in partial fulfillment of the requirements for the degree of

Doctor of Philosophy

in

Water Resources Engineering

Department of Civil and Environmental Engineering

Fall 2012

Edmonton, Alberta

Abstract

Due to the complexity of breakup ice jam processes deterministic modelling cannot yet forecast every aspect of the timing and severity of possible consequent flooding, especially when some lead-time is needed. In most northern regions, the sparse network and short record of data have impeded the successful development of empirical and statistical models. In this study, a multi-layer modeling approach was investigated for forecasting breakup ice jam flooding using the two soft computing techniques: artificial neural networks and fuzzy logic systems. The Town of Hay River in NWT, Canada was chosen as the case study site, where the breakup ice jam flooding is an annual threat.

This thesis first presents the development of index variables as potential predictors to breakup severity and timing. For the case study site, it was found that water level at the onset of freeze-up and accumulated degree-days of freezing during the winter could be potential predictors for breakup severity. The indicator variable of the timing of the onset of breakup was found to be completely nonlinear with respect to any of the index variables. Then the feed-forward artificial neural network (ANN) modeling technique was assessed for its applicability in forecasting of onset of breakup. Detailed results of the ANN model calibration and validation are presented and discussed. It was found from the calibration results, that the ANN model has greater potential for successfully forecasting the onset of river ice breakup (i.e. the first transverse cracking of the

ice cover) compared to the conventional multiple linear regression technique. However, rigorous validation also indicated that the accuracy of such ANN models can be optimistically overestimated by looking only at the calibration results. Finally, the applicability of a Mamdani-type fuzzy logic system to forecast the peak snowmelt runoff during breakup for a long lead-time of ~3 to 4 weeks prior to breakup was assessed, and was found to be a good predictor of breakup flood severity at the Town of Hay River. In particular, it was found that the fuzzy logic model could predict most of the high flow, the exception being those that were triggered by short intense rainfall events during the breakup period (a factor that cannot be included in a long lead-time forecast).

This study contributes new knowledge and techniques, advancing the breakup ice jam flood forecasting capabilities for the northern communities. The two most common soft computing techniques (e.g. ANN and fuzzy logic system) were studied comprehensively for their potential in river ice breakup forecasting and demonstrated step by step at the case study site. A hydrometeorological data base for the Town of Hay River was also established for the further research.

Acknowledgements

The author would like to first thank his supervisor, Dr. Faye Hicks for her tremendous unselfish help and guidance in this study. Dr. Hicks' comprehensive professional knowledge, great scientific insight, persistent passion for research has a great influence and is a lifetime example to the author. It is also much appreciated for the opportunities of take part in the field work attending the conferences supported by Dr. Hicks. The author is also grateful to his co-supervisor Dr. Aminah Robinson Fayek for her advice and support over the course of this study. Dr. Robinson Fayek's keen interest and knowledge in the fuzzy logic technique has great helped this study keep going on the right track. Her time is greatly appreciated. The author also would like to thank the rest of the defense committee, Dr. Mark Loewen, Dr. Witold Pedrycz, Dr. Karen Dow Ambtman, and in particular the external examiner Dr. Leonard Lye from Memorial University of Newfoundland, for their time and effort in reviewing this thesis.

The author was financially supported by the University of Alberta through the F.S. Chia and QE II scholarships, the R (Larry) Gerard Memorial Graduate Scholarship in Ice Engineering, and various teaching and research assistantships. The author's study was also funded by NSERC through the Strategic Grants, Discovery Grants and Northern Research Supplement programs. The travel awards to the author by the Canadian Geophysical Union's Committee on River

Ice Processes and the Environment, the University of Alberta's Graduate Student Association, through the Professional Development Grant and from Alberta Advanced Education and Technology through the Profiling Alberta's Graduate Students Award are also acknowledged.

Many thanks to Aboriginal Affairs and Northern Development Canada (AANDC) for their participation in, and support of, the research with particular thanks to Shawne Kokelj and Meg McCluskie. Sincere thanks to Water Survey of Canada for providing extensive amounts of data in support of this study and in particular thank Randy Wedel, Roger Pilling, Dennis Lazowski and Shayla Pagonis as well as their staff and co-workers. Thanks also to the Town of Hay River for their interest in and extensive support of this research.

Thanks also go to the whole river ice group at the University of Alberta: Robyn Andrishak, Maxime Belanger, Michael Brayall, Perry Fedun, Agata Hall, Nadia Kovachis, Chris Krath, Joshua Maxwell, Janelle Morley, Jennifer Nafziger, Yuntong She, David Watson, and in particular Wendy Howard and Brett Howard for their assistance in processing the Hay River historical data. All the helps and friendships make this study memorable at the University of Alberta.

Finally, I would give special thanks to my wife, Jianan Cai, for her endless encouragement to me to complete this thesis, to my newborn baby girl, Chenyi

Zhao, for giving me much motivation to finish the thesis writing, and to my parents and parents-in-law for their forever love and always standing by me.

Table of Contents

List of Tables

List of Figures

List of Variables

$\boldsymbol{ADDF_{-5}}$ = the accumulated degree-days of freezing (referred to a base air temperature of -5°C) during the pre-breakup period at a climate station;

$\boldsymbol{ADDF_W}$ = the accumulated degree-days of freezing for the winter at a climate station;

$\boldsymbol{ADDT_{-5}}$ = the accumulated degree-days of thaw (referred to a base air temperature of -5°C) during the pre-breakup period at a climate station;

$\boldsymbol{AP_W}$ = the accumulated precipitation during the winter time at a climate station;

$\boldsymbol{AR_S}$ = the accumulated rainfall during spring at a climate station before the date of peak discharge (D_p);

$\boldsymbol{AS_S}$ = the accumulated snowfall during spring at a climate station before the date of peak discharge (D_p);

$\boldsymbol{BS}$ = the qualitative descriptor for breakup flooding severity at the Town of Hay River;

$\boldsymbol{D_{cl}}$ = the date when the river is clear of ice;

$\boldsymbol{DECAY}$ = the index variable to account for potential ice strength decay during pre-breakup;

$\boldsymbol{D_{FC}}$ = the date of H_{FC};

$\boldsymbol{D_{HM}}$ = the date of H_{MB};

$\boldsymbol{D_i}$ = the date of measurement of t_i;

$\boldsymbol{D_{MO}}$ = the date when the snow on ground melts out at a climate station;

$\boldsymbol{D_{OF}}$ = the date of the onset of freezing degree-days at a climate station;

$\boldsymbol{D_{OR}}$ = the date of the onset of water level rise due to spring snowmelt at a WSC gauge;

$\boldsymbol{D_{OT}}$ = the date of the onset of thawing degree-days at a climate station;

$\boldsymbol{D_P}$ = the date of Q_P;

$\boldsymbol{D_{QM}}$ = the date of Q_{MB};

$\boldsymbol{H_{FC}}$ = the water level when the first transverse cracking occurs at a WSC gauge site;

$\boldsymbol{H_{MB}}$ = the maximum instantaneous water level during breakup at a WSC gauge;

$\boldsymbol{H_{OF}}$ = the daily water level on D_{OF} at a WSC gauge;

$\boldsymbol{H_{OR}}$ = the daily water level on D_{OR} at a WSC gauge;

$\boldsymbol{Q_{MB}}$ = the maximum daily discharge during the breakup period at a WSC gauge;

$\boldsymbol{Q_P}$ = the peak snowmelt runoff at a WSC gauge;

$\boldsymbol{RN_{PB}}$ = the accumulated rainfall during the pre-breakup period at a climate station;

$\boldsymbol{SNG_{OT}}$ = the depth of snow on the ground on D_{OT} at a climate station;

$\boldsymbol{SN_{PB}}$ = the accumulated snowfall during the pre-breakup period at a climate station;

$\boldsymbol{SWE}$ = snow water equivalent;

$\boldsymbol{SWE_{SC}}$ = the SWE measured during the late winter surveys at a snow course;

$\boldsymbol{t_i}$ = the ice thickness from the last direct measurement by WSC near a gauge site;

Year = the Calendar year of the breakup event.

List of Abbreviations

CRHL = the acronym for the Water Survey Canada gauge Chinchaga River Near High Level (07OC001);

EC = Environment Canada;

HLA = the acronym for the Environment Canada climate station High Level A (3073146);

HRA = the acronym for the Environment Canada climate station Hay River A (2202400);

HRHR = the acronym for the Water Survey Canada gauge Hay River near Hay River (07OB001);

HRMR = the acronym for the Water Survey Canada gauge Hay River near Meander River (07OB003);

HRNB = the acronym for the Water Survey Canada gauge Hay River near ALTA/NWT Boundary (07OB008);

MF = membership function;

THR = the Town of Hay River;

WSC = Water Survey of Canada.

Chapter 1 Introduction

Flooding is one of the most damaging natural disasters faced by mankind. It can be triggered by heavy rainfall, rapid snowmelt, as well as by ice jams and not uncommonly a combination of them. In northern river basins such as in Canada, ice jams are a major cause of significant flooding (Andrews 1993). For instance, in the period 1983 to 1987, over one third of flood events in Canada were caused by ice jams (Environment Canada 1988). The estimated economic loss each year due to ice jams is around $60 million dollars in Canada (Beltaos 1995) and $120 million dollars (USD) in United States (White *et al.* 2007).

Ice jams can develop during freeze-up, during a mid-winter thaw and/or during spring breakup. In this study, only breakup ice jams are considered, as these are common in northern Canada and almost universally the most severe of the three. For a major ice jam, due to its blockage of the river channel and much bigger hydraulic resistance by its rough interface with the water, the water level is elevated much higher than what occurs for the open channel condition at the same discharge. As a result, ice jam flooding can occur even with a moderate flow discharge (e.g. see Figure 1-1). Additionally, breakup ice jam floods are always sudden, as water level associated with a major ice jam can rise several meters in minutes. The competent ice floes carried with the ice jam flood water increase risk to life and damage to property. In the context of climate change, the frequency of extreme ice jam floods may possibly be expected to increase (e.g.

Beltaos and Prowse 2001; Mahabir *et al.* 2007). Therefore, it is crucial to have the capability of forecasting such events with enough lead-time for northern riverside communities.

The goal of the study is to enhance our capability to predict the flooding severity and the timing of river ice breakup in northern communities. In the following of this chapter, a background of river ice breakup problems is first given; A literature review of the state of art forecasting models on the flood severity and timing of river breakup is then presented; Finally the objectives of the study and the structure of the thesis is outlined.

1.1 Background

River ice breakup is a very complex process involving many disciplines such as thermodynamics, structural mechanics, hydraulics, hydrology, and meteorology. It has been the focus of intense research over the past few decades. Beltaos (2008) provides a comprehensive review of the state of knowledge of river ice breakup processes and related phenomena. The whole breakup process can be divided into five phases: *pre-breakup, onset, drive, jamming, and wash.* In the pre-breakup phase, the strong ice cover is subject to thermal decay by the positive energy inputs; for example, solar radiation from above, and heat transferred to the underside by flowing water. Meanwhile, the river discharge starts to increase along with the snowmelt runoff and the associated rising water levels and

increased flow shear stresses cause the decayed ice cover to crack. This finally results in the onset of breakup, which was defined as *"the first sustained movement of the winter ice cover"* by Beltaos (1997). As the snowmelt runoff continues to cause river water levels rise, the fragmented ice sheets are carried along the flow downstream (this is *drive*) until they are stopped by, for example, a stronger and intact ice cover. Ice jamming results. An ice jam can either stay in place until it melts out, or it might release under the pressure of building water storage upstream, or as a result of an incoming wave of ice and water. The ice jam release wave or 'jave' (e.g. see Beltaos and Burrell 2005; Kowalczyk Hutchison and Hicks 2007), comprised of release water and ice, can stall and reform a new ice jam somewhere downstream, or may instigate an ice jam release when it impacts on an existing downstream ice jam. In particular, on dynamic systems, such as the Hay River, NWT, the breakup front can proceed downstream in a cascade of driving, jamming and releasing events until the last phase of wash, in which the ice blocks are cleared from the river by the runoff or the remnants of ice jams just melt out in place.

Currently, the main focus of river ice breakup research is in studying the dynamics of ice jam formation and release. Extensive literature on these ice jam processes include field investigations and data collections (e.g. Jasek 2003; Shen and Liu 2003; Beltaos and Burrell 2005; Kowalczyk Hutchison and Hicks 2007; She *et al.* 2009a), experimental studies (e.g. Zufelt 1990; Healy and Hicks 2006, 2007; Dow Ambtman *et al.* 2011a, 2011b) and numerical simulations (e.g. see

Shen *et al.* 1990, 1995; Beltaos 1993; Zufelt and Ettema 2000; She and Hicks 2006; She *et al.* 2009b). All of these efforts have aimed to provide a capability to predict the formation and release of ice jams and to quantify their potential flood impacts. More recently, Carson *et al.* (2011) provided the test results of three phases for the 8 numerical models (i.e. CRISSP 2D by Manitoba Hydro/Clarkson University; HEC-RAS by AMEC Earth and Environmental; ICEJAM by University of Alberta; ICEPRO by KGS Group; ICESIM by Hatch Energy; MIKE 11 by LaSalle Consulting Group; RIVER1D by University of Alberta and RIVJAM by Environment Canada). They concluded that when these models were calibrated against the proper field data, they all were able to reproduce the measured data; when no field data were provided to calibrate the ice parameters of each model (i.e. in a "blind test"), their performances were more variable, and highly dependent on the modelers' judgments. Though much success has been achieved, these models need more verification in practice and the data requirements for calibrating them are intensive and time-consuming. Many features of the phenomenon (e.g. ice jam thickness) are logistically difficult to measure safely, which may reduce the reliability of such models for practical forecasting purposes. In addition, although such models provide a promising tool for short lead-time forecasting of potential ice jam flood levels (i.e. providing a few hours advanced warning of expected water levels given knowledge of incoming ice runs or javes), in the context of long lead-time forecasting (e.g. days to weeks in advance of breakup) they are not generally applicable.

Breakup ice jam floods have been documented along many rivers in northern Canada. For example, the Town of Hay River in Northwest Territories (NWT) has a very long history of moderate and significant spring ice jam flooding. Flooding occurred in 20 of the 47 years between 1963 and 2010, and 8 of these were severe flood events (Kovachis *et al.* 2011). For a small town of about 3600 population (2006 census accessed from www.hayriver.com), the estimated losses and property damages were between 0.6 million and 1 million Canadian dollars for the two largest documented floods: in 1963 (Stanley Grimble Roblin Ltd. 1963) and 1985 (Environment Canada 1988). Ice jam flooding is also frequent in other rivers across Canada such as the Athabasca River at Fort McMurray, Alberta (see Mahabir 2007), the Pease River at Peace River, Alberta, the Red River at Winnipeg, Manitoba, and the St John River at New Brunswick. Though ice jams have some beneficial ecological impacts (e.g. see Beltaos *et al.* 2006), their destructive threat to properties and human lives is a major concern in northern communities such as the Town of Hay River.

For hundreds of communities across Canada, practical and reliable forecasting tools are imperative to provide advance warning of the expected timing and magnitude of ice jam floods. The ultimate objective of this study was to develop such an operational tool, by integrating modern ice jam flood forecasting technologies within an expert system interface in the development of an *Emergency Operations Ice Jam Flood Forecasting Expert System* (Brayall *et al.* 2008). To achieve these goals, a comprehensive suite of ice jam flood forecasting

models was proposed, which was comprised of the following three key components (see Figure 1-2):

1. A long lead-time preparedness forecasting model (i.e., providing a few weeks warning), based on soft computing techniques. This component produces as output a qualitative forecast of the expected severity of breakup flooding (e.g., a low, moderate, or high degree of flooding), which helps to define the appropriate level of emergency preparedness planning required by both the local disaster services agency and the community's residents. This also produces as output a forecast of expected timing of the onset of breakup, i.e. the first transverse crack of the ice cover, with a lead-time of ~ 1 week.

2. A moderate lead-time event forecasting model (i.e., 12 to 24 hours warning), based on ice jam release event modeling. This component produces as output the expected timing of the ice jam flood event in the community. This model will be closely integrated with event detection technologies such as water level sensors, remote cameras, and satellite imagery.

3. A short lead-time evacuation forecasting model (i.e., 6 to 12 hours warning), based on ice jam formation event modeling, which produces as output the extent and depths of flooding anticipated in the community. This model will be closely integrated with community Emergency Operations systems, to facilitate the orderly and efficient execution of an evacuation plan.

For detailed studies of the second and third components, the reader is referred to Watson (2011) and Brayall (2011), respectively. This study focuses on the long lead-time forecasting model (i.e. the first component) and aims to investigate and enhance our ability to forecast the breakup ice jam floods. To some extent, flooding is a natural event that cannot be completely prevented. However, due to the rapidity with which ice jam flood events develop, an advanced warning and preparedness measures are greatly desired for the riverside communities to minimize the potential for property damage and, in some cases, they may even save human lives. Considerable efforts have been undertaken to develop empirical and statistical models to forecast the severity of breakup ice-jam flooding. A small number of models are also available in respect to forecast the timing of breakup. This literature is discussed below.

1.2 Forecasting breakup flood severity

In terms of breakup flood severity, to be useful a forecasting model should provide a quantitative flood level forecast for a specific site with adequate lead-time. In current practice, there exists no such a model. Empirical, statistical and artificial intelligence models are quite prevalent in operational river ice jam/flooding prediction. Techniques range from simple threshold models to complex nonlinear models.

1.2.1 Threshold models

Historically, some forecasting models have attempted only to produce a dichotomous outcome, i.e. whether or not a breakup ice jam will occur, since this is a necessary condition for any ice jam flooding. Shulyakovskii (1963) first presented a simple one-variable threshold model to predict the risk of ice jams on the Yenisei River downstream of the town of Krasnoyarsk, Russia, using the freeze-up stage as the only independent variable. There existed a lower threshold when ice jams would never happen and an upper threshold when ice jam would surely happen. White (2003) then used the same data to develop a quantitative probability distribution function for ice jam occurrence between the two threshold values. However, this is the only successful single-variable threshold model that can be found in literature. Due to the complexity of factors precipitating ice jams, it is rare that such a simple threshold model could be found for each case. For example, Robichaud (2003) tested 16 hydrometeorological indices as potential single variable threshold indicators of breakup flooding for the Athabasca River at the Town of Fort McMurray, Alberta Canada, and none were successful.

Multivariate threshold models have also been investigated: Shulyakovskii (1963) presented an example of a two-variable threshold model for the Neman River downstream of Kaunas (before the construction of the Kaunas hydroelectric plant), Lithuania, based on the mean rate of water level rise before the onset of breakup and on the air temperature at the time of breakup. He found that ice jams

occurred when the air temperature was positive at the time of breakup, and the rate of water level rise was not lower than 24 cm/day at the water gauge of Kaunas.

Galbraith (1981) developed a more complex threshold model to predict the likelihood of ice jams on the Saint John River in New Brunswick. Four meteorological indices were analyzed on the available data set (from 1954 to 1980): the accumulated degree-days of thaw (*ADDT*, referred to a base temperature of 0 °C); the average rate of heat transfer during the breakup period; the snowmelt index (*SMI*); and the accumulated precipitation during the breakup period. An operational procedure was then used to estimate the likelihood of a breakup ice jam based on the weather forecast data in the coming 5 days. When *ADDT* reached 50 °C-days or the *SMI* reached 90mm in less than 15 days, the risk of ice jam will be high. Also, when the accumulated precipitation exceeded 40 mm over a three day period, the risk of serious flooding was increased. However, the author also mentioned that these threshold values could only be regarded as guidelines as confidence in them was not very high due to a small sample size and the rare occurrence of ice jam events.

Similar studies have been performed to develop multivariate threshold models (e.g. see Wuebben and Gagnon 1995; White and Kay 1996; White and Daly 2002). However, as summarized by White (2003), the main drawback of these models is that they tend to have a high rate of false-positive errors (i.e. false

predictions of ice jams that did not happen) in order to minimize the false-negative errors (i.e. non-predicted ice jams that did happen). Another weakness of these threshold models is that they do not give any quantitative or qualitative evaluation of the flood severity; they only attempt to predict whether an ice jam will or will not occur. On many Canadian northern rivers such the Athabasca River in Alberta and the Hay River in NWT, ice jams happen almost every spring, but not all of them have caused flooding. Therefore, it is necessary to investigate models to forecast the breakup ice jam flood severity other than occurrence of ice jam in these cases.

1.2.2 Multiple linear regression models

Because of the limited capability of the threshold models, more complex models have been investigated for predicting potential breakup ice-jam flood severity, either qualitatively or quantitatively, for example, the applicability of statistical techniques, such as multiple linear regression models, have been explored. Shulyakovskii (1963) first developed a linear regression model to predict the maximum water level rise above the initial water level at the onset of breakup for the Tom River at the Town of Tomsk, Russia. The model validation was not discussed by the author, neither the error range of the model. However, it is worth noting that the following independent variables were chosen in the model development:

- $ADDF_w$, which is the accumulated degree-days of freezing during winter (e.g. the period from the day of freeze-up to January inclusive for the site);
- the depth of snow cover on the ice and in the river basin;
- the rate of water level rise before the onset of breakup;
- and the ratio of $ADDT_{jam}$ to $ADDT_{snw}$, which are respectively the accumulated degree-days of thaw at the jam location and a upper basin location.

Mahabir *et al.* (2006a) also developed a multiple linear regression model for predicting the maximum breakup water level at the Town of Fort McMurray, Alberta Canada from an extensive database of 106 variables. The selection of independent variables was done by Pearson's correlation coefficient analysis. The jackknife approach was used to assess the model stability and the best model was determined by the adjusted R^2 criterion. The final model had a standard error of ±0.7 m and was the most successful statistical model to date for this study site. The authors commented that the validation of the model was limited by the unavailability of the data for the extreme events, i.e. the performance of the model on these events was verified.

1.2.3 Logistic regression models

Logistic regression is another form of regression, in which only a small number of ordinal outputs rather than a continuous output are modeled. Its two biggest advantages over the linear regression models are that no distribution assumption is needed for the input and output variables and the output variable can have a nonlinear relationship with the input variables. White (1996) used a logistic regression model to predict ice jams on the Platte River at North Bend, Nebraska USA, which provided a dichotomous outcome (e.g. jam/no jam). However, a cut-off point, i.e. a probability value for the occurrence of ice jam, has to be chosen subjectively. For the study site at the 0.36 probability level, the model had 1 of the 28 jam years falsely classified as a non-jam year and 8 of the 11 non-jam years falsely classified as jam years.

1.2.4 Discriminant function analysis

Discriminant function analysis is a statistical method that predicts a category output using independent variables. Using two linear discriminant functions, Zachrisson (1990) presented a model to predict the ice jam flood risk on the Tornealven River along the Finish-Swedish border by using three output categories: *Safe, Medium, and Critical*, and four input variables: total winter precipitation, total April precipitation, change of discharge in 5 days before breakup and the date when the accumulated thawing degree-days reaches 40°C.

The model showed a promising result in 1989 but a poor result in 1990. The author commented that it was due to limited data on the ice thickness and strength. White and Daly (2002) applied the same technique to predict ice jam risk at Oil City, Pennsylvania, USA. However, unlike Zachrisson, they used a dichotomous outcome, e.g. jam or no jam. They found that, at this site, the discriminant function analysis model had fewer false positive errors than the empirical threshold model. However, it did have more false negative errors (i.e. 6 out of 39 ice jam events were falsely classified as non-jam events). White and Daly also developed the 90% confidence intervals for the prediction result by using a bootstrap simulation (Efron and Tibshirani 1993): when a non-jam event is predicted, the chance of a jam occurring ranges from 7% to 25%; when a jam event is predicted, the chance of it not occurring ranges from 0 to 20%. In terms of flood forecasting, this model could only provide a prediction of the ice jam occurrence, not the severity of breakup flooding.

1.2.5 Artificial neural networks (ANNs)

In recent years, the advances in soft computing techniques suggest great potential for application to the breakup forecasting problem. The ANN method is one of the most commonly used. ANNs self-learning capabilities enable them to represent the inherent relationships between the input and output variables, without the need for a priori knowledge about the nature of the relationship. This special advantage over other techniques makes it very suitable for the river ice problems: for

example, Massie *et al.* (2002) developed an ANN to produce a daily forecast of jam/no jam at Oil City, Pennsylvania USA. The ANN model decreased both the false positive error rate and the false negative error rate comparing to the alternative regression and threshold methods at the same location.

The viability of using ANNs to model at least some river ice processes has been demonstrated by modeling ice thickness growth in several studies. Seidou *et al.* (2006) investigated a one-hidden-layer neural network with a sigmoid transfer function for the nodes in the hidden layer and a linear transfer function in the output layer. They also used a trial and error process to find the optimal number of both input nodes and hidden nodes. They found that choosing a proxy variable for solar radiation as one of the inputs made the model more physically rigorous, but at the same time it decreases its practical utility due to the complexity in calculating the variable. Hicks *et al.* (1995) found that the less data intensive linear heat transfer model outperformed a full energy budget model for modeling thermal breakup on the Mackenzie River at the outlet of Great Slave Lake, NWT Canada. This suggests that a more practical simplified method for river ice forecasting, in which air temperature is an important meteorological factor.

Chokmani *et al.* (2007) also assessed the ability of ANNs in river ice thickness modeling using easily available climate data. In the preliminary data set analysis, the outliers were excluded. It was found that the developed ANNs were not able to model the low and high ice thickness values correctly. They suggested that

rescaling of the data set in an interval of [0.1, 0.9] and using more hidden nodes might improve the model performance. Another problem is that they did not test the sensitivity of the number of hidden nodes to the model performance.

1.2.6 Fuzzy logic systems

Based on the concept of fuzzy set proposed by Zadeh (1965), fuzzy logic systems have the best advantage over others to deal with linguistic variables (e.g. low, average, and high) and generalized expert knowledge (i.e. "rules of thumb") in an "IF-THEN" format. A good example of a general rule for the breakup flood severity can be found in Beltaos (1997): when the freeze-up stage is low and spring runoff is average or high, the breakup flood risk will be moderate; or when the freeze-up stage is high and spring runoff is low (or high), the breakup flood risk will be low (or high).

Mahabir *et al.* (2002) proposed the first fuzzy logic system to predict the breakup water level of the Athabasca River at the Town of Fort McMurray, Alberta, Canada by using only long lead-time variables, specifically: antecedent basin moisture, later winter snowpack, and late winter ice thickness. By giving ~ 3 weeks of lead-time, the model could correctly predict all the high water events with only one false positive error.

Mahabir *et al.* (2006b) enhanced their fuzzy logic model by investigating a hybrid neuro-fuzzy model and applied it in the same site. This hybrid model combined both the advantages of the ANN's self-learning capability from the historical data and the fuzzy logic system's ability to incorporate linguistic variables and qualitative understanding and knowledge of the river ice breakup process. Specifically, the rule base of the fuzzy logic system was trained using the ANN approach. Their model was found to perform much better than the MLR model for the same site, while using fewer input variables and providing a longer lead-time forecast.

1.2.7 Discussions

From the above reviews it is apparent that, due to the extremely complex mechanism of breakup ice jams in natural rivers, most of the current forecasting approaches are highly site specific and empirical. The variables used in these methods are usually arbitrary and not known or possible to be forecasted more than a few days prior to breakup, which greatly reduces their potential as a practical forecasting tool for a long lead-time prediction. In less populated regions like northern Canada, a short record of historical data and the sparsity of data network further impede successful development of such models, such as statistical models which usually need a large data set to make them more reliable. In addition, the severity of breakup ice jam flooding was not considered by most of these earlier models, either quantitatively or qualitatively, only the occurrence of

ice jams. Though fuzzy logic models (e.g. Mahabir *et al.* 2006a and 2006b) have showed much potential in respect to forecasting flood severity, quantitative data collection is still a big problem for less populated northern regions. For instance, at the town of Hay River, the collection of a reliable maximum breakup water level set is not possible for the variety of the ice jam locations at the town (Mahabir *et al.* 2007). In this case, the direct evaluation of breakup flooding severity (i.e. flood water level) is impossible; only other possible indicators can be used, such as peak snowmelt runoff during breakup. These indirect breakup indicators will be discussed in this study.

1.3 Forecasting the timing of breakup

For advance warning purposes, the onset of breakup is of great interest in the practice of river ice breakup forecasting. As has been discussed earlier, the onset of breakup is the result of the increase of river discharge (and water level) from snowmelt and/or rainfall runoff and the decay of the ice cover by extra energy input (e.g. solar radiation). Thus in the literature, either the water level or the date of the onset of breakup has been used for the purpose of forecasting. Using the water level at the onset of breakup (defined as H_{OB}) as the predictive variable in practical forecasting has been quite common in the past since it is closely related to the physical mechanism of the ice cover deflection and fracture. It is especially useful when the historical water level hydrographs are available at gauge sites as they can be used to extract the required breakup data, i.e. H_{OB}. The predictions of

H_{OB} can be translated to the time scale based on real time water level observations, usually based on a projection of the prevailing rate of water level rise during the pre-breakup period.

1.3.1 Semi-empirical models

Most early studies focused on river ice breakup mechanisms. In those studies, the breakup water level rather than the time of breakup has been used to develop the breakup forecasting models. Billfalk (1981) investigated the formation of shore cracks parallel to the river banks by considering a floating ice cover as an infinitely long beam on an elastic foundation. In his study, the required water level changes to create cracks were computed both for cases of a fixed end beam (see Equation [1-1]) and a hinged end (see Equation [1-2]).

$$\Delta h = 0.0058\sigma_i\sqrt{t_i/E} \quad [1\text{-}1]$$

$$\Delta h = 0.018\sigma_i\sqrt{t_i/E} \quad [1\text{-}2]$$

where Δh is the water level change; σ_i is flexural strength of the ice; t_i is the ice thickness; and E is modulus of elasticity of the ice.

A laboratory experiment was also designed to validate the theory; however, the results showed considerable scatter in the data. The author discussed the possible reasons such as the limitation of displacement of the support (which was not infinitely long) in the laboratory experiments and the variability of the flexural strength of thin ice covers. These two factors reflect the limitation of the theory when applied to practical problems: the finite channel width of the river and the non-uniform ice thickness across the width.

Tang and Davar (1984) developed a semi-empirical forecasting approach to predict the onset of breakup and maximum breakup water level. They first extracted the water level data from the historical hydrographs, including the maximum stable freeze-up water level (H_F), the breakup water level (H_{OB}), and the maximum water level during breakup (H_M). They used a simplified method to calculate the heat index, $\sum q$, which was taken as the sum of net incoming solar radiation, emitted long wave radiation, and conduction and convection heat exchange to the ice cover. The ice thickness (t_i) was estimated based on the accumulated degree-days of freezing. Using the five variables, two empirical relationships were found: the plot of the deviation, $2.5t_i - H_{OB} - H_F$, against $\sum q$; and the plot of the deviation, $H_M - 1.22 - 1.18H_F$, against $\sum q$. When they were validated, it was found that the model only worked successfully for winter thaw events within a 24-hour range of the forecast, but was *very poor* for the spring breakup events. By providing a procedure to predict the probable water level a few days in advance, they showed that the model had potential as an operational

tool for a case study of the 1982-83 breakup events at the Nashwaak River in New Brunswick Canada. The prediction error for the maximum breakup water level was 0.3m and the timing of onset of breakup was correctly predicted. However, they noted that the model was very sensitive to the accurate data extraction from the hydrometric records, which means that the poorly extracted data would result in poor model performance.

1.3.2 Empirical models

Many site-specific empirical and semi-empirical approaches have been developed as more practical tools for forecasting purposes. These employ the historical records of hydro-meteorological data (e.g. snowfall, air temperature, and freeze-up water level) in a conceptual modelling framework. Shulyakovskii (1963) first proposed the relationship between the onset of breakup (i.e. *"the first ice-cover push"*) and required heat input to the ice cover, which is a function of several factors, such as ice thickness, depth of snow on the ice cover, morphological characteristics of the river, flow velocity under the ice cover and the rise of water level. He further proposed that the water level at which the first ice push occurs was directly correlated to the maximum water level or the mean water level during the first 5 days of the stable ice period. This provides the simplest model that can be used for a long lead-time forecasting of the required water level to initiate the river ice breakup (i.e. no short term variables are needed, such as expected air temperatures).

Beltaos (1990) presented a similar approach as that proposed by Billfalk (1981) for the idealized case of an infinitely wide channel and further discussed the results for the finite channel width case. In the same study, Beltaos also discussed the boundary constraint criterion for the onset of breakup (defined as "*the time when the local ice cover is set in motion"*) and proposed a practical approach to forecast the onset of the breakup, as shown in Equation [1-3] below.

$$H_{OB} - H_F = kt_i \quad [1\text{-}3]$$

where, H_{OB} is the water level at which the onset of breakup occurs; H_F is the water level at the preceding freeze-up; t_i is the ice thickness; and, k is an empirical coefficient that depends on the river channel geometry and hinge crack distance from the edge.

Beltaos (1997) proposed a more general equation for cases where significant heat input to the ice cover has occurred during the pre-breakup period (Equation [1-4]).

$$H_{OB} - H_F = kt_i - f(ADDT_{-5}) \quad [1\text{-}4]$$

where H_{OB}, H_F, k, and t_i are the same as those in Equation [1-4]; f is a site-specific function; and $ADDT_{-5}$ is defined as the accumulated degree-days of thaw referred to a base temperature of -5 °C. Here, the $ADDT_{-5}$ is considered as an

index of the accumulated heat input to the ice cover during the pre-breakup period.

Aside from the water level, other indicators can be used for forecasting the onset of breakup, such as the accumulated degree-days of thaw, based on mean daily air temperatures. For instance, Kovachis (2011) examined three variations of accumulated degree-days of thaw as an indicator of the onset of breakup at Hay River, NWT: the accumulated degree-days of thaw on a base of 0 °C, $ADDT_0$; the accumulated degree-days of thaw on a base of -5 °C, $ADDT_{-5}$; and the total degree-days of thaw on a base of 0 °C, *TDDT*. It was found none of these variables produced particularly consistent results as an indicator of the timing of breakup at a specific site within the study area. Nevertheless, it is very worthwhile to test other factors such as the winter snowfall, spring rainfall as potential breakup indicators.

1.3.3 Soft computing methods

More recently, soft computing methods have been investigated for forecasting the timing of river breakup. Chen and Ji (2005) developed a three-layer neural network model using fuzzy optimization to forecast the freeze-up and breakup dates of the Yellow River at Inner Mongolia, China. Four input variables were used in their study: the accumulated degree-days of thaw, the average water level, the average streamflow and the maximum ice thickness. Five nodes were used in

the intermediate layer. The first 28 data points (1969 to 1996) were used to train the neural network model and the last 5 (1997-2001) were used to test the model. The results showed moderate success on the test set (1 to7 days of error for breakup dates) while the calibration results were not shown in the paper. Later, Zhou *et al.* (2009) used a Support Vector Machine (SVM) model for ice breakup prediction for the same site on the Yellow River using the same calibration and test data set as Chen and Ji (2005). They showed that SVM had better results than ANN both for the training and testing data. However, it is significant to note that they also found that the error on the testing data was smaller than the error on the training data. In the author's opinion, this result shows the disadvantage of the split-data method used for the model validation: when the error on the testing data is smaller than that on the training data, it is not convincing that the model will have as good performance in another split-data pattern. More comprehensive validations should be conducted in developing an ANN model.

Wang *et al.* (2008) used a feed-forward ANN model trained by a Levenberg-Marquardt algorithm to forecast the ice run date, freeze-up date and breakup date at this same site of the Yellow River, China. For the three sites of study reach, both the prediction errors for the data of ice run and for the freeze-up date ranged from 0 to 2 days. However, they found that for the breakup date, the error ranged from 2 to 7 days.

Hu *et al.* (2008) further employed a hybrid feed-forward ANN model (particle swarm optimization and back propagation) to predict the timing of breakup on the Ningxia and Inner Mongolia Reach of the Yellow River, China and concluded that the hybrid ANN model outperforms both the empirical and combined empirical and statistical methods. The errors ranged from -4 to +8 days for the breakup date. In both of these studies, 7 input variables were used: water temperature, air temperature, discharge, water channel storage, ice concentration on the water surface, ice thickness, and water level. Detailed definitions of the variables were not provided.

Guo (2009) further applied the Non-linear Combined Forecast (NCF) method to predict the freeze-up and breakup dates of the Yellow River China. Based the structure of a fuzzy optimization neural network (Chen 1998), he combined a fuzzy pattern recognition model (FPR), a FPR-ANN model and an intelligent forecast model. Using the mean absolute error as the evaluating index, he found that the new model (i.e. combination of the three) outperformed both of the original models. The mean error for the freeze-up date was 1.17 days, while the error for the breakup date was not shown. It should be noted that the change in performance between the FPR-ANN model and the new model was very small.

1.3.4 Discussions

The timing of river breakup is difficult to predict due to its great dependence on the short-term weather conditions during the pre-breakup period. The semi-empirical models consider the physical mechanisms associated with of the onset of breakup and, therefore, have the advantage of being more physically rigorous. However, the data requirements for these methods are necessarily more extensive. From a forecaster's point of view, these models or approaches are too complicated to use: some parameters (e.g. ice strength and thickness just prior to breakup) are highly site and case specific and take many years of field data collection to calibrate adequately. On the other hand, most empirical models are also very site-specific and need a large data set to gain a high level of confidence. Thus the utility of both approaches in forecasting practice are very limited.

Those recent studies have illustrated the potential applicability of soft computing methods, especially ANNs, for forecasting the timing of the river ice breakup. However, there are still many questions yet to be answered. One of the biggest questions is: in the context of northern rivers, where the available data is relatively limited, how reliable will the calibrated ANN model be, given a small data set? Also how does the size of the intermediate layer affect the performance of an ANN model in the same (data limited) situation. Further studies are needed to investigate these questions.

1.4 Objectives of this study

Expanding on the previous research by Mahabir (2007), which investigated direct relationships between raw data and breakup severity using regression methods, fuzzy logic and neuro-fuzzy logic models, in this study, a multi-layer approach is to be explored to address the data sparsity issue in northern regions. Though both ANN and fuzzy logic systems have been shown to be universal approximators, an explicit methodology to develop these models has not yet come into existence, particularly for the river ice breakup applciation. On the one hand, this gives model developers the freedom to choose any model configuration they want; however, the other side is that it is hard to verify choices and the performance of the calibrated model on the "blind" data is forever unknown.

The specific objectives of this study were to:

- to investigate a multi-layer modeling approach to forecast breakup ice jam flood severity for northern communities, where the sparsity and short record of the hydrometeorological data is a constraining issue;
- to assess the applicability of feed-forward artificial neural networks (ANNs) and the Mamdani-type fuzzy logic systems (FLSs) to the river ice breakup forecasting problem. To achieve this, ANNs and FLSs were developed and demonstrated. Based on the suitability of the typical data available and given the type of forecasts generally needed, it was determined that the ANN approach was best suited to the problem of

predicting the timing of river ice breakup and the FLS was best suited to the problem of forecasting the breakup ice jam flood severity.

1.5 Outline of the thesis

This thesis has a paper-based format and follows the specifications brought forward by the Faculty of Graduate Studies and Research, University of Alberta. One conference paper and two journal papers make up the three main chapters of the thesis:

- Chapter 2 describes the multi-layer modeling approach proposed in this study and presents the hydro-meteorological data set for the study site, the Hay River basin at NWT Canada. This is an extended version of the paper which was presented by the author at the 20th Canadian Hydrotechnical Conference, Canadian Society for Civil Engineering (Zhao *et al.* 2011).
- Chapter 3 presents the results of investigating the applicability of ANN models to the onset of breakup, as published in the Journal of Cold Regions Science and Technology (Zhao *et al.* 2012a).
- Chapter 4 shows the detailed results of the investigation of using the fuzzy logic technique to predict the peak snowmelt runoff during breakup, which is to be submitted to the Journal of Cold Regions Science and Technology in the near future (Zhao *et al.* 2012b).
- Chapter 5 makes the conclusions for this study and some recommendations for future research.

- Appendix A presents the development of the raw hydrometeorological data set of the Hay River study site.
- Appendix B summarizes all the data tables of the index variables extracted or processed from the raw hydrometeorological data for the Hay River study site.
- Appendix C presents the detailed discharge hydrographs for the three WSC gauges in the Hay River basin and the extractions of the peak snowmelt runoff.
- Appendix D presents the result of the study using ANN models to predict the timing of breakup at the Town of Hay River NWT.

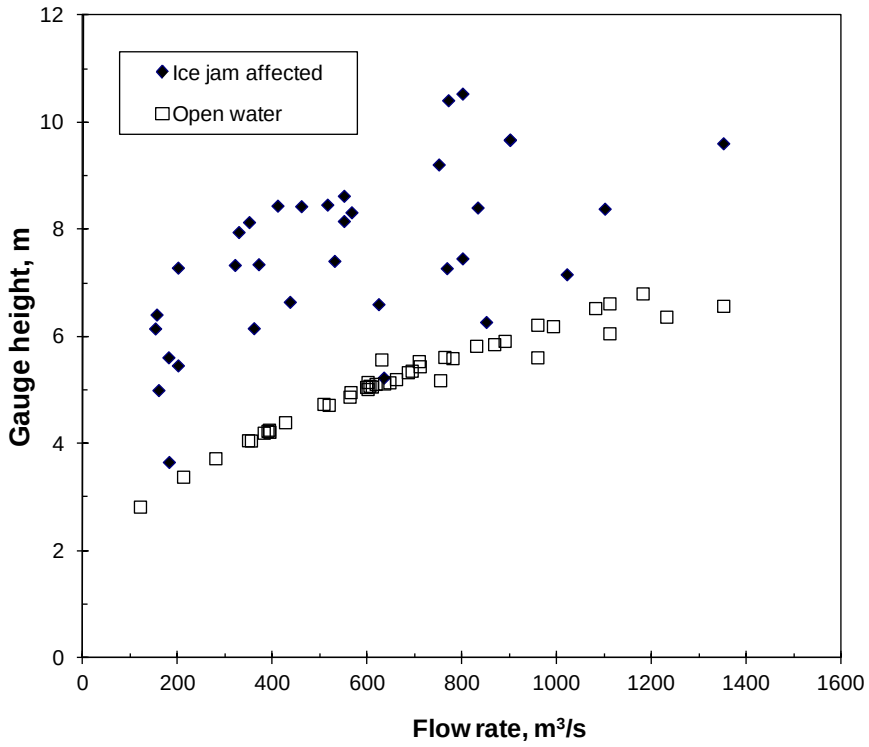

Figure 1–1: Comparison between the annual open water maximum and ice jam affected maximum water level at WSC Hay River near Hay River gauge (07OB001).

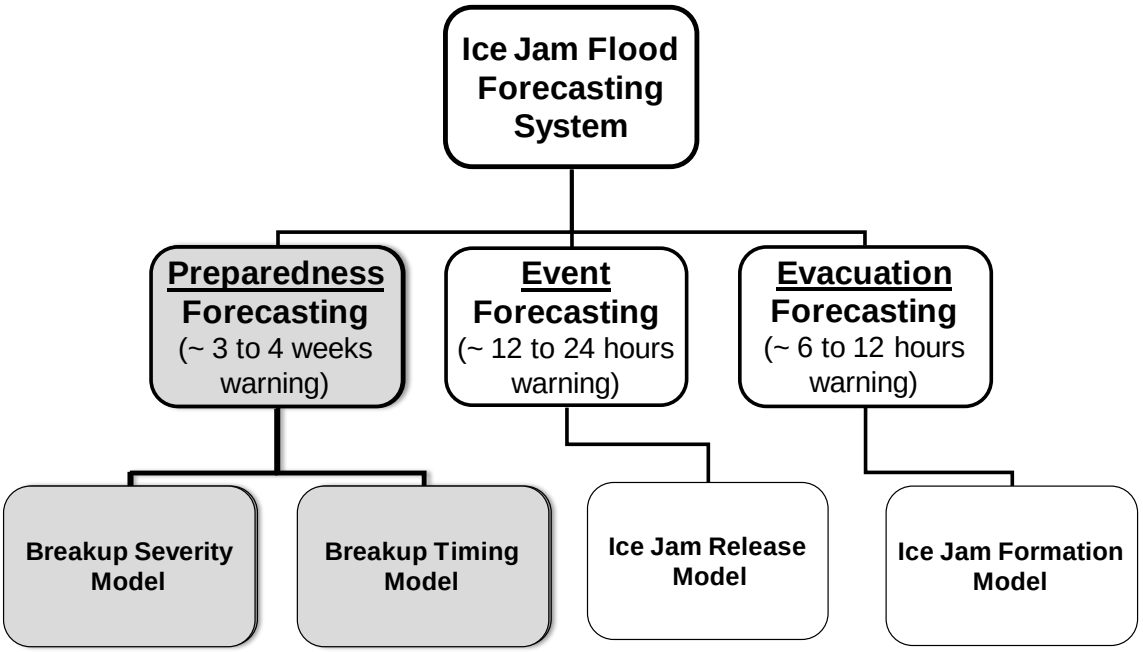

Figure 1–2: A multi-stage river ice jam flood forecasting system (adapted from Brayall *et al*. (2008)).

1.6 List of references

Andrews, Jeanne (Ed.) 1993. Flooding Canada Water Book. Ecosystem Sciences and Evaluation Directorate, Economics and Conservation Branch, Environment Canada. Ottawa, Ontario. 171pp.

Beltaos, S. 1984. A conceptual model of river ice breakup. Canadian Journal of Civil Engineering, 11(3): 516-529.

Beltaos, S. 1990. Fracture and breakup of river ice cover. Canadian Journal of Civil Engineering, 17(2): 173-183.

Beltaos, S. 1993. Numerical computation of river ice jams. Canadian Journal of Civil Engineering, 20(1): 88-99.

Beltaos, S. (Ed.) 1995. River Ice Jams. Water Resources Publications, LLC, Highlands Ranch, Colorado, 372 pp.

Beltaos, S. 1997. Onset of river ice breakup. Cold Regions Science and Technology, 25(3): 183-196.

Beltaos, S. (Ed.) 2008. River ice breakup. Water Resources Publications, LLC, Highlands Ranch, Colorado. 462pp.

Beltaos S. and Burrell, B.C. 2005. Field measurements of ice-jam-release surges. Canadian Journal of Civil Engineering, 32(4): 699-711.

Beltaos, S. and Prowse, T.D. 2001. Climate impacts on extreme ice-jam events in Canadian rivers. Hydrological Sciences Journal, 46(1): 157-181.

Beltaos, S., Prowse, T.D., and Carter, T. 2006. Ice regime of the lower Peace River and ice-jam flooding of the Peace-Athabasca Delta. Hydrological Processes, 20(19): 4009–4029.

Billfalk, L. 1981. Formation of shore cracks in ice covers due to changes in the water level. Proceedings of the 6th IAHR Symposium on Ice, Quebec City, Canada, Vol. II: pp. 650-660.

Brayall, M. 2011. 2-D Hydraulic and Ice Process Modeling at Hay River, NWT. Thesis presented in partial fulfillment of the degree of Master of Science in Water Resources Engineering, Department of Civil and Environmental Engineering, University of Alberta, Edmonton, Alberta. 173pp.

Brayall, M., Andrishak, R., and Hicks, F. 2008. Ice jam flood forecasting expert system for the Hay River at Hay River, (NWT Canada). Proceedings of 19th IAHR Ice Symposium, Vancouver, Canada, Vol. 1:339-352.

Carson, R., Beltaos, S., Groeneveld, J., Healy D., She, Y., Malenchak, J., Morris, M., Saucet, J., Kolerski, T., Shen, H. T. 2011. Comparative testing of numerical models of river ice jams. Canadian Journal of Civil Engineering, 38(6): 669-678.

Chen, S. 1998. Multiobjective decision making theory and application of neural network with fuzzy optimum selection. Journal of Fuzzy Mathematics, 6(4):957-967.

Chokmani, K., Khalil, B., Ouarda, T., Bourdages, R. 2007. Estimation of river ice thickness using artificial neural networks. Proceedings of the 14th Workshop on the Hydraulics of Ice Covered Rivers. CGU HS Committee on River Ice Processes and the Environment (CRIPE), Québec, Canada. 12 pp.

DeWalle, D.R. and Rango, A. 2008. Principles of snow hydrology. Cambridge University Press, Cambridge, UK; New York. 410 pp.

Dow Ambtman, K., Steffler, P. and Hicks, F. 2011a. Analysis of the stability of floating ice blocks. ASCE Journal of Hydraulic Engineering, 137(4): 412-422.

Dow Ambtman, K., Steffler, P. and Hicks, F. 2011b. Experimental investigation of the pressure distribution beneath a floating ice block. ASCE Journal of Hydraulic Engineering, 137(4): 399-411.

Efron, B. and Tibshirani, R.J. 1993. An introduction to the bootstrap. Chapman and Hall, New York. 456pp.

Environment Canada. 1988. Flood events in Canada 1983-1987. Inland Waters Directorate, Water Planning and Management Branch. 84pp.

Galbraith, P.W. 1981. On estimating the likelihood of ice jams in the Saint John River using meteorological variables. Proceedings of the 5th Canadian Hydrotechnical Conference, Fredericton, N.B., May 26-27, 1981. Canadian Society for Civil Engineering, Montreal, Québec, pp. 219-237.

Guo, Y. 2009. Application of system NCF method to ice flood prediction of the Yellow River. Fuzzy Information and Engineering, 2: 191-204.

Healy, D. and Hicks, F. 2006. Experimental study of ice jam formation dynamics. ASCE Journal of Cold Regions Engineering, 20(4): 117-139.

Healy, D., Hicks, F., 2007. Experimental study of ice jam thickening under dynamic flow conditions. ASCE Journal of Cold Regions Engineering, 21 (3): 72–91.

Hicks, F.E., Steffler, P.M. and Gerard, R. 1992. Finite element modeling of surge propagation and an application to the Hay River, NWT, Canadian Journal of Civil Engineering, 19(3): 454-462.

Hicks, F.E., Cui, W. and Andres, D. 1995. Breakup forecasting on the Mackenzie river at the Ft. Providence ferry crossing, NWT. Proceedings of the 8th Workshop on the Hydraulics of Ice Covered Rivers, Kamloops, B.C. pp. 483-551.

Hu, J., Liu, L., Huang, Z., You, Y., and Rao, S. 2008. Ice breakup date forecast with hybrid artificial neural networks. Proceedings of the 4th International Conference on Natural Computation, ICNC, Vol. 2: 414-418.

Jasek, M. 2003. Ice jam release surges, ice runs, and breaking fronts: field measurements, physical descriptions, and research needs. Canadian Journal of Civil Engineering 30(5): 113–127.

Kovachis, N., Zhao, L. and Hicks, F. 2011. A summary of historical records of Hay River breakup, 1894 to 2011. Water Resources Engineering Report 2011_FH_01, University of Alberta, Edmonton.

Kowalczyk Hutchison, T. and Hicks, F. 2007. Observations of Ice Jam Release Events on the Athabasca River, AB. Canadian Journal of Civil Engineering, 34 (4): 473-484.

Mahabir, C. 2007. River ice breakup forecasting with fuzzy and neuro-fuzzy models. Thesis presented in partial fulfillment of the degree of Doctor of Philosophy in Water Resources Engineering, Department of Civil and Environmental Engineering, University of Alberta, Edmonton, Alberta. 308pp.

Mahabir, C., Hicks, F., Fayek, A. Robinson, 2002. Forecasting ice jam risk at Fort McMurray, AB using fuzzy logic. 16th IAHR International Symposium on Ice. Dunedin, New Zealand, pp. 112–118.

Mahabir, C., Hicks, F. E., Robichaud, C., and Robinson Fayek, A. 2006a. Forecasting breakup water levels at Fort McMurray, AB, using multiple linear regression. Canadian Journal of Civil Engineering, 33(9):1227-1238.

Mahabir, C., Hicks, F.E., and Robinson Fayek, A. 2006b. Neuro-fuzzy river ice breakup forecasting system. Cold Regions Science and Technology, 46(2): 100-112.

Mahabir, C., Hicks, F.E., and Robinson Fayek, A. 2007. Transferability of a neuro-fuzzy river ice jam flood forecasting model. Cold Regions Science and Technology, 48(3): 188-201.

Massie, Darrell D., White, Kathleen D. and Daly, Steven F. 2002. Application of neural networks to predict ice jam occurrence. Cold Regions Science and Technology, 35(2): 115-122.

Robichaud, C. 2003. Hydrometeorological factors influencing breakup ice jam occurrence at Fort McMurray, Alberta. Thesis presented in partial fulfillment of the degree of Master of Science in Water Resources Engineering, Department of Civil and Environmental Engineering, University of Alberta, Edmonton, Alberta.

Seidou, O., Ouarda, T.B.M.J., Bilodeau, L., Hessami, M., St-Hilaire, A., Bruneau, P. 2006. Modeling ice growth on Canadian lakes using artificial neural networks. Water Resources Research 42, W11407. doi:10.1029/2005WR004622.

She, Y. and Hicks, F., 2006. Modeling ice jam release waves with consideration for ice effects. Cold Regions Science and Technology, 20(3): 137-147.

She, Y., Andrishak, R., Hicks, F., Morse, B., Stander, E., Krath, C., Keller, D., Abarca, N., Nolin, S., Tanekou, F., Mahabir, C., 2009a. Athabasca River ice jam formation and release events, 2006 and 2007. Cold Regions Science and Technology, 55(2): 249-261.

She, Y., Hicks, F., Steffler, P., and Healy, D. 2009b. Constitutive model for internal resistance of moving ice accumulations and Eulerian implementation for river ice jam formation. Journal of Cold Regions Science and Technology, 55(2):286-294.

Shen, H.T., Shen, H., Tsai, S.M., 1990. Dynamic transport of river ice. Journal of Hydraulic Research, 28 (6): 659–671.

Shen, H.T., Wang, D.S., Lal, A.M.W., 1995. Numerical simulation of river ice processes. Journal of Cold Regions Engineering, 9 (3): 107–118.

Shen, H.T., Liu, L., 2003. Shokotsu River ice jam formation. Journal of Cold Regions Science and Technology, 37(1): 35–49.

Chen, S. and Ji, H. 2005. Fuzzy optimization neural network approach for ice forecast in the Inner Mongolia reach of the Yellow River. Hydrological Sciences Journal, 50(2): 319-326.

Shulyakovskii, L.G. (Ed.) 1963. Manual of forecasting ice-formation for rivers and inland lakes. Manual of Hydrological Forecasting No. 4, Central Forecasting Institute of USSR. Translated from Russian 1966, Israel Program for Scientific Translations, Jerusalem, Israel.

Stanley, Grimble, Roblin Ltd. 1963. Engineering report on flood protection at Hay River, N.W.T. 74pp.

Tang, P.W. and Davar, K.S. 1984. Forecasting the initiation of ice breakup on the Nashwaak River N.B. Proceeding of the 3rd Workshop on the Hydraulics of Ice Covered Rivers Fredericton, New Brunswick. pp. 65-93.

Wang, T, Yang, K., and Guo, Y. 2008. Application of artificial neural networks to forecasting ice conditions of the Yellow River in the Inner Mongolia reach. Journal of Hydrologic Engineering, 13(9): 811-816.

Watson. D. 2011. Observation and modeling of ice jam release events on the Hay River, NWT. Thesis presented in partial fulfillment of the degree of Master of Science in Water Resources Engineering, Department of Civil and Environmental Engineering, University of Alberta, Edmonton, Alberta. 114pp.

White, K.D. 1996. Predicting breakup ice jams using logistic regression. ASCE Journal of Cold Regions Engineering, 10(4): 178-189.

White, K.D. 2003. Review of prediction methods for breakup ice jams. Canadian Journal of Civil Engineering, 30(1): 89-100.

White, K.D., and Daly, S.F. 2002. Predicting ice jams with discriminant function analysis. Proceedings of the 21st International Conference on Offshore Mechanics and Arctic Engineering, Oslo, Norway, June 23-28, 2002. American Society of Mechanical Engineers, New York, N.Y., pp. 683-690.

White, K.D. and Kay, R.L. 1996. Ice jam flooding and mitigation: lower Platte River basin, Nebraska. Special Report 96-1, U.S. Army Cold Regions Research and Engineering Laboratory, Hanover, N.H. 88 pp.

White, K.D., Tuthill, A.M. and Furman, L. 2007. Studies of ice jam flooding in the United States. In Vasiliev, O.F. *et al.* (Eds.), Extreme Hydrological Events: New Concepts for Security: pp. 255-268.

Wilby, R. L., Abrahart, R. J. and Dawson, C. W. 2003 Detection of conceptual model rainfall–runoff processes inside an artificial neural network. Hydrological Sciences Journal, 48(2): 163-181.

Wuebben, J.L. and Gagnon, J.J. 1995. Ice jam flooding on the Missouri River Near Williston, North Dakota. CRREL Report CR 95-19, U.S. Army Cold Regions Research and Engineering Laboratory, Hanover, N.H. 25pp.

Zachrisson, G. 1990. Severe break-ups in the River Tornealven: measures to mitigate damages from ice jamming. Proceedings of the 10th IAHR Symposium on Ice, Espoo, Finland, August 20–23, 1990. Madrid, Spain, Vol. 2: 845-857.

Zadeh, L.A. 1965. Fuzzy sets, Information and Control, 8: 338-353.

Zhao, L., Hicks, F and Robinson Fayek, A. 2012a. Applicability of multilayer feed-forward neural networks to model the onset of river breakup. Journal of Cold Regions Science and Technology, 70 (2012): 32-42.

Zhao, L., Hicks, F. and Robinson Fayek, A. 2012b. Long lead forecasting of spring peak runoff using Mamdani-type fuzzy logic systems. In preparation for submission to the Journal of Cold Regions Science and Technology. Manuscript length: 75pp.

Zhao, L., Hicks, F and Robinson Fayek, A. 2011. River breakup forecasting by hydro-meteorological data. Proceeding of the 20th Canadian Hydrotechnical

Conference, Canadian Society for Civil Engineering, Ottawa, July 14-17, 2011, HY-048: 11pp.

Zhou, H., Li, W., Zhang, C., and Liu, J. 2009. Ice breakup forecast in the reach of the Yellow River: the support vector machines approach. Hydrology and Earth System Sciences Discussions, 6 (2): 3175-3198.

Zhukova, M.A. 1979. Formation of ice jams and their distribution. Soviet Hydrology: Selected Papers, 18: 7-13.

Zufelt, J.E. 1990. Experimental observations of shoving and thickening: comparison to equilibrium thickness theory. Proceedings of the 10th IAHR Ice Symposium, Espoo, Finland, Vol.1: pp. 500–510.

Zufelt, J.E. and Ettema, R., 2000. Fully coupled model of ice-jam dynamics. Journal of Cold Regions Engineering, 14 (1): 24–41.

Chapter 2 Available hydro-meteorological data and proposed river breakup forecasting model structure[1]

2.1 Introduction

Unlike open-water floods, breakup ice jam floods are always sudden, as water levels associated with a major ice jam can rise several meters in just minutes. For example, Kowalczyk Hutchison and Hicks (2007) documented a water level rise of 0.81 m/min during an ice jam release event on the Athabasca River. Due to their obstructive effects on the river flow, ice jams can result in severe flooding even at relatively low flow rates. Moreover, competent ice floes carried with flood waves can pose significant risk to life and property of the riverside communities. Therefore, for those communities faced with this annual threat, predicting the timing and anticipated severity of breakup flooding can be extremely valuable in flood preparedness planning.

Considerable physical understanding on the river ice breakup process has been gained in the last 50 years or so (e.g. see Beltaos 2008). However, due to the complex interactions between meteorological, hydrological, and hydraulic factors during the progression of the river ice breakup, a completely physically based

[1] This chapter is an extended version of the published paper: Zhao, L., Hicks, F. and Robinson Fayek A. 2011. "River breakup forecasting by hydro-meteorological data", 20th Canadian Hydrotechnical Conference, Canadian Society for Civil Engineering, Ottawa, July 14-17, 2011, HY-048: 11pp.

prediction model is not yet feasible. Thus, most forecasting models are highly site specific and empirical in nature (e.g. see White 2003). Furthermore, because of the dependence of breakup timing and severity on meteorological conditions immediately prior to and during breakup, most of the input variables in forecasting models are limited by the time range of accurate weather forecasts (i.e. typically only one to two days).

The process of river ice breakup and subsequent ice-jam flooding is influenced by many factors such as ice cover thickness and strength, as well as the volume of snowmelt runoff and consequent stream flow rate. In practice, these variables cannot safely be measured or quantified just prior to or during breakup and the resulting lack of data usually poses a major limitation in developing reliable forecasting models for ice-jam floods. Fortunately, these factors are closely related to hydro-meteorological conditions, which are readily available or forecasted through hydrometric gauges and climate stations. In less populated regions like northern Canada, a short record of historical data and the sparsity of the data networks further impede successful development of forecasting models. The challenge in this case becomes one of trying to incorporate information from a variety of sources and measurement techniques. For example, snow water equivalent (SWE) data may be available from snow courses, snow pillows, climate stations and satellite image. It may not be practical to directly combine this data to estimate basin average SWE, but it may be possible to consider all of the data in the determination of a basin representative spring snowmelt runoff

index useful for breakup forecasting. In addition, for those communities prone to breakup ice jam floods, valuable historical breakup information can be obtained from technical flood reports and local newspaper reports. These raw data, either qualitative or quantitative, provide valuable information to investigate and develop forecasting models of river ice breakup. The goal of the research was to consider all relevant historical data by employing a new multi-layer modeling approach for forecasting river ice breakup.

As illustrated in Figure 2-1, the proposed approach is comprised of four layers: raw data, index variables, breakup indicators, and output variables. All of the pertinent historical information and archived raw hydro-meteorological data from different sources are collected in the first layer (e.g. historical breakup reports, air temperature, snowfall, water level, *etc.*). In Layer 2, index variables are either directly extracted (e.g. day of the onset of freezing and thaw) or calculated from the raw data (e.g. accumulated degree days of freezing and thaw). The resulting set of index variables are then tested for their potential as predictors for breakup severity and timing. The promising index variables are carried forward as input data to Layer 3, where various complex models are investigated to determine key breakup indicators (e.g. peak flow of snowmelt runoff or water level at the onset of breakup). For example, the index variables for basin SWE derived from various data sources (as discussed above) might be used as inputs to a model for the spring snowmelt runoff (a key breakup severity indicator). Soft computing techniques (e.g. fuzzy logic systems and artificial neural networks (ANNs)) are

ideally suited to the development of these breakup indicators. The predictions of the Layer 3 variables are finally used to project the timing of breakup (i.e. using the real time gauged water level) and the flood severity (i.e. using the established relationship between flood severity and peak flow during breakup) in Layer 4. A parallel approach is used to collate records for the output variables, i.e. the timing of breakup and flood severity, in Layer 4.

This chapter illustrates the development of the first two model layers (i.e. the collection of the raw data and development of the index variables) for the case study site at the Town of Hay River, NWT, a northern community frequently at risk of ice jam flooding during breakup. The development of the data set of the output variables in Layers 3 and 4 is also presented, as well as the results of the screening for key predictors of the output variables.

2.2 Study site and raw data collection

The Town of Hay River is located in the Hay River delta on the south shore of Great Slave Lake, Northwest Territories, Canada (see Figure 2-2). The Hay River experiences a highly dynamic breakup each spring (typically in late April or early May), which ultimately results one or more large ice runs approaching the community. Because Great Slave Lake does not melt out until early June, these ice runs can jam in the delta causing flooding at the Old Town and KFN Reserve along the East Channel and the Fishing Village along the West Channel (see the

inset in Figure 2-2). Several weeks advanced warning of the expected breakup severity would be valuable to the town for emergency preparedness planning. A timely and accurate prediction of the expected timing of the initiation of breakup near the town would also be extremely useful, since the subsequent breakup evolution can unfold within as little as 24 to 48 hours following the first cracking at the town site (Kovachis *et al.* 2010).

All of the available raw hydro-meteorological data and other records were assembled and processed to build the raw data set for this study. Meteorological stations run by Environment Canada (EC) and hydrometric gauges by Water Survey of Canada (WSC) provide the best readily available raw data in direct relation to river ice breakup. Specifically, in the Hay River basin, there are four active WSC streamflow gauges along the main stem. From upstream to downstream these are: the Chinchaga River near High Level (WSC station number: 07OC001), the Hay River near Meander River (WSC station number: 07OB003), the Hay River near ALTA/NWT Boundary (WSC station number: 07OB008) and the Hay River near Hay River (WSC station number: 07OB001). Water levels (instantaneous and daily) and stream flow data (daily) are collected and archived by WSC as well as ice thickness data from the field winter discharge measurements.

There are also several active meteorological stations in and near the Hay River basin (see Figure 2-2). The two most pertinent stations are: High Level A

(Meteorological Service of Canada Climate ID: 3073146), located near the Chinchaga River basin at High Level airport, Alberta; and Hay River A (Meteorological Service of Canada Climate ID: 2202400), located at the Hay River airport. Both stations are principal climate stations with daily forecast and archived hourly observations readily available in near-real-time from online climate data at the EC website[2]. The complete record of daily air temperature (including mean, maximum and minimum), precipitation (including rainfall, snowfall, and total precipitation) and snow-on-the-ground for these stations were obtained from National Climate Data Archive of Environment Canada[3].

There are also several other sources for winter snow water equivalent data. For example, Alberta Environment (AE for short, see River Forecast Section 2011) and the Aboriginal Affairs and Northern Development Canada (AANDC for short, see Water Resources Division 2011) operate snow courses. Also, volunteers from the Town of Hay River (THR) have conducted intermittent snow depth measurements during winter over many years. For the purpose of studying breakup, the snowpack condition in late winter (usually at the end of March or the beginning of April) is of most interest, since it has been found to be a very good indicator of the expected snowmelt runoff volume and peak (Zhao *et al.* 2009). The SWE data from the snow course surveys near the Hay River basin used in this study included: High Level (AE ID: 07JF801) and Assumption (AE ID: 07OA801); Hay River (AANDC ID: 07OB-SC02) and Swede Creek (AANDC

[2] http://climate.weatheroffice.gc.ca/climateData/canada_e.html
[3] Archived Canadian Daily Climate Data is accessible at ftp://arcdm20.tor.ec.gc.ca/pub/dist/CDCD/

ID: 07OB-SC03); and various locations in and around the Town of Hay River from THR volunteers.

Other available sources for the breakup information for this study were also collected including the technical reports, local newspaper reports on river breakup and flooding, and scientific studies by the river ice research group at the University of Alberta (UA) and AANDC. Specifically, Gerard and Stanley (1988) provided a detailed summary of historical breakup information on the Hay River; this database was then updated by Gerard *et al.* (1990), Jasek *et al.* (1993), Jasek (1993), and Kovachis *et al.* (2011). All of the qualitative data (i.e. descriptions of breakup flood severity) and quantitative data in these reports were used to define the breakup severity for the years between 1964 and 1993. For the years between 1994 and 2002, the reports from the newspaper at the Town of Hay River (HUB Publications Ltd 1994-2002) were only source of information regarding breakup severity. More recently, from 2003 to 2010, the breakup severity was determined based on direct observations by the UA river ice research group.

All the raw data mentioned above are provided via a data CD attached at the end of the thesis and the corresponding descriptions are presented in Appendix A.

2.3 Development of index variables

All of the raw data collected from the above sources were used to develop the index variables for this breakup study. Figure 2-3 presents the raw data (Layer 1) and index variables (Layer 2). These variables include the directly extracted water levels and the processed indices from the meteorological data. To facilitate the subsequent development of multiple breakup forecasting models, the index variables were divided into two subsets according to their availability for forecasting purposes: a long lead-time subset (e.g. variables known more than one week in advance of breakup) and a short lead-time subset (e.g. variables only obtained, or forecasted, a few days before breakup).

Based on the daily air temperature and water level data, three key dates related to river ice freeze-up and breakup were first defined. These dates were then used to define the other index variables as discussed below.

- D_{OT}: the date of the onset of thawing degree-days, considered as the time from which the ice cover decay and snowmelt starts. It is taken as the date of the first of five consecutive days of mean daily air temperatures above -5°C each year (so as to take into account the melting effect of maximum daily temperatures above freezing). This was found to be best choice to account for ice cover decay by Bilello (1980). If a cold spell of more than 5 days of below -5°C temperatures occurs, it is reset as the date when above -5°C air temperatures resume (again requiring 5 consecutive days).

- D_{OF}: the date of the onset of freezing used in the calculation of freezing degree-days. This is taken as the date of the first of five consecutive days of subzero daily air temperatures each year. If a warm spell of more than 5 days of above freezing temperatures occurs, it is reset as the date when the freezing air temperatures resume (again requiring 5 consecutive days). It is considered as the start of the winter snow accumulation and river freeze-up.
- D_{OR}: the date of the onset of water level rise due to spring snowmelt. This is defined as the day when the rate of rise first achieves a specified value (e.g. 5cm/day was used for the HRHR gauge).

2.3.1 Long lead-time variables

The following independent variables are known sufficiently in advance of breakup to be useful for a long lead-time forecast.

- *API*: the antecedent precipitation index. This is the accumulated precipitation during the previous summer (between July 1 and September 30). It is considered as an index of soil moisture that affects the spring snowmelt runoff process.
- H_{OF}: the water level on the date of the onset of freeze-up (D_{OF}), which gives a general idea of the required water level to initiate the breakup in spring. As a rule of thumb, the higher H_{OF} is, the greater the water level and snowmelt runoff required to initiate breakup. It is also an alternative

of API, considered as a surrogate of soil infiltration capacity during snowmelt period.

- $ADDF_W$: the accumulated degree-days of freezing for the winter period, defined as the sum of the negative degree-days for the winter period, which begins on D_{OF} and ends on D_{OT}. This is considered as an index of the winter severity and late winter ice cover condition.
- SWE variables: These are considered an important index of expected spring snowmelt runoff, which in turn affects the breakup process directly. Also SWE influences the ice cover decay potential during pre-breakup. The higher the depth of snow cover, the slower the ice cover decay.
    - AP_w: the accumulated winter snowfall (measured at climate stations using a Nipher shielded standard snow gauge), defined as the sum of the precipitation during the winter period (between D_{OF} and D_{OT}).
    - SWE_{SC}: the SWE measured during the late winter snow course surveys (usually at the end of March or the beginning of April).
    - SNG_{OT}: the depth of snow on the ground (reported at climate stations), taken on the day of the onset of thaw (D_{OT}).
- Ice variables: The thickness and strength of the late winter ice cover also affects the breakup severity and timing. In this study, late winter ice thickness data were obtained from the records of direct winter discharge measurement by WSC. In these records, the date of the measurement of ice thickness (D_i) could be either before or after the onset of thaw (D_{OT}).

If D_i is prior to D_{OT}, the ice thickness from the measurement can be a good estimate of the ice thickness at the onset of thaw, D_{OT}, since there is usually not much ice growth during the last week or two of winter. On the other hand, the ice cover deterioration must be considered if D_i is measured after the onset of thaw, D_{OT}. The following two index variables are defined from these records.

  - t_i: the ice thickness from the last direct measurement by WSC each winter (usually conducted in mid-April).
  - *DECAY:* an index variable to account for potential ice decay when D_i is after D_{OT}: If D_i is 7 or more days after D_{OT}, *DECAY* is set to 1; otherwise *DECAY* is set to 0. The choice of 7 days is based on the estimated time required for the ice cover to become isothermal before starting to decay.

- H_{OR}*:* the water level on the day of onset of rise *(*D_{OR}*)*. This indicates the ice level at late winter.

2.3.2 Short lead-time variables

The following variables are defined using the daily meteorological data during the pre-breakup period.

- $ADDT_{-5}$: the accumulated degree-days of thaw during the pre-breakup period, referred to a base air temperature of -5°C and calculated from the onset of thawing degree-days (D_{OT}) up to the day of breakup (D_{FC}, as

defined in the following section). It is considered as an index of the accumulated heat input to the ice cover which decreases ice thickness and/or ice strength during the pre-breakup period.

- $ADDF_{-5}$: the accumulated degree-days of freezing (referred to a base air temperature of -5°C) during the pre-breakup period (i.e. between D_{OT} and D_{FC}). This accounts for the occurrence of a cold spell (i.e. mean daily air temperature is below -5°C) after the onset of thaw, which would be expected to delay ice cover deterioration.
- RN_{PB}: the accumulated rainfall during the pre-breakup period, which would be expected to enhance the rate of snowmelt runoff and accelerate ice cover deterioration.
- SN_{PB}: the accumulated snowfall during the pre-breakup period. Because of its high albedo, snowfall during the pre-breakup period tends to delay snowmelt runoff and ice cover deterioration.
- AR_S: the accumulated rainfall during the spring snowmelt period (i.e. from the onset of thawing degree-days, D_{OT}, to the day just before the peak flow at HRHR). This is considered as a positive impact to the peak snowmelt runoff.
- AS_S: the accumulated snowfall during the spring snowmelt period. This is considered as another factor that would affect the peak snowmelt runoff. It could either increase the peak flow rate by additional amount of snowmelt or decrease the peak by reducing the snowmelt rate.

2.4 Development of output variables

Figure 2-4 presents the output variables (Layer 4) that were defined using the raw data in the case of Hay River breakup study. These were grouped into two subsets: one for breakup severity and the other for breakup timing.

2.4.1 Breakup severity

This refers to the flood severity resulting from ice jams during breakup. For the case of the Town of Hay River, a quantitative variable (e.g. a flood water level at a specific location) is difficult to establish because of the variety of flood prone areas in the Hay River delta and the lack of a comprehensive water level record for each. Fortunately, considerable qualitative information on breakup flood severity is available from historical flood descriptions in technical reports, personal accounts and newspapers articles.

- *BS*: the qualitative descriptor for breakup severity at the town. It has three possible values: ‘severe flooding, ‘some flooding’, and ‘no flooding’. ‘Severe flooding’ applies to major floods in which the flood extent and damage to property were extensive, as explicitly described in historical/technical reports and newspaper accounts. ‘Some flooding’ applies to those events when minor or moderate flooding was documented, though insufficient information is available to distinguish between the two.

Typically for these events vulnerable areas (e.g. the government dock, as well as businesses and residences closest to the river) were flooded to some extent and people were evacuated as a precaution. 'No flooding' refers to those events described as 'quiet' and unnoticeable in the newspaper accounts or field notes.

The period of record for this investigation was limited to between 1964 and 2010. Although some variables are known prior to that, and in particular, it is known that the most severe flood on record occurred in 1963, the HRHR gauge was only installed in 1964. Since that data is critical to the forecasting effort (particularly in terms of the output variables), its period of operation is the constraining factor in this analysis.

2.4.2 Breakup timing

In this study, the initiation of breakup was defined as the first evidence of transverse cracking near the HRHR gauge site. The following variables were first determined using the historical hydrometric data.

- H_{FC}: the water level at which cracking first occurs. It was determined by identifying the first spike in the historical instantaneous water level hydrographs and confirmed as applicable using direct observations in 2005, and 2007 to 2010.

- D_{FC}: the date corresponding to H_{FC}. When H_{FC} comes before the noon of the day, D_{FC} is set as the previous day. Otherwise, D_{FC} is the day when the H_{FC} occurs. This definition was chosen to facilitate more realistic correspondence with those index variables represented by mean daily values.

From the perspective of practical forecasting, the variable D_{FC} is using the date format and not a common choice for developing forecasting models. Since the rise of water level in the snowmelt season is the most direct driving force initiating the breakup, it is practical to use the onset of rise of water level as the starting point to define the output variable ΔD_{FC}.

- ΔD_{FC}: the length of the duration required from the onset of rise of water level (D_{OR}) to the day of first cracking (D_{FC}).

Another more direct way to define the timing of breakup at the Town of Hay River is the day of the first push:

- D_B: the day of the first push of ice at the town site. They were obtained from historical breakup reports and newspaper accounts (prior to 2003) and recent field work (from 2004 to 2011).

Similar to the forecasting of the first crack, D_B is not a feasible variable to use in operational forecasting directly. The alternative output variable was calculated:

- ΔD_B: the number of days until breakup, D_B, from the onset of water level rise at the HRHR gauge (D_{OR}).

2.5 Screening of predictors to the output variables

Generally, the severity of breakup is controlled by the magnitude of snowmelt runoff and ice cover competence prior to breakup, while the timing of breakup is more related to weather conditions during the pre-breakup period. Thus it is more feasible to develop a long lead-time forecasting model for breakup severity than for breakup timing. Late winter ice cover conditions can be related to freeze-up water level and winter severity. Spring snowmelt runoff can be predicted based on the late winter SWE and antecedent soil moisture, though incident rainfall during breakup may accelerate the snowmelt runoff process. In this study, the long lead-time index variables were first tested to assess their potential as direct predictors of breakup severity, *BS*. However, it was found that none of these index variables were strongly indicative of *BS* (see Appendix B for details). Nevertheless, there were some qualitative tendencies demonstrated as discussed below.

It appears that flooding events are associated with higher freeze-up levels, H_{OF}. As shown by Figure 2-5(a), when H_{OF} is above 2.8 m, the probability of flooding is high, with some or severe flooding occurring in 7 of 10 cases. The three exceptions (1998, 1993 and 1977) were associated with low snowmelt runoff events, specifically: 390, 159 m^3/s and 530 m^3/s, respectively, all of which are

below the average snowmelt runoff peak flow of 638 m^3/s. Flooding occurred in only 3 (18%) of the 17 years for which the freeze-up level, H_{OF} was below 2.1 m, and none of these events were significant in severity. These findings are consistent with the logic of breakup severity forecasting discussed by Beltaos (1995).

- When H_{OF} is low: neither low nor high snowmelt runoff would be expected to induce severe flooding.
- When H_{OF} is high: a low snowmelt runoff would be more likely to result in a thermal breakup (no flooding), and a high snowmelt runoff would be expected to induce severe flooding.

Thus, these findings will be very useful in developing the 'IF-THEN' rule base and fuzzy sets for the final fuzzy logic model to predict breakup severity.

A competent and thick ice cover is typically considered necessary for any significant breakup event. Therefore, the ice variables (t_i and *DECAY*) at the HRHR gauge were also assessed for their potential as predictors of breakup severity. The results are shown in Figure 2-5(b), where the letter 'Y' indicates that some ice decay occurred prior to breakup. As the figure illustrates, there is no clear pattern. Two examples are 1977 and 2008: in 1977, the index ice thickness was relatively high (1.2 m) yet no flooding occurred; in 2008, the index ice thickness was 0.6 m (below the average of 0.7 m), yet severe flooding occurred. There also appears to be no particular trend towards lower breakup severity for those years in which decay was thought to have occurred prior to breakup.

Figure 2-5(c) shows the freezing degree-days, $ADDF_W$, at the Hay River Airport, coded by breakup severity. It appears that most of the severe flooding events are associated with a higher $ADDF_W$: 7 of the 8 years (88%) with severe flooding have $ADDF_W$ exceeding the threshold 2900. Considering that $ADDF_W$ is as an index of the winter severity and late winter ice cover condition, it makes sense that higher $ADDF_W$ may be indicative of a severe breakup. However, this indication is very weak: non-flooding events occurred as many times as flooding events when $ADDF_W$ exceeded this value. This suggests that the initial ice cover condition prior to deterioration plays a minor role in the case of Hay River breakup.

It was also found that neither the *API* or SWE index variables were indicative of breakup severity, as exemplified by Figure 2-5(d) for the *API* at Hay River A station and Figure 2-5(e) for the SWE_W at the High Level snow course. This result implies that none of these variables are individually sufficiently representative of the late winter snowpack condition and runoff potential in the Hay River basin. This illustrates the need for the multi-layer modeling approach; their effects will be combined to facilitate inclusion of all SWE data sources and API in a Layer 3 breakup indicator.

Based on the above results, the potential predictors for a long lead-time forecasting model of breakup severity include H_{OF}, $ADDF_W$, and a combination of

the *API* and SWE variables to indicate the expected magnitude of snowmelt runoff, i.e. the breakup indicator in Layer 3. This will be discussed in details in Chapter 4.

For the prediction of breakup timing, the most important factors are the rise of water level and the extent of ice cover decay. Thus practically, two other variables could be used indirectly as indicators of the timing of breakup:

- ΔH_{FC}: the amount of water level rise required from the onset of rise of water level (H_{OR}) to the first cracking (H_{FC}). This is used in most of the literature (e.g. see Beltaos 2008). It can be evaluated by using the real time hydrographs at WSC gauges.
- $ADDT_{FC}$: the amount of the degree-days of thaw ($ADDT_{-5}$) required from the onset of thaw (D_{OT}) to the day of first cracking (D_{FC}). This provides an indirect prediction of breakup timing in terms of heat input to the ice cover required to initiate the breakup, with degree-days of thaw providing an index of this heat input. It can be evaluated several days in advance using readily available weather forecasts from EC.

Forecasting the timing of breakup is more complex than forecasting the severity, because timing is more affected by the weather conditions during the pre-breakup period. Simple analyses were conducted to screen the predictors for the output variables for the prediction of breakup timing. When the available data were plotted for the index variables against each of the output variables, a large degree

of scatter was seen. For example, simple linear correlations between some of the index variables and the output variable, ΔH_{FC}, are shown in Figure 2-6. The very small coefficients of determination (R^2 values) (see Figure 2-6(a)-(f)) mean that none of the input variables are significantly linearly correlated with the output variable. Also, there is no obvious pattern between ΔH_{FC} and DECAY (see Figure 2-7). This implies that the relationships between the index variables and the output variable are nonlinear. In Chapter 3, the ANN modeling approach is investigated to assess its applicability to this nonlinear problem.

2.6 Summary

This chapter introduces a new multi-layer modeling approach for the river ice breakup forecasting problem. The results of the first two layers of the approach are presented: the collection of all raw historical and hydrometeorological data and development of index variables. The detailed process for constructing the index variables from the raw data is described and demonstrated for the case of Hay River, NWT. The potential predictors of breakup severity were also identified for the case study site, the Town of Hay River, such as the water level at the onset of freeze-up and the accumulated degree-days of freezing during winter. The antecedent precipitation index and the SWE variables are to be combined as an indicator for the magnitude of snowmelt runoff, which will be discussed in Chapter 4 as the important indicator of breakup flood severity. In practice, these variables could be determined well in advance of breakup, thus can

be used for a long lead-time forecast of breakup severity. The nonlinearity of the timing of breakup was also discussed and the applicability of ANN modeling technique will be investigated in Chapter 3.

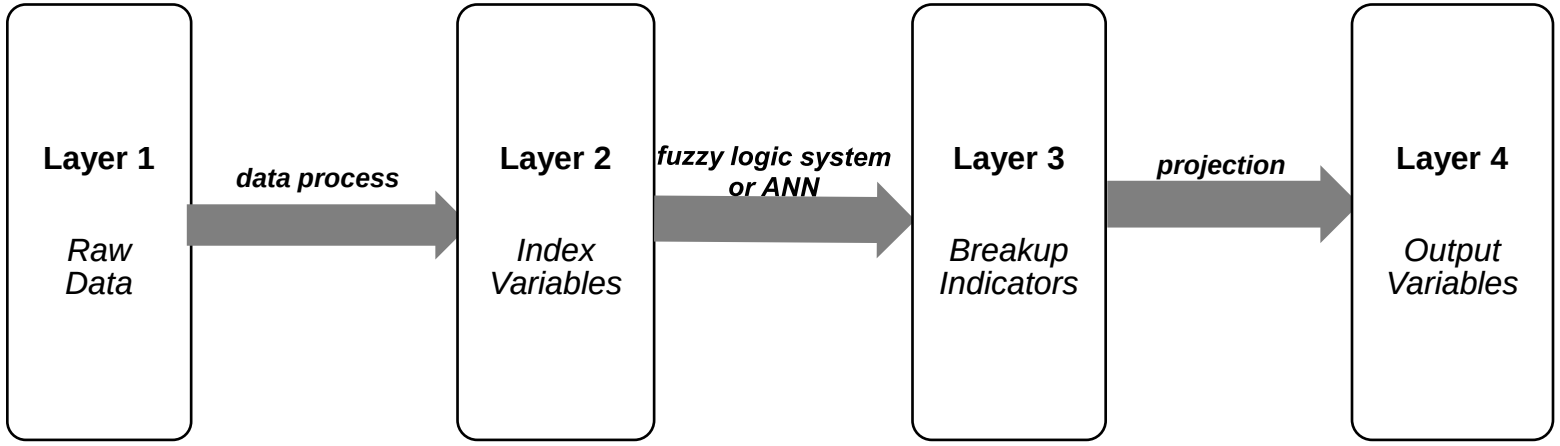

Figure 2–1: Proposed multi-layer modeling approach for river ice breakup forecasting.

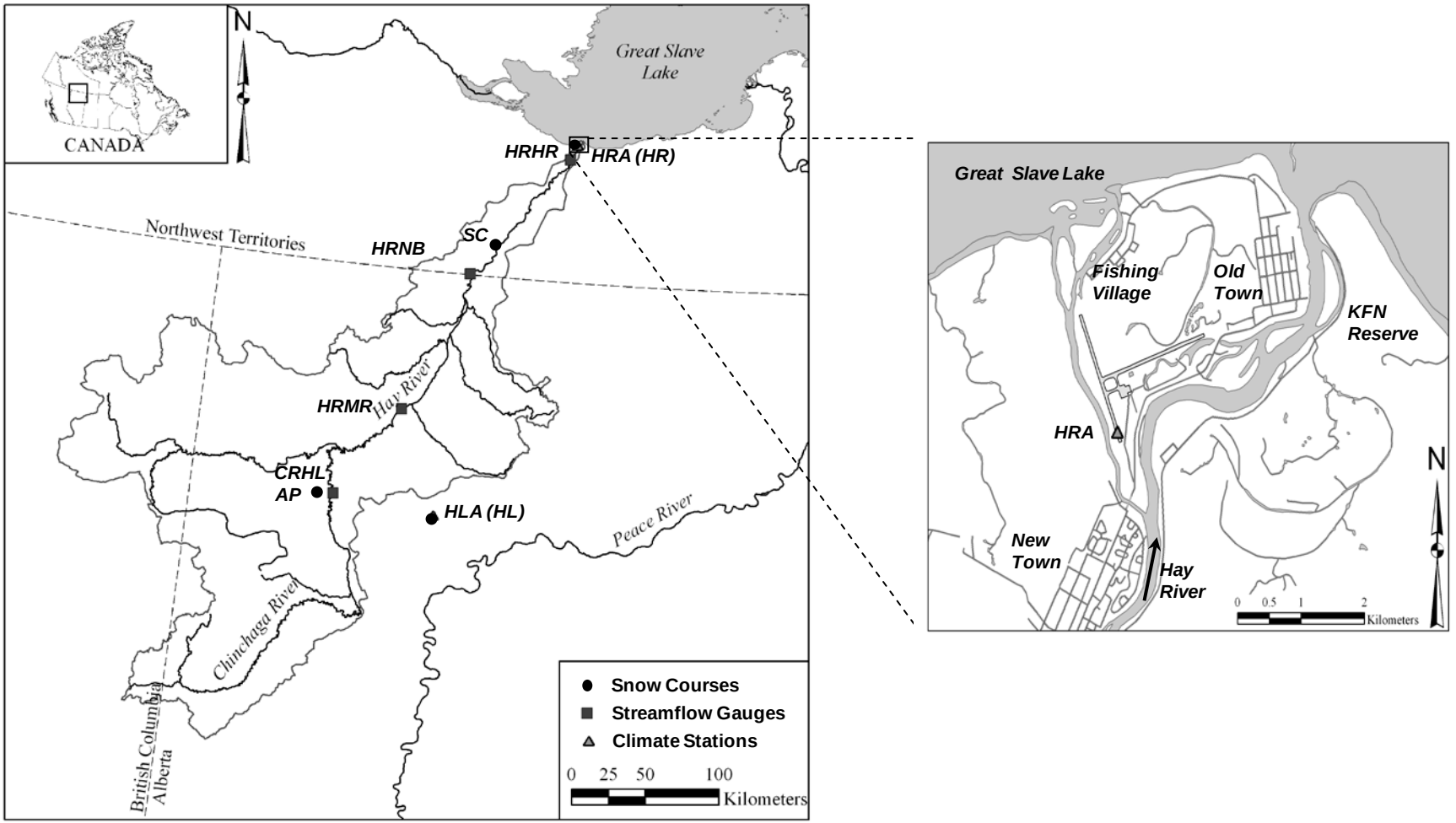

Figure 2–2: Location of the Hay River basin and map of the Town of Hay River.

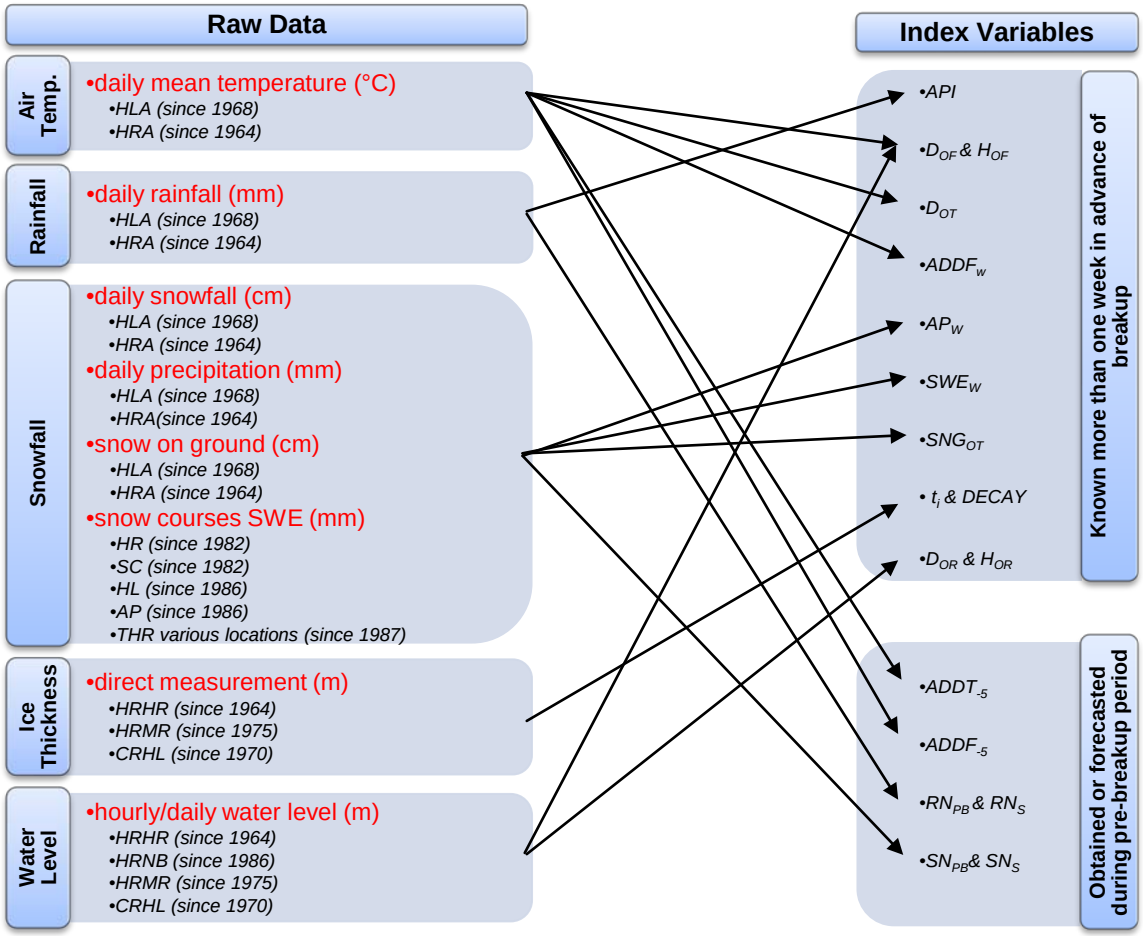

Figure 2–3: Layers 1 and 2 in the Hay River breakup forecasting model.

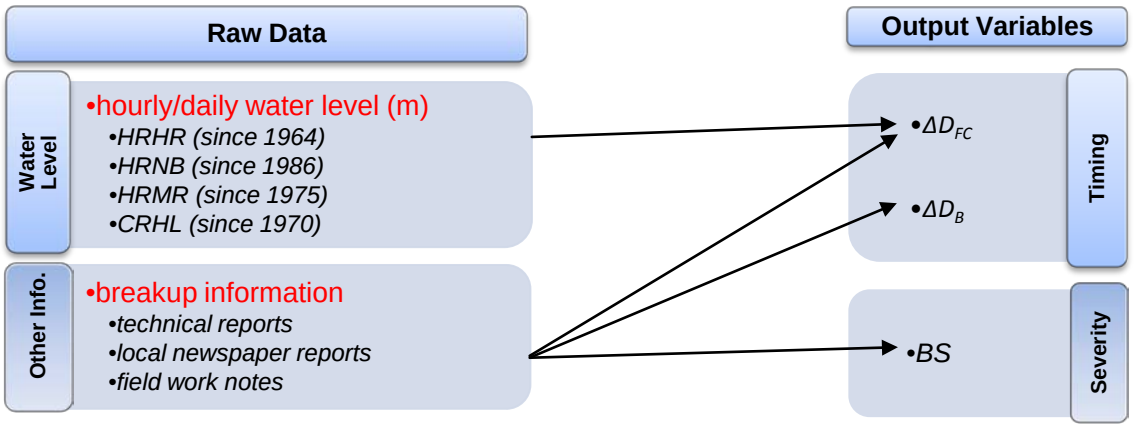

Figure 2–4: The output variables in Layer 4 for the Hay River breakup study.

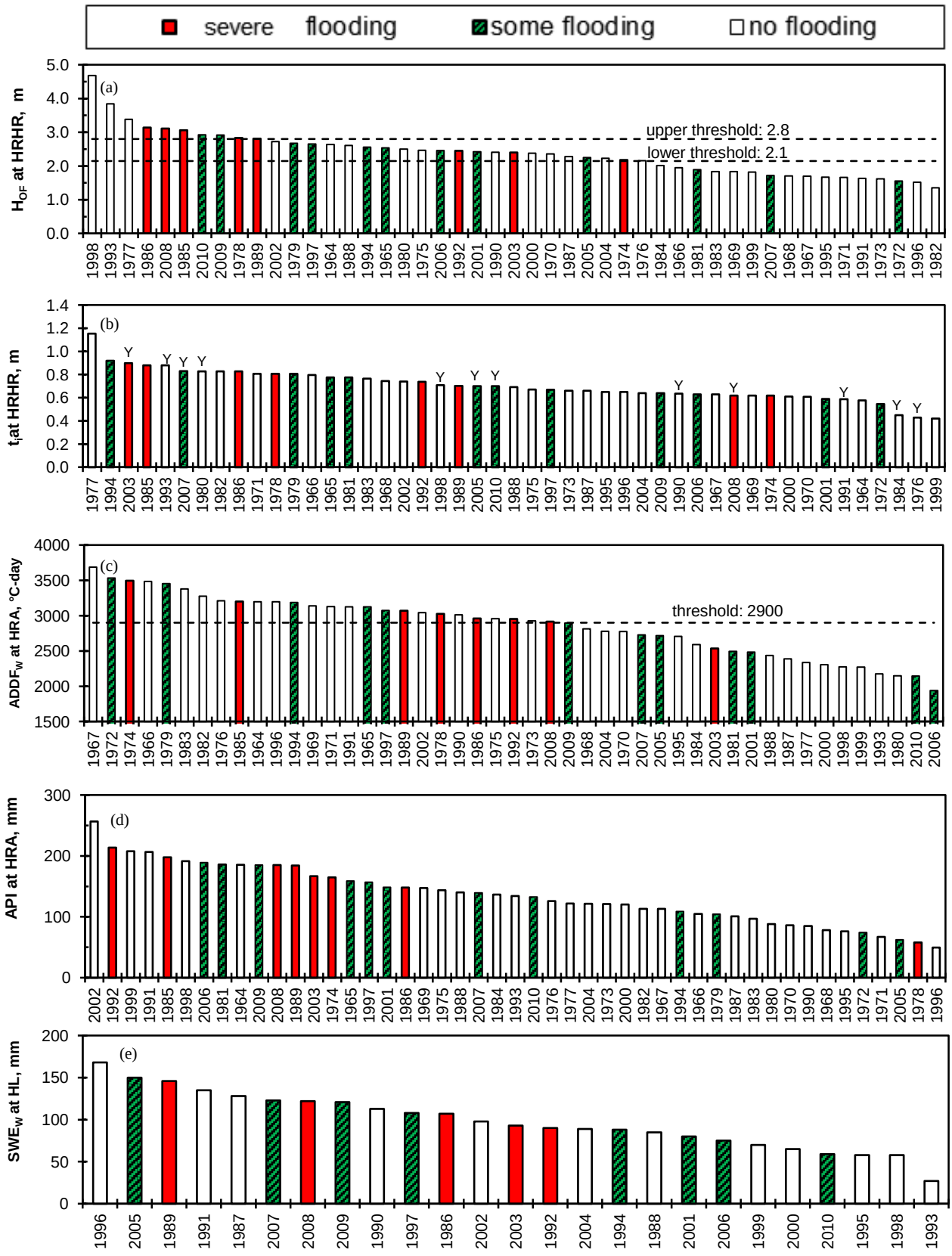

Figure 2–5: Potential predictors for breakup severity at the Town of Hay River. Note: the letter 'Y' in (b) indicates that some ice decay occurred prior to breakup.

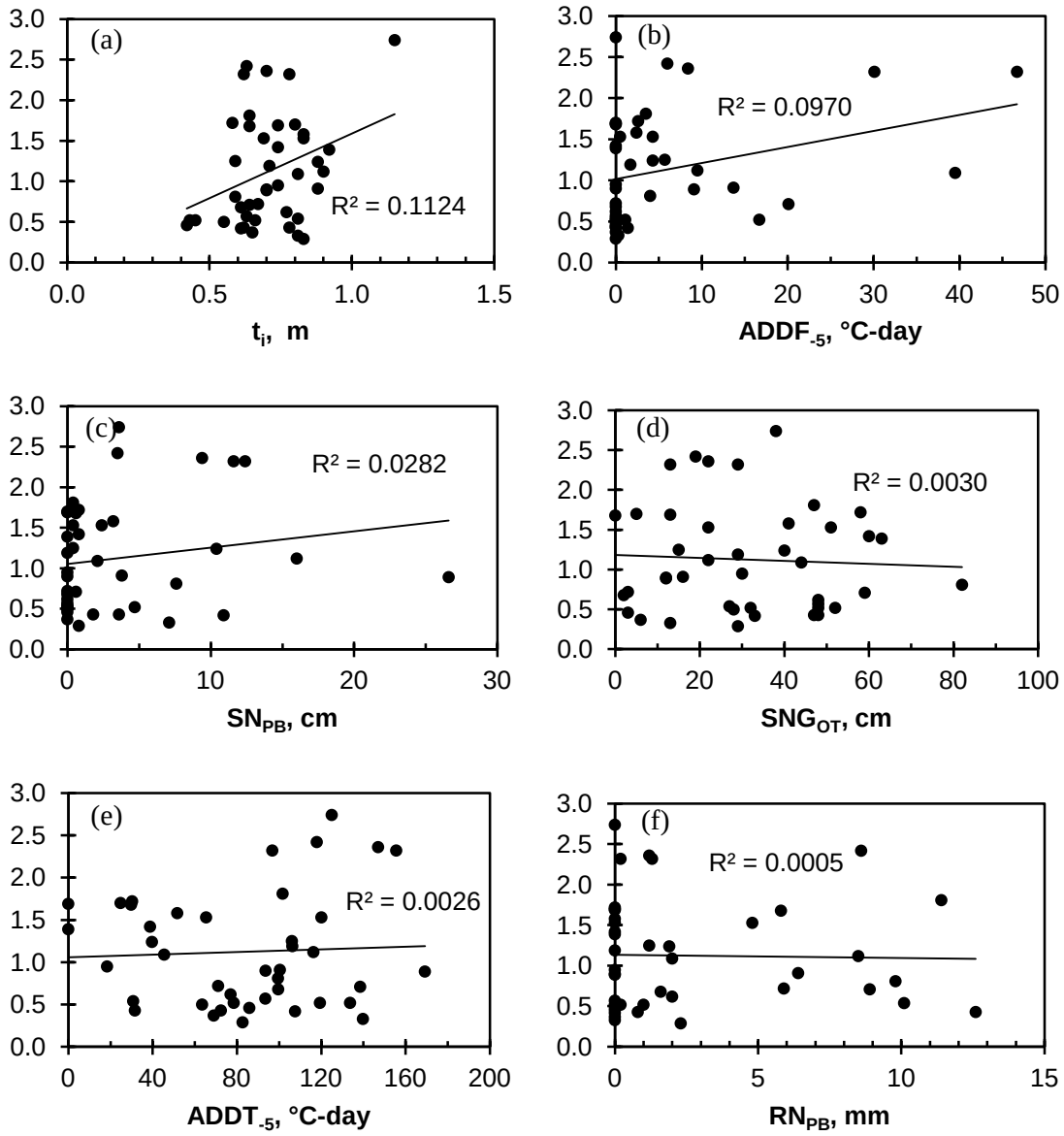

Figure 2–6: Simple correlations between the index variables (x axis) and ΔH_{FC} (y axis). Note the sample size is 42 for all the cases.

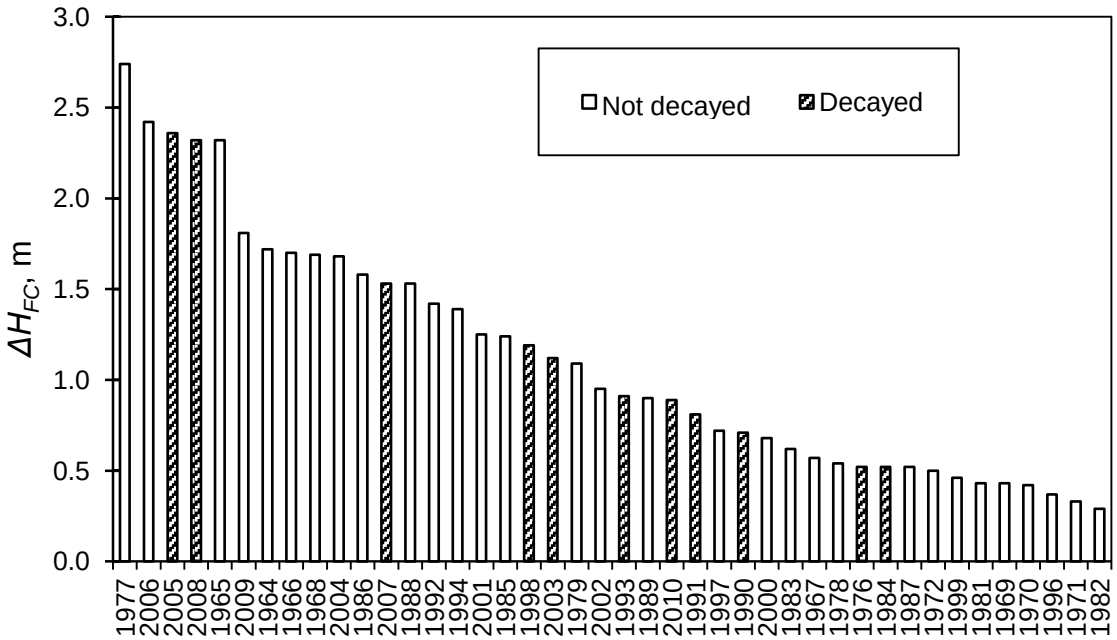

Figure 2–7: Required water level rise (ΔH_{FC}) coded with the extent of ice cover decay.

2.7 List of references

Beltaos, S. (Ed.) 2008. River ice breakup. Water Resources Publications, LLC, Highlands Ranch, Colo.

Beltaos, S. 1995. Breakup forecasting. Proceedings of the 8th Workshop on River Ice Winter Environments of Regulated River, Kamloops, British Columbia, 463-482.

Bilello, M.A., 1980. Maximum thickness and subsequent decay of lake, river and fast sea ice in Canada and Alaska. U.S. Army Cold Regions Research and Engineering Laboratory, Report 80-6, Hanover, NH, 165 pp.

Gerard R. and S. Stanley. 1988. Ice jams and flood forecasting, Hay River, NWT. Water Resources Engineering Report No. 88-6, Dept of Civil Engineering, University of Alberta, Edmonton, Canada.

Gerard, R. and Jasek, M. 1990. Break-up observations and ice jam flood forecast algorithm evaluation, Hay River, N.W.T., 1989. Water Resources Engineering Report 90-3, Dept of Civil and Environmental Engineering, University of Alberta, Edmonton, Canada.

Gerard, R., Hicks, F. and Jasek, F. 1990. Ice jams and flood forecasting, Hay River, N.W.T. - Phase 2: surges and interactive computer program. Prepared for Environment Canada and Indian and Northern Affairs Canada, Yellowknife, N.W.T.

HUB Publications Ltd. 1994-2002. HUB. The newspaper for the Town of Hay River.

Jasek, M. 1993. Hay River Flood Control: Hay River, N.W.T.. The Town of Hay River, N.W.T.

Jasek, M, Stanley, S., and Gerard, R. 1993. Update of Ice Jam Flood Database, Hay River, N.W.T.. Indian and Northern Affairs Canada, Yellowknife, N.W.T.

Kovachis, N., Hicks, F., Zhao, L. and Maxwell, J. 2010. Development of an expert system for forecasting the progression of breakup at Hay River, NWT, Canada. Proceedings of the 20th IAHR International Symposium on Ice, Lahti, Finland, June 14 to 18, 2010. 12pp.

Kovachis, N., Zhao, L. and Hicks, F. 2011. A summary of historical records of Hay River breakup, 1894 to 2011. Water Resources Engineering Report 2011_FH_01, University of Alberta, Edmonton.

Kowalczyk Hutchison, T. and Hicks, F. 2007. Observations of Ice Jam Release Events on the Athabasca River, AB. Canadian Journal of Civil Engineering, 34(4): 473-484.

River Forecast Section. 2011. Plains Snow Course Results as of Apr 1 2011. Water Management Operations Branch, Alberta Environment (AE). Data URL: http://www.environment.alberta.ca/forecasting/data/snow/apr2011/plains_highlevel.pdf.

Water Resources Division. 2011. Snow Survey Data. Renewable Resources and Environment, Aboriginal Affairs and Northern Development Canada (AANDC). Data URL: http://www.aadnc-aandc.gc.ca/eng/1100100027479.

White, K.D. 2003. Review of prediction methods for breakup ice jams. Canadian Journal of Civil Engineering, 30(1): 89-100.

Zhao, L., Hicks, F., and Robinson Fayek, A. 2009. Long lead forecasting of peak flow during breakup using fuzzy logic. Proceedings of 15th Workshop on River Ice. 15-17 Jun 2009, CGU - Hydrology Section, Comm. on River Ice Processes and the Env. , St. John's, NL, Canada. pp. 300-315.

Zhao, L., Hicks, F., Robinson Fayek, A. and Kovachis, N. 2010. Forecasting the onset of breakup using artificial neural networks. Proceedings of the 20th

IAHR International Symposium on Ice, Lahti, Finland, June 14-18, 2010, 11pp.

Chapter 3 Applicability of multilayer feed-forward neural networks to model the onset of river ice breakup[4]

3.1 Introduction

The occurrence of ice jams during river breakup presents a significant flood risk to many northern communities and, for those communities faced with this annual threat, predicting the onset of breakup can be extremely valuable in flood preparedness planning. However, the complexity of the problem, combined with our limited ability to forecast many of the relevant hydrometeorological factors driving the river ice breakup process, makes this a particularly challenging problem. Nowhere is this more evident than in remote northern communities (e.g. in the Northwest Territories of Canada), where the data is sparse and historical records are generally limited.

Forecasting river ice breakup has been the focus of intense research over the past few decades. Beltaos (2008) provides an excellent review of the state of knowledge of breakup processes and related phenomena. Although a few researchers have employed deterministic methods based on the dynamics of the ice cover deflection and fracture caused by water waves (e.g. see Shulyakovskiy

[4] A version of this chapter has been published as a journal paper: Zhao, L, F Hicks and A Robinson Fayek (2012) "Applicability of multi-layer feed-forward neural networks to model the onset of river breakup", Journal of Cold Regions Science and Technology,70:32-42.. It has been slightly revised here to accommodate revisions required by the thesis committee.

1972; Billfalk 1981; Daly 1995; Beltaos 1990 and 2004; Nzokou *et al.* 2009), due to the complexity of the problem and the logistical difficulties in measuring many aspects of the phenomenon, site specific empirical methods still predominate (e.g. see White 2003). This is particularly true with respect to predicting the onset of breakup, as the properties of the ice cover at the onset of breakup can be difficult to measure in the field, due to safety concerns. Semi-empirical methods, such as the boundary constraint criterion (Beltaos 1997), have also been developed for considering the actual mechanisms influencing the onset of breakup. These employ physical information (e.g. channel geometry and ice competence) to incorporate more deterministic effects and have the advantage of being more physically rigorous. However, the data requirements for these methods are necessarily more extensive.

Recent studies have investigated the practical application of artificial intelligence techniques to the field of civil engineering, and the application of artificial neural network (ANN) techniques is one of the most commonly used approaches (e.g. see Flood and Kartam 1994a and 1994b; ASCE 2000a and 2000b; Dawson and Wilby 2001; Maier and Dandy 2000; Maier *et al.* 2010). ANNs self-learning capabilities enable them to represent the inherent relationship between the input and output variables, without the need for a priori knowledge about the nature of the relationship. This special advantage over other techniques makes it very suitable for complex nonlinear problems which cannot yet be solved analytically.

A number of researchers have successfully employed ANNs for various river ice applications: for example, Seidou *et al.* (2006) and Chokmani *et al.* (2007) illustrated the viability of using ANNs to estimate lake and river ice thickness growth; Massie *et al.* (2002) developed an ANN to produce a daily forecast of jam/no jam with improved accuracy over statistical and empirical methods; and Chen and Ji (2005) and Hu *et al.* (2008) employed ANNs in attempting to predict the timing of breakup on the Yellow River, China with moderate success. Mahabir *et al.* (2006) developed a neuro-fuzzy model for river ice breakup forecasting in which the rule base was trained using ANNs. Their model was found to perform much better than a multiple linear regression (MLR) model for the same site, while using fewer input variables and providing a longer lead-time forecast. These earlier investigations have illustrated the potential applicability of ANNs for forecasting the complex and nonlinear river ice breakup problem.

The objective of this study was to investigate the practical applicability of ANN modeling to forecast the timing of river ice breakup particularly in the context of limited data, as is typical in less populated northern regions and to illustrate their correct implementation and validation for this problem. To achieve this, a three-layer feed-forward ANN model was developed to forecast the onset of river ice breakup using variables extracted from the readily available hydro-meteorological data record for the demonstration site at the Town of Hay River, NWT Canada. This Chapter first provides descriptions of the study site and data sources along with details of the process employed to determine the input and output variables.

This is followed by details of the ANN model development, calibration and validation. Comparisons of model performance to results obtained using the more conventional MLR modeling approach are also presented and discussed. Finally, recommendations for future study are presented.

3.2 Study site and data sources

The test site for this investigation was the Town of Hay River, which is located at the mouth of the Hay River on the south shore of Great Slave Lake, NWT, Canada (Figure 3-1). The north flowing nature of the river means that spring snowmelt runoff in the upper basin makes its way downstream into strong competent ice. This, combined with steep gradients along the river (including two waterfalls, 33 m and 15 m high, respectively), leads to a highly dynamic breakup in most years, with a cascade of ice jam formation and release events progressing down the Hay River. The resulting ice runs eventually reach the Town of Hay River where the ice cover on Great Slave Lake obstructs their further passage. As a result, the town is prone to severe ice jamming and consequent flooding during spring breakup.

University of Alberta researchers have been monitoring breakup at this site and assisting in the flood forecasting efforts since 2004. A timely and accurate prediction of the initiation of breakup near the town is extremely desirable from an emergency preparedness perspective, since the subsequent breakup evolution

can unfold quite rapidly. For example, the peak stage at the town has followed the first transverse cracking within zero to two days in 23 of the 38 cases documented since 1933, and within 6 days in all but one of the remaining documented cases (Kovachis 2011). Thus, prediction of the initiation of breakup local to the Town of Hay River was the key focus of this study.

As is typical of northern Canada, there is only a sparse network of hydrometric gauges and climatic stations in the Hay River basin (see Figure 3-1). The two stations in closest proximity to the town were chosen for use in this study, specifically: the Water Survey of Canada (WSC) streamflow gauge 07OB001, Hay River near Hay River (HRHR), which is located about 10 km upstream of the town site (Figure 3-1(a)) and Environment Canada's (EC) climate station 2202400, which is situated at the Hay River airport (Figure 3-1(b)). The WSC HRHR gauge has the longest hydrometric record of all the gauges on the Hay River (1963 to present). For this study, instantaneous and daily water level data were supplied by WSC, as well as ice thickness data from winter discharge measurements. The EC station at the Hay River airport is a principal climate station with hourly observations available in near-real-time. This station provides the longest record of meteorological data in the Hay River basin area. The historical daily air temperature (e.g. mean, maximum and minimum), precipitation (rainfall, snowfall, and total precipitation) and snow-on-the-ground records from year 1964 to 2007 were obtained from National Climate Data Archive of Environment Canada. Data after 2007 were available from their website

(http://climate.weatheroffice.gc.ca/climateData/canada_e.html). These raw hydro-meteorological data records were accessed and processed to build the data set for this study.

3.3 Determination of input and output variables

A practical definition of the onset of breakup was introduced by Shulyakovskiy (1963) and adopted by Beltaos (1997) as *"the time when the first sustained movement of the winter ice cover takes place"*. Unfortunately, this definition was not practical for the Hay River case because of the rapidity at which the breakup unfolds: once this sustained movement occurs, flooding can ensue within as little as one to two hours. Therefore, for the purposes of this study, the onset of breakup was defined as the first evidence of transverse cracking near the WSC HRHR gauge site. In a manner similar to earlier researchers (e.g. Shulyakovskii 1963 and Beltaos 1997), the forecast is achieved by predicting the expected rise of water level associated with the onset of cracking, ΔH. The expected timing is then determined based on the real time water level data, by projecting the rate of rise of the water level hydrograph.

Considering all of the available hydro-meteorological data presented in the last section and from a physical point of view, the two categories of factors controlling the water level associated with the first cracking are:

- driving forces: the heat input into the ice cover that decreases ice thickness and/or strength; and
- resisting forces: the competence (or strength) of the ice cover.

In this study, the following one output and seven input variables can be extracted from the developed data set to describe these processes.

3.3.1 Rise of water level at the onset of breakup, ΔH

As noted above, the rise of water level at the onset of breakup, ΔH, is the primary output parameter (dependent variable) of the forecasting model. To facilitate the model development, ΔH was defined as the difference between the water level at the onset of rise of spring runoff, H_{OR}, and the water level at the onset of breakup (i.e. at the time of the first transverse crack), H_{FC}, both of which were extracted from the measured data at the WSC gauge site (i.e. from the actual strip charts for 1964 to 1996 and from the continuous electronic water level data for 1997 to 2010).

Based on direct observations from 2005 to 2010 (excluding 2006), it has been determined that fluctuations in the WSC water level record provide a consistent indication of the shifting of ice sheets associated with the development of the first transverse cracks at the gauge site. Figure 3-2 illustrates this using two examples from the data record for which actual observations are available (2005 and 2008). As the figures illustrate, this initial transverse cracking tends to be associated with

the slope break in the water level hydrograph that is followed by a water level drop. Thus, for those years where no direct visual observations were available, the water level associated with the first crack, H_{FC}, was identified from the WSC gauge records as the first slope break preceding a water level drop in the measured instantaneous water level hydrograph. No water level data were available during breakup in 1973, 1974, 1975, 1980 and 1995, leaving a total of $N = 42$ years of record between 1964 and 2010. The corresponding date on which H_{FC} occurred was also documented as a variable: D_{FC}. In cases where H_{FC} occurred before noon, D_{FC} was set as the previous date; otherwise, D_{FC} was assigned the date on which H_{FC} occurred. This definition was chosen to facilitate more realistic correspondence with those independent variables represented by mean daily values (as discussed further below).

For this study, H_{OR}, the observed water level just prior to the arrival of the spring runoff wave, provided an index of the actual pre-breakup flow. This measured stage was used (as opposed to the discharge deduced from this measured stage) because the WSC discharge data are not immediately available to facilitate real-time forecasting. H_{OR} also represents the base level that must be exceeded by some incremental rise, ΔH, before the ice can crack and thus shift a small amount, causing a slope break in the local water level hydrograph. In this context then, H_{FC} (which is equal to $H_{OR} + \Delta H$) is slightly analogous to the threshold water level "*that must be exceeded in the spring before the ice is detached from the banks and other river boundary supports"* (Beltaos 1997). Some earlier

researchers have found the freeze-up stage, H_F, directly represents the threshold water level that must be exceeded for the ice cover to detach and move; others have found that the freeze-up stage must be exceeded by some incremental rise for the ice to detach and move (e.g. Hicks et al., 1995). In this study, the freeze-up stage was not found to be a useful representation of either, possibly because the objective here was to predict the stage associated with first cracking, not to predict the threshold stage for detachment and sustained movement of the ice. In particular, it was found that freeze-up stage values extracted from the instantaneous water level data for this site exhibited no correlation with the observed stage at first cracking, H_{FC}. In fact, in many cases the observed freeze-up stage was higher than H_{FC}. This makes physical sense if the freeze-up stage is indicative of the threshold stage for sustained ice movement, since first cracking occurs prior to sustained ice movement and thus should occur at a lower stage. However, it also means that the freeze-up stage was not of any practical value for predicting the first transverse crack.

H_{OR} was also extracted from the WSC HRHR gauge record. However, in this case, daily water level data were found to be more useful than instantaneous data. Based on an examination of the gauge records, it was found that H_{OR} could most reliably be identified by taking it as the mean daily water level on the first day that the rate of water level rise attains 5cm/day and continues to increase afterwards. Specifically, in examining the actual data record, it was found that variations in water level less than 5 cm could be spurious fluctuations. For real-time

forecasting purposes, it has also been determined that the mean daily water level can reasonably be approximated by the observed value at noon, since the water level is rising gradually in the pre-breakup period. Figure 3-2 illustrates the H_{OR} values determined for the two example cases, 2005 and 2008.

Figure 3-3 shows the resulting dependent variable ΔH (=H_{FC} - H_{OR}) in descending order, color coded according to breakup flood severity at the Town of Hay River. Although there is no definitive threshold relationship between ΔH and breakup flood severity, it appears that severe flood events are more likely to occur when ΔH exceeds about 0.7m, for which 16 of 26 (61% of) events involved flooding. This includes 6 of the 7 documented severe flood events and 10 of the 12 cases in which some flooding occurred. For ΔH less than 0.7m, only 3 of 16 (19% of) events involved flooding.

3.3.2 Heat input factors

The heat input to the ice cover during the pre-breakup period is described by five variables, processed from the available meteorological data. Two of these five variables were formulated from the mean daily air temperature data: $ADDT_{-5}$ and $ADDF_{-5}$. $ADDT_{-5}$ was taken as the accumulated degree-days of thaw, referred to a base air temperature of -5°C as suggested by Bilello (1980), in the pre-breakup period (e.g. between the onset of thaw, D_{OT}, and the day of the first crack, D_{FC}). The onset of thaw, D_{OT}, was defined as the date after which the mean daily air

temperature persisted above -5°C (e.g. for five consecutive days). Any mean daily temperatures below -5°C in the pre-breakup period were used to count towards the accumulated degree-days of freezing, $ADDF_{-5}$ referenced to the same base temperature. It should be noted that a number of other degree-day accumulation conventions were tested, but this one was found to produce the most consistent results. $ADDT_{-5}$ is considered as an index of the accumulated heat input to the ice cover, which in turn decreases ice thickness and/or ice strength. Thus $ADDF_{-5}$ provides an index of the delay of ice cover deterioration during the pre-breakup period.

The three remaining variables: RN_{PB}, SN_{PB}, and SNG_{OT}, were formulated using the daily precipitation and the snow-on-the-ground data, since rainfall and snowfall during the pre-breakup period are also important factors that can affect ice cover competence. RN_{PB} is the accumulated rainfall during the pre-breakup period. It is considered as an index that accelerates snowmelt process and the ice cover deterioration. SN_{PB} is the accumulated snowfall during the pre-breakup period. It is considered as an index important in delaying snowmelt and ice cover deterioration. SNG_{OT} is the depth of snow on the ground at the onset of thaw, D_{OT}. It is considered as a factor which can delay ice cover decay and breakup: the higher the depth of snow cover, the slower the ice cover decays and the later the ice cover breaks up.

3.3.3 Initial ice cover condition

In terms of ice competence, the initial ice cover condition is described by two variables: t_i and *DECAY*. t_i is the ice thickness, based on the data collected during WSC's final winter discharge measurement each year. The date of the measurement is recorded as D_i. There are usually several measurements for each winter season, but the last one each year (usually taken in mid-April) is considered most representative of the actual ice cover thickness just prior to breakup.

The other index variable for ice cover condition, *DECAY,* was introduced to identify whether the ice cover has been significantly decayed or not at the time of this ice thickness measurement. *DECAY* was assigned one of two values: 1 or 0, by comparing the D_i with the onset of thaw, D_{OT}. If D_i was seven days, or more, later than D_{OT}, which means that the ice cover had been exposed to the thawing temperatures for longer than seven days at the time of the measurement, *DECAY* was set to 1; otherwise *DECAY* was set to 0. A zero or one classification for the ice decay was chosen because the breakup evolves quickly at this site (over just a few days, as discussed earlier) and, based on direct observations since 2004, there usually appears to be a dramatic change in the degree of thermal deterioration of the ice cover from one day to the next. The model was tested with and without this variable, and its inclusion was confirmed to reduce the model error.

All seven variables discussed above: t_i, *DECAY*, SNG_{OT}, $ADDT_{-5}$, $ADDF_{-5}$, RN_{PB} and SN_{PB} were used as the models' input variables. The first three (t_i, *DECAY* and SNG_{OT}) are known approximately one to three weeks in advance of the onset of breakup, whereas the other four variables ($ADDT_{-5}$, $ADDF_{-5}$, RN_{PB} and SN_{PB}) must be updated during the pre-breakup period, based on the actual meteorological conditions and short range weather forecasts.

3.4 Multiple linear regression (MLR) models

The multiple linear regression (MLR) technique is currently one of the most prevalent methods used in river ice forecasting. Correct application of MLR first requires that the data set have the characteristics of normality of distributions and independence of input variables. Despite this, to the authors' knowledge, none of the earlier studies applying this technique to the river ice forecasting problem has checked this requirement. The typical river ice breakup data used in the forecasting models do not meet these requirements, yet the method is still widely applied. In the context of this study, because of its prevalent use in practice, the MLR technique was employed purely to provide a conventional (though not necessarily valid) basis of comparison for the proposed ANN model later.

A backwards stepwise regression was performed, in which all the input variables were first entered into the equation and then were successively removed upon meeting the criterion of the significance level of the F-statistic being greater than

0.1 (In this context, the significance level indicates the probability of making an incorrect inference in the hypothesis that the removed variable is not significantly improving the model performance). The significance level of 0.1 was chosen to achieve a more parsimonious model (IBM SPSS Inc., 2009).

This process produced six successive MLR models: the first, employing all seven input variables, is shown in Equation [3-1]. As Figure 3-4(a) illustrates, this model provides relatively poor predictive capability.

$$\Delta H = 1.6543 * t_i - 0.0517 * DECAY - 0.0019 * SNG_{OT} + 0.0004 * ADDT_{-5} + 0.0206 * ADDF_{-5} - 0.0064 * RN_{PB} - 0.0017 * SN_{PB} - 0.1002 \quad [3\text{-}1]$$

The final MLR model from the stepwise regression, which employed only two input variables (ice thickness, t_i and $ADDF_{-5}$), is shown in Equation [3-2]. As Figure 3-4(b) shows, the performance of this simpler MLR model was comparable to the one obtained using all seven input variables.

$$\Delta H = 1.6232 * t_i + 0.0199 * ADDF_{-5} - 0.1351 \quad [3\text{-}2]$$

3.5 Artificial neural network models

3.5.1 Model structure

As a data-driven black-box model, ANN is suitable for complex non-linear problems when an explicit relationship between the input and output variables is difficult to formulate. This method has a parallel and layered structure consisting of artificial neurons (or nodes) that process a number of input signals to produce an output signal. Among the different structures for developing ANN models, Maier and Dandy (2000) and Maier *et al.* (2010) found that multilayer feed-forward networks have been, and are, the most commonly used in the applications of ANNs to water resources problems. It has also been shown that a three-layer feed-forward network with sufficient nodes in the intermediate layer can approximate any function to any desired degree of accuracy (Hornik *et al.* 1989). For this investigation, the most common three-layer feed-forward structure was employed, as illustrated in Figure 3-5. The first is the input layer comprised of all the input variables. The last is the output layer which is the output variable. The intermediate (or hidden) layer is composed of a number of artificial nodes. Nodes of adjacent layers are connected by weighting factors. The analytical form of the model depicted in Figure 3-5 can be expressed by Equation [3-3]. The original values of the nodes in the input layer (X_i) are first summed by their weights (w_{ij}). Each weighted sum is then taken as the input to the nonlinear transfer function (f_1) for the hidden nodes HN_j. The outputs of the nodes in the hidden layer (HN_1 to

HN_h) are again summed up by their weight (w_j) and then taken as the input for the node in the output layer (Y). These weighted sums are converted into the final output using either a linear or non-linear transfer function (f_2) for the node in the output layer (Y).

$$Y = f_2\left(\sum_{j=1}^{h} f_1\left(\sum_{i=1}^{n}(X_i\, w_{ij})\right) w_j\right) \qquad [3\text{-}3]$$

where: n is the number of input variables (7 in this case); and h is the number of nodes in the intermediate layer.

The number of nodes, in the intermediate (hidden) layer, h, is the most critical parameter for a feed-forward ANN structure because an inappropriate choice could result in a model with little generalization capability. If too few hidden nodes are used, the model will not be able to express the complex relationship between the input and output variables. If too many hidden nodes are used an over-fitting situation results, causing the model to perform much better for the calibration data than for the unseen validation data. Currently there is no deterministic method to find the optimal number of nodes to use in the intermediate layer. Sarle (1997) discussed the use of empirical guidelines noting that they are all very case specific and, thus fundamentally no better than the simple trial-and-error method. Therefore, in this study, the trial-and-error method was implemented: first by training a number of networks with different numbers of hidden nodes, then choosing the one with the best performance as the final

model. The smallest number of hidden nodes was taken as 2 in this study. The NeuroShell® 2 Release 4.2 (Ward Systems Group, Inc., 1995) software, used for this study, recommends specifying the number of hidden nodes for a three-layer network by Equation [3-4].

$$h = \frac{1}{2}(N_I + N_O) + \sqrt{N} \qquad [3\text{-}4]$$

where: N_I is the number of the input variables; N_O is the number of output variables; and N is the available number of the calibration data cases. For this case, with seven input variables, one output variable and 42 calibration data cases, Equation [3-4] suggests that it would be appropriate to use 11 nodes in the hidden layer. Therefore, a range of 2 to 11 for the number of hidden nodes was tested and compared. Two larger values, 15 and 20 hidden nodes, were also tested to see if larger model structures could give better performance. The 12 model structures investigated in this study are summarized in Table 1, categorized into three groups by the ratio of the degree of freedom, *DF* (i.e. the number of connection weights for calibration) to the size of calibration data set, *N*, so that the average performance of structures in each group can be compared. The degrees of freedom are calculated using Equation [3-5]:

$$DF = h(N_I+1) + (h+1)\,N_O \qquad [3\text{-}5]$$

The ‘small’ group includes three structures (h=2, 3 and 4) where the ratio, DF/N, is less than 1. The ‘moderate’ group includes another five structures (h=5 to 9) when the ratio is between 1 and 2. The ‘large’ group is comprised of the cases for which the ratio is larger than 2 (h=10, 11, 15 and 20).

3.5.2 Model calibration

Calibration of an ANN model involves iteratively updating the connection weights between the nodes of adjacent layers (i.e. w_{ij} and w_j in Equation [3-3]) to minimize the overall mean squared error between the actual and modeled output for all calibration data. In this investigation, the calibration data were first pre-processed and standardized; then the back-propagation (BP) algorithm proposed by Rumelhart *et al.* (1986) and ‘early stopping’ scheme (see Sarle 1997) were used to calibrate the models proposed above; the performance of the calibrated models were then compared to determine the best model structure.

3.5.2.1 Data pre-processing

The range in magnitude of each variable in the calibration data set can be quite different. For example, in this study, the variable $ADDT_{.5}$ ranges from 0.0 to 169.2 °C-day whereas the variable t_i only varies from 0.4 to 1.1 m. If the original values of these variables were used in calibrating the ANN model, very small

weightings would be assigned for these widely ranging variables. Therefore, to avoid the effect of uneven absolute ranges of variables, the original data should be transformed. Among the different transformation techniques (e.g. the linear, logarithmic, histogram equalization, seasonal and normal transformations), Bowden *et al.* (2003) found that the linear transformation gave the best results. Therefore, in this study, all of the input and output data were linearly scaled to the range of -1 and 1 using Equation [3-6]:

$$S_i = [2x_i - (x_{max} + x_{min})]/(x_{max} - x_{min}) \quad [3\text{-}6]$$

where: S_i is the scaled non-dimensional value of the variable; x_i is its original value; and x_{max} and x_{min} are the maximum and minimum value of the variable in the data set, respectively.

All of the input and output variables were scaled into non-dimensional numerical values between -1 and 1 using Equation [3-6]. A box plot of the scaled values for each variable (except the nominal variable *DECAY*) is shown in Figure 3-6, illustrating the fact that none of the variables are normally distributed. This is an advantage of ANN modeling over traditional statistical models such as MLR, as it is not appropriate to apply MLR modeling to non-normally distributed data (Masters 1993). It should be noted that non-linear data transformations might resolve this issue for the MLR modeling technique; however, as the historical applications of MLR modeling to this problem have not employed such

transformations, and this research was focused on the ANN modeling approach, such investigations were considered beyond the scope of this study. To measure the model performance against observed data, the output from the calibrated model was rescaled by the reverse process to obtain values in the original unit.

3.5.2.2 Calibration algorithm

The BP algorithm was chosen to train the proposed ANN models, as it has been the most commonly used in water resources related applications (Maier *et al.* 2010). There are several parameters associated with the BP algorithm including: the initial weight range, the transfer functions, the learning rate, α and the momentum factor, m. The initial weight range defines the range of the randomly assigned connection weights as the initial condition for the iteration process. In this study, since the BP algorithm cannot guarantee globally optimal results from the calibration, successive values for the initial weight range, ranging from 0.01 to 0.3 with a step size of 0.01, were tried. Then the initial weight range which provided the best model performance was used in the final version of the model.

The transfer functions in the BP algorithm (i.e. f_1 *and* f_2 in Equation [3-3]) can be any differentiable and bounded function. In this study, a hyperbolic tangent was chosen as f_1 and a linear (identity) function was chosen as f_2. This combination is recommended by Sarle (1997) and NeuroShell® 2 Release 4.2, and has been used

most frequently for forecasting problems in the literature (Maier and Dandy 2000).

Since the computational time required for calibration was not a constraint in this study, relatively small learning rates and momentum factors were used: α = 0.1 and m = 0.1 for the intermediate layer and α = 0.05 and m = 0.5 for the output layer. These are recommended by NeuroShell® 2 Release 4.2 and were kept the same throughout the calibration process.

To avoid over-fitting (i.e. a situation in which the model is overly calibrated such that it even reproduces the 'noise' in the calibration data and thus has a poor generalization capability), the 'early stopping' scheme (Sarle 1997) was also employed in this study. In this scheme, the calibration data set is split into two subsets: one for training the model and the other for testing the model during the calibration process. The model calibration proceeds using the training subset, and each successive calibration is assessed using the testing subset. The calibration result that produces the minimum root mean squared error for the testing subset ($RMSE_{tst}$), as calculated by Equation [3-7], is then chosen as the optimal model.

$$RMSE_{tst} = \sqrt{\frac{1}{N_{tst}} \sum_{s=1}^{N_{tst}} \frac{1}{2} (\widehat{Y^s} - Y^s)^2} \qquad [3\text{-}7]$$

where: $\widehat{Y^s}$ and Y^s are respectively the modeled and actual output for the sth of the N_{tst} testing data.

For this study, the calibration data was split manually so as to avoid any extrapolation by the ANN model in the testing phase; specifically, those data with one or more extreme values of any input or output variable were kept in the training subset. Also to make the best use of the available data, 90% of data was kept in the training subset and the remaining 10% was left in the testing subset. As a result, the data for 1970, 1992, 1997 and 2005 were chosen as the testing subset and the remaining 38 years data were used as the training subset (as noted in Figure 3-3).

3.5.3 Model validation

Before implementing an ANN model in practice, it is necessary to determine how well the model will make predictions for cases that are not in the calibration data set by validating its generalization capability. Given the small data set available in this study (N = 42 years), it was not valid to employ the commonly used split-sample validation method due to the subjective approach required for the sample splitting (Sarle 1997). This was confirmed by testing the split-sample approach for multiple combinations of calibration/validation subsets. As expected, it was found that resulting model error depended on the sample split selected, even though sub-samples were chosen to have consistent statistics for all variables. Consequently, the 'leave-one-out cross validation' (LOOCV) technique (Stone 1974) was employed here. In this method, the ANN model is calibrated and

validated *N* times, each time calibrating with all but one of the data set (i.e. with a sample size of *N*-1 for training and testing). The calibrated model is then validated by the reserved (single) data case not used in the calibration. This calibration and validation process is repeated until each data case is used as a validation data once. The average of the resulting validation errors is then used as an estimate of the true error of the model.

As discussed above, in this study, four cases were chosen for the testing subset (1970, 1992, 1997 and 2005) in the calibration process. When one of the four test cases was reserved for validation in the LOOCV procedure, another case having an output of comparable magnitude was substituted in the calibration testing subset. The data cases used as substitutes in the testing subset are marked with '☆' in Figure 3-3.

3.6 Results and Discussions

3.6.1 Calibration and determination of the final ANN model

Figure 3-7 illustrates the comparative performance of three of the calibrated models (for h = 2, 6 and 20), as a function of initial weight range (IWR). As seen in Figure 3-7(a), models with fewer hidden nodes (e.g. h = 2) have the largest errors; this is because small networks have a limited capability to express the

types of complex relationships considered in this study. The model performance improved when the number of hidden nodes were increased, as illustrated by Figure 3-7(b) for h = 6. However, when too many hidden nodes were employed the model performance became unpredictable, as illustrated in Figure 3-7(c) for h = 20. In particular, for some trials, such as IWR = 0.05, 0.10, 0.13, 0.14 and 0.28, the calibration fit the testing data better than the training data (Figure 3-7(c)). These results imply that a medium size network is likely to exhibit better performance than a large size network in the case of a small data set.

Figure 3-7 also illustrates that the optimal IWR was identified for each model as the value associated with the minimum RSME for the testing subset. Figure 3-8 compares the optimal values of IWR for all 12 cases of h tested. This comparison shows that that medium sized models (e.g. for h = 6 to 9) exhibited better performance than the small models (e.g. for h = 2 to 5). Although the larger models suggest even better performance, potentially unpredictable results are possible. Specifically, when the testing errors are smaller than the training errors (e.g. as they were for h = 11 and 20), the testing error is no longer representative of the model error, which means that the 'early stopping' scheme has essentially failed.

Based on the above results, the model with 6 hidden nodes and an initial weight range of 0.29 showed the smallest $RMSE_{tst}$ and was chosen as the optimal model. The performance of this proposed ANN model is shown in Figure 3-9. The R^2 for

the whole calibration set was 0.93, which is much better than seen for the two MLR models discussed earlier (0.22 and 0.21). Also, $RMSE_{tst}$ was 0.23 m, which is much smaller than the SEE for the two MLR models (0.65 m and 0.61 m). This good performance implies the great potential of the ANN model to generalize the complex relationships for the river ice breakup forecasting.

3.6.2 Validation of the ANN model

The results for the 42 LOOCV calibrations are shown in Figure 3-10, illustrating that they varied substantially in terms of the resulting training and the testing errors. This demonstrates how sensitive the ANN calibration results are to small changes in the calibration data, especially for small data sets. However, the average of the $RMSE_{trn}$ (0.14 m) and the $RMSE_{tst}$ (0.26 m) for the LOOCV analysis are very close to those for the proposed ANN model calibration (also shown on the figure), which were 0.16 m and 0.23 m, respectively.

The results of the validation of the 42 LOOCV models are shown in Figure 3-11. The range of validation errors (0.00 to 4.77 m) is much larger than that for the testing errors (0.11 to 0.42 m as seen in Figure 3-10). This implies that the accuracy of the ANN model could be overestimated by looking only at the calibration testing errors, especially if the data set is small, which is the case in this study. For the 9 anomalous years, in which one or more variables were outside of the range of the corresponding calibration data, the errors were

generally larger. In addition, the modeled outputs were negative (i.e. physically meaningless) for 4 of the anomalous cases and beyond the maximum of the observed values for 2 of the anomalous cases. This illustrates that problems associated with extrapolating ANN models. It should also be noted that, to prevent these non-physical (i.e. negative) outputs, a sigmoid transfer function could be tried for the node in the output layer. This needs further investigation in future studies.

There could be two possible reasons for this poor predictive capability of the feed-forward ANN models in this study. The first is the small size of the calibration data set compared to the large structure of the ANN model. In the case of this study, the ratio of degrees of freedom to the size of the calibration data set was 1.31 for $h = 6$ (see Table 1), which is larger than 1. This can cause the ANN model training to become trapped in some local minima that is far away from the global optimum, which tends to result in poor validation performance. One possible solution to this problem would be to perform a sensitivity analysis on the input variables and then eliminate those found to be insensitive, so as to reduce the complexity of the model structure. It is also possible that model performance could reflect errors in the data set, especially as the occurrences of the first transverse cracks were, in most cases, deduced from the historical raw water level data rather than by direct observation. Despite these issues, the forecast stage at breakup for 2011 was found to be within 0.1 m of the actual observed value.

3.6.3 Potential of the ANN model to predict the timing of breakup

To test the potential applicability of the ANN model for predicting the timing of river ice breakup, these forecasted water levels were translated into a date of occurrence (D_{FC}) by referring to the raw strip chart or instantaneous water level data from WSC to determine the date on which the modelled H_{FC} occurred. For some cases, the modelled H_{FC} was outside the range of the available water level data; in those cases, the predicted D_{FC} was estimated as the date on which the water level was closest to the modelled H_{FC}.

Figure 3-12 illustrates the comparisons of the proposed ANN model predictions to the actual data and to the 2-variable MLR model (i.e. Equation [3-2]). As expected, given the lower RMSE in the calibrated ANN model, the performance is encouraging, with the predicted dates for the onset of breakup all within one day of the actual occurrence (see Figure 3-12(a)). In comparison the 2-variable MLR model performs relatively poorly. However, the results of the validations in the LOOCV analysis, shown in Figure 3-12(b), probably illustrate a more realistic picture of the potential accuracy of the forecasts: 28 of the 47 events have an error equal to or greater than 2 days, which is comparable to that of the 2-variable MLR model. This fact suggest that, despite the encouraging calibration results of the ANN model, its true performance in forecasting practice still has much uncertainty and needs further study. Nevertheless, the optimal model suggested in this study did correctly predict the timing of breakup in 2011.

3.6.4 Relative importance of the input factors to the timing of river ice breakup

To make the most use of the calibrated ANN model, the relative importance of input variables to the output variable was calculated by Garson's method (Garson 1991), using the calibrated connection weights. The results are shown in Figure 3-13. The five most important variables are the SNG_{OT}, $ADDF_{-5}$, *DECAY*, $ADDT_{-5}$, and t_i, which are all of a similar level of relative contribution (from 14% to 20%). The remaining two variables (i.e. RN_{PB} and SN_{PB}) are less important. This analysis was also performed for all the calibrations in the LOOCV (see Chapter 3). The rank of the relative contributions of each input variable to the output variable are shown by the box plot in Figure 3-14. This result indicates that the four most important input variables are t_i, $ADDT_{-5}$, $ADDF_{-5}$ and SNG_{OT} and the least important is SN_{PB}. This result is more or less consistent with those empirical criteria for the onset of river ice breakup found in the literature (e.g. see Beltaos 1997), except for the following newly introduced variables: the accumulated degree-days of freezing during the pre-breakup period ($ADDF_{-5}$) and the snow-on-the-ground at the onset of thaw (SNG_{OT}) which were also found to be important factors affecting the initiation of river ice breakup in this study. The result of this analysis is also consistent with that of the MLR models (see Equations [3-1] and [3-2]). In the backward stepwise regression, the last model contained the two variables: t_i and $ADDF_{-5}$. It is understandable, given that when a cold spell occurs during the pre-breakup period, the decay of ice cover could be delayed, which

thus affect the initiation of breakup. $ADDF_{-5}$ is a good indicator of this effect and should be included in developing river ice breakup models. These results also suggest that snowfall during the pre-breakup period (SN_{PB}) is not as important as the other factors and can be neglected in practical models for river breakup forecasting.

3.7 Conclusions

This Chapter explored the practical applicability of feed-forward ANN models to the river ice breakup forecasting problem. All of the independent and dependent variables related to river ice breakup were processed from the readily available historical hydrometric and meteorological records. These variables were then used to develop a three-layer feed-forward ANN model. The results for the Hay River case study showed that the feed-forward ANN model has more potential than conventional multiple linear regression models employed historically to express the complex nonlinear relationship between the input and output variables in the river ice breakup forecasting problem. However, limited available data remains a key constraint in forecasting this complex phenomenon.

It is important to note that an ANN model's performance can be optimistically overestimated by looking only at the calibration testing results. The results of the independent validation for this example case study clearly illustrate that the error of the calibrated ANN model on the unseen validation data could be much larger

than those indicated by the calibration testing data. It was also found that the error is generally larger for the extrapolation cases than for interpolation. Thus independent validation, using data not employed in the training and testing processes, is essential to obtain a clear picture of the actual potential errors of any ANN model.

Table 3–1: The 12 ANN model structures tested in this study.

Size of network	**Number of hidden nodes (*h*)**	**Degree of freedom (*DF*)**	**Ratio of *DF* to *N***
Small	2	19	0.45
	3	28	0.67
	4	37	0.88
Medium	5	46	1.10
	6	55	1.31
	7	64	1.52
	8	73	1.74
	9	82	1.95
Large	10	91	2.17
	11	100	2.38
	15	136	3.24
	20	181	4.31

(a)

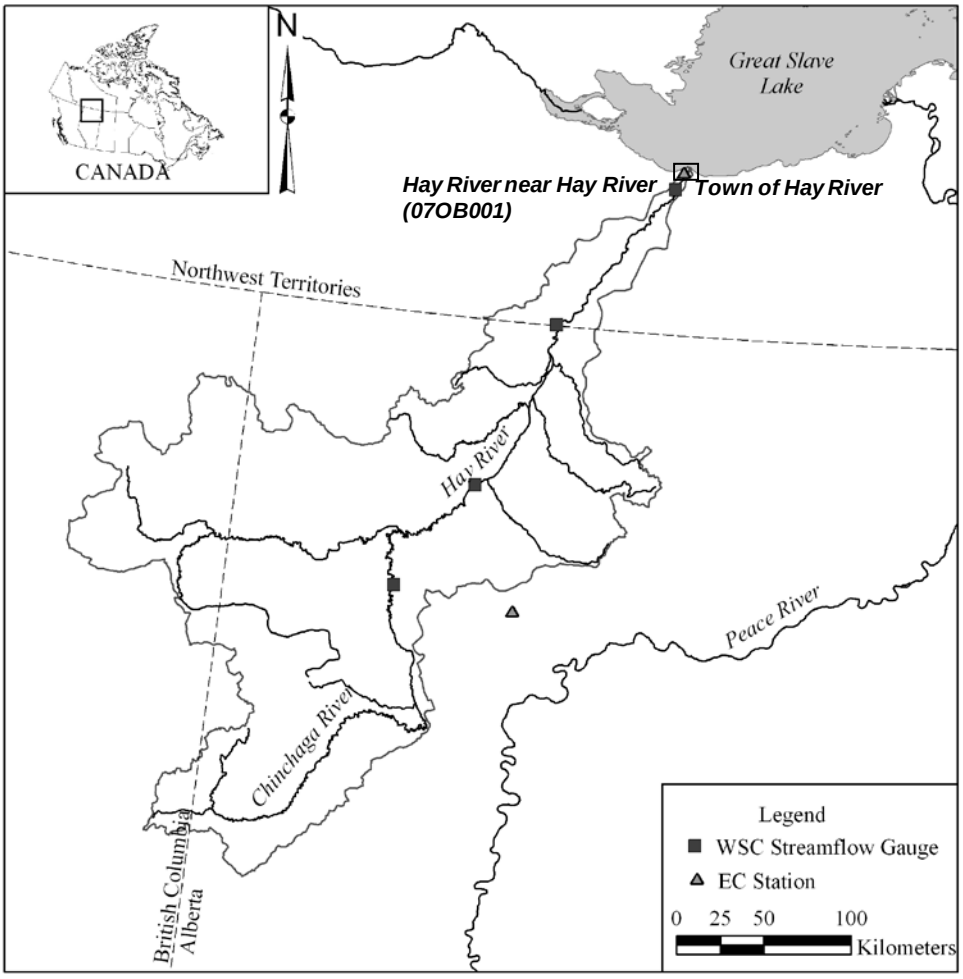

(b)

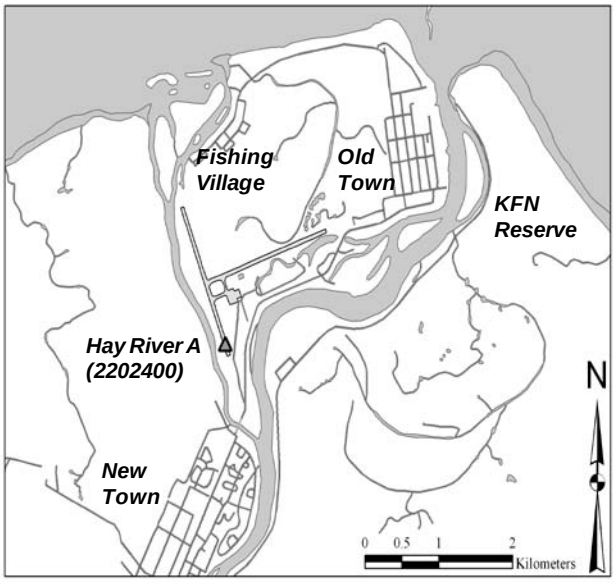

Figure 3–1: Map of (a) the Hay River basin and (b) the Town of Hay River.

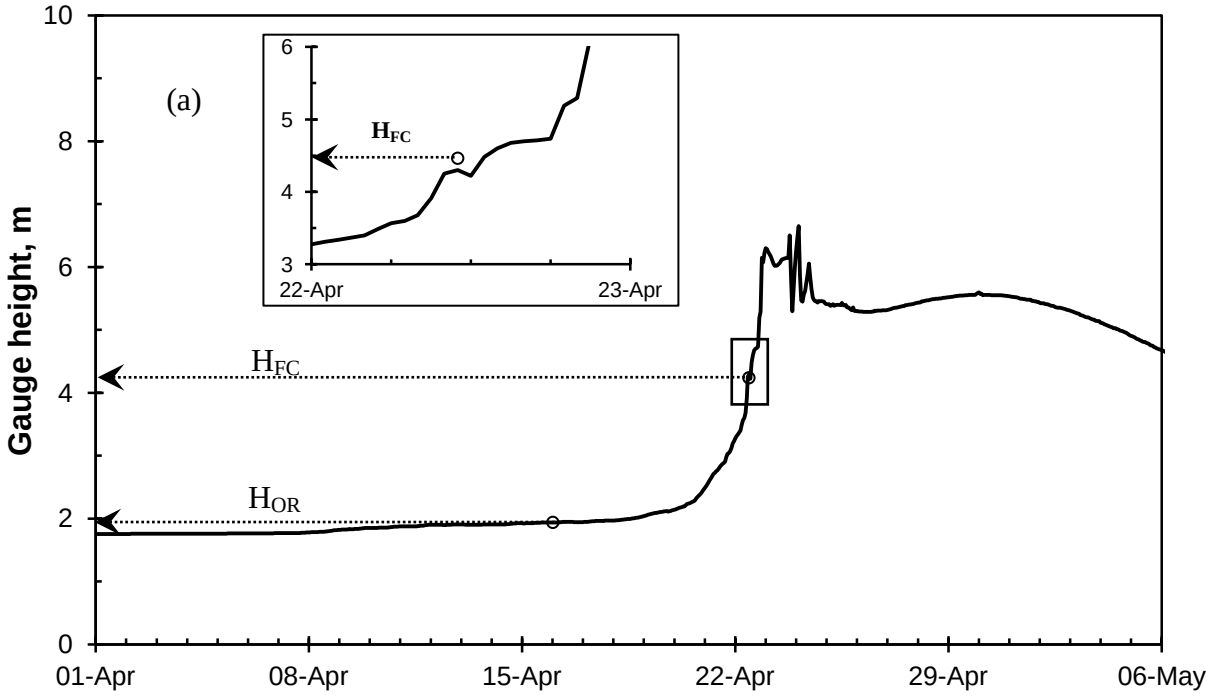

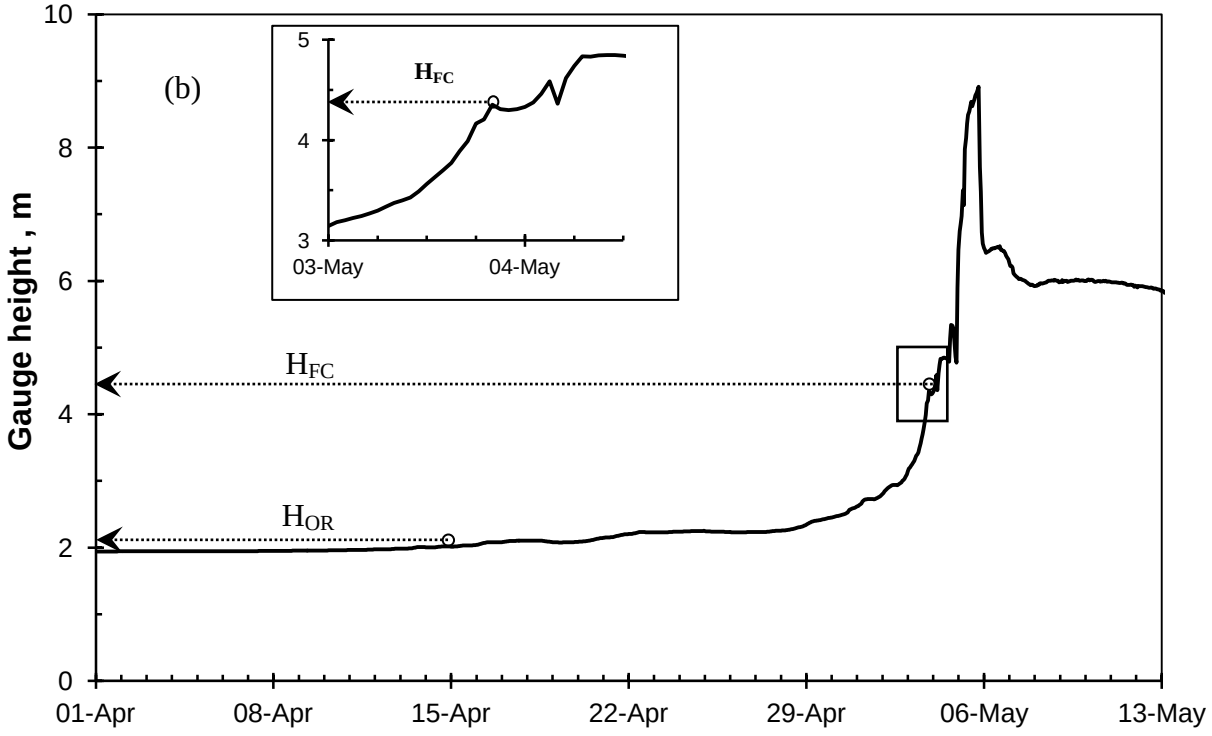

Figure 3–2: Examples of H_{FC} and H_{OR} determination at the WSC 07OB001 (HRHR) gauge for (a) year 2005 and (b) year 2008.

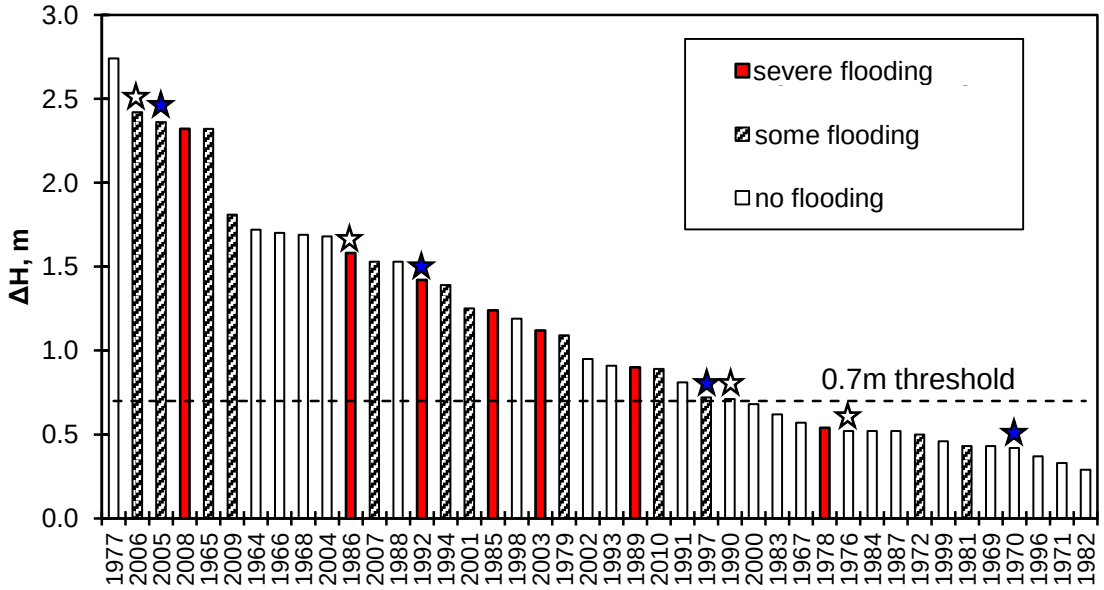

Figure 3–3: The amount of rise of water level required to initiate river ice breakup (ΔH), and breakup flood severity, at the Town of Hay River. Note: the years marked with symbol '★' were used in the testing subset in the calibration of the ANN model; the years marked with the symbol '☆' were the substitutes used when members of the testing subset were reserved cases in the in the leave-one-out cross validation.

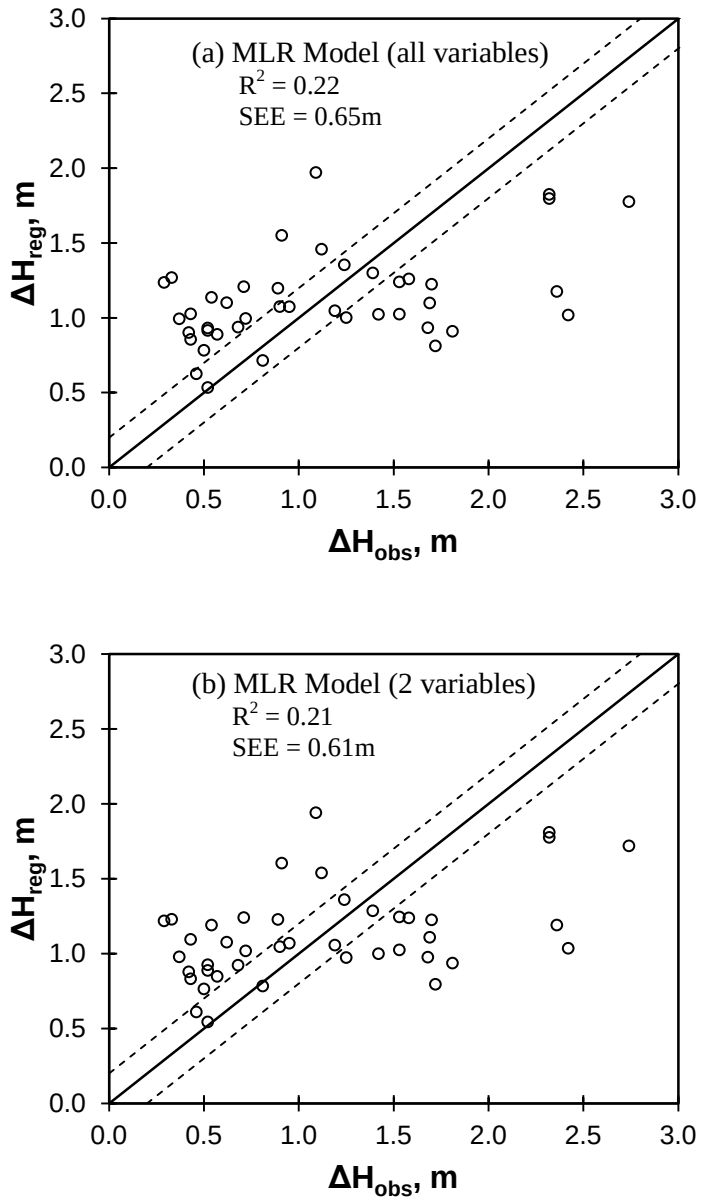

Figure 3–4: Comparison between the predicted stage change at the onset of breakup (ΔH_{reg}) and the observed stage change (ΔH_{obs}) for the two multiple linear regression models: (a) with the most input variables and (b) with the least input variables. Note: the dashed lines enclose ±0.2 m difference from the perfect agreement (solid line). R^2 is the coefficient of determination and SEE is the standard error of the estimate. Sample size is 42 in this study.

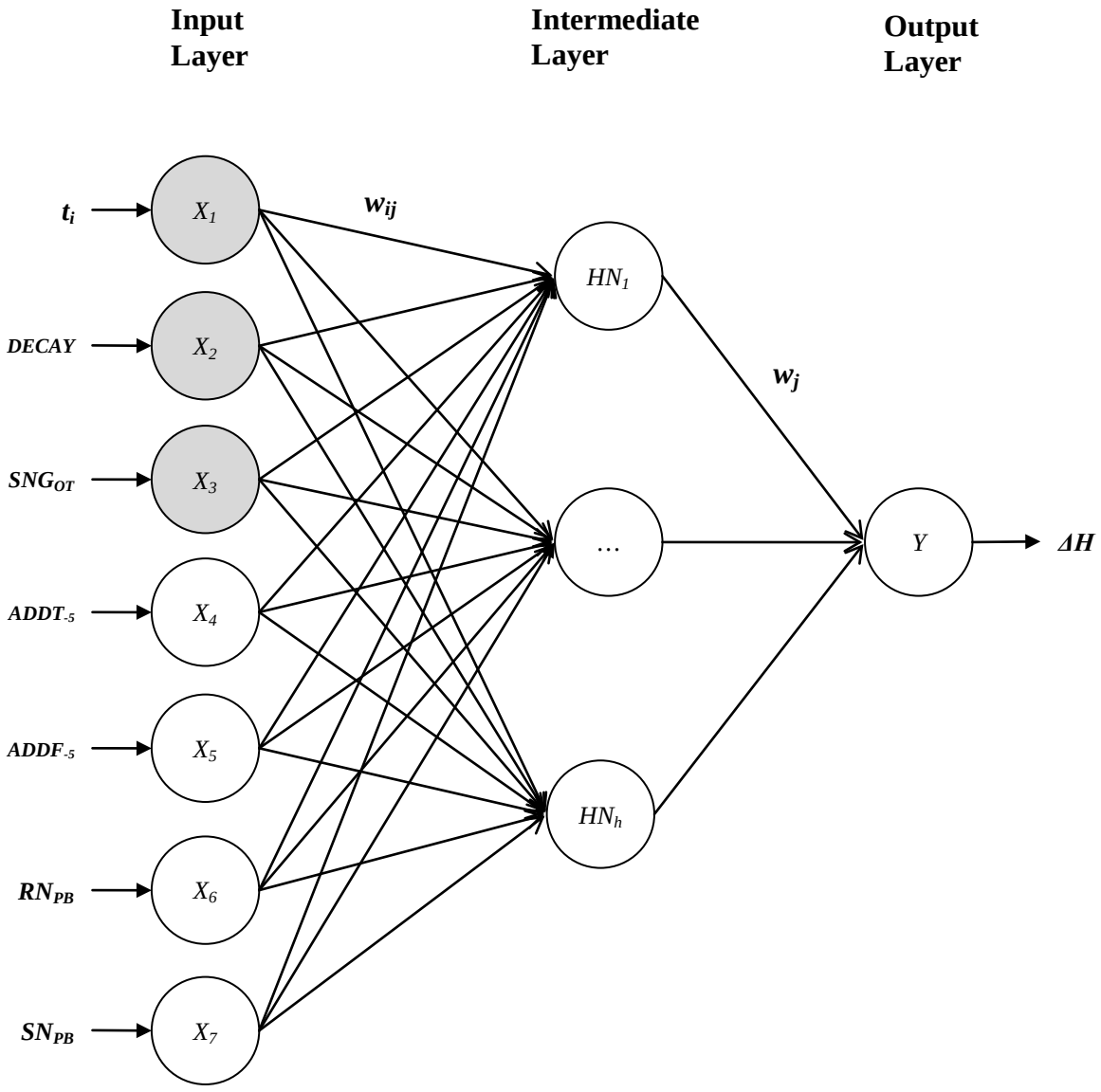

Figure 3–5: The three-layer feed-forward ANN structure employed in this study. Note: shaded nodes in the input layer are variables known one to three weeks prior to the onset of breakup; unshaded nodes are variables based on the actual situation and weather forecasts during the pre-breakup period; w_{ij} is the connection weight between an input node (X_i) and a hidden node (HN_j); w_j is the connection weight between a hidden node (HN_j) and the output node Y.

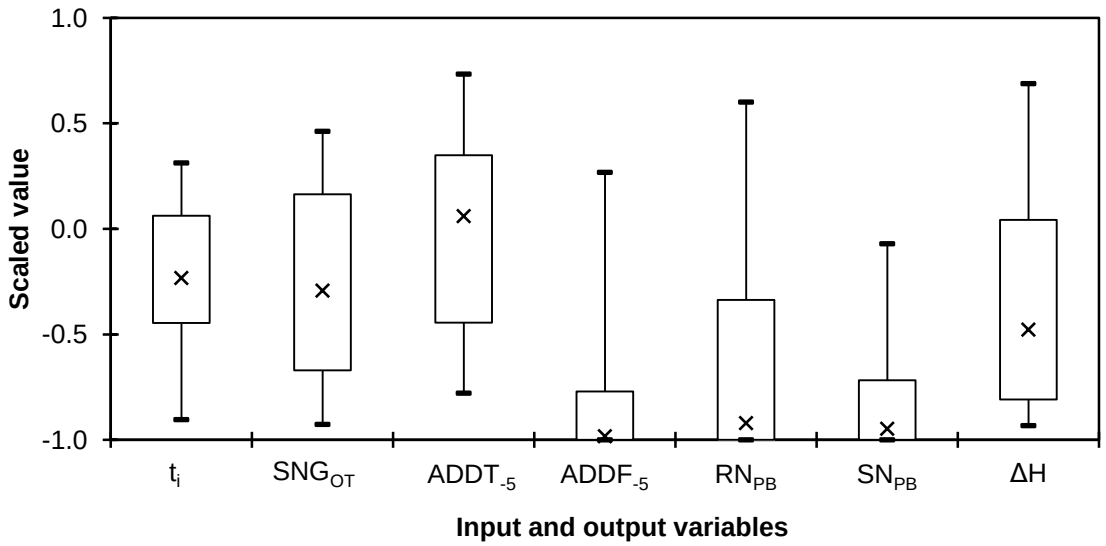

Figure 3–6: Box plot for the scaled values of all input and output variables. Note: 'x' indicates the median value; the bottom and top of the box are the 25^{th} and 75^{th} percentiles, respectively; and the lower and upper ends of the whiskers are the 5^{th} and 95^{th} percentiles, respectively.

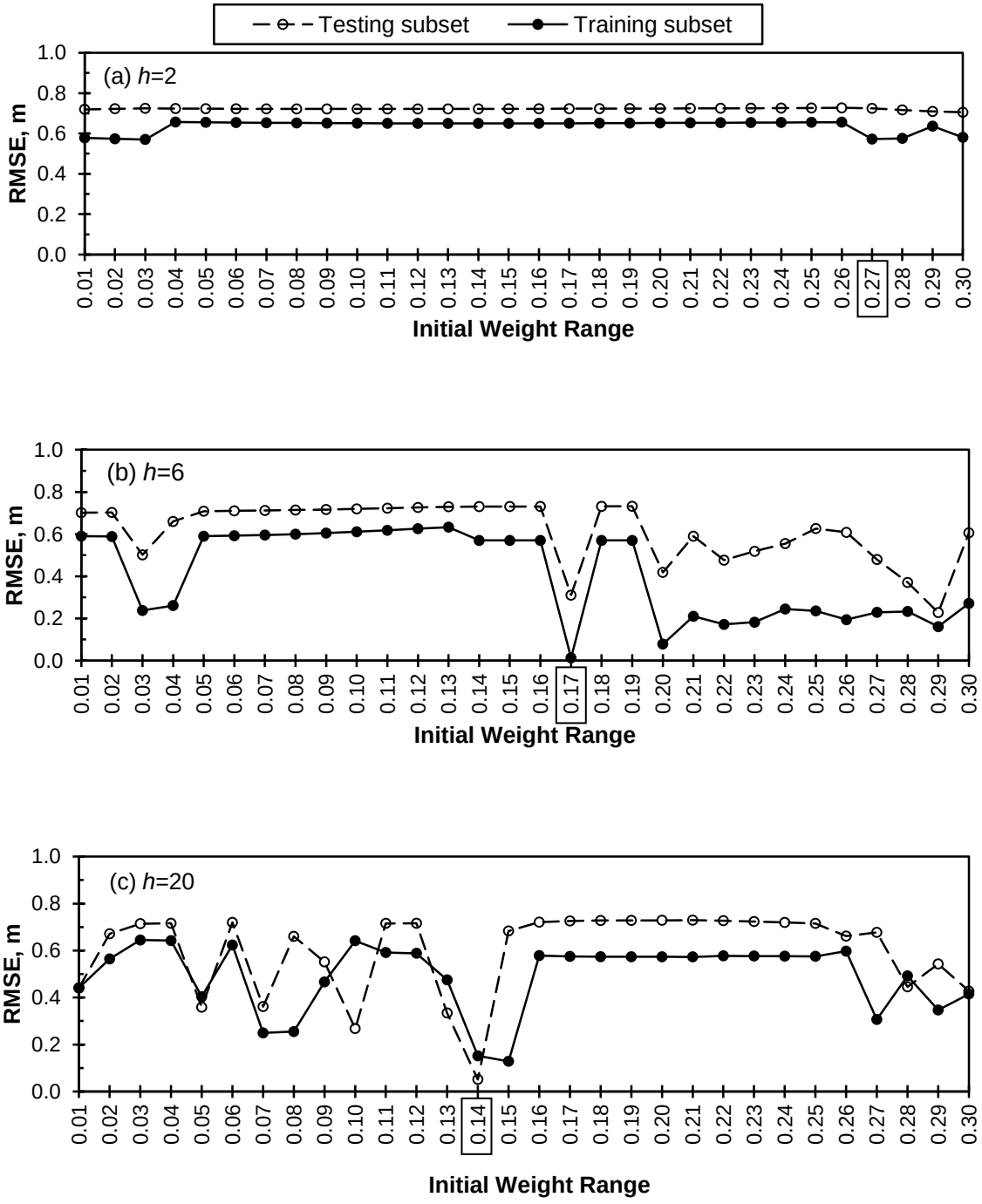

Figure 3–7: Root mean squared error (RSME) as a function of the initial weight range (IWR) for three of the calibrated models: (a) h=2, (b) h=6, and (c) h=20, where h is the number of hidden nodes. The boxed number indicates the optimal IWR for each model.

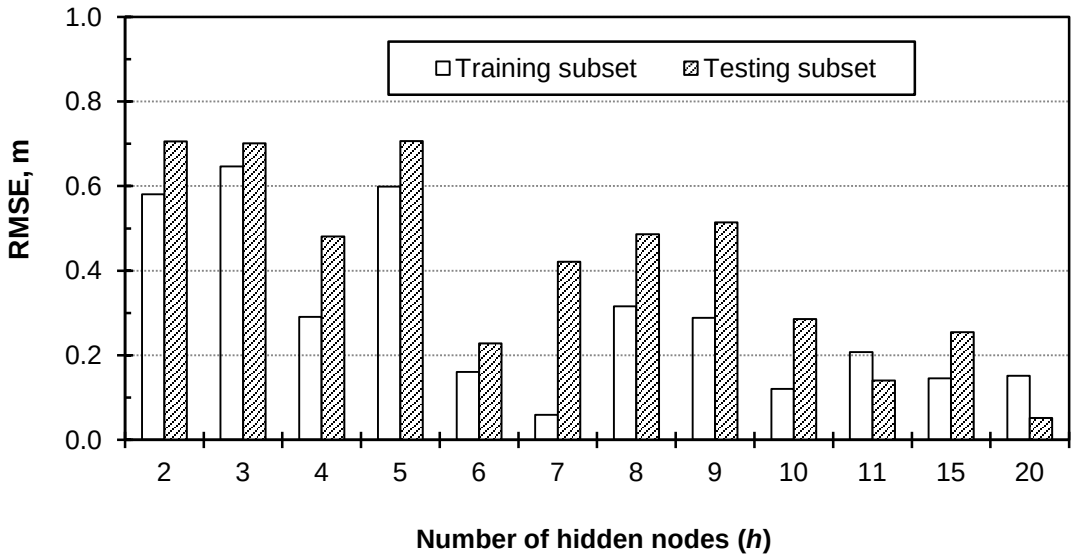

Figure 3–8: Comparison between the best performances of the trained ANNs with different numbers of hidden nodes.

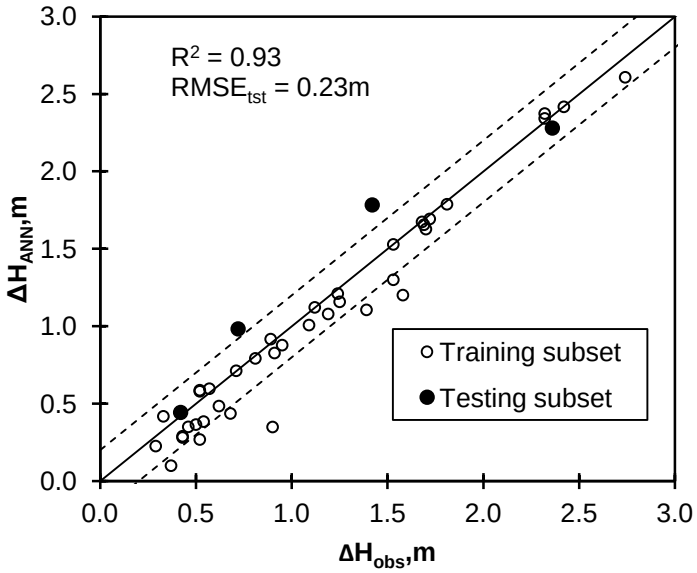

Figure 3–9: Comparison of the modeled ΔH of the final ANN model (ΔH_{ANN}) with the corresponding observed values (ΔH_{obs}). Note: the dashed lines enclose ±0.2 m difference from the perfect agreement (solid line); $RMSE_{tst}$ is the root mean squared error for the testing subset.

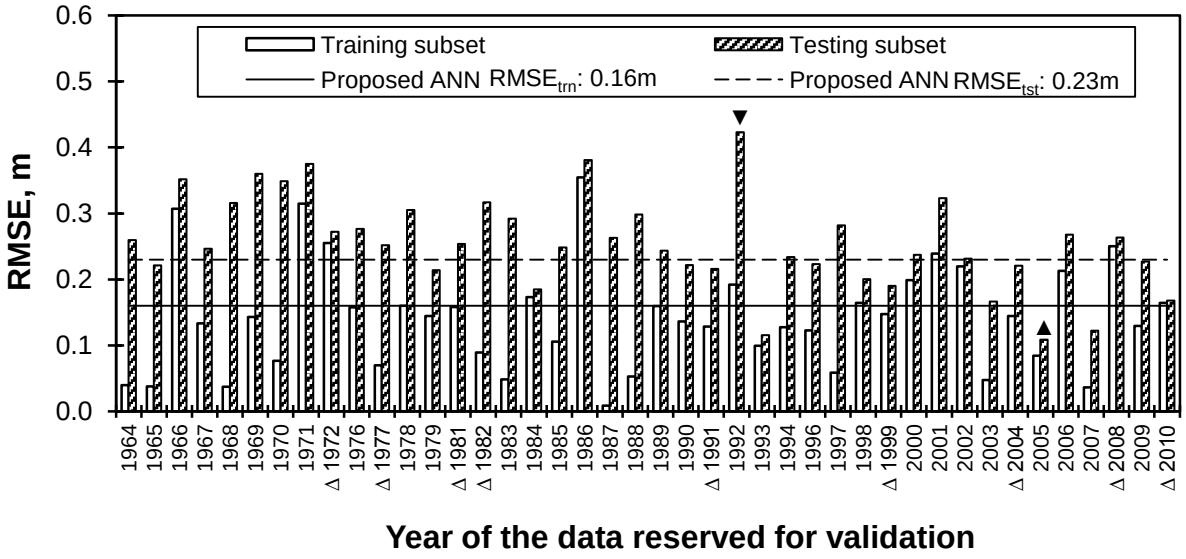

Figure 3–10: Results of the 42 calibrations in the LOOCV. Note: 'Δ' indicates the anomalous years, in which one or more of the variables were outside of the range of the calibration data; '▼' and '▲' indicate the maximum and minimum testing errors, respectively.

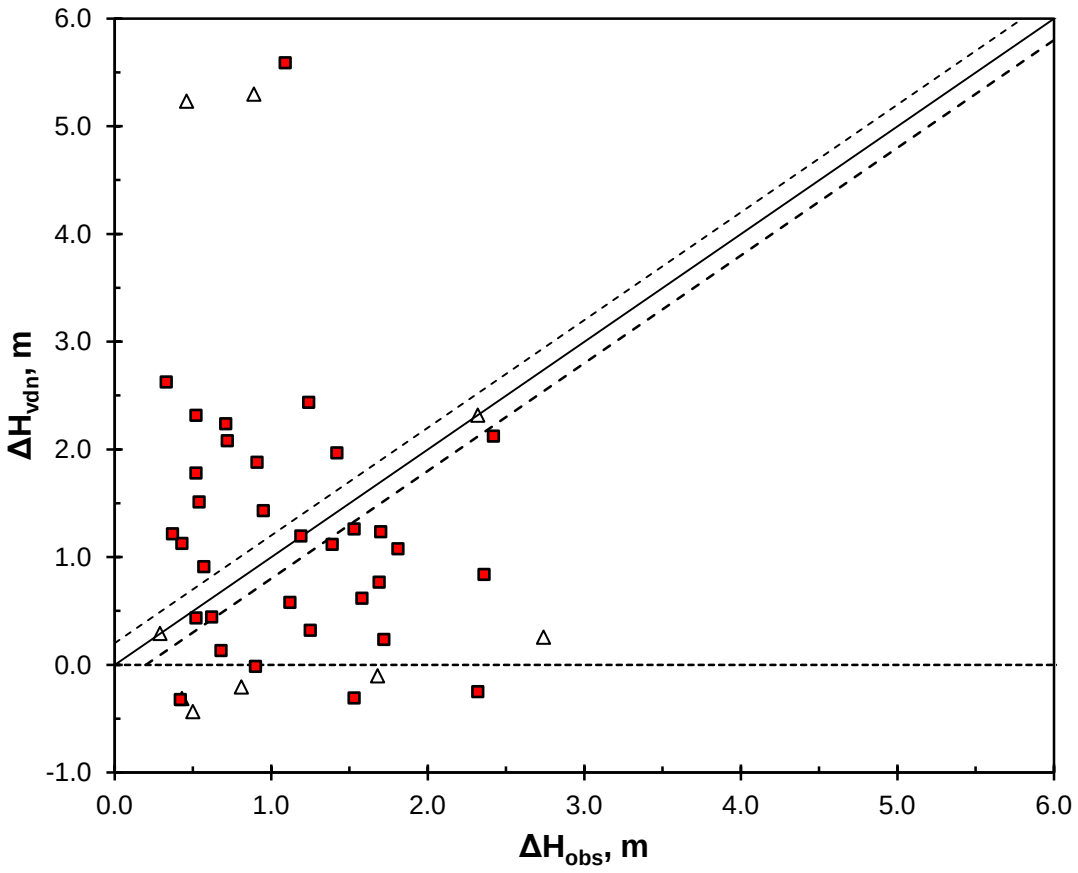

Figure 3–11: Comparison of the output values for the validating data (ΔH_{vdn}) compared to the corresponding observed values (ΔH_{obs}). Note: 'Δ' indicates the anomalous years, in which one or more of the variables were outside of the range of the calibration data.

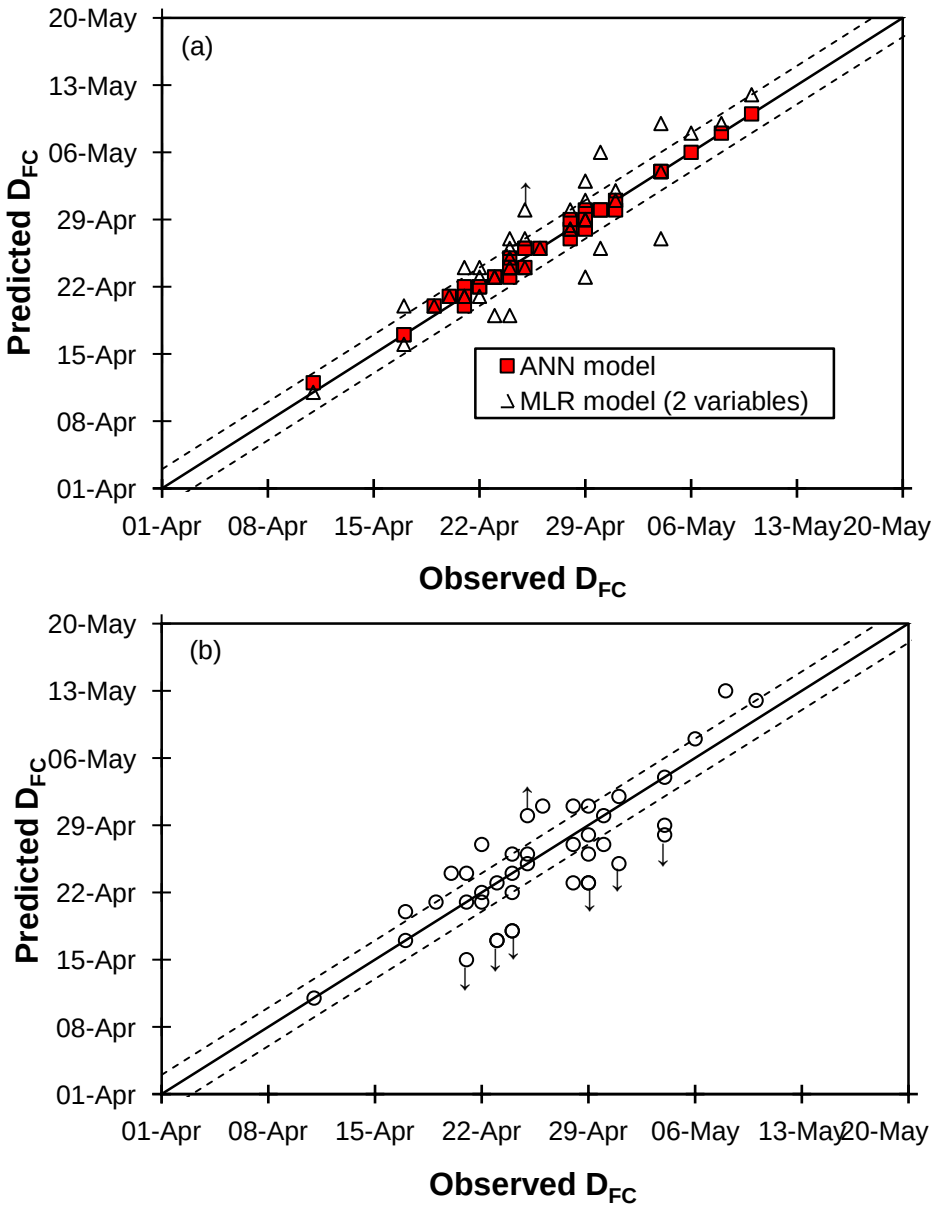

Figure 3–12: Comparison of the predicted date of the onset of breakup (D_{FC}) to the observed data for (a) the calibrated ANN and MLR model (i.e. Equation [3-2]) and (b) the validations in the LOOCV. Note: ↓ indicates that the predicted D_{FC} was estimated and is known to be less than shown and ↑ indicates that the predicted D_{FC} is greater than shown (for cases which could not be precisely determined due to incomplete hydrographs).

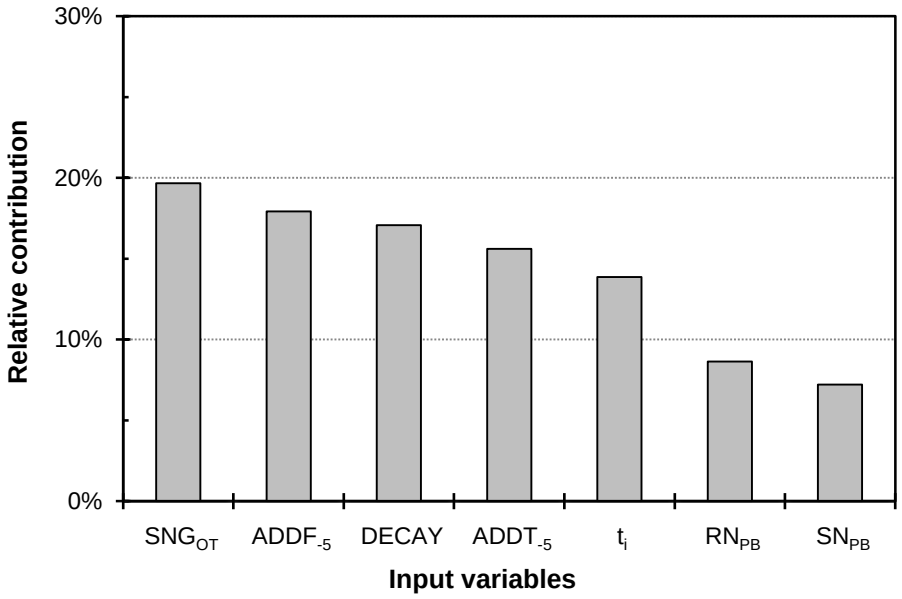

Figure 3–13: Relative contributions of input variables to the output variable for the calibrated ANN model with 6 hidden nodes.

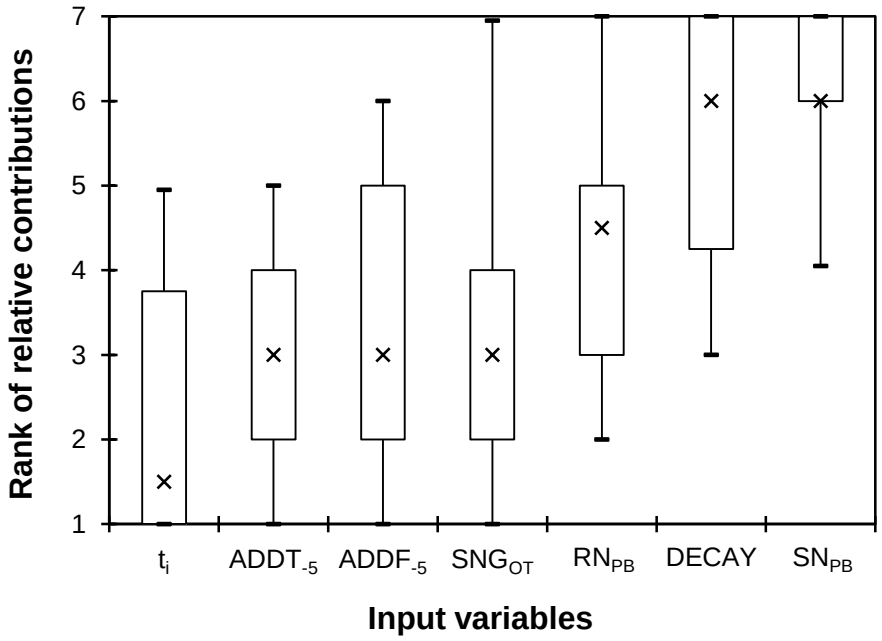

Figure 3–14: Box plot of the ranks of relative contributions of input variables to the output variable for the different calibrations in the LOOCV. Note: 'x' indicates the median value; the bottom and top of the box are the 25^{th} and 75^{th} percentile; the ends of the whiskers are the 5^{th} and 95^{th} percentile.

3.8 List of references

ASCE Task Committee on Application of Artificial Neural Networks in Hydrology, 2000a. Artificial neural networks in hydrology. I: preliminary concepts. Journal of Hydrologic Engineering, ASCE 5 (2), 115-123.

ASCE Task Committee on Application of Artificial Neural Networks in Hydrology, 2000b. Artificial neural networks in hydrology. II: hydrologic applications. Journal of Hydrologic Engineering 5 (2), 124-137.

Beltaos, S., 1990. Fracture and breakup of river ice cover. Canadian Journal of Civil Engineering, 17(2): 173-183.

Beltaos S., 1997. Onset of river ice breakup. Cold Regions Science and Technology 25(3): 183-196.

Beltaos, S., 2004. Wave-generated fractures in river ice covers. Cold Regions Science and Technology 40 (3), 179-191.

Beltaos, S. (Ed.), 2008. River ice breakup. Water Resources Publications, LLC, Highlands Ranch, Colo. 462pp.

Bilello, M.A., 1980. Maximum thickness and subsequent decay of lake, river and fast sea ice in Canada and Alaska. U.S. Army Cold Regions Research and Engineering Laboratory, Report 80-6, Hanover, NH, 165 pp.

Billfalk, L., 1981. Formation of shore cracks in ice covers due to changes in the water level. Proceedings of the 6th IAHR Symposium on Ice, Quebec City, Canada, Vol II, 650-660.

Bowden, G. J., Dandy, G. C. and Maier, H. R., 2003. Data transformation for neural network models in water resources applications. Journal of Hydroinformatics 5, 245–258.

Chen, S. and Ji, H., 2005. Fuzzy optimization neural network approach for ice forecast in the Inner Mongolia reach of the Yellow River. Hydrological Sciences, 50(2): 319-326.

Chokmani, K., Khalil, B., Ouarda, T. and Bourdages,R., 2007. Estimation of river ice thickness using artificial neural networks. Proceedings of the 14th Workshop on the Hydraulics of Ice Covered Rivers. CGU HS Committee on River Ice Processes and the Environment (CRIPE). Québec, Canada. 12pp.

Daly, S.F., 1995. Fracture of river ice covers by water waves. Journal of Cold Regions Engineering 9(1), 41-52.

Dawson, C.W. and Wilby, R.L., 2001. Hydrological modelling using artificial neural networks. Progress in Physical Geography 25 (1), 80-108.

Flood, I. and Kartam, N., 1994a. Neural networks in civil engineering. I: Principles and understanding. Journal of Computing in Civil Engineering 8 (2), 131-148.

Flood, I. and Kartam, N., 1994b. Neural networks in civil engineering. II: Systems and application. Journal of Computing in Civil Engineering 8 (2), 149-162.

Garson, G.D., 1991. Interpreting neural-network connection weights. Artificial Intelligence Expert 6, 47-51.

Hicks, F.E., Cui, W. and Andres, D. (1995) "Breakup Forecasting on the Mackenzie River at the Ft. Providence Ferry Crossing" Water Resources Engineering Report No. 95-H2, Department of Civil Engineering, University of Alberta, Edmonton, Alberta, 202 pp.

Hornik, K., Stinchcombe, M. and White, H., 1989. Multilayer feedforward networks are universal approximators. Neural Networks 2, 359-366.

Hu, J., Liu, L., Huang, Z., You, Y. and Rao, S., 2008. Ice breakup date forecast with hybrid artificial neural networks. Proceedings of the 4th International Conference on Natural Computation, ICNC, 2: 414-418.

Kovachis, N. 2011. Patterns of river breakup timing and sequencing, Hay River, NWT. A thesis submitted to the Faculty of Graduate Studies and Research in partial fulfillment of the requirements for the degree of Master of Science in Water Resources Engineering, Department of Civil and Environmental Engineering, University of Alberta.

Mahabir, C., Hicks, F.E., and Robinson Fayek, A., 2006. Neuro-fuzzy river ice breakup forecasting system. Cold Regions Science and Technology 46(2): 100-112.

Maier, H.R. and Dandy, G.C., 2000. Neural networks for the prediction and forecasting of water resources variables: a review of modelling issues and applications. Environmental Modelling & Software 15(1), 101-124.

Maier, H.R., Jain, A., Dandy, G.C. and Sudheer, K.P., 2010. Methods used for the development of neural networks for the prediction of water resource variables in river systems: Current status and future directions. Environmental Modelling & Software 25(8), 891-909.

Massie, Darrell D., White, Kathleen D. and Daly, Steven F., 2002. Application of neural networks to predict ice jam occurrence, Cold Regions Science and Technology 35(2): 115-122.

Masters, T., 1993. Practical neural network recipes in C++. Academic, San Diego, California, 493pp.

Nzokou, F., Morse, B. and Quach-Thanh, T., 2009. River ice cover flexure by an incoming wave. Cold regions Science and Technology 55(2): 230–237.

Rumelhart, D. E., Hinton, G. E. and Williams, R. J., 1986. Learning representations by back propagating errors. Nature 323(9): 533-536.

Sarle, W.S., (ed.) 1997. Neural Network FAQ, periodic posting to the Usenet newsgroup comp.ai.neural-nets, URL: ftp://ftp.sas.com/pub/neural/FAQ.html.

Seidou, O., T. B. M. J. Ouarda, L. Bilodeau, M. Hessami, A. St-Hilaire and P. Bruneau (2006), Modeling ice growth on Canadian lakes using artificial neural networks, Water Resour. Res., 42, W11407, doi:10.1029/2005WR004622.

Shulyakovskiy, L.G. (Ed.), 1963. Manual of forecasting ice-formation for rivers and inland lakes. Manual of Hydrological Forecasting No. 4, Central Forecasting Institute of USSR. Translated from Russian 1966, Israel Program for Scientific Translations, Jerusalem, Israel.

Shulyakovskiy, L.G., 1972. On a model of the break-up process. Soviet Hydrology: Selected Papers 1, 21-27.

IBM SPSS, Inc., 2009. PASW® Regression 18.0 help files.

Stone, M., 1974. Cross-validatory choice and assessment of statistical predictions (with discussion). Journal of the Royal Statistical Society, Series B, 36, 111-147.

Ward Systems Group, Inc., 1995. NeuroShell 2 (Release 4.2) help files, URL: http://www.wardsystems.com/manuals/neuroshell2/.

White, K.D., 2003. Review of prediction methods for breakup ice jams. Canadian Journal of Civil Engineering, 30(1): 89-100.

Chapter 4 Long lead forecasting of spring peak runoff using Mamdani-type fuzzy logic systems[5]

4.1 Introduction

Breakup ice-jams are frequent on many northern rivers, particularly in the vicinity of river confluences, islands, tight channel bends and in deltas. Although there are beneficial aspects for northern eco-systems (e.g. Beltaos *et al.* 2006), the consequent severe floods that ice jams cause can also lead to significant property loss and even threat to human safety in riverside communities. The magnitude of the snowmelt runoff peak is generally one of the most significant controlling factors in determining potential breakup severity, because of its direct hydraulic influence on ice jam induced flood levels. Therefore it is of great potential value, in terms of ice jam flood preparedness planning, to be able to predict the magnitude of the peak snowmelt runoff hydrograph for communities threatened by spring ice jam floods.

Forecasting snowmelt runoff has been a very important practice in cold regions. Physically based snowmelt runoff modeling has been actively studied for decades (e.g. see DeWalle and Rango 2008; Ferguson 1999). Generally, these models

[5] A slightly condensed version of this chapter is being submitted to the *Journal of Cold Regions Science and Technology* with my thesis supervisors (F. Hicks and A. Robinson Fayek) as co-authors.

focus on the prediction of the snowmelt runoff process by the energy budget method, which is very data intensive. In northern regions, where the data network is sparse and the record is relatively short, there is seldom sufficient data for calibration and validation of the numerous model parameters involved. Thus, such data intensive models are often of limited value for the application of long lead-time ice jam flood forecasting in northern communities.

Compared to the long-term and large investments required to develop a physically based, distributed, hydrologic model under changing environmental conditions, more cost-efficient, flexible and robust soft computing methodologies (e.g. ANN models and fuzzy logic systems) offer promising alternatives. However, despite its attractive ability to self-learn using historical data, as a pure 'black-box' approach ANN model structures cannot be investigated analytically (e.g. see ASCE 2000a and 2000b). Also, for cases where there is only a small calibration data set, the ANN models' reliability in forecasting is still questionable (e.g. see Zhao *et al.* 2011). Therefore, the potential suitability of fuzzy logic systems for forecasting peak runoff during spring snowmelt was investigated in this study.

Since first proposed by Zadeh (1965), fuzzy set theory has been widely used in many problems. The concept of fuzzy sets is an extension of classic crisp set mathematics in which the bivalent membership (i.e. 0 or 1) is replaced with an interval (i.e. [0, 1]) of real numbers. Consequently, it is more suitable for dealing with imprecise data and the qualitative nature of vagueness of heuristic

knowledge, especially in the context of hydrological modeling for northern regions where data networks are sparse and records are short. For example, in this study, a spatially limited dataset of point-wise snowfall measurements was used to provide an index of late winter snow pack conditions over a whole basin. Two overlapping fuzzy sets can be used to capture the impreciseness of this index variable, for example, describing a particular case as "Low" to a degree of 0.4 and "Average" to a degree of 0.6. By using crisp inputs and outputs, a fuzzy logic system implements a nonlinear mapping from its input space to its output space. It works like an expert system by using fuzzy sets to describe expert knowledge (i.e. an "IF-THEN" rule base). Thus the primary advantages of a fuzzy logic model over an ANN model are its interpretability and transparency, and it is tolerant of imprecise data.

Although known as universal approximators (e.g. see Wang 1992; Kosko 1992), there is no single architecture or configuration generally employed in the design of a fuzzy logic system for a particular problem. Neither a construction method nor the determination of the size of the optimal fuzzy system have been developed theoretically (Castro and Delgado 1996). Though automatic rule generation and system optimization are possible by a hybrid approach of soft computing techniques, for example neuro-fuzzy (e.g. see Jang *et al.* 1997) or genetic algorithms (e.g. see Herrera 2008), the transparency of fuzzy logic systems is sacrificed if calibrated by any of these techniques. For example, in investigating the transferability of fuzzy logic systems Mahabir *et al.* (2006) demonstrated that

expert knowledge based fuzzy logic models outperform neuro-fuzzy models, especially for the extreme flood events. They also mentioned that a possible reason for this was that the rule base calibrated by ANNs introduced some site specific factors, which is not transferable from one site to another.

Although fuzzy logic systems are attracting more and more attention in water resources engineering research (e.g. see Mujumdar and Ghosh 2008), alternative methodologies for model development, such as the partitions of membership functions, generation of rule base (e.g. most appropriate one), the choices of inference operators and defuzzification methods, have seldom been systematically investigated. In most cases, model development has been conducted subjectively and so the models' sensitivity to these various component approaches is not known. Therefore, it was a particular goal of this study to conduct such investigations in order to achieve a better understanding of the fuzzy logic modeling approach.

In this chapter, the extraction of peak snowmelt runoffs from the available historical daily discharge data is first presented and assessed as a potential indicator of breakup flood severity with the Hay River, NWT Canada taken as the study case. Then the selection of the three long lead-time input variables and the impacts of the short-term meteorological data (e.g. rainfall and snowfall) on the long lead-time forecasting model are discussed. Next, the model configuration for the study case is introduced, followed by the detailed descriptions for developing

each component of the model. Finally the results of experiments on the models are discussed.

4.2 Description of study site and available data

The Hay River originates from the Rocky Mountains in northern British Columbia and Alberta, Canada. It flows northeast into Great Slave Lake in the Northwest Territories (Figure 4-1(a)), forming a small delta at the Town of Hay River (THR, Figure 4-1(b)). Due to the northerly flow direction of the Hay River, breakup commences in the upper (southern) portion of the basin first; as a result snowmelt runoff from the upper basin typically encounters strong competent ice in the lower basin, driving a highly dynamic breakup down the river. This combined with the fact that the ice on Great Slave Lake does not melt out until several weeks after river ice breakup, means that spring ice jams are an annual occurrence at the town site. Flooding tends to occur when the spring snowmelt runoff event is large, especially if the peak flow is coincident with the formation of ice jams. Thus any reliable breakup flood forecasting tool must include information regarding the expected snowmelt peak magnitude.

There is only a sparse network of hydrometeorological stations in the Hay River basin. As shown in Figure 4-1(a), there are four streamflow gauges operated by the Water Survey of Canada (WSC) along the main stem of the Hay River. Two are located in the upper basin: Chinchaga River near High Level (CRHL,

07OC001) and Hay River near Meander River (HRMR, 07OB003). The third is situated at the AB/NWT border (070B008) and the fourth is located 13km upstream of the town site Hay River near Hay River (HRHR, 07OB001). The border gauge only operates seasonally and reports only water levels, therefore, its data was not relevant to this study. Daily water levels and flow data from three remaining gauges were used in this study.

Two long term active climate stations, operated by Environment Canada (EC), were relevant to this study: High Level A (HLA, 3073146) is located near the upper basin at the Town of High Level, Alberta; and Hay River A (HRA, 2202400) is located in the lower basin at the THR. The historical daily data archives for these two stations include air temperature, rainfall, snowfall, precipitation and depth of snow on the ground. Additionally, there are also snow course survey data, e.g. snow water equivalent (SWE), available near the Town of High Level (07JF801, Alberta Environment 2011) and near the THR (07OB-SC02, Aboriginal Affairs and Northern Development Canada 2011) for a shorter period than the climate stations. Record periods for all of the raw historical data assembled for this study are summarized in Table 4-1. These data were processed to develop the data base of input and output variables discussed below.

4.3 Assessment of peak snowmelt discharge at HRHR and its relationship to breakup flood severity at THR

For both open water and ice affected flooding scenarios, peak flow is one of the most decisive factors. In the case of the Hay River, summer rainfall induced annual peak flows have never been a concern for the THR. It is high spring snowmelt runoff events combined with severe breakup ice jams that have caused all of the severe flood events in the history of the town. The spring peak discharge not only controls the water level directly from the viewpoint of hydraulics, it also affects the initiation of ice jams, which is another necessary condition for breakup ice-jam floods. Therefore, in the context of long lead forecasting of breakup ice-jam flooding, it is reasonable to investigate the peak snowmelt runoff as an indicator of flood severity associated with breakup ice jams. To assess the potential influence of the peak spring snowmelt discharge, Q_P, at HRHR on the breakup flood severity at the THR, the raw historical daily flow data at HRHR was used to extract Q_P. Next all of the data related to historical breakup at the town were collected from various sources and used to define breakup flood severity at THR. Then the relationship between the two was analyzed.

4.3.1 Extraction of Q_P at the three WSC gauges

On the Hay River, the peak spring snowmelt discharge, Q_P, usually occurs in late April or early May. It can either be prior to, along with, or after, the breakup event

at the town site. Great care was taken to correctly identify the Q_P for each year at all three WSC gauges. In some cases this was straightforward; for example, when there was only one single peak during the snowmelt period. However, because of the dynamic nature of breakup along the Hay River, discharge fluctuations due to variable ice effects are very common in the WSC spring daily flow data. These are not snowmelt peaks; they are typically either erroneous discharge interpretations (caused by assuming the validity of a winter rating curve in the backwater zone of an ice jam) or actual discharge fluctuations caused by ice jam release waves. For the purposes of this discussion, peaks associated with such ice affected discharge fluctuations during the breakup period are defined as Q_{MB}. Figure 4-2 illustrates one such example for the HRHR gauge from 1988; here the spring peak snowmelt discharge, Q_P, followed the ice clearing. This example illustrates how simply picking the largest value from a published table of mean daily flows could greatly overestimate the actual snowmelt runoff peak. Though Q_{MB} was not the primary focus of this study, it was also extracted from the historical data of HRHR for a comparison with Q_P to understand its impact to the breakup flood severity at the THR.

All the Q_P data were also extracted at the other two gauges (HRMR and CRHL) from the available daily flow data using the same methodology as for the HRHR gauge. However, it should be noted that for the HRMR and CRHL gauges, in some cases the ice effect on the flow hydrographs is not as obvious as that for the HRHR gauge, which made the identification of Q_P at these gauges more difficult.

Therefore, in this study, the timing of Q_P at the HRHR gauge was used to extract the most probable Q_P at the HRMR and CRHL gauge when the hydrographs showed more than one peak during spring snowmelt period. A good example of these cases is illustrated in Figure 4-2 for 1988: when both the Q_P for the HRHR and HRMR occurred on May 12, the most possible Q_P for the CRHL is the one on May 9 (*i.e.* three days ahead) compared to the other two on May 3 and May 20 because of the nearest approximation of the CRHL gauge to the HRMR gauge. The detailed information on all the historical Q_P for the three gauges can be found in Appendix C.

4.3.2 Determination of breakup flood severity at THR

Kovachis *et al.* (2011) summarize the information on the THR breakup flood severity dating back to 1984, based on historical flood descriptions in technical reports, personal accounts, and newspapers articles. Three qualitative descriptors were applied for all the cases: ‘severe flooding’, ‘some flooding’, and ‘no flooding’. ‘Severe flooding’ describes major events in which the flood extent and damage to property were extensive, as explicitly described in the available sources. ‘Some flooding’ refers to both minor and moderate flood events, since it was often the case that insufficient information was available to distinguish between the two. ‘No flooding’ refers to those events described as ‘quiet’ and unnoticeable in historical accounts.

4.3.3 Relationship between Q_P at HRHR and breakup flood severity at THR

It is possible to investigate a relationship between Q_P and breakup severity for those years in which Q_P is available at HRHR (1964 to 2010). Figure 4-3 shows the 47 ranked Q_P values at HRHR (Q_{P_HRHR} for short) coded according to breakup flood severity at the THR, illustrating that flooding events are more prone to occur when Q_{P_HRHR} is greater than or equal to the median value (635 m^3/s). Of the 24 cases falling in this range, there were 8 with 'severe flooding' (i.e. in 33% of the cases where $Q_P \geq 635$ m^3/s) and 9 cases (38%) with 'some flooding'. In contrast, of the remaining 23 cases, where Q_P was below the median value, there were no 'severe flooding' events and only 3 years when 'some flooding' occurred (i.e. only 13% of cases when $Q_P < 635$ m^3/s). This result suggests that Q_{P_HRHR} is a good indicator of expected ice jam flood severity at THR.

It is important to note that a high value of Q_{P_HRHR} did not always result in flooding (e.g. 1969) and, conversely, flooding did occur in some cases where Q_{P_HRHR} was relatively low (e.g. 2006, 2010, and 2001). To investigate this further, a comparison was made between the timing of Q_{P_HRHR} and the timing of ice clearing at the town site. (This time lag, in days, is provided over the bars in Figure 4-3.) It was found that, in most cases, where a high value of Q_{P_HRHR} came more than 4 days after ice clearing at the town site, there was no flooding at all (e.g. in 1969, 1967, 1987, 1964, 1976, 1975, and 1996). Because the ice jam formed in the community well before the snowmelt runoff hydrograph peaked, the

resulting ice jam was not high enough to cause flooding. There were two exceptions to this: in 1992 and 1986 where, Q_{P_HRHR} followed ice clearing by 10 and 7 days, respectively, but 'severe flooding' occurred. In these cases, despite the delayed snowmelt peak the ice jams still formed at relatively high discharges, due to a particularly dynamic breakup evolution (Gerard and Stanley 1988; Jasek *et al.* 1993). These variabilities illustrate the need to develop a more complex model to predict potential breakup severity. However, it is clear that any such model must depend heavily on a good prediction of Q_P, which was the focus of this modeling effort.

4.4 Screening of input variables for a long lead forecasting model of Q_P

The important factors controlling snowmelt runoff include the late winter snow pack condition, antecedent soil moisture conditions, the depth of frozen soil, the rate of energy influx causing snowmelt and, possibly, rain-on-snow effects. From the perspective of providing a long lead forecast of the snowmelt runoff peak (i.e. ~3 to 4 weeks in advance of breakup), the latter two factors would be unknowns. Therefore, only the first three variables were considered in this study. However, due to the potential significance of the rain-on-snow effect (e.g. see Todhunter 2001), the influence of spring rainfall on the snowmelt peak was assessed in order to facilitate an estimate of the range of error caused by this effect; this can be provided along with the long lead forecast.

To facilitate the development of the input variable dataset, two key dates were first defined from the daily air temperature data. The date of the onset of freezing degree-days, D_{OF}, was taken as the date of the first of five consecutive days of subzero daily air temperatures each fall. If a warm spell of more than 5 days of above freezing temperatures occurred, then the onset of freezing was reset as the date when the freezing air temperatures resumed (again requiring 5 consecutive days). The date of the onset of thawing degree-days, D_{OT}, was taken as the date of the first of five consecutive days of mean daily air temperatures above -5°C (so as to take into account the melting effect of maximum daily temperatures above freezing) each spring. If a cold spell of more than 5 days of below -5°C temperatures occurred, the date of the onset of thawing degree-days was reset as the date when above -5°C air temperatures resumed (again requiring 5 consecutive days). The period between D_{OF} and D_{OT} was then defined as the winter period and used to develop the three input variables.

4.4.1 Accumulated precipitation during the winter period

The late winter snow pack condition indicates the potential volume of snowmelt runoff. Many hydrological studies have used the pack's late winter snow water equivalent (SWE) and/or remotely sensed snow cover data to model the snowmelt runoff process. The spatial and temporal variations of snow pack conditions are generally used as the explanatory variables of these predictive models. Dyer (2008) used three snow cover parameters (i.e. the timing and value of the

maximum snow volume, and the duration of snowmelt) to predict the spring peak discharge using multiple linear regression analysis for five large North American watersheds. The best coefficient of determination (R^2) he obtained: 0.56, was for the high-latitude Yukon basin. He suggested that using more detailed SWE data would enhance model accuracy. Similarly, Yang *et al.* (2003) found that remotely sensed data describing snow cover extent can be used to predict spring discharge with acceptable accuracy. In particular, they studied the relation between streamflow and remotely sensed snow cover information (e.g. SWE and snow cover extent) in the Yukon River basin and found a general association of high (low) flow peak with high (low) maximum SWE over the basin. However, they also noted a much higher variability in peak flows than in the basin SWE, which suggested uncertainties in the reliability of the basin SWE data from remotely sensed data.

Basin-averaged SWE data, based on remote sensing images, are also available for the Hay River basin; however these data have been found to show very little annual variation. For example, Mahabir *et al.* (2006) showed the Hay River basin satellite SWE data had a standard deviation (SD) of only 5 mm over 24 years and absolutely no correlation to the snowfall data measured by Environment Canada ($R^2 < 0.05$). Yang *et al.* (2009) found a similar lack of variation in satellite SWE data for the Yukon River basin, with a SD of only 13 mm. Thus satellite SWE data are considered to be of questionable value to represent the true SWE over the Hay River basin.

In the Hay River basin, snow course surveys (i.e. direct snow depth and/or SWE measurements) are conducted only monthly and records date back only to 1986. In contrast, the daily snowfall/precipitation data records at the HLA and HRA climate station date back to 1968 (see Table 4-1). Therefore, to maximize the length of record available for this study, the accumulated precipitation during the winter period, AP_W, based on data from the HLA and HRA climate stations, were used to provide an index of the late winter snowpack condition over the upper and lower Hay River basin areas, respectively.

4.4.2 Water level at the onset of freeze-up

Soil infiltration loss during the snowmelt period reduces the direct runoff and, therefore, the magnitude of the snowmelt peak. Although it is not generally practical to measure soil moisture basin wide, and such data certainly do not exist for most northern basins such as the Hay River basin, reasonable indices of soil moisture are readily available. The most common is the antecedent precipitation index, or API (Gray 1970) which, in this context, would simply be a summation of all of the rainfall in the preceding open water season. However, API is generally more relevant to hydrologic modeling on an event by event basis, and a seasonal accumulation is not necessarily representative of soil moisture conditions in late fall just prior to freeze-up. In this application, actual groundwater levels would generally be a more robust indicator of basin soil moisture and since in late

fall/early winter the river level itself is an indicator of ground water levels, the daily average water level on the date of the onset of freezing degree-days (i.e. on D_{OF}), H_{OF}, was taken as an indicator for the antecedent soil moisture that would affect the infiltration loss of the snowmelt. A higher H_{OF} suggests a higher soil moisture content, which would limit the available infiltration storage volume and increase the snowmelt runoff peak. Conversely, a lower value of H_{OF} would be expected to be associated with a lower snowmelt runoff peak.

4.4.3 Accumulated degree-days of freezing during the winter period

The accumulated degree-days of freezing during the winter period, $ADDF_W$, was used to provide an indirect index to account for both snow sublimation and ground freezing effects. Mass loss due to snow sublimation is a very important component of the snow water balance; it can amount to as much as 15 to 32% of the snowfall (e.g. see MacDonald *et al.* 2008; Strasser *et al.* 2008; Hood *et al.* 1999), greatly reducing potential snowmelt runoff. Although it is very difficult to quantify snow sublimation through direct measurements, the accumulated degree-days of freezing during the winter period, $ADDF_W$, can be considered as an index of the factors that affect the sublimation loss during the snowfall accumulation period. For example, Yang *et al.* (2009) evaluated the compatibility of snow cover data in the Yukon River basin and found a wide range in the ratio of basin-averaged SWE to accumulated precipitation over the winter period, AP_W, (i.e. ratios of 0.37 to 1.20). The lower ratios were generally associated with high

values of AP_W and warm winters; while the higher ratios were associated with low values of AP_W and cold winters. Thus one would expect a positive correlation between the peak snowmelt runoff and $ADDF_W$; that is, greater snowmelt runoff after colder winters (i.e. winters with lower snow sublimation) and lesser snowmelt runoff after warmer winters (i.e. winters with greater snow sublimation).

The degree of ground freezing during the winter is also potentially important to snowmelt runoff, since the deeper the ground is frozen, the lower the infiltration loss expected during the snowmelt runoff period. Since deeper ground freezing (and thus lower infiltration loss) would be expected to be associated with larger values of $ADDF_W$, again it is expected that $ADDF_W$ would be positively correlated with the peak snowmelt runoff.

4.4.4 Effect of superimposed rainfall/snowfall during snowmelt runoff to Q_P

Incident intense rainfall is superimposed on snowmelt runoff when saturated soil layers are frozen and the infiltration loss is minimal. This can directly increase the spring snowmelt runoff and its peak. In addition, rainfall during this period can accelerate the snowmelt process substantially, also resulting in an increased snowmelt runoff peak. To assess the potential effect of spring rainfall events on Q_P, the following accumulated rainfall ratio for the spring snowmelt runoff period, ARR_S, was defined:

$$ARR_S = AR_S / AP_W \qquad [4-1]$$

where AR_S is the accumulated rainfall during the spring period and AP_W is the accumulated precipitation (snow plus rain) over the entire winter.

Figures 4-4(a) and (b) present the results of correlation analyses between ARR_S and the Q_P at HRMR (Q_{P_HRMR}) and HRHR (Q_{P_HRHR}), respectively. The goodness of fit (i.e. a linear regression model), R^2 are both very small for the two cases (0.119 and 0.017). The p values for the null hypothesis tests (i.e. the slope of the linear regression model is zero), 0.040 for Figure 4-4(a) and 0.390 for Figure 4-4(b), indicate that there is a statistically significant linear relationship between Q_{P_HRMR} and ARR_{S_HLA} (i.e. the ARR_S at HLA) and none between Q_{P_HRHR} and ARR_{S_HRA} (i.e. the ARR_S at HRA). Although this relationship is not very evident because of very small R^2 in Figure 4-4(a), it is interesting to note that when ARR_{S_HLA}, is greater than ~0.17, all but one of the Q_{P_HRMR} values are above the regression line (note the exception in 1982, when the accumulated winter precipitation was relatively small). Below this threshold, the Q_{P_HRMR} values are scattered around the regression line. Therefore, 0.17 was chosen as the threshold value for AAR_{S_HLA}, beyond which Q_{P_HRMR} has the potential to be significantly enhanced by the spring rainfall. Such cases cannot not be predicted with a long lead forecast model (since rainfall cannot be reliably predicted several weeks in advance). In addition, those cases in the historical record that fell into this

category were excluded when evaluating the long lead forecast model (1978, 1979, 1981, 1982, 1994, 1997, 2003, and 2007) leaving 28 years of record in the dataset. It was for the consistency purpose to discard the year 1982 though it was an exception case among other intense spring rainfall events. This will be further discussed in the model results. As Figure 4-4(b) illustrates, no comparable threshold was evident for the ARR_S at HRA (ARR_{S_HRA}).

A later snowfall event that occurs during the spring snowmelt period might be expected to diminish Q_P, by temporarily delaying the snowmelt, or it might enhance Q_P by adding additional SWE to the pack. To investigate whether there is a consistent tendency one way or the other, the following accumulated snowfall ratio for the spring snowmelt runoff period, ASR_S, was defined:

$$ASR_S = AS_S / AP_W \qquad [4-2]$$

where AS_S is the accumulated snowfall occurring during the spring snowmelt period.

As Figures 4-4(c) and (d) illustrate, the accumulated snowfall ratios during the spring snowmelt period at HLA (ASR_{S_HLA}) and HRA (ASR_{S_HRA}) show no significant relationship with Q_P (see the very small R^2 and very high p values), nor is any threshold value apparent. Therefore, there is no evidence that a late

snowfall (occurring during the snowmelt period) has any significant, consistent effect on Q_P.

Based on these data analyses, the six long lead-time input variables: AP_{W_HLA}, $ADDF_{W\_HLA}$, H_{OF_HRMR}, AP_{W_HRA}, $ADDF_{W\_HRA}$, and H_{OF_HRHR} were used to develop the predictive model for Q_{P_HRHR}. This enables a lead-time of approximately 3 to 4 weeks before breakup. Twenty-eight years of historical data were available to evaluate the model.

4.5 Configuration of the fuzzy logic system for Q_P at HRHR

To incorporate the spatial variation of contributing snowmelt to the peak flow at the basin outlet, the Hay River basin was divided into two sub-basins: the upper Hay River basin (i.e. upstream of the HRMR gauge) and the lower Hay River basin (i.e. downstream of the HRMR gauge). The configuration of the fuzzy logic system for Q_{P_HRHR} is illustrated by Figure 4-5: Submodel-1 and Submodel-2 were first developed to model Q_P for the upper basin (Q_{P_HRMR}) and the lower basin (Q_{P_Lower}), each using three of the six input variables; Q_{P_HRMR} and Q_{P_Lower} were then used as the inputs of Submodel-3 to determine the Q_P at the Hay River outlet (Q_{P_HRHR}). Note that there is no actual numerical output produced for Q_{P_Lower} in Submodel-2, only linguistic values (i.e. a fuzzy set). This highlights a key advantage of fuzzy logic models, in that they can even accept non-numerical linguistic values as inputs.

To determine the appropriate model structure for the sub-models, two types of fuzzy logic systems (FLS) were considered, Sugeno or Takagi-Sugeno type (Takagi and Sugeno 1985) and Mamdani-type (Mamdani and Assilian 1975). Both are commonly used in fuzzy control and fuzzy modeling (e.g. see Ying 2000). The primary distinction is in their different structures for "IF-THEN" rules. For the Sugeno-type, the consequent of each rule (i.e. the "THEN" part of each "IF-THEN" rule) is a (linear or nonlinear) function of the input variables; for the Mamdani-type, the consequent of each rule is a fuzzy set (i.e. a linguistic term). Though it is potentially more powerful, the Sugeno-type typically needs a large data set to reliably calibrate the function parameters for the consequent. By using linguistic terms for both the input ("IF" part) and the consequent, the Mamdani-type describes expert knowledge (e.g. rules of thumb) in a more intuitive manner by mimicking human thinking. As it is widely accepted for capturing expert knowledge more explicitly than the Sugeno-type, the Mamdani-type structure was applied for all the three sub-models in this study.

Figure 4-6 shows the flow chart of a Mamdani-type FLS, as well as an example of detailed model components, in this case for Submodel-1. The development of each of the following components was explored in detail for this study. In the FUZZIFICATION component, the input variables are classified into membership functions (MFs) based on linguistic terms. In the example shown, three linguistic terms ("Low", "Average", and "High") have been used to describe each of the

three input variables, resulting in a total of nine MFs to be defined in the model development. A key aspect of fuzzification is that the membership functions overlap such that particular values of an input variable can be classified (i.e. have non-zero membership) to some degree in more than one linguistic category. For example, as illustrated in Figure 4-6, an AP_{W_HLA} value of 90 mm has a membership degree of 0.30 in "Low" and "0.70" in "Average" (summing for a total membership of 1.00 overall). Thus, the input data is actually classified into sets of numbers, not just assigned qualitative descriptors. Membership functions are also used to classify all possible values of the output variable though, generally, more linguistic terms (than those used for the input variables) are employed. Figure 4-6 also illustrates an example for Q_{P_HRMR} under the DEFUZZIFICATION heading. Five linguistic terms ("Very Low", "Low", "Average", "High" and "Very High") were used for the output variable in this example.

In the INFERENCE component of a FLS, the "IF-THEN" rule base is developed, describing the outcomes for all possible combinations of the input variables. This is illustrated linguistically in Figure 4-6 under the INFERENCE heading; for example, IF all of the input variables are "Average" THEN, conceptually, the 'consequent' (i.e. the result for the output variable) could reasonably be expected to be "Average" as well (i.e. Rule 14). Again, this requires consideration of sets of numbers (specifically the degree of membership involved for each input variable in each category), not simply a qualitative assessment. As a result,

consideration of all possible inputs using the "IF-THEN" rule base and fuzzy operators produces an output fuzzy set. The degree of truth of each rule's consequent is first computed using an "AND" operator (e.g. MIN or PROD) to combine the linguistic terms of the fuzzified inputs (i.e. the "IF" part). To illustrate this for the MIN operator, consider an example in which the AP_{W_HLA} is 0.70 degree of "Average", $ADDF_{W\_HLA}$ is 0.60 degree of "Average", and H_{OF_HRMR} is 0.20 degree of "High". The THEN part (Q_{P_HRMR}) for this IF is 0.20 (i.e. the minimum of 0.70, 0.60, and 0.20) degree of "Average" by Rule 15 shown in Figure 4-6. When PROD is used, Q_{P_HRMR} will become 0.084 (i.e. the product of 0.70, 0.60, and 0.20) degree of "Average". Also the MIN and PROD produce the output MF shape in different ways: MIN clips the corresponding output MF at the validated degree of truth (see Figure 4-7(a)); PROD scales it by the validated degree of truth (see Figure 4-7(b)). All the MFs with a non-zero membership for Q_{P_HRMR} are then aggregated to form a complex output fuzzy set by the aggregation operator (e.g. MAX or BSUM). MAX and BSUM respectively choose the maximum and the sum (with a bound of 1.0) of all the degree of truth for each MF of the output variable. This would result in four different combinations of inference operators: MIN-MAX, MIN-BSUM, PROD-MAX, and PROD-BSUM. In the example provided in Figure 4-6, it is the shaded portion shown on the output variable membership functions illustrated under the DEFUZZIFICATION heading by the MIN-MAX operator.

DEFUZZIFICATION is then the final component of the FLS, in which the inference result (i.e. the output fuzzy set) is converted to a crisp value (e.g. a specific value of Q_{P_HRMR} in this example) or a linguistic term, by a specific algorithm. Details of the development of each of these FLS model components are discussed the following sections.

4.6 Development of the model components

Though it has been accepted that a fuzzy logic model can approximate any continuous function, there is not yet a general theory to guide the development of its component (i.e. the number and shape of MFs, rule base and inference operators, and the defuzzification method) and so multiple approaches still exist. Though other soft computing methods such as neural networks or genetic algorithms (e.g. see Jang *et al.* 1997; Herrera 2008) have been employed in the development of various fuzzy logic model components, the main weaknesses of such methods are that they reduce the transparency of fuzzy logic models and the resultant models may exhibit unreliability in cases with limited data sets (e.g. see Zhao *et al.* 2011). Therefore, in this study, each component of Submodel-1 was developed explicitly in a series of independent experiments. The results of these experiments were then used as guidelines for developing the components of the Submodel-2 and Submodel-3. Measured by the designed criterion indices, those configurations with best performance were chosen for the final model. The details of the designed experiments and indices are as follows.

4.6.1 Development of MFs

To determine the number and shape of MFs is very context specific. For most practical problems, the number of MFs for each variable should be no more than the number of conceptual entities that can readily perceived by a human being for that variable, which is typically between 3 and 7 MFs. However, a practical rule is to use as small a number as possible in order to make the model structure (e.g. the rule base) tractable by avoiding the problem of "rule explosion". Specifically, a complete rule base contains all the possible combinations of different MFs for each input variable; therefore, the number of rules required is equal to MF^n, where n is the number of input variables. As illustrated in the example in Figure 4-6, where 3 MFs (i.e. Low, Average and High) were used for each of the 3 input variables, 27 (i.e. 3^3) rules were required to complete the rule base. If 5 MFs are used, the size of rule base expands to 125 (i.e. 5^3); if 7 MFs are used, then 343 (i.e. 7^3) rules must be defined. Not only does it become conceptually intractable to define such a complex array of rules, it would require an extremely large set of data to reliably test and validate the resulting model. Given that only 28 years of data are available for evaluating the developed models in this study, if 7 MFs were employed for each input variable, then the vast majority of the 343 rules would not be evaluated; this would make the resulting rule base debatable. Therefore, 3 and 5 MFs for the input variables were considered in the study.

As mentioned earlier, often more MFs are used for the output variable than the input variables; this is done in an effort to make a smoother transition for the output MFs (Inform GmbH 2010). In this study, two schemes for the number of MFs for the input and output variables were implemented: the first one (I3O5) uses 3 MFs ("Low", "Average", and "High") for the input variables and 5 MFs ("Very Low", "Low", "Average", "High", and "Very High") for the output variable; the second one (I5O7) uses 5 MFs for the input variables and 7 MFs ("Extremely Low", "Very Low", "Low", "Average", "High", "Very High", and "Extremely High") for the output variable.

Once the number of MFs is determined, the characteristic points (e.g. the values associated with zero and full membership) for each variable can then be assigned; and the intermediate points can be interpolated either linearly or nonlinearly, resulting in a triangular, trapezoidal, Gaussian, or bell shape. Nguyen *et al.* (1994) showed that a piecewise linear function is the least sensitive (i.e. "the change in an input value x will lead to the smallest possible change in the value of membership") for FLSs. Mahabir *et al.* (2006) also found that the FLS did not appear to be sensitive to the shape of MFs in comparing results for linear and cubic spline shapes. Pedrycz (1994) showed that 50% overlapping between adjacent triangular MFs for the output variable produces zero defuzzification error using the centroid method. Therefore, in this study, triangular shape MFs were considered first.

To develop the optimal model, the following general constraints for constructing the MFs (e.g. see Pedrycz and Oliveira 1996) were also employed: (a) all the MFs must be normal (i.e. there exists at least one point having full membership); (b) only partial overlapping is allowed between two adjacent MFs such that no more than two linguistic terms are used for expressing the fuzziness of a crisp value; (c) all the MFs must be convex, i.e. their shapes should be unimodal; and (d) the universe of discourse (i.e. all possible values) for each variable should be fully covered; thus each point should have a non-zero membership value for at least one MF.

Following these general constraints, the statistics of the historical data for the input and output variables were used to develop their MFs. Specifically, zero and full memberships were first defined at some points for each MF; then linear interpolation was used to define the intermediate points. For example, the partitions of the MFs for the input and output variables tested in scheme I3O5 for the Submodel-1 are illustrated in Figure 4-8. For each of the input variables, three scenarios were tested for partitioning the MFs. For scenario (a): the zero percentile value (i.e. the minimum value in the historical record) was assigned full membership for L and zero membership for A(a) and H(a); the 50^{th} percentile value (i.e. the median value) was assigned full membership for A and zero membership for L(a) and H(a); and the 100^{th} percentile value (i.e. the maximum value) was assigned full membership for H(a) and zero membership for L(a) and A(a). These points of zero and full membership for each MF were then connected

by straight lines to form the full definitions of the MF (i.e. the solid line triangular shapes shown in Figure 4-8). For scenario (b), the points with the full membership of L and H were changed to range from the 0 to the 5^{th} percentile values for L(b) and from the 95^{th} to the 100^{th} percentile values for H(b), making the shapes of L(b) and H(b) trapezoidal, as shown in Figure 4-8(b). Scenario (c) was similar to scenario (b), except that the trapezoidal ranges extended from 0 to the 10th percentile values for L(c) and from the 90^{th} to the 100^{th} percentile value for H(c). These trapezoidal shapes for the "Low" and "High" MFs were intended to test if a range is better than a single point for representing the full membership zone for these extreme MFs. The corresponding partitions of MFs for the output variable in scheme I3O5 are shown in Figure 4-8(d). As explained above, two additional MFs classifications: "Very Low" (VL) and "Very High" (VH) were introduced. The 15^{th}, 20^{th} and 25^{th} percentile values were used to define the full membership range for L(a), L(b) and L(c), respectively; and the 85^{th}, 80^{th} and 75^{th} percentile values were used to define the full membership range for H(a), H(b) and H(c), respectively. For all scenarios, the L (or VL) and H (or VH) MFs are also extended backward or forward so that when the actual value of the variable is lower or higher than the historical minimum or maximum, they would be assigned a full membership of 1.

The partitions of MFs for the input and output variables in the scheme I5O7 for the Submodel-1 are shown in Figure 4-9. In this case, the three scenarios for the MFs for the input variables employed the same percentile points as were used for

as the output variable in scheme I3O5, (i.e. as in Figure 4-8(d). Two additional partitions were tested for the output variable's MFs in this case (Figure 4-9(d)): "Extremely Low" (EL) and "Extremely High" (EH). The percentile values for full membership of each MF were respectively 0([0, 2.5], [0, 5]), 15(17.5, 20), 30(32.5, 35), 50(50, 50), 70(67.5, 65), 85(82.5, 80), 100([97.5, 100], [95, 100]).

Due to the sensitivity of the defuzzification algorithm to definitions of the MFs of the output variable, different practical ranges were tested in choosing its universe of discourse. First the output was assumed to range only between the historical minimum and maximum values, as shown in Figure 4-8(d) and 4-9(d). Then the range was broadened beyond the historical minimum and maximum, first by 5% and then by 10%. These three sets of MFs for the output variables, combined with the 3 different input variable MF test scenarios and the two MF schemes (I3O5 and I5O7), resulted in a total of 18 experiments for testing partitions of the MFs for the input and output variables of Submodel-1.

4.6.2 Development of the rule base and inference operators

The rule base is the determinative and the most sensitive component of any FLS since it explicitly represents the knowledge of the system (Inform GmbH 2010). It directly defines the relationships between the MFs of the input and output variables. Although extreme cases can usually be defined by experts easily, interpretations of the relationships between input and output variables are often

considerably less definitive for the intermediate cases. Therefore, in this study, a correlation analysis of the input and output variables from the historical data set was used to assist in the rule base development, with the most correlated input variable considered to have the most significant impact on the output variable. Figure 4-10 presents the results of correlation analysis between the three input variables (AP_{W_HLA}, $ADDF_{W\_HLA}$, and H_{OF_HRMR}) and the output variable (Q_{P_HRMR}) for Submodel-1. As seen in Figure 4-10(a), the input variable, AP_{W_HLA}, had the strongest correlation to Q_{P_HRMR} (i.e. correlation coefficient (r) = 0.734). Therefore, the first guideline in developing the rule base was that the resulting MF (i.e. the linguistic term) for the output variable should not be much higher or lower than the corresponding MF for AP_{W_HLA}. Consider an example case for the I3O5 experiment where AP_{W_HLA} is "Low"; no matter what the other two inputs are, the output MF should be the same (i.e. "Low") or at least be a MF that overlaps with "Low" (i.e. "Very Low" or "Average"). The second input variable $ADDF_{W\_HLA}$ had the next strongest impact on Q_{P_HRMR} (i.e. r = 0.529 as shown in Figure 4-10(b)) and so was used to decrease these three possibilities to two. Continuing with the same example case, where the MF for AP_{W_HLA} is "Low", if $ADDF_{W\_HLA}$ is also "Low" then the output Q_{P_HRMR} should only be "Very Low" or "Low". Alternatively, if $ADDF_{W\_HLA}$ is "Average" or "High", the output Q_{P_HRMR} should only be "Low" or "Average". To narrow down the output MF for each rule to a single outcome the last input variable, H_{OF_HRMR}, was considered; however, given the lower correlation between this input variable and Q_{P_HRMR} (r = 0.088 shown in Figure 4-10(c)), it was not always easy to make a definitive judgement.

Therefore, for this study, three slightly different rule bases were developed for each scheme of experiments (i.e. I3O5 and I5O7), with each successive rule base assuming a slightly stronger influence of H_{OF_HRMR} compared to the previous. In addition, a fourth rule base was automatically generated in fuzzyTECH, using a qualitative interpretation of the correlation analysis as input (i.e. a 'very positive' correlation for AP_{W_HLA}, a 'somewhat positive' correlation for $ADDF_{W\_HLA}$ and a 'very small positive' correlation for H_{OF_HRMR}). Tables 4-2 and 4-3 show the four rule bases developed and tested for Submodel-1 for schemes I3O5 and I5O7, respectively. In these tables, RB1d and RB2d refer to the rule bases generated in fuzzyTECH.

Four rule bases were also developed and tested for Submodel-3. Since Q_{P_HRMR} shows a strong correlation with Q_{P_HRHR} (see Figure 4-11), it was considered to have a strong positive impact on the output. However, as there is no actual numerical value for the variable Q_{P_lower} on which to perform a correlation analysis, its impact on Q_{P_HRHR} was tested by the first three rule bases as shown in Table 4-4: in RB3a, Q_{P_HRHR} does not change with Q_{P_lower} and it is considered as the same as Q_{P_HRMR}; in RB3b, Q_{P_HRHR} changes slightly with Q_{P_lower} (e.g. the output is upgraded only when Q_{P_HRMR} is "high" or "very high"); in RB3c, Q_{P_HRHR} is more sensitive to Q_{P_lower} (e.g. when Q_{P_HRMR} is "very low", the output is degraded). As well, a fourth rule base, RB3d in Table 4-4, was generated in fuzzyTECH and used for a comparison with the former three. It should be noted that, when generating up the fuzzyTECH rule base (i.e. RB3d), Q_{P_lower} was

assumed to have a smaller positive impact on Q_{P_HRHR} than Q_{P_HRMR} because the lower basin represents only 30% of the whole basin area.

Apart from the design of these rule bases, the inference operators are also very important in the REFERENCE process as discussed above. In this study, four sets of fuzzy operators (i.e. MIN-MAX, MIN-BSUM, PROD-MAX, and PROD-BSUM) were all tested, along with each of the rule bases, to compare their impacts on model performance.

4.6.3 Experiments on choosing the defuzzification method

Defuzzification (or reconstruction) is the reverse process of fuzzification (i.e. it is the transformation of a fuzzy set into a representative crisp value). While not essential to all applications, it is desirable in most practical problems because crisp values can be more easily understood and explicitly compared. As with the choices of MFs and rule base, defuzzification is also a very sensitive component for a FLS (e.g. see Robinson Fayek and Sun 2001). Choosing a defuzzification method is very context specific as no one method is universally better than others. For most FLSs, two categories of defuzzification methods are used: one is used to achieve the most plausible value from the output fuzzy set; and the other is used for computing the best compromise value among all the MFs of the complex output fuzzy set. Those methods relevant to the former objective (achieving the most plausible value) include the mean-of-maximum (MoM), largest-of-

maximum (LoM) and smallest-of-maximum (SoM) methods. They only account for the part of the solution set with the highest degree of truth (e.g. the segment "*bc*" in Figure 4-12 for which the degree of membership is the highest, 0.60) by selecting a typical value, e.g. mean (i.e. $(x_b+x_c)/2$) for MoM, largest (i.e. x_c) for LoM, or smallest (i.e. x_b) for SoM. These methods are often used in pattern recognition and classification applications when a plausible solution is most appropriate.

The latter objective (computing the best compromise value) is most commonly achieved using the center-of-area (CoA) method (also known as the centroid or center-of-gravity method) or the center-of-maximum (CoM) method. The COA method computes the horizontal coordinate of the centroid of the polygon for the output fuzzy set (e.g. the centroid of polygon "*abcdefgh"* in Figure 4-12), as expressed by Equation $[4-3]$.

$$\bar{x}_{COA} = \frac{\int_{x_a}^{x_h} x\mu_x dx}{\int_{x_a}^{x_h} \mu_x dx} \qquad [4-3]$$

where x denotes the Q_{P_HRMR} as in Figure 4-12; μ_x denotes the degree of membership at a specific value of x (e.g. at the solid line in Figure 4-12).

Due to the intensive computing requirements of the CoA method, fuzzyTECH® uses a "fast CoA" (FCoA) method to approximate it, which neglects the

overlapping portion between the different parts of the output fuzzy set (e.g. the shaded area in Figure 4-12). This method has a much higher computational efficiency than the real CoA algorithm and has been proven to provide sufficient accuracy for the vast majority of applications (Inform GmbH 2010).

The CoM method computes the weighted average of the values at its maximum degree of truth for each part of the output fuzzy set, as expressed by Equation $[4-4]$.

$$\bar{x}_{COM} = \frac{\sum \mu_{MF} * \overline{x_{MF}}}{\sum \mu_{MF}} \qquad [4-4]$$

where μ_{MF} denotes the degree of truth for a specific MF, e.g. 0.6 for "L", 0.4 for "A" and 0.3 for "H" in Figure 4-12; $\overline{x_{MF}}$ donates the average value at which the MF achieves its full membership, e.g. the horizontal coordinate of the peak of the triangular shape "L" (x_L), "A" (x_A), and "H" (x_H) in Figure 4-12; when the peak of a MF is a range (e.g. a trapezoidal shape), the mid-point value of the range is used.

In this study, the latter category of defuzzification methods, e.g. CoA (approximated by FCoA in fuzzyTECH) and CoM, were considered more appropriate to this specific application because they provide the best comprise value among all the fuzzy sets of the output variable. Nevertheless, one method of

the former category (e.g. MoM) was also used for the purpose of comparison as it only considers the fuzzy set with the highest membership.

4.6.4 Numerical measurement criteria for model performance

The performance of FLMs can be evaluated by comparing the model outputs with actual observations in the historical record. In this study, two sets of numerical indices were used to assess the model performance. The root mean squared error (RMSE) (Equation $[4-5]$) was first chosen as an index to assess the crisp output.

$$RMSE = \sqrt{\frac{\sum_{i=1}^{N}\left(Q_i - \widehat{Q}_i\right)^2}{N}} \qquad [4-5]$$

where Q_i and $\widehat{Q}_i$ are the i^{th} observed and modeled values of Q_P, respectively and N is the total number of historical observations available for comparison (e.g. 28 in this study).

The total error (TE) was used as another index for assessing the model performance, as it is useful from the perspective of qualitative forecasting. TE was defined as the sum of the false positive errors (PE) and false negative errors (NE). To calculate PE or NE, the universe of discourse of the output variable Q_P was first divided into 5 (for the I3O5 scheme) or 7 (for the I5O7 scheme) sub-

ranges by the points of intersection of the defined MFs. Each of the sub-ranges was assigned the linguistic term (i.e. MF) which has the highest membership for the values in this sub-range. In cases where the memberships for two adjacent terms were both 0.5, the higher (or right-hand side) term was chosen to be conservative in the context of flood forecasting. For example, as shown by Figure 4-13, the linguistic terms used for the sub-ranges of Q_P in the I3O5 scheme were "Very Low" (VL), "Low" (L), "Average" (A), "High" (H), and "Very High" (VH). Both the observed and modeled values of Q_P were transformed to their corresponding linguistic terms by the interval values of each sub-range. These categorized values of measured and modeled Q_P were then compared to determine the PE and NE: PE is the count of the modeled outputs, which are "H" or "VH" and higher than the corresponding actual values; and NE is the count of the modeled outputs lower than the corresponding actual values, which are "H" or "VH".

4.7 Results and discussions

To determine the best configuration for the fuzzy logic model, a series of experiments were first conducted for Submodel-1, as summarized in Table 4-5. In each of the two schemes of experiments, different number of partitions of MFs for the input and output variables were used, (i.e. I3O5 used 3 partitions for the input variables and 5 partitions for the output variable and I5O7 used 5 partitions for the input variables and 7 partitions for the output variable). As well, different shapes

of MFs (e.g. all triangular shapes and combinations of triangular and trapezoidal shapes) were tried. This resulted in a total of 18 experiments for Submodel-1. Four groups of rule bases were also tried for each experiment to test the impacts of different input variables to the output variable (as discussed earlier). For each rule base, four inference operators (i.e. MIN-MAX, MIN-BSUM, PROD-MAX, and PROD-BSUM) were tried. Finally, three different defuzzification methods were tested. All of model variations were tested and compared against the historical data to determine the best configuration for Submodel-1 and this optimal configuration was then adopted for Submodel-2. A series of experiments were then designed for Submodel-3, as shown by Table 4-6, adopting the MF partitions from Submodel-1. Four rule bases, four inference operators and three defuzzification methods were tested; and the configuration with the best performance compared to the historical data was chosen for the final model. The following discussion presents the results of the various test experiments and comparisons.

4.7.1 Results of experiments on Submodel-1

The quantitative criterion index (i.e. RMSE) and the qualitative criterion index (i.e. TE) were used separately to assess the relative performance of the different experimental configurations for Submodel-1. In terms of RMSE, the results for of all 18 experiments are summarized in Table 4-7, which shows the best RMSEs for the different configurations of Submodel-1 and their corresponding TE, PE, and

NE. These results suggest that the performances in RMSE were more or less consistent for all the 18 experiments, within a narrow range from 90 to 99 m^3/s and this variation is considered negligible in the context of flood forecasting at this site. However, the corresponding qualitative error index, TE, has a wider range, from 4 to 8, for these experiments. It was found that using 5 partitions of MFs for the input variables (i.e. experiments I5O7-a1 to I5O7-c3) does not result in any better performance compared to using 3 partitions (i.e. experiments I3O5-a1 to I5O5-c3). For each of the 9 experiments in each scheme (i.e. of the same number of partitions of MFs), RMSEs were also consistent within a narrow range, (e.g. from 90 to 98 m^3/s for I3O5 and from 94 to 99 m^3/s for I5O7). The minimum RMSE of 90 m^3/s was achieved in experiment I3O5-c1 with rule base RB1c, using PROD-MAX and the CoM defuzzification method. The corresponding TE for this experiment was 7, with 4 PEs and 3 NEs, respectively. As discussed in Section 4.6.2, the rule base RB1c includes the input variable H_{OF} with a somewhat strong influence on the output variable Q_{P_HRMR}. This is not the same indication as shown in Figure 4-10 (c) (i.e. very poor correlation between the two). This finding suggests that the linear correlations do not explain the physical rules. From this point of view, more research is needed to investigate more comprehensive techniques to develop the rule base of fuzzy logic systems.

Similar results were also found when TE was used as the criterion to select the best performance for the 18 experiments designed in this study, as shown in Table 4-8. The biggest difference between these TEs is 3, with the minimum being 4

and the maximum 7. The I5O7 partitions did not have a better result than the I3O5 partitions, and were even worse in many cases. The corresponding RMSEs for each of the best TEs were generally greater than those shown in Table 4-7. This suggests that the two performance indices used in this study are not consistent with each other (i.e. the configuration with the best RMSE is not the one with the lowest TE). However, given the relatively tight range in RMSE for all experiments, and the fact that the RMSE for the two experiments with the lowest TE (I3O5-a1 and I3O5-a2) was only 8 m^3/s higher than the minimum RMSE of 90 m^3/s (for experiment I3O5-c1), It seems that TE is a more robust and practical index of model performance. Since I3O5-a1 had the simplest partition of MFs (e.g. all triangular shape) of the two experiments with the lowest TE, this configuration was considered as the optimal one for Submodel-1.

The comparison between the modeled and observed Q_{P_HRMR} is shown in Figure 4-14, where the division of the five sub-ranges (i.e. the linguistic terms) is also illustrated. From the perspective of flood forecasting, the model has a very good performance in the H and VH events, for which only one VH event (1992) was underestimated as an H event. This can be explained by the fact that there was an intense rainfall event of 16 mm just prior to the runoff peak in that year. Though this rainfall was not quite high enough to exceed the threshold (i.e. ARR_{S_HLA} = 0.17) for classification as having a significant effect on Q_{P_HRMR}, it appears that the AP_W was relatively high and the combined effect was enough to nudge the actual runoff peak event from H to VH. Of the A events, three were

overestimated as H (1976, 1987, and 1991). In all the three years, the AP_W was very high and they were predicted as H events. Although the VL and L events are not really of great importance when assessing this model's performance, it should be noted that they did seem to be slightly overestimated by this model. However, in the context of flooding forecasting, these results are not interpreted as false positive errors because they could not cause any real concern in terms of advanced warning.

4.7.2 Results of the final model performance

In this study, there was no numerical value for the output variable of Submodel-2, i.e. Q_{P_Lower}. Considering the knowledge based nature of the FLS and the similar characteristics of the upper and lower Hay River basin, the best configuration for Submodel-1 was adapted for the development of Submodel-2: the I3O5-a1 (3 for the input variables and 5 for the output variable) partitions of MFs with the triangular shape, RB1c, PROD-BUSM inference operator and CoA defuzzification method. The outputs of these two sub-models were then used as the intermediate inputs (see Inform GmbH 2010) of Submodel-3. As discussed above, similar experiments were implemented to test the four rule bases (i.e. RB3a, RB3b, RB3c, and RB3d shown in Table 4-4), the inference operators and the defuzzification methods. The same indices were also used to assess the performances of different configurations of Submodel-3.

The results in terms of RMSE for all experiments are shown in Table 4-9. The minimum RMSE has a range of 23 m^3/s from 168 m^3/s for RB3d to 191 m^3/s for RB3c. Also the corresponding TE for each configuration is different: 5 for RB3d and 8 for RB3c. The results on TE for all experiments are also shown in Table 4-10, where the same configuration for RB3d has the best performance of all. Therefore, the configuration for the RB3d with the MIN-MAX inference operator, CoM defuzzification method was chosen as the optimal one for Submodel-3.

The comparison between the modeled and observed Q_{P_HRHR} is shown in Figure 4-15. It is apparent that two (1983 and 1976) of the four PEs are just located at the border of the A and H sub-ranges. Of the remaining two PEs for the final model (1991 and 1990), the former can likely be explained by weather conditions occurring after the 'forecast' date. Specifically, in 1991, there was a 6-day long cold snap just before the runoff peak and so not all the snow at HRA had melted when peak came. The only NE was for the year 1985, which was one of the biggest flood events in the THR. In this year, there was an intense rainfall of 18.1 mm at HRA in the three days just prior to the peak.

4.7.3 Corrections of underestimate of Q_P for the rainfall events during snowmelt period

In the context of flood forecasting it is very important to quantify the exacerbation of the snowmelt peak flow caused by rainfall during the snowmelt runoff period.

For this purpose the 8 discarded events from the historical records, for which significant spring rainfall occurred (see Section 4.4.4), were tested to assess Submodel-1 and Submodel-3. It was found that for Q_{P_HRMR} (Submodel-1), the errors of these events were *all* negative (i.e. the peak runoff discharge was underestimated, as would be expected) and were very scattered when plotted against ARR_{S_HLA}, as shown in Figure 4-16(a). An interesting point is that the eight cases can be divided into two groups: one with small errors and prediction falling into the correct category as the observations when ARR_{S_HLA} was below 0.20 (as indicated in Figure 4-16(a)); and the other with greater errors when ARR_{S_HLA} was over 0.20. For the latter group, the errors averaged 248 m^3/s (ranging from 109 to 360 m^3/s), which resulted in all the 6 cases where High or Very High events were incorrectly categorized by the model as less severe (i.e NE). For Submodel-3, the result is shown in Figure 4-16(b): when ARR_{S_HLA} was below 0.20 (2 cases), the error was very small, 20 m^3/s and 34 m^3/s, respectively (positive, not shown in the figure); otherwise, Q_{P_HRHR} was underestimated with an average of 313 m^3/s (ranging from 193 to 490 m^3/s), which caused 4 High events to be classified as less severe (4 NEs). This implies that a better threshold value of ARR_{S_HLA} for screening rainfall events might be 0.20 for the Hay River basin (not 0.17, as was originally assumed). It is also worthwhile to note that sporadic rainfall events that occur during the snowmelt runoff period may be of less significance, in terms of increasing the spring runoff peak, compared to intense rainfall storms, even when the total rainfall amount is greater. A good example of this occurred in 1982 (see Figure 4-16(a) and (b)) when the ARR_{S_HLA} was as high as 0.51, but was scattered

over a prolonged duration (23 days), thus the resulting errors in the Q_{P_HRMR} and Q_{P_HRHR} predictions were not large.

4.8 Sensitivity of model performance to inference operators and defuzzification methods

The effects of using different inference operators and defuzzification methods on model performance were compared for Submodel-1 (e.g. the I3O5-a1 experiment with RB1c) and Submodel-3 (e.g. the experiment with RB3d). The results for Submodel-1 are shown in Figure 4-17. The resulting RMSE was comparable for the CoA and CoM defuzzification methods, (both categorized as seeking a compromise result). However, when the MoM defuzzification method was used, larger RMSEs resulted (see Figure 4-17(a)). Model results were also relatively insensitive to the type of inference operator; as seen in Figure 4-17(a) for the same defuzzification method, the RMSEs for different inference operators were very close to each other. In contrast, the other performance index, TE (shown in Figure 4-17(b)) shows more variability in the model results: the CoA method gave the best results among the three defuzzification methods for each inference operator and for this defuzzification method (CoA), TE also showed some sensitivity to inference operators. It had a minimum value of 4 for PROD-BSUM and a maximum value of 6 for MIN-MAX. The MoM method gives the worst TE and RMSE of all cases. This indicates that MoM method is not as useful as CoA and CoM to this application, which has been discussed above (i.e. MoM only

accounts for partial output fuzzy set). The relative performance of the CoA and CoM methods were very similar in terms of RMSE, though the CoA method gave a slightly better result than the CoM in terms of TE.

The results for Submodel-3 are shown in Figure 4-18. Again, the resulting RMSE was not sensitive to inference operators under the same defuzzification method (see Figure 4-18(a)), and it was much higher when MoM was used compared to the results for CoA and CoM. The resulting TE, shown in Figure 4-18(b), was also more sensitive to defuzzification methods than inference operators: there was no difference greater than 1 for all operators under the same defuzzification method; there was the greatest difference (i.e. 2) for the MIN-BSUM operator with the CoA and CoM methods.

It should be noted that the optimal versions of Submodel-1 and Submodel-3, involved different choices for the inference operator and defuzzification method. This illustrates the fact that there is not one universal approach that will be ideal for all scenarios. Therefore, a good practice is to try them all and to then choose the one with the best performance.

4.9 Interpreting Q_{P_HRHR} in terms of breakup flood severity at THR

Figure 4-19 shows the distributions of occurrences of historical breakup events at THR for each partition of Q_{P_HRHR} in Submodel-3 (note the record data before

1975 were also included though they were not considered in assessing the models). It is apparent that most of the severe flooding events fall into the partitions of “High” and “Very High”, with the exception of one event (2003), which was “Average”. The corresponding percentages of each kind of breakup events are also shown in Figure 4-19. This information can be used to develop some preliminary guidelines for predicting breakup severity at THR:

1) When Q_{P_HRHR} is “Low” or “Very Low”, there is very little likelihood that a flooding event will occur;
2) When Q_{P_HRHR} is “Average”, the likelihood of a non-flooding event is about twice that for a flooding event (~2 in 3 likelihood for non-flooding, compared to ~1 in 3 likelihood of at least some flooding occurring). Also if flooding does occur, the likelihood of it being severe is small (only about 1 in 5 of actual flooding events are likely to be severe);
3) When Q_{P_HRHR} is “High”, there is a very strong likelihood (~3 in 4) that a flooding event will occur; and it is just as likely to be a severe flood event as it is to be a moderate or minor flood event;
4) When Q_{P_HRHR} is “Very High”, it is almost certain that a flooding event will occur; and the chance of a severe flooding event is twice as much as that a moderate or minor flooding event.

Although these preliminary guidelines are useful, it is important to remember that there is still a great amount of uncertainty in long lead-time forecasts (e.g. ~3 to 4 weeks ahead of breakup), as discussed earlier (see Section 4.3.3). A high Q_{P_HRHR}

does not necessarily cause any flooding at THR when it comes after breakup and the flow during the breakup is not high. Also, for long lead-time forecasting, the actual meteorological conditions just prior to breakup or during the snowmelt runoff period are unknown when the prediction is made. Thus in practice, occurrences such as intense rainfall events can affect the snowmelt peak, and thus the potential breakup severity. Based on the available historical data for the case of the Hay River, it is estimated that, for cased where the ARR_{S_HLA} is greater than 0.20, Submodel-3 may underestimate Q_{P_HRHR} by ~300 m^3/s.

4.10 Summary

A reliable long lead forecasting of breakup ice-jam flood severity is of extreme importance for protecting properties and human lives in northern communities. In this study, the peak snowmelt runoff during breakup was assessed as an indicator of breakup flood severity, using the Town of Hay River as the test case. Due to a sparse network and short record of hydrometeorological data in remote northern regions, the techniques of fuzzy set and fuzzy logic were applied to make optimal use of limited data and available heuristic knowledge. Specifically, a Mamdani-type fuzzy logic system was developed to model the peak runoff at the Town of Hay River using three long lead-time variables: the accumulated precipitation during winter, the accumulated degree-days of freezing during winter and the local river water level at the onset of freeze-up. The Hay River basin was also

divided into two sub-basins to incorporate the spatial variations of the contributions to the snowmelt runoff at the outlet.

By designing a series of experiments for the different configurations of the submodels, it was found that the optimal fuzzy logic model could provide very good performance for the “High” and “Very High” events. Overall, there was only one “Very High” event that was underestimated (because of an intense rainfall just prior to the peak runoff). The possible error range due to rainfall events were also assessed by evaluating the model using those data with a ratio of accumulated rainfall to the winter precipitation in the upper basin higher than 0.20. It resulted in an underestimation error of ~300 m^3/s for the peak snowmelt runoff at the basin outlet.

Preliminary guidelines for predicting the breakup severity based on the expected peak snowmelt runoff were also provided. However, it should be noted that some uncertainty exist when the peak comes later than the breakup event. The timing of snowmelt peak and breakup can only predicted using the short lead-time meteorological data (e.g. air temperature and rainfall). This needs to be further investigated.

Table 4–1: List of hydrometeorological data used in this study.

Data source	Data type	Station/gauge name (ID)	Duration of record
WSC	daily discharge and water level	HRHR (07OB001)	1964-2010
		HRMR (07OB003)	1975-2010
		CRHL (07OC001)	1970-2010
EC	daily air temperature, rainfall, snowfall, total precipitation, and depth of snow on the ground	HRA (2202400)	1964-2010
		HLA (3073146)	1968-2010
Alberta Environment	late winter SWE	High Level (07JF801)	1986-2010
Aboriginal Affairs and Northern Development Canada	late winter SWE	THR(07OB-SC02)	1982-2010

Table 4–2: The four rule bases tested in scheme I3O5 for Submodel-1.

Rule No.	IF			THEN Q_{P_HRMR}			
	AP_{W_HLA}	$ADDF_{W\_HLA}$	H_{OF_HRMR}	in RB1a	in RB1b	in RB1c	in RB1d
1	L	L	L	VL	VL	VL	VL
2	L	L	A	VL	VL	VL	VL
3	L	L	H	VL	VL	***L***	***L***
4	L	A	L	L	L	L	L
5	L	A	A	L	L	L	L
6	L	A	H	L	***A***	***A***	L
7	L	H	L	A	A	***L***	***L***
8	L	H	A	A	A	A	A
9	L	H	H	A	A	A	A
10	A	L	L	L	L	L	L
11	A	L	A	L	L	L	***A***
12	A	L	H	L	L	***A***	***A***
13	A	A	L	A	A	A	A
14	A	A	A	A	A	A	A
15	A	A	H	A	***H***	***H***	A
16	A	H	L	H	H	***A***	***A***
17	A	H	A	H	H	H	H
18	A	H	H	H	H	H	H
19	H	L	L	A	A	A	A
20	H	L	A	A	A	A	A
21	H	L	H	A	A	***H***	***H***
22	H	A	L	H	H	H	H
23	H	A	A	H	H	***VH***	H
24	H	A	H	H	***VH***	***VH***	H
25	H	H	L	VH	VH	VH	***H***
26	H	H	A	VH	VH	VH	VH
27	H	H	H	VH	VH	VH	VH

Note: the italics indicate the differences between RB1b, RB1c, and RB1d and RB1a.

Table 4–3: Four rule bases tested in scheme I5O7 for Submodel-1.

Rule No.	IF			THEN Q_{P_HRMR}			
	AP_{W_HLA}	$ADDF_{W\_HLA}$	H_{OF_HRMR}	in RB2a	in RB2b	in RB2c	in RB2d
1	VL	VL	VL	EL	EL	EL	EL
2	VL	VL	L	EL	EL	EL	EL
3	VL	VL	A	EL	EL	EL	EL
4	VL	VL	H	EL	EL	EL	EL
5	VL	VL	VH	EL	EL	***VL***	***VL***
6	VL	L	VL	EL	EL	EL	EL
7	VL	L	L	EL	EL	EL	EL
8	VL	L	A	EL	EL	EL	***VL***
9	VL	L	H	EL	EL	***VL***	***L***
10	VL	L	VH	EL	***L***	***VL***	***L***
11	VL	A	VL	VL	VL	VL	***L***
12	VL	A	L	VL	VL	VL	***L***
13	VL	A	A	VL	VL	VL	***L***
14	VL	A	H	VL	***L***	***L***	***L***
15	VL	A	VH	VL	***L***	***L***	***L***
16	VL	H	VL	L	L	***VL***	L
17	VL	H	L	L	L	***VL***	L
18	VL	H	A	L	L	L	L
19	VL	H	H	L	L	L	L
20	VL	H	VH	L	L	L	***A***
21	VL	VH	VL	L	L	***VL***	L
22	VL	VH	L	L	L	L	L
23	VL	VH	A	L	L	L	***A***
24	VL	VH	H	L	L	L	***A***
25	VL	VH	VH	L	L	L	***A***
26	L	VL	VL	VL	VL	VL	VL
27	L	VL	L	VL	VL	VL	***L***
28	L	VL	A	VL	VL	VL	***L***
29	L	VL	H	VL	VL	VL	***L***
30	L	VL	VH	VL	VL	***L***	***L***
31	L	L	VL	VL	VL	VL	***L***
32	L	L	L	VL	VL	VL	***L***
33	L	L	A	VL	VL	VL	***L***
34	L	L	H	VL	VL	***L***	***L***
35	L	L	VH	VL	***A***	***L***	***L***
36	L	A	VL	L	L	L	L
37	L	A	L	L	L	L	L

Rule No.	IF			THEN Q_{P_HRMR}			
	AP_{W_HLA}	$ADDF_{W\_HLA}$	H_{OF_HRMR}	in RB2a	in RB2b	in RB2c	in RB2d
38	L	A	A	L	L	L	L
39	L	A	H	L	***A***	***A***	***A***
40	L	A	VH	L	***A***	***A***	***A***
41	L	H	VL	A	A	***L***	A
42	L	H	L	A	A	***L***	A
43	L	H	A	A	A	A	A
44	L	H	H	A	A	A	A
45	L	H	VH	A	A	A	A
46	L	VH	VL	A	A	***L***	A
47	L	VH	L	A	A	A	A
48	L	VH	A	A	A	A	A
49	L	VH	H	A	A	A	A
50	L	VH	VH	A	A	A	A
51	A	VL	VL	L	L	L	L
52	A	VL	L	L	L	L	L
53	A	VL	A	L	L	L	L
54	A	VL	H	L	L	L	L
55	A	VL	VH	L	L	***A***	L
56	A	L	VL	L	L	L	L
57	A	L	L	L	L	L	L
58	A	L	A	L	L	L	***A***
59	A	L	H	L	L	***A***	***A***
60	A	L	VH	L	***H***	***A***	***A***
61	A	A	VL	A	A	A	A
62	A	A	L	A	A	A	A
63	A	A	A	A	A	A	A
64	A	A	H	A	***H***	***H***	A
65	A	A	VH	A	***H***	***H***	A
66	A	H	VL	H	H	***A***	***A***
67	A	H	L	H	H	***A***	***A***
68	A	H	A	H	H	H	***A***
69	A	H	H	H	H	H	H
70	A	H	VH	H	H	H	H
71	A	VH	VL	H	H	***A***	***A***
72	A	VH	L	H	H	H	H
73	A	VH	A	H	H	H	H
74	A	VH	H	H	H	H	H

Rule No.	IF			THEN Q_{P_HRMR}			
	AP_{W_HLA}	$ADDF_{W\_HLA}$	H_{OF_HRMR}	in RB2a	in RB2b	in RB2c	in RB2d
75	A	VH	VH	H	H	H	H
76	H	VL	VL	A	A	A	A
77	H	VL	L	A	A	A	A
78	H	VL	A	A	A	A	A
79	H	VL	H	A	A	A	A
80	H	VL	VH	A	A	***H***	A
81	H	L	VL	A	A	A	A
82	H	L	L	A	A	A	A
83	H	L	A	A	A	A	A
84	H	L	H	A	A	***H***	A
85	H	L	VH	A	***VH***	***H***	A
86	H	A	VL	H	H	H	***A***
87	H	A	L	H	H	H	***A***
88	H	A	A	H	H	H	H
89	H	A	H	H	***VH***	***VH***	H
90	H	A	VH	H	***VH***	***VH***	H
91	H	H	VL	VH	VH	***H***	***H***
92	H	H	L	VH	VH	***H***	***H***
93	H	H	A	VH	VH	VH	***H***
94	H	H	H	VH	VH	VH	***H***
95	H	H	VH	VH	VH	VH	***H***
96	H	VH	VL	VH	VH	***H***	***H***
97	H	VH	L	VH	VH	VH	***H***
98	H	VH	A	VH	VH	VH	***H***
99	H	VH	H	VH	VH	VH	***H***
100	H	VH	VH	VH	VH	VH	VH
101	VH	VL	VL	H	H	H	***A***
102	VH	VL	L	H	H	H	***A***
103	VH	VL	A	H	H	H	***A***
104	VH	VL	H	H	H	H	***A***
105	VH	VL	VH	H	H	***VH***	H
106	VH	L	VL	H	H	H	***A***
107	VH	L	L	H	H	H	H
108	VH	L	A	H	H	H	H
109	VH	L	H	H	H	***VH***	H
110	VH	L	VH	H	***EH***	***VH***	H
111	VH	A	VL	VH	VH	VH	***H***

Rule No.	IF			THEN Q_{P_HRMR}			
	AP_{W_HLA}	$ADDF_{W\_HLA}$	H_{OF_HRMR}	in RB2a	in RB2b	in RB2c	in RB2d
112	VH	A	L	VH	VH	VH	***H***
113	VH	A	A	VH	VH	***EH***	***H***
114	VH	A	H	VH	***EH***	***EH***	***H***
115	VH	A	VH	VH	***EH***	***EH***	***H***
116	VH	H	VL	EH	EH	EH	***H***
117	VH	H	L	EH	EH	EH	***H***
118	VH	H	A	EH	EH	EH	***VH***
119	VH	H	H	EH	EH	EH	EH
120	VH	H	VH	EH	EH	EH	EH
121	VH	VH	VL	EH	EH	EH	***VH***
122	VH	VH	L	EH	EH	EH	***VH***
123	VH	VH	A	EH	EH	EH	***VH***
124	VH	VH	H	EH	EH	EH	EH
125	VH	VH	VH	EH	EH	EH	EH

Note: the italics indicate the differences between RB2b, RB2c, and RB2d and RB2a.

Table 4–4: Four rule bases applied for Submodel-3.

Rule No.	**IF**		**THEN Q_{P_HRHR}**			
	Q_{P_HRMR}	Q_{P_Lower}	in RB3a	in RB3b	in RB3c	in RB3d
1	VL	VL	VL	VL	VL	VL
2	VL	L	VL	VL	VL	VL
3	VL	A	VL	VL	***L***	***L***
4	VL	H	VL	***L***	***L***	***L***
5	VL	VH	VL	***L***	***L***	***L***
6	L	VL	L	L	***VL***	L
7	L	L	L	L	L	L
8	L	A	L	L	L	L
9	L	H	L	***A***	***A***	***A***
10	L	VH	L	***A***	***A***	***A***
11	A	VL	A	A	***L***	A
12	A	L	A	A	A	A
13	A	A	A	A	A	A
14	A	H	A	***H***	***H***	A
15	A	VH	A	***H***	***H***	A
16	H	VL	H	H	***A***	***A***
17	H	L	H	H	H	***A***
18	H	A	H	H	H	H
19	H	H	H	***VH***	***VH***	H
20	H	VH	H	***VH***	***VH***	*H*
21	VH	VL	VH	VH	***H***	***H***
22	VH	L	VH	VH	VH	***H***
23	VH	A	VH	VH	VH	***H***
24	VH	H	VH	VH	VH	VH
25	VH	VH	VH	VH	VH	VH

Note: the italics indicate the differences between the rules RB3b, RB3c, and RB3d and the rule RB3a.

Table 4–5: Design of experiments on the Submodel-1.

Experimental scheme	Membership function partitions	Rule base	Inference operator	Defuzzification method
I3O5	a). all triangular shape 1. historical range only; 2. extended by 5% for the historical minimum and maximum; 3. extended by 10% for the historical minimum and maximum b). composite of triangular and trapezoidal shape 1 1. historical range only; 2. extended by 5% for the historical minimum and maximum; 3. extended by 10% for the historical minimum and maximum c). composite of triangular and trapezoidal shape 2 1. historical range only; 2. extended by 5% for the historical minimum and maximum; 3. extended by 10% for the historical minimum and maximum	RB1a; RB1b; RB1c; RB1d	MIN-MAX; MIN-BSUM; PROD-MAX; PROD-BSUM	CoA; CoM; MoM
I5O7		RB2a; RB2b; RB2c; RB2d	MIN-MAX; MIN-BSUM; PROD-MAX; PROD-BSUM	CoA; CoM; MoM

Table 4–6: Design of experiments on the Submodel-3.

Experiment schemes	MF partitions	Rule base	Inference operator	Defuzzification method
adopted based on tests of Submodel-1		RB3a; RB3b; RB3c; RB3d	MIN-MAX; MIN-BSUM; PROD-MAX; PROD-BSUM	CoA; CoM; MoM

Table 4–7: Results of experiments on the Submodel-1 when RMSE was used as the criterion.

No.	Rule base	Inference operators	Defuzzification	RMSE, m^3/s	TE	PE	NE
I3O5-a1	RB1c	PROD-BSUM	CoA	98	4	3	1
I3O5-a2	RB1c	PROD-BSUM	CoA	98	4	3	1
I3O5-a3	RB1c	PROD-BSUM	CoA	99	6	5	1
I3O5-b1	RB1c	PROD-MAX	CoA	94	6	5	1
I3O5-b2	RB1c	PROD-MAX	CoA	96	6	5	1
I3O5-b3	RB1c	PROD-MAX	CoA	98	6	5	1
I3O5-c1	***RB1c***	***PROD-MAX***	***CoM***	***90***	***7***	***4***	***3***
I3O5-c2	RB1c	PROD-MAX	CoM	91	7	4	3
I3O5-c3	RB1c	PROD-MAX	CoM	92	7	4	3
I5O7-a1	RB2b	MIN-BSUM	MoM	98	8	4	4
I5O7-a2	RB2b	MIN-BSUM	MoM	99	8	4	4
I5O7-a3	RB2b	MIN-BSUM	MoM	99	8	4	4
I5O7-b1	RB2d	MIN-BSUM	CoA	98	9	2	7
I5O7-b2	RB2d	MIN-BSUM	CoA	97	8	2	6
I5O7-b3	RB2d	MIN-BSUM	CoA	96	8	2	6
I5O7-c1	RB2b	MIN-MAX	CoA	96	7	3	4
I5O7-c2	RB2b	MIN-MAX	CoA	95	7	3	4
I5O7-c3	RB2b	MIN-MAX	CoA	94	7	3	4

Note: the italics indicate the one with the best performance.

Table 4–8: Results of experiments on the Submodel-1 when TE was used as the criterion.

No.	Rule base	Inference operators	Defuzzification	TE	PE	NE	RMSE, m^3/s
I3O5-a1	***RB1c***	***PROD-BSUM***	***CoA***	***4***	***3***	***1***	***98***
I3O5-a2	RB1c	PROD-BSUM	CoA	4	3	1	98
I3O5-a3	RB1b	MIN-BSUM	CoM	4	3	1	108
I3O5-b1	RB1c	PROD-BSUM	CoM	5	4	1	97
I3O5-b2	RB1c	PROD-BSUM	CoM	5	4	1	98
I3O5-b3	RB1c	PROD-BSUM	CoM	5	4	1	100
I3O5-c1	RB1c	PROD-MAX	CoA	7	5	2	90
I3O5-c2	RB1c	PROD-MAX	CoA	6	5	1	93
I3O5-c3	RB1a	PROD-BSUM	CoA	6	3	3	112
I5O7-a1	RB2a	PROD-BSUM	CoM	5	2	3	116
I5O7-a2	RB2a	MIN-MAX	CoM	5	2	3	115
I5O7-a3	RB2a	MIN-MAX	CoM	5	2	3	116
I5O7-b1	RB2a	MIN-BSUM	CoM	5	2	3	114
I5O7-b2	RB2a	MIN-BSUM	CoM	5	2	3	115
I5O7-b3	RB2a	MIN-BSUM	CoM	5	2	3	116
I5O7-c1	RB2a	MIN-BSUM	CoM	6	2	4	120
I5O7-c2	RB2a	MIN-BSUM	CoM	6	2	4	122
I5O7-c3	RB2a	MIN-BSUM	CoM	6	2	4	123

Note: the italics indicate the one with the best performance.

Table 4–9: Results of experiments on the Submodel-3 when RMSE was used as the criterion.

No.	Rule base	Inference operators	Defuzzification	RMSE, m^3/s	TE	PE	NE
1	RB3a	MIN-BSUM	CoA	174	7	4	3
2	RB3b	MIN-MAX	CoA	191	7	5	2
3	RB3c	MIN-BSUM	CoA	191	8	7	1
4	***RB3d***	***MIN-MAX***	***CoM***	***168***	***5***	***4***	***1***

Note: the italics indicate the one with the best performance.

Table 4–10: Results of experiments on the Submodel-3 when TE was used as the criterion.

No.	Rule base	Inference operators	Defuzzification	TE	PE	NE	RMSE, m^3/s
1	RB3a	MIN-BSUM	CoM	7	6	1	176
2	RB3b	MIN-MAX	CoA	7	5	2	191
3	RB3c	MIN-MAX	CoA	7	5	2	195
4	***RB3d***	***MIN-MAX***	***CoM***	***5***	***4***	***1***	***168***

Note: the italics indicate the one with the best performance.

(a)

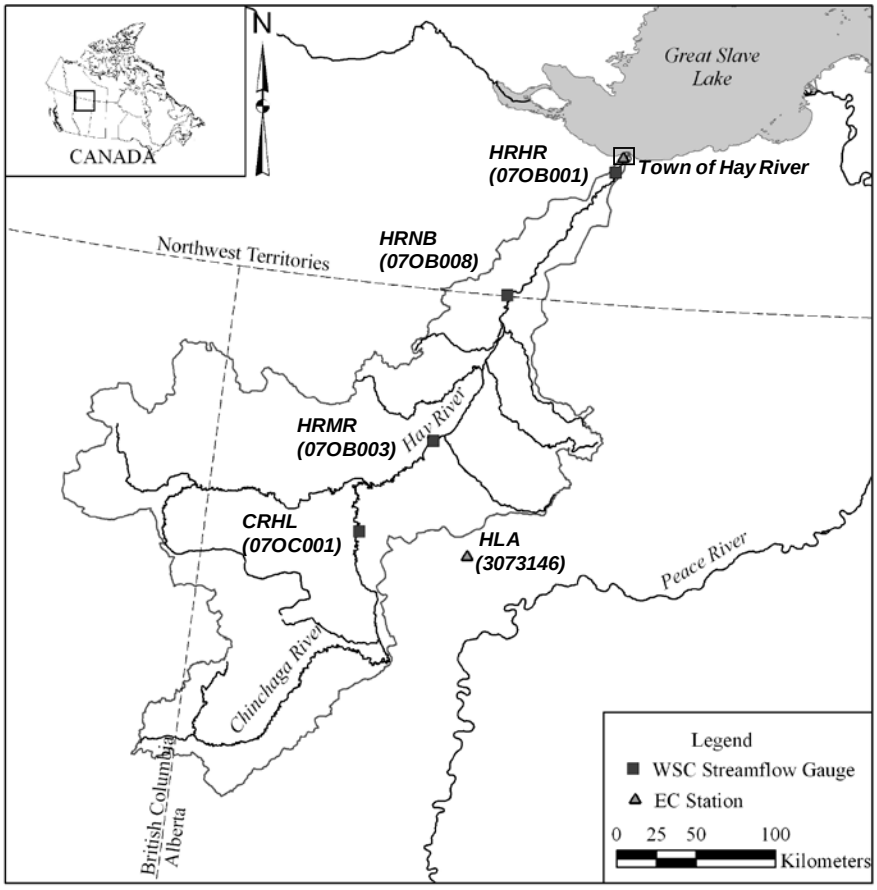

(b)

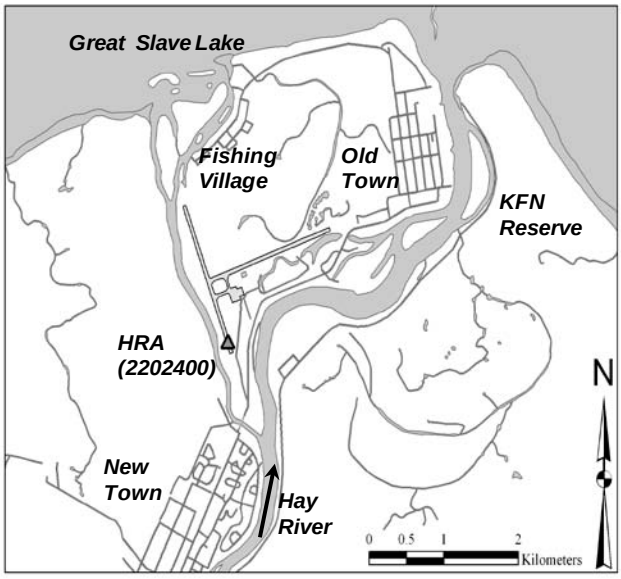

Figure 4–1: Map of (a) the Hay River basin and (b) the Town of Hay River.

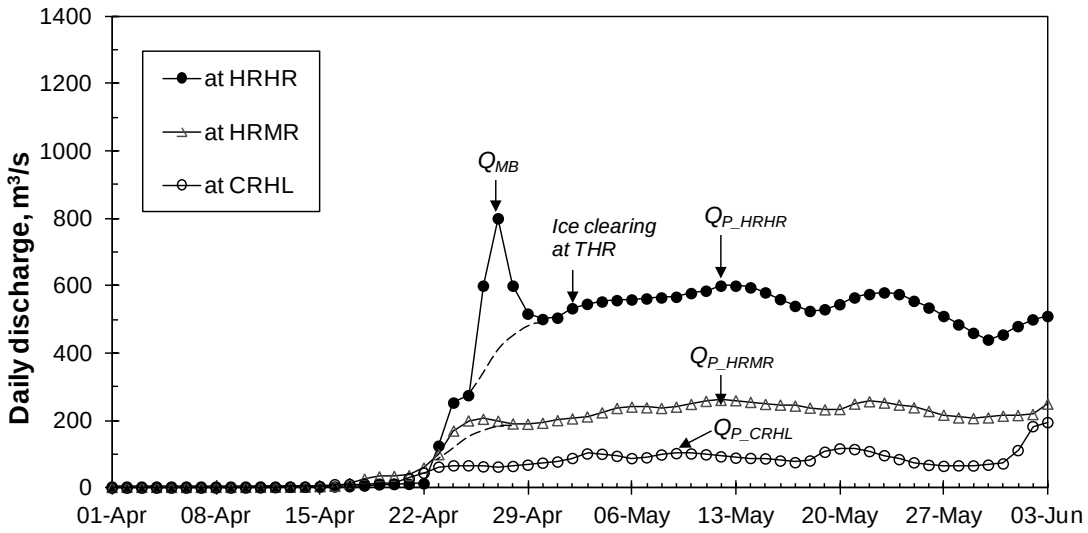

Figure 4–2: An example of an ice affected discharge hydrograph at the HRHR WSC gauge for 1988. Note: The dashed line is the assumed snowmelt runoff hydrograph (i.e. estimated ice effects separated).

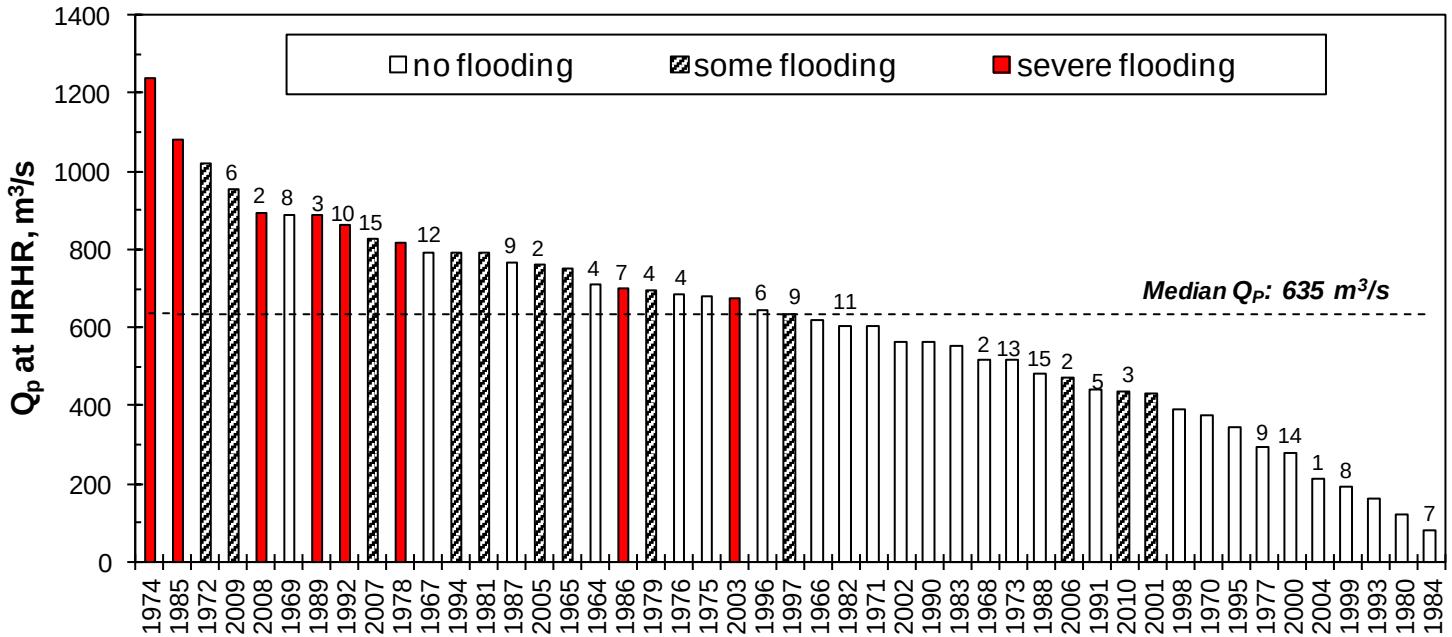

Figure 4–3: Historical Q_P at HRHR coded according to breakup flood severity at the THR. Note that the number above the bar indicates the number of days between ice clearing at the THR and Q_P (no number shown means that Q_P occurred before ice clearing at the THR).

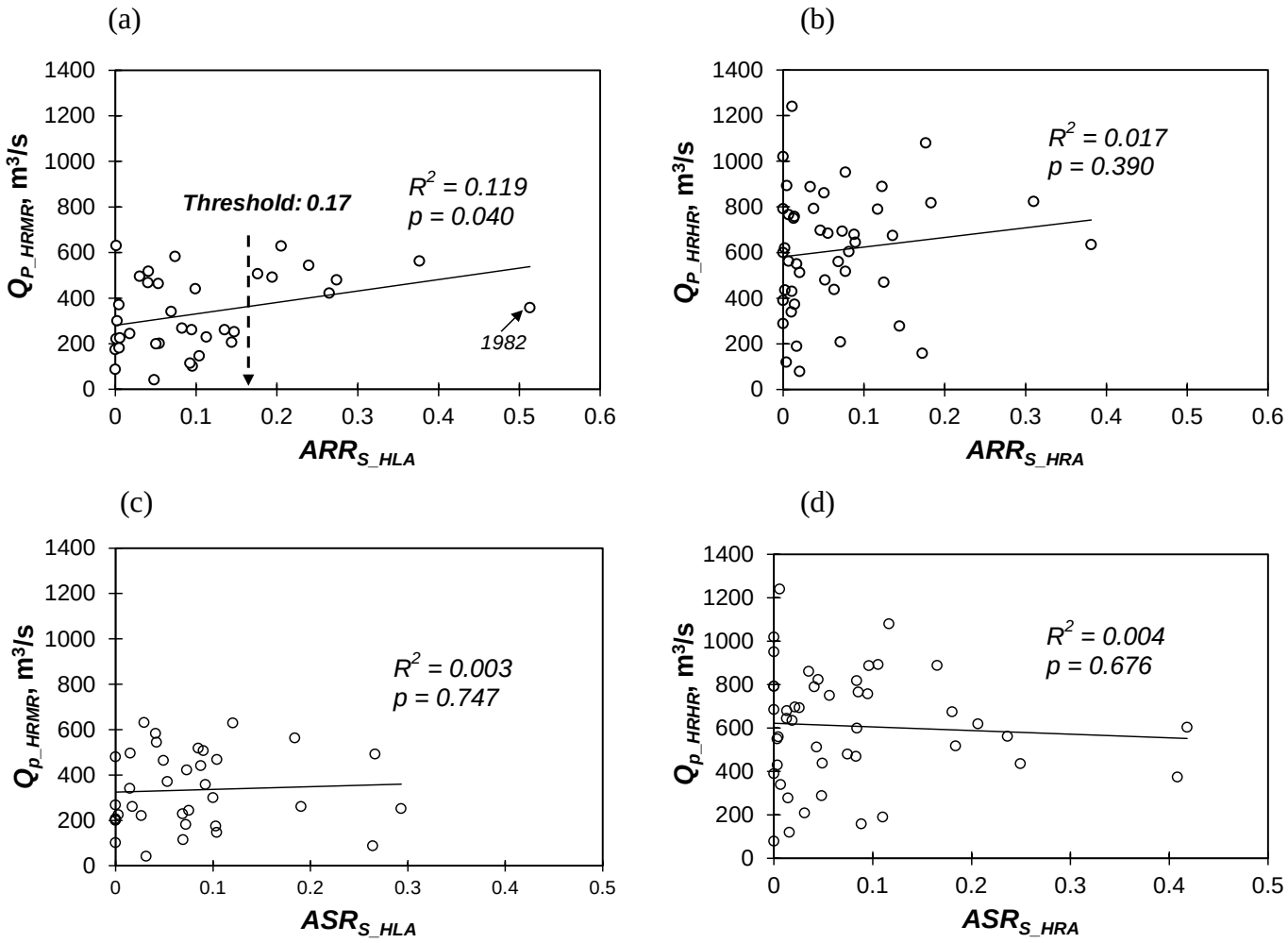

Figure 4–4: Influence of spring rainfall and snowfall during snowmelt to Q_p by correlation analysis between (a) Q_{p_HRMR} and ARR_{S_HLA}; (b) Q_{p_HRHR} and AAR_{S_HRA}; (c) Q_{p_HRMR} and ASR_{S_HLA}; (d) Q_{p_HRHR} and ASR_{S_HRA}. Note the sample sizes for each case are respectively 36, 46, 36, and 46.

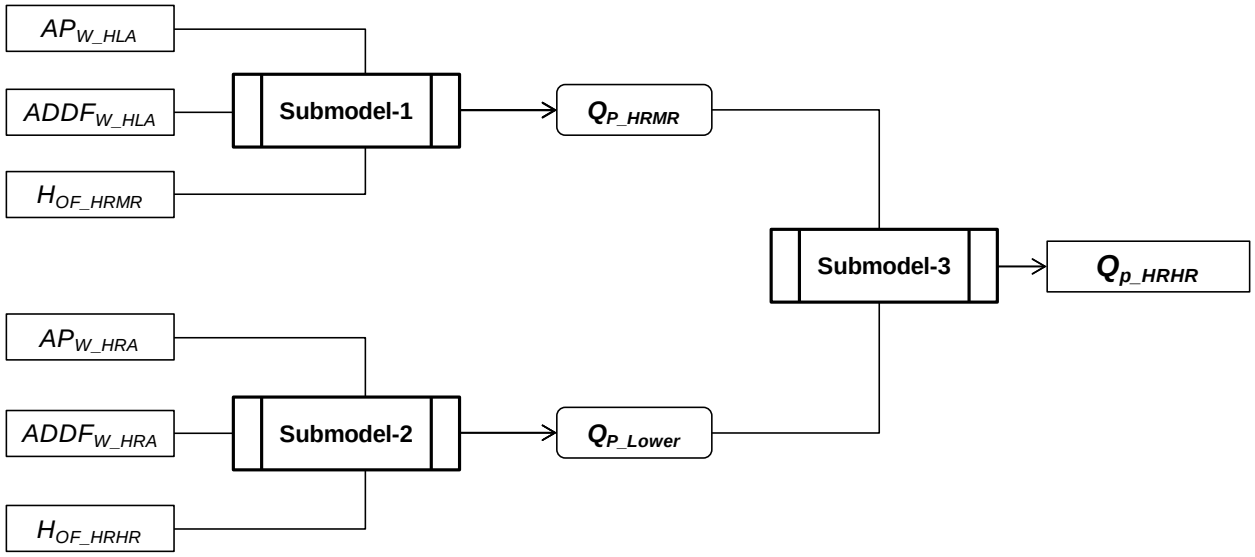

Figure 4–5: Configuration of the fuzzy logic system for predicting Q_{P_HRHR}.

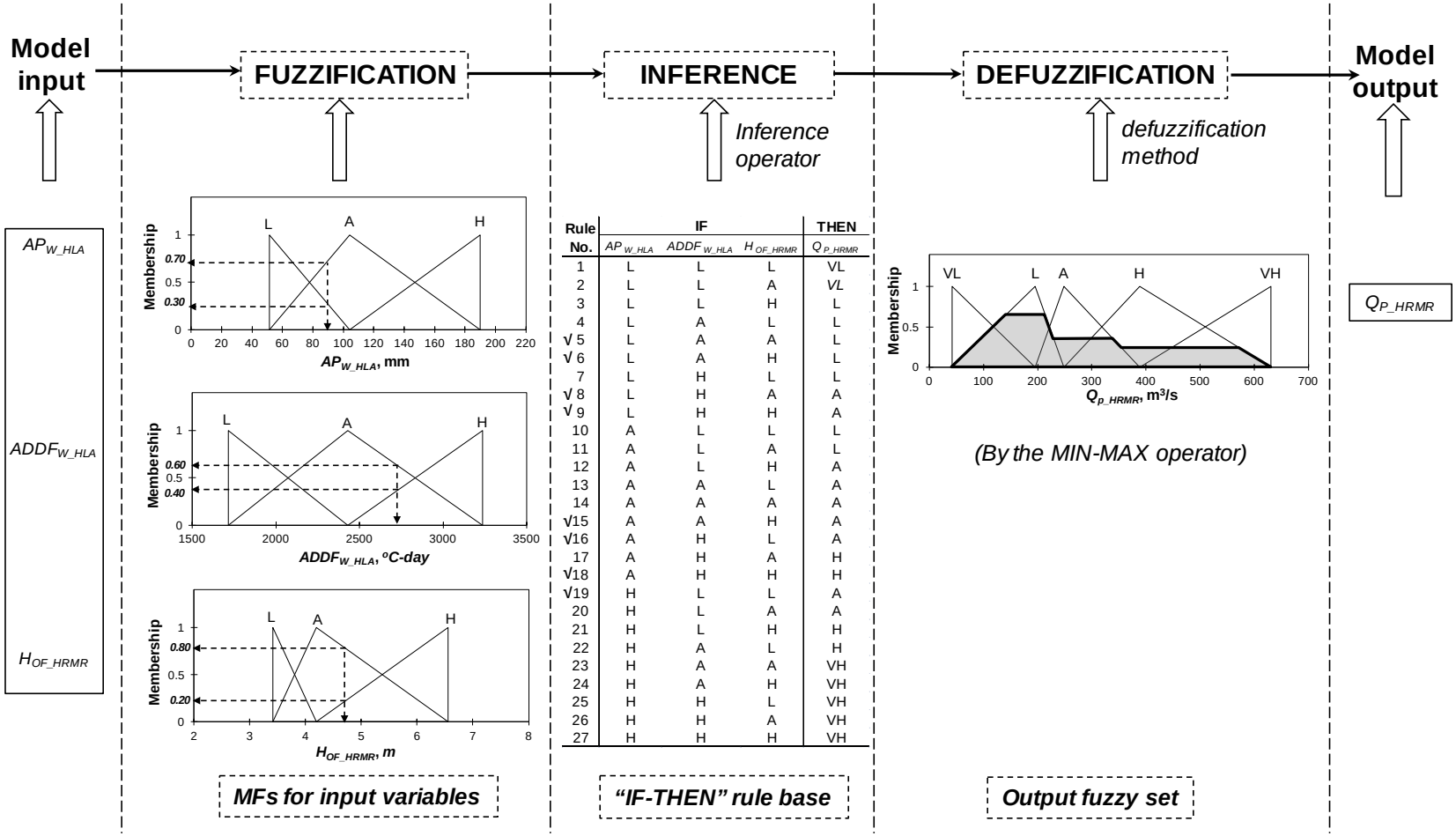

Figure 4–6: Flow chart for a Mamdani-type FLS and an example of components of Submodel-1. Note: the symbol"√" indicates the rules associated with the given example input; the shaded area in the output MF indicates the output fuzzy set (e.g. the result of inference for the given example input and rule base) by the MIN-MAX operator.

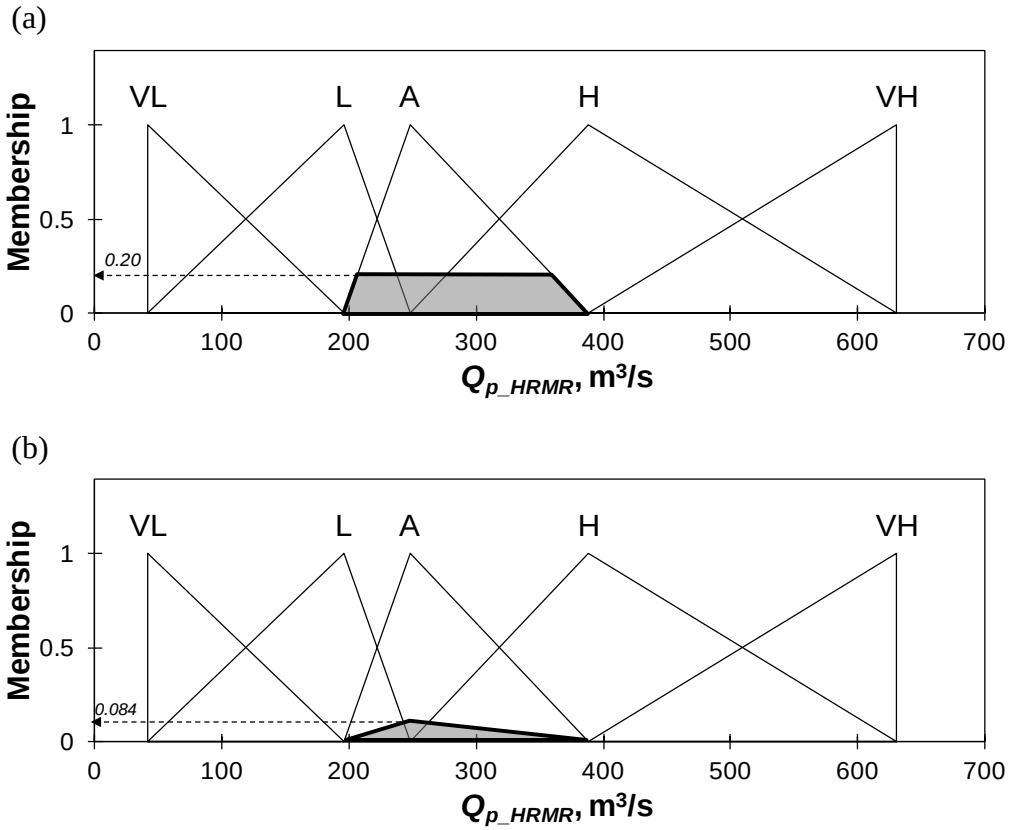

Figure 4–7: Different operators in INFERENCE component for producing the output MF: (a) MIN (clip); (b) PROD (scale).

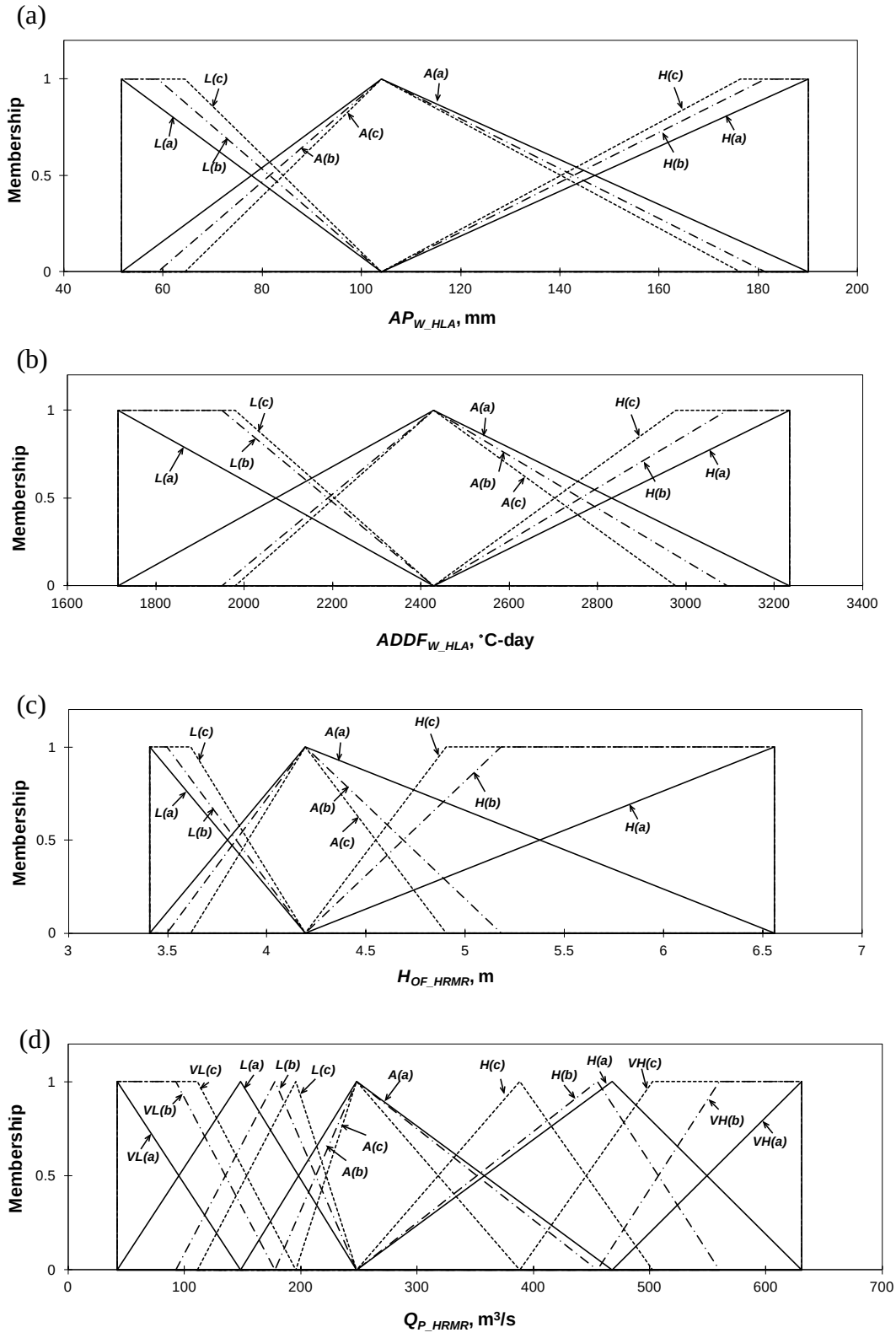

Figure 4–8: Three different partitions of MFs for the input and output variables in the I3O5 scheme.

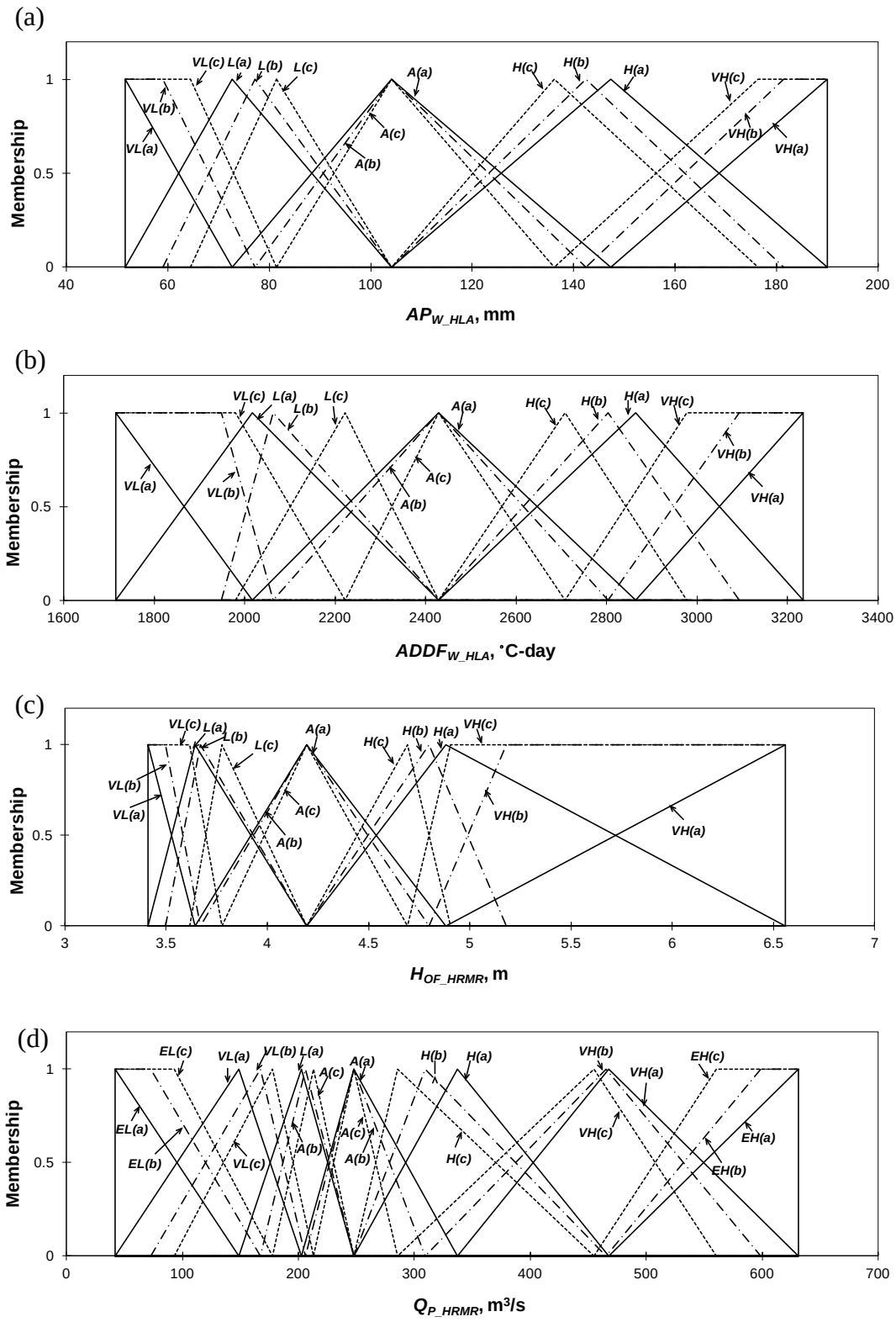

Figure 4–9: Three different partitions of MFs for the input and output variables in the I5O7 scheme.

(a)

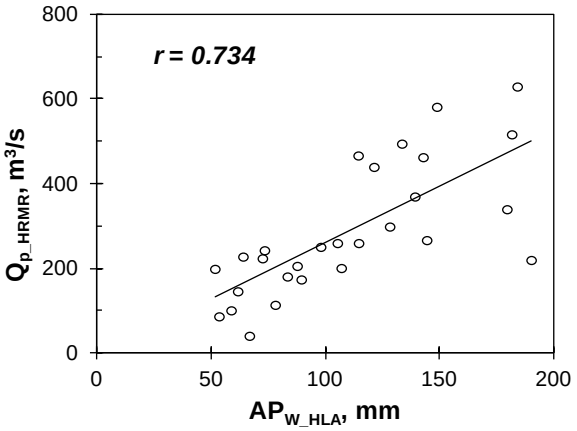

(b)

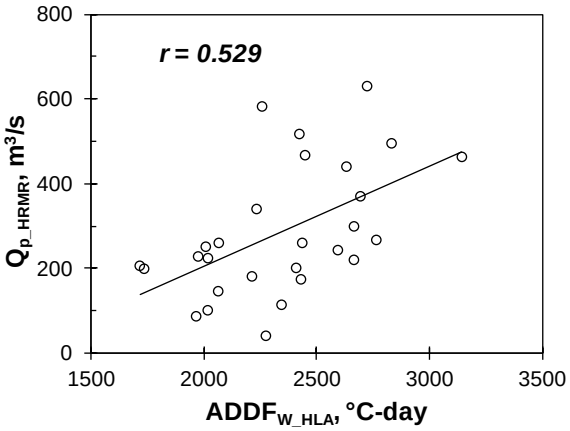

(c)

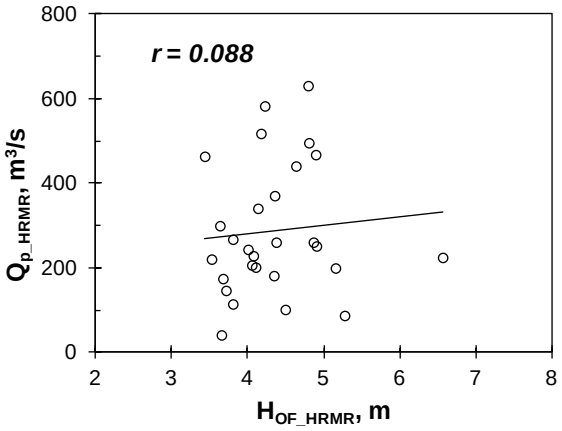

Figure 4–10: Correlations between the numerical input variables and the output variable of the Submodel-1. Note *r* is Pearson's correlation coefficient. The sample size for all the three cases is 28.

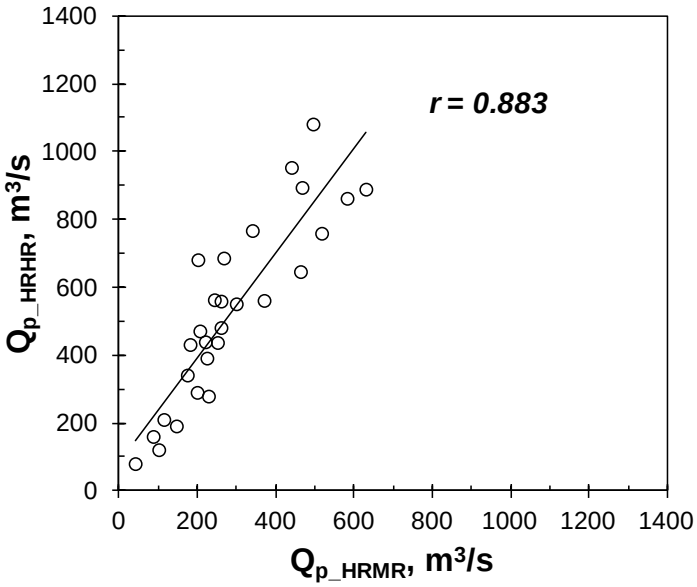

Figure 4–11: Correlation between observed values of Q_{P_HRHR} and Q_{P_HRMR}. Note the sample size is 28.

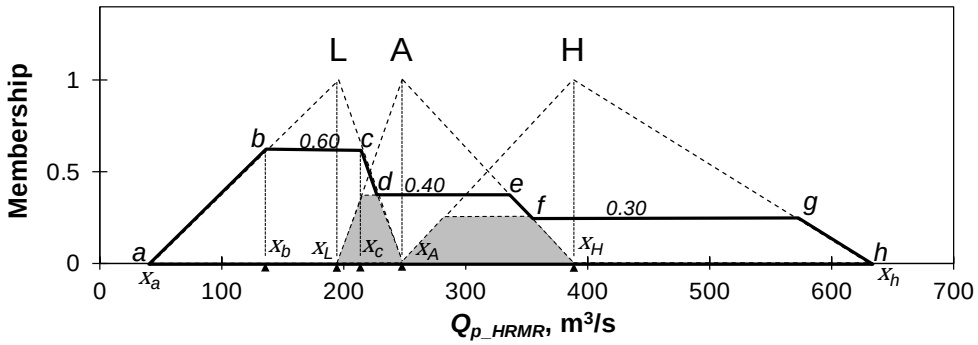

Figure 4–12: An example of the polygon (i.e. solid line) for the output fuzzy set for Q_{P_HRMR}. Note the numbers indicate the validated degree of truth for each MF; the shaded areas indicate the overlaps between the adjacent MFs that have been validated.

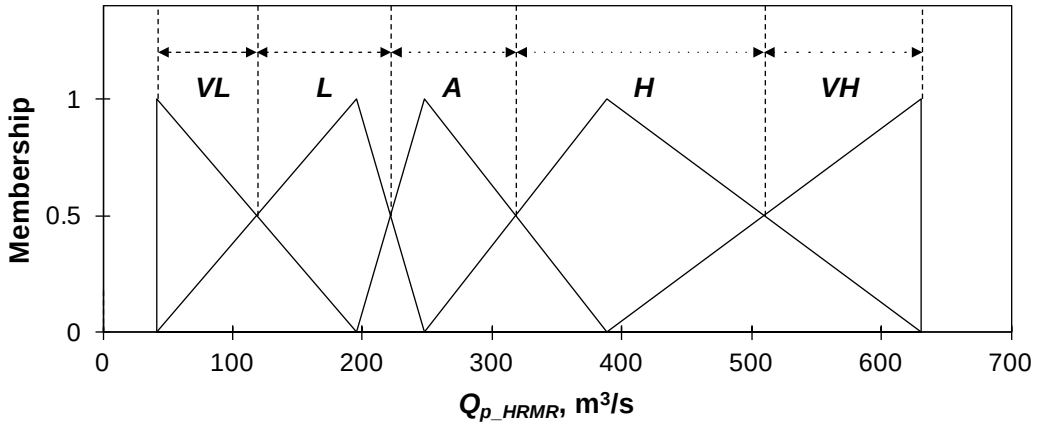

Figure 4–13: Categorization of the actual observed values of Q_{P_HRMR} using defined MFs.

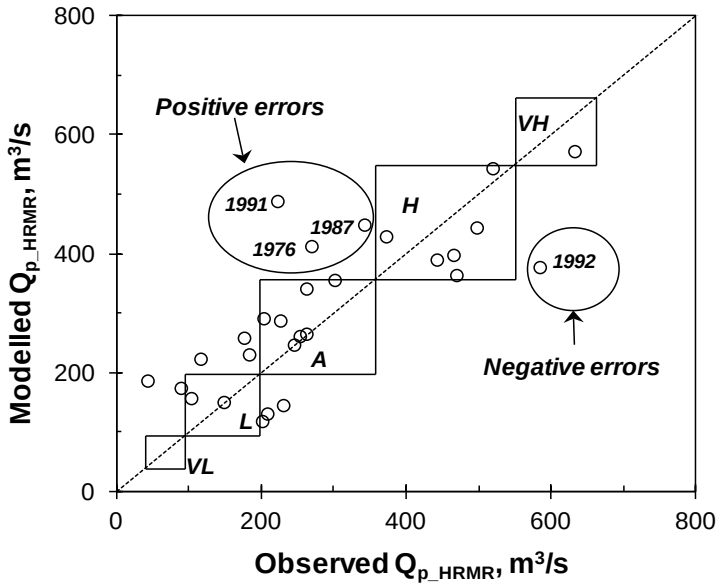

Figure 4–14: Model performance for the final Submodel-1.

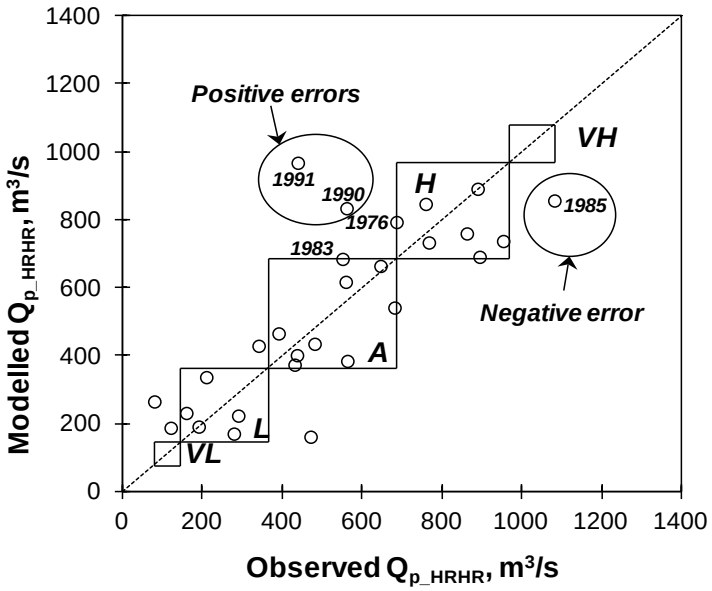

Figure 4–15: Model performance for the final Submodel-3.

(a)

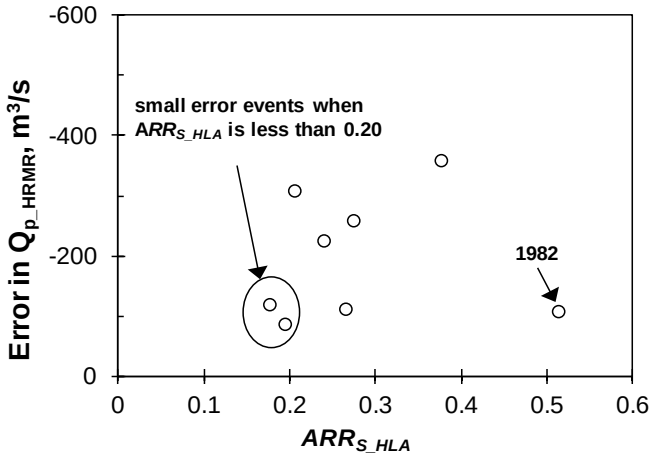

(b)

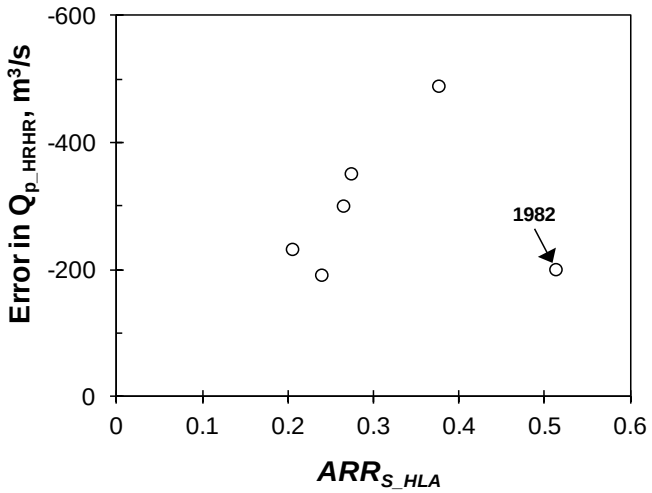

Figure 4–16: Error in modeled peak discharges for the intense rainfall events at HLA by (a) Sub-model 1 and (b) Sub-model 3.

(a)

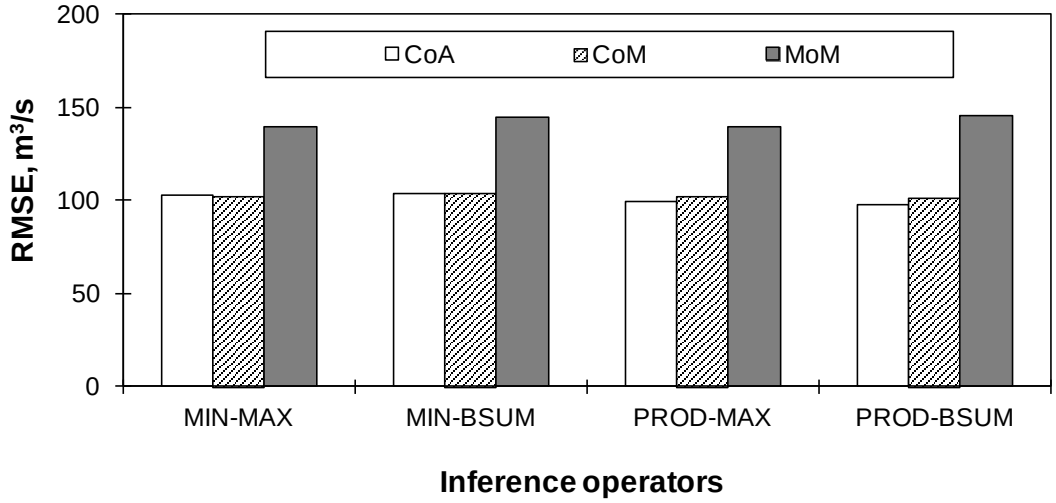

(b)

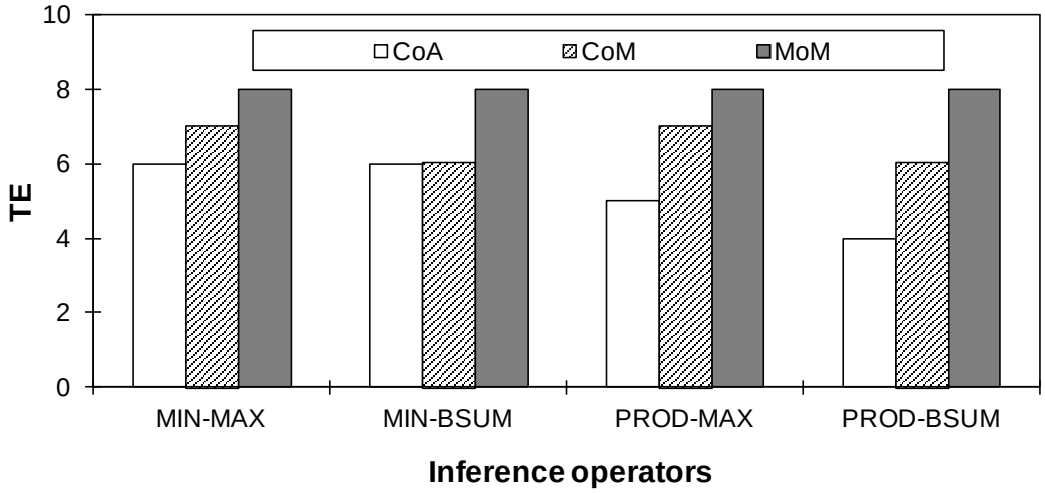

Figure 4–17: Comparison of model performances for Submodel-1 using different inference operators and defuzzification methods in terms of (a) RMSE and (b) TE.

(a)

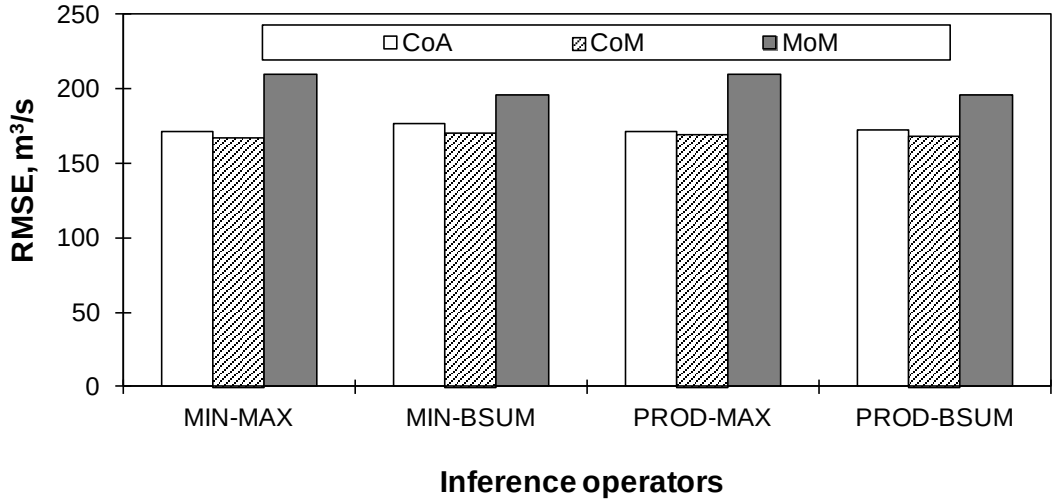

(b)

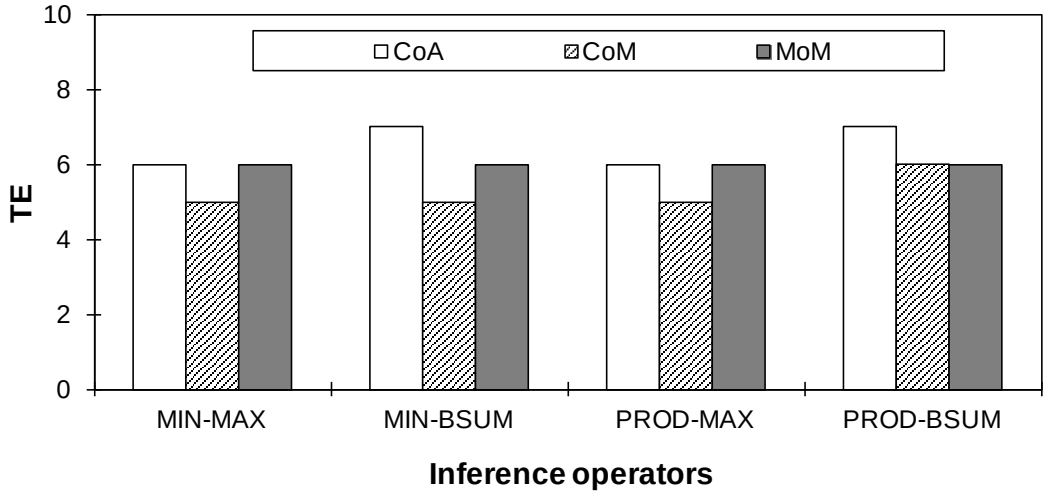

Figure 4–18: Comparison of model performances for the Submodel-3 using difference inference operators and defuzzification methods in terms of (a) RMSE and (b) TE.

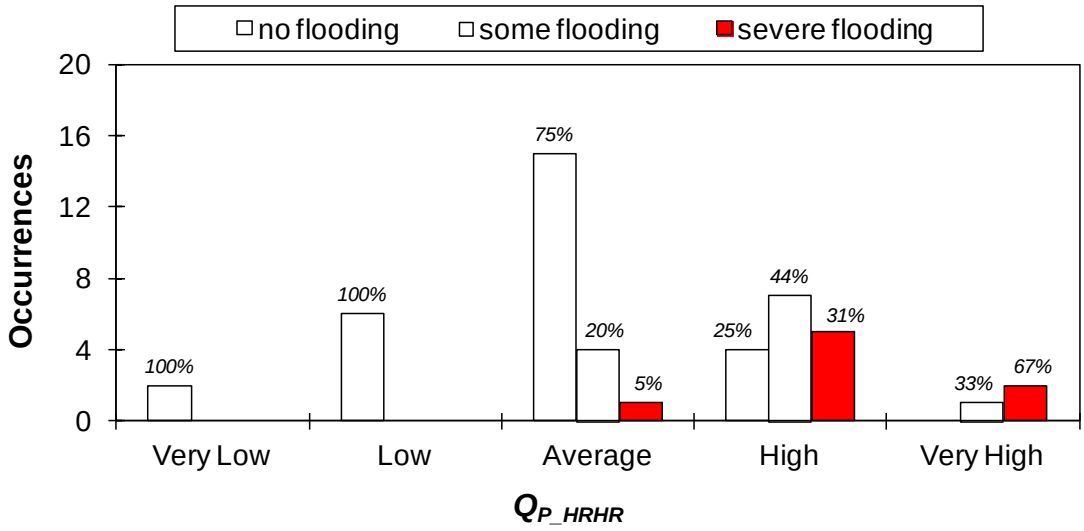

Figure 4–19: Comparison of the ooccurrences of historical breakup events at THR for each partition of Q_{P_HRHR}.

4.11 List of references

Aboriginal Affairs and Northern Development Canada. 2011. Snow Survey Data. Renewable Resources and Environment, Water Resources Division. Data URL: http://www.ainc-inac.gc.ca/eng/1100100027479.

Alberta Environment. 2011. Plains Snow Course Results as of Apr 1 2011. Water Management Operations Branch, River Forecast Section. Data URL: http://www.environment.alberta.ca/forecasting/data/snow/apr2011/plains_highlevel.pdf.

ASCE Task Committee on Application of Artificial Neural Networks in Hydrology, 2000a. Artificial neural networks in hydrology. I: preliminary concepts. Journal of Hydrologic Engineering, ASCE 5(2), 115-123.

ASCE Task Committee on Application of Artificial Neural Networks in Hydrology, 2000b. Artificial Neural Networks in Hydrology. II: hydrologic applications. Journal of Hydrologic Engineering, ASCE 5(2), 124-137.

Beltaos, S., Prowse, T.D., and Carter, T. 2006. Ice regime of the lower Peace River and ice-jam flooding of the Peace-Athabasca Delta. Hydrological Processes, 20(19): 4009-4029. doi:10.1002/hyp.6417.

Castro, J.L. and Delgado, M. 1996. Fuzzy systems with defuzzification are universal approximators. IEEE Trans Syst Man Cybern B Cybern. 26(1):149-52.

DeWalle, D.R. and Rango, A. 2008. Principles of snow hydrology. Cambridge University Press, Cambridge, UK; New York.

Dyer, J. 2008. Snow depth and streamflow relationships in large North American watersheds, Journal of Geophysical Research, 113, D18113. doi:10.1029/2008JD010031.

Ferguson, R. I. 1999. Snowmelt runoff models. Progress in Physical Geography. 23(2): 205-227.

Gerard, R. and S. Stanley. 1988. Ice jams and flood forecasting, Hay River, NWT. Water Resources Engineering Report No. 88-6, Dept of Civil Engineering, University of Alberta, Edmonton, Canada.

Gray, D. M. (Ed) 1970. Handbook on the principles of hydrology: with special emphasis directed to Canadian conditions in the discussions, applications, and presentation of data. Canadian National Committee for the International Hydrological Decade.

Herrera, F. 2008. Genetic fuzzy systems: taxonomy, current research trends and prospects. Evol Intell 1:27–46.

Hood, E.,Williams, M., and Cline, D. 1999. Sublimation from a seasonal snowpack at a continental, mid-latitude alpine site, Hydrol. Process., 13: 1781-1797.

Inform GmbH. 2010. FuzzyTECH® 5.81 user's manual, Aachen, Germany.

Jasek, M, Stanley, S., and Gerard, R. 1993. Update of Ice Jam Flood Database, Hay River, N.W.T.. Indian and Northern Affairs Canada, Yellowknife, N.W.T.

Jang, J. R., Sun, C. T., and Mizutani, E. 1997. Neuro-Fuzzy and Soft Computing: A Computational Approach to Learning and Machine Intelligence. Prentice Hall, pp 614.

Kosko, B. 1994. Fuzzy Systems as Universal Approximators. IEEE Transactions on Computers, vol. 43, no. 11, 1329-1333. doi:10.1109/12.324566.

Kovachis, N, L Zhao and F Hicks. 2011. A Summary of Historical Records of Hay River Breakup, 1894 to 2011. Water Resources Engineering Report 2011_FH_01, University of Alberta, Edmonton.

MacDonald, M.K., Pomeroy, J.W. and Pietroniro, A. 2010. On the importance of sublimation to an alpine snow mass balance in the Canadian Rocky Mountains. Hydrology and Earth System Sciences 14: 1401-1415.

Mahabir, C., F. Hicks, and A. Robinson Fayek. 2007. Transferability of a Neuro-fuzzy River Ice Jam Flood Forecasting Model, Journal of Cold Regions Science and Technology, 48(3): 188-201.

Mamdani, E. H. and Assilian, S. 1975. An experiment in linguistic synthesis with a fuzzy logic controller. International Journal of Man-Machine Studies, 7(1):1-13.

Mujumdar, P. P., and Ghosh, S. 2008. Fuzzy Logic-Based Approaches in Water Resource System Modeling. Practical Hydroinformatics, R. J. Abrahart, L. M. See, and D. P. Solomatine, eds., Springer Berlin Heidelberg, 165-176.

Nguyen, T. H., Kreinovich, V. and Tolbert, D. 1994. A measure of average sensitivity for fuzzy logics. International Journal of Uncertainty, Fuzzyness and Knowledge-Based Systems, 2(4): 361-375.

Pedrycz, W. 1994. Why triangular membership functions? Fuzzy Sets and Systems, 64(1):21-30.

Pedrycz, W. and V. de Oliveira. 1996. Optimization of fuzzy models. IEEE Trans. on Systems, Man, and Cybernetics Part B: Cybernetics, 26(4): 627-637.

Robinson Fayek, A. and Sun, Z. 2001. A fuzzy expert system for design performance prediction and evaluation. Can. J. Civ. Eng., 28, 1-25.

Strasser, U., Bernhardt, M., Weber, M., Liston, G. E., and Mauser, W. 2008. Is snow sublimation important in the alpine water balance? The Cryosphere, 2, 53-66, doi:10.5194/tc-2-53-2008, 200.

Takagi, T. and Sugeno, M. 1985. Fuzzy identification of systems and its application to modeling and control. IEEE Trans. Syst. Man Cybern. 15 (1): 116-132.

Todhunter, P.E. 2001. A hydroclimatological analysis of the Red River of the North snowmelt flood catastrophe of 1997. Journal of the American Water Resources Association, 37, 1263-1278.

Wang, L. 1992. Fuzzy systems are universal approximators. IEEE Trans. Syst., Man, Cybern., vol. SMC-7, no. 10, 1163-1170.

Yang, D, Robinson, D, Zhao, Y, Estilow, T andYe B. 2003. Streamflow response to seasonal snow cover extent changes in large Siberian watersheds. Journal of Geophysical Research 108(D18): 4578, doi:10.1029/2002JD003149.

Yang, D., Zhao, Y., Armstrong, R. and Robinson, D. 2009. Yukon River streamflow response to seasonal snow cover changes. Hydrological Processes. 23:109-121.

Ying, H. 2000. Fuzzy Control and Modeling: Analytical Foundations and Applications. IEEE Press, pp 310.

Zadeh, L.A. 1965. Fuzzy sets. Information and Control 8(3):338-353.

Zhao, L., Hicks, F and Robinson Fayek, A. 2012. Applicability of multilayer feed-forward neural networks to model the onset of river breakup. Journal of Cold Regions Science and Technology, 70 (2012): 32-42.

Chapter 5 Summary and conclusions

River breakup ice jam flooding is one of the most dangerous natural disasters in northern communities. Due to the suddenness and rapidness of rise of flood water level, an advance forecast, in terms of the expected flood severity and timing of the onset of breakup, is extremely helpful in the preparedness planning for the riverside communities. Unfortunately, current knowledge and understanding of ice jam dynamics has not allowed us to predict every aspect of the ice jam flooding. In particular, there is a great need to have long lead-time forecasts of the expected breakup flood severity. Moreover, the highly dynamic and swift nature of ice jam events results in a very limited amount of data available to develop and validate reliable ice jam forecasting models. Thus the present capability to forecast the occurrence, extent, and duration of breakup ice jam flooding is very limited. The existing small amount of forecasting models are all highly site specific and empirical. The variables used in these methods are usually arbitrary (due to the lack of an analytical breakup ice jam model) and not possibly achieved or forecasted more than a few days prior to breakup. In less populated regions like northern Canada, a short record of historical data and the sparsity of data network further impede successful development of such models.

With the continuing growth of northern communities, a reliable forecasting tool for breakup ice jams is most urgent. Being part of the Operational River Ice Jam Flooding Forecasting System (see Section 1.3), this study aimed to explore a

multi-layer modeling approach by incorporating all the readily available hydrometeorological data into the river ice breakup forecasting. Two soft computing techniques, artificial neural networks and fuzzy logic systems, were comprehensively assessed for their applicability to the river breakup problems and demonstrated in the study site, the Town of Hay River, NWT.

In this thesis, a new multi-layer modeling approach for the river ice breakup forecasting problem was first proposed in Chapter 2. The approach was comprised of four layers:

1. *The raw data layer:* all the raw hydrometeorological data (e.g. air temperature, precipitation, water level, etc.) and other pertinent historical information (e.g. qualitative breakup flooding reports from local newspapers or personal communications with local residents) are collected in this layer.
2. *The index variable layer:* the raw data are processed to develop proper variables, such as accumulated degree-days of freezing and thaw, accumulated precipitation during winter, and the water level at the onset of freeze-up, which are carried forward to use as input data to the next layer.
3. *The breakup indicator layer:* the key breakup indicators (e.g. in terms of breakup timing and flooding severity) are identified in this layer and complex soft computing techniques are employed to model these variables.

4. *The output variable layer:* the output variables of river breakup forecasting, the timing of onset of breakup and a qualitative descriptor of the expected breakup flooding severity, are then projected from the predictions of the breakup indicators in the last layer.

The details on the data processing and definitions of all the variables in the four layers were presented and demonstrated for the Town of Hay River in Chapter 2. The most promising potential predictors of breakup severity were found to be water level at the onset of freeze-up and the accumulated degree-days of freezing during winter. The variable related to the timing of breakup, ΔH_{FC} (i.e. the difference between the water level at the onset of breakup and that at the onset of rise of snowmelt runoff) was found to be completely nonlinear with respect to the independent index variables: the three long lead-time variables were the late winter ice thickness, whether the ice cover was significantly decayed or not, and the depth of snow on the ground at the onset of thaw. The four short lead-time variables were the accumulated degree-days of thaw, the accumulated degree-days of freezing, the accumulated snowfall, and the accumulated rainfall during the pre-breakup period.

Chapter 3 explored the applicability of feed-forward artificial neural network models for forecasting of the timing of the onset of river ice breakup. It represents the first application of ANNs to river ice breakup forecasting for which the model is actually independently validated. Specifically, in this case, the objective was to

predict the onset of cracking (i.e. the first transverse crack.) The output variable of the model was chosen as the water level rise between the onset of the spring snowmelt runoff and first cracking. The input included three long lead-time variables (each known several weeks prior to breakup): the ice thickness, the ice cover condition prior to breakup, and the depth of snow cover at the onset of thaw, as well as four short lead-time variables (each either know or forecasted during the breakup period): the accumulated degree-days of thaw, the accumulated degree-days of freezing, the accumulated rainfall and snowfall during pre-breakup. The "early stopping" scheme was employed in the calibration of the ANN model as well as a trial-and-error procedure for the optimization of the model performance with respect to the number of the hidden nodes and the initial weight range. The 'leave-one-out cross validation' method was used to assess the model error. It was found that:

- The calibrated ANN model showed more potential than conventional multiple linear regression models for this specific problem.
- A medium-size structure of the ANN model exhibited better performance than either a large-sized or small-sized structure. The optimal value for the ratio of the degrees of freedom to the calibration data size was ~1.3.
- Even with the same number of hidden nodes, the ANN model was very sensitive to the assignment of the initial weight range. A trial-and-error procedure is essential for determining its optimal value.
- The independent validation results showed that the error of the calibrated ANN model on the unseen validation data could be much larger than those

indicated by the calibration testing data and that the error is generally larger for the extrapolation cases than for the interpolation cases. In practice, the ANN model should be recalibrated whenever the new data is available.

Chapter 4 explored and assessed the applicability of the technique of the Mamdani-type fuzzy logic systems to predict the peak snowmelt runoff during breakup and its viability as an indicator of breakup flood severity. It represents the first time that the Mamdani-type fuzzy logic system has been comprehensively studied, in terms of each single component, for the river ice breakup forecasting problem, including the development of membership functions, rule base and inference operator, and the defuzzification method. Specifically, in this part of study, the relationship between the breakup flood severity and peak snowmelt runoff was first established for the case study site using the available historical data. Three long lead-time variables were used as inputs to the model: the accumulated precipitation during winter, the accumulated degree-days of freezing during winter and the local river water level at the onset of freeze-up. Furthermore, the whole basin was divided into two sub-basins to account for spatial variations in the contributions to snowmelt runoff. Based on this investigation, it was found that:

- The optimal fuzzy logic model could provide very good performance for the “High” and “Very High” events, which are of most interest from the flood forecasting perspective. However, significant underestimation errors

(i.e. ~300 m^3/s) should be expected whenever intense spring rainfall events occur in the interval between the day of the long term forecast and the actual breakup (i.e. when the spring rainfall ratio is over 0.20).

- Using more membership functions for the input and output variables did not result in better model performance. The I3O5 scheme (i.e. using 3 membership functions for the input variables and 5 membership functions for the output variable) was more suitable for this specific problem than the I5O7 scheme.
- The fuzzy logic model was very sensitive to the fuzzy operators and defuzzification methods. For best performance, different model configurations were associated with different combination of fuzzy operators and defuzzification method. However, for the case of peak snowmelt runoff, it was found that the COA and COM methods outperformed the MOM method. A trial-and-error practice would be necessary to determine the best combination of these.

From the point view of the model transferability, it should be noted that the peak discharge during breakup is the single most important factor affecting the ice jam flood severity and thus this model is relevant to all ice jam flood affected sites, not just the Hay River case study presented here. The demonstrated fuzzy logic system can be easily applied to any other sites only by directly using the established rule base; however, site-specific data would be needed to develop the

relevant membership functions and for performing a sensitivity analysis on the inference operators.

The demand of the practical methodology for river ice breakup flooding will continue to be of importance as the northern region communities continue to expand. Furthermore, the warming trend of the global climate is likely to exacerbate the severity of breakup ice jam flooding. This is because, in the context of a warming climate, the early spring snowfall will become rainfall, which would cause much higher peak snowmelt runoff (see Chapter 4). In addition, there will be a greater risk of mid-winter thaws and potentially multiple breakup events in some years. As the majority of the river ice engineering community focuses on numerical simulations of the breakup ice jam process, the author recommends continued research on the soft computing methodology, which could provide a less time-consuming and more cost-efficient complement to the current research paradigm:

1) Further research on ANNs should be performed for other sites, for which plentiful data is available. The early stopping calibration scheme and the leave-one-out cross validation technique should always be used to see if the model's performances will improve for such cases.
2) An analysis of the calibrated ANN model should be performed in each case, to determine the impact of each input variable on the output variable. This is important for understanding the key factors that affect the timing of

river ice breakup. This result can also be used to simplify the model structure by only selecting the important input variables.

3) More meteorological factors can be incorporated into the fuzzy logic system directly, such as spring rainfall and air temperature, to enhance its capability to forecast the breakup ice jam flooding severity. The layered structure should be used to avoid the rule base explosion problem. For example, the spring rainfall ratio (ARR_S) should come into the model in the same layer as the long lead-time forecast of the snowmelt peak, but not in the same layer as other long lead-time input variables (see Figure 5-1). Though this would limit the lead-time of practical forecasting, the enhanced rainfall effect on the peak snowmelt runoff can be significant and worthy of this consideration. There is also a need to collect the solar radiation data to account for the ice cover decay extent just prior to breakup rather than just using ADDT as a surrogate.
4) More work also needs be done on the Mamdani-type fuzzy logic system. For example, to determine how to develop a more rigorous rule base using more sophisticated techniques. This is especially important for the cases when data are plentiful; a hybrid model (e.g. neuro-fuzzy system, genetic fuzzy system) should be tested and compared for their performance.

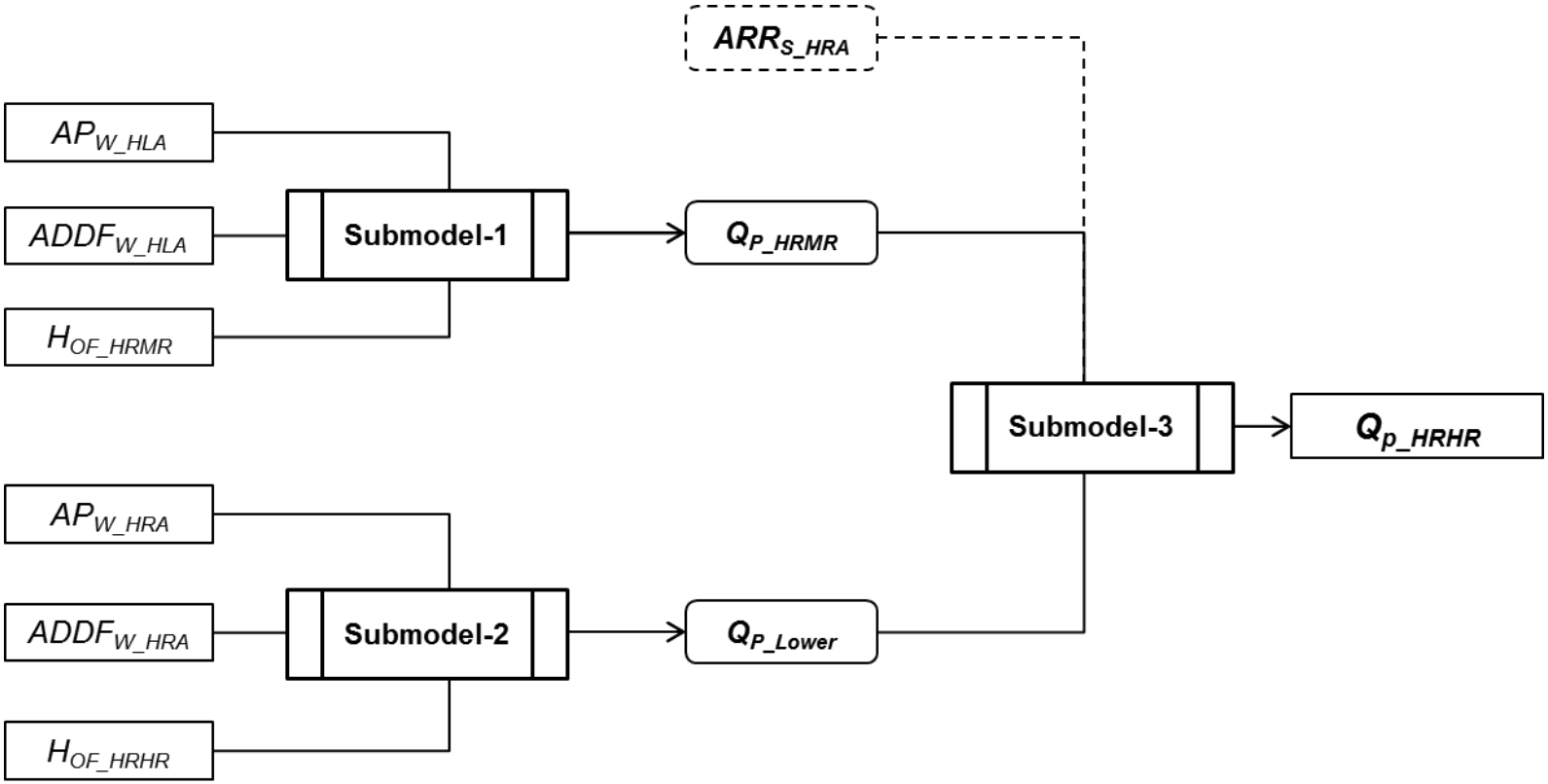

Figure 5–1: Proposed layered structure for the new fuzzy logic system to incorporate the spring rainfall information.

Appendix A Development of the raw hydrometeorological database for Hay River breakup forecasting

This appendix presents a summary of the collated hydrometeorological data from a variety of available data sources in the Hay River basin. This includes: hydrometric data (e.g. discharge and water levels) gauged by WSC, meteorological data (e.g. mean daily air temperature, daily precipitation, and snow-on-the-ground condition) from EC climate stations, late winter snowpack data by snow course surveys (e.g. snow pack depth and water equivalence), and river ice measurement data (ice thickness).

A.1 Raw hydrometric data

The raw hydrometric data are available at the four WSC gauges in the Hay River basin (See Figure 2-2). These include water level and/or discharge data on an hourly and/or daily basis. Also the winter discharge measurements performed by WSC provide a useful data source for the seasonal development of the river ice thickness. All these data were collected and discussed below.

A.1.1 Instantaneous and daily stage/discharge data

For the three gauges, HRHR, MRMR, and CRHL, both the stage and discharge data are available from WSC. The historical records for these data are

summarized in Table A-1. All these raw data can be found in the attached compact disc, in the folder of "*hydrometric data*".

Apart from these digitized data, there are also raw stripe charts provided by WSC for the early periods of HRHR. These are the breakup water levels that have not ever been digitized by WSC. A lot of efforts were made to digitize these raw charts and the results are summarized in the file '*Ungraphed hourly WL at HRHR 1964-1996*' (also the raw charts can be found in the folder *'HRHR Strip Charts during breakup period'*).

A.1.2 Ice thickness data extracted from the winter discharge measurements

At the three gauges of HRHR, HRMR and CRHL, WSC performs winter discharge measurement 3 to 5 times per year, in which the ice thickness is also measured. The raw data sheets of discharge measurements provided by WSC were digitized and summarized. Among these measurements, the last one at the end of winter is very useful to be considered as an estimation of the maximum ice thickness of the year. All the raw data of measurement records are summarized in the folder of "winter ice thickness measurement" in the attached compact disc. Please note that the actual ice thickness data before 1992 at the HRHR gauge were extended by the relationship shown in Figure A-1. The complete late winter ice thickness data are presented in Table A-2.

The Town of Hay River also performed ice thickness measurements at various locations around the town. The available data are collected and summarized in the data file of '*THR ice thickness measurements*'.

A.2 Raw meteorological data

The main sources of the meteorological data are the EC climate stations in the Hay River basin. The two stations chosen in this study are shown in Figure 2-2. They are the Hay River A at the Town of Hay River and High Level A at the Town of High Level. Apart from these, there are several snow courses surveyed in the basin, which are also shown in Figure 2-2.

The raw meteorological data achieved from these EC climate stations include the daily mean air temperature, daily rainfall, daily snowfall, daily total precipitation, and snow depth on the ground. The records of these data are summarized in Table 4-1 and the raw data are organized in the folder "*Mete data*" in the attached data disc. The available snow course surveys data are also organized in the same folder with a name of '*Snow course surveys*'.

Table A-1: Historical records of hydrometric data at WSC gauges in Hay River Basin.

No	Station No	Station Name	Instantaneous Water Level	Hourly Discharge	Daily Water Level	Daily Discharge
1	07OB001	HRHR	1997-2010: all the year (15 mins interval) 1964-1996: only the pre-breakup periods (hourly)	NA	1964-2010	1964-2010
2	07OB003	HRMR	1991-2008: March/April to November	2000-2008	1975-2008	1975-2010
3	07OB008	HRNB	2003-2010: March/April to November	NA	1987-2010	NA
4	07OC001	CRHL	1978-2008: all the year	1999-2008	1970-2008	1970-2010

Table A-2: Actual late winter ice thickness data at HRHR.

Year	Measurement Date	actual ice thickness (t_i), m	the water surface to bottom of ice (WSBI), m
1964	17/04/1964	*0.58*	0.55
1965	09/03/1965	*0.78*	0.74
1966	06/04/1966	*0.80*	0.76
1967	12/04/1967	*0.63*	0.60
1968	19/03/1968	*0.74*	0.71
1969	08/04/1969	*0.62*	0.59
1970	13/04/1970	*0.61*	0.58
1971	15/04/1971	*0.81*	0.77
1972	25/04/1972	*0.55*	0.52
1973	10/04/1973	*0.66*	0.63
1974	09/04/1974	*0.62*	0.59
1975	10/04/1975	*0.67*	0.64
1976	13/04/1976	*0.43*	0.41
1977	04/04/1977	*1.15*	1.10
1978	26/04/1978	*0.81*	0.77
1979	14/04/1979	*0.81*	0.77
1980	10/04/1980	*0.83*	0.79
1981	22/04/1981	*0.78*	0.74
1982	15/04/1982	*0.83*	0.79
1983	24/03/1983	*0.77*	0.73
1984	18/04/1984	*0.45*	0.43
1985	19/04/1985	*0.88*	0.84
1986	02/04/1986	*0.83*	0.79
1987	15/04/1987	*0.66*	0.63
1988	07/04/1988	*0.69*	0.66
1989	07/04/1989	*0.70*	0.67
1990	10/04/1990	*0.64*	0.61
1991	12/04/1991	*0.59*	0.56
1992	14/04/1992	0.74	0.72
1993	07/04/1993	0.88	0.82
1994	18/04/1994	0.92	0.92
1995	18/04/1995	0.65	0.62
1996	18/04/1996	0.65	0.58
1997	14/04/1997	0.67	0.64
1998	14/04/1998	0.71	0.68
1999	14/04/1999	0.42	0.39
2000	10/04/2000	0.61	0.57
2001	17/04/2001	0.59	

Year	Measurement Date	actual ice thickness (t_i), m	the water surface to bottom of ice (WSBI), m
2002	22/04/2002	0.74	0.73
2003	17/04/2003	0.90	0.84
2004	12/04/2004	0.64	0.60
2005	13/04/2005	0.70	0.67
2006	06/04/2006	0.63	0.59
2007	17/04/2007	0.83	0.77
2008	15/04/2008	0.62	0.62
2009	16/04/2009	0.64	0.61
2010	13/04/2010	0.70	0.68

Note: the italics indicate that they were estimated from the WSBIs using the relationship shown in Figure A-1.

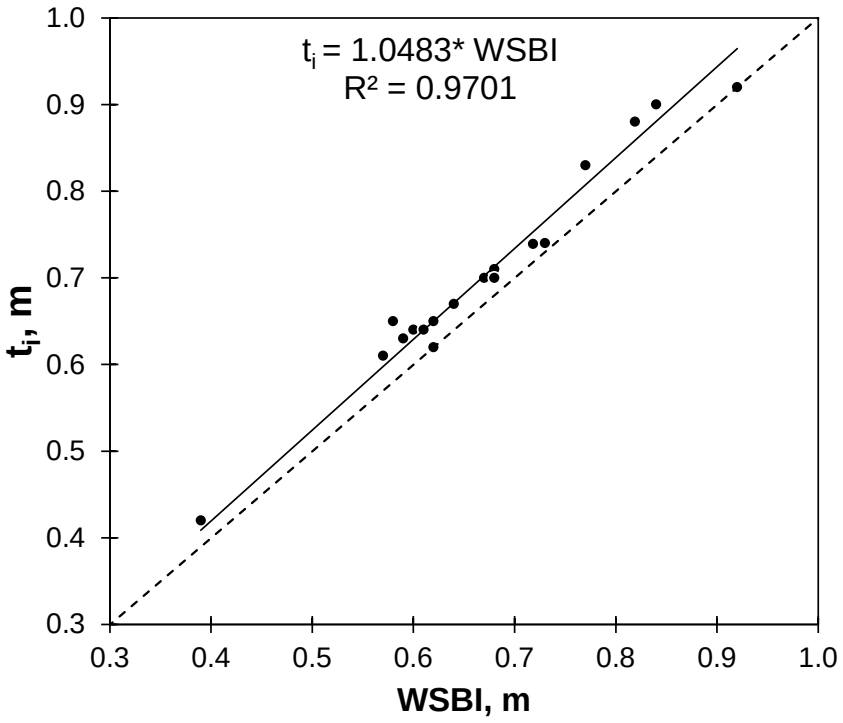

Figure A-1: Relationship between the actual ice thickness (t_i) and the measured water surface to the bottom of ice (WSBI) at HRHR gauge from 1992 to 2010.

Appendix B Data tables of all the developed variables for the Hay River breakup forecasting

This appendix summarizes all the data tables of the variables extracted or processed from the raw hydrometeorological data for the Hay River breakup forecasting. Please refer to Chapter 2 for the detailed definition for these variables.

Table B-1: Classification of historical breakup severity at the Town of Hay River.

Breakup Severity	Year
severe flooding (8 years)	1974, 1978, 1985, 1986, 1989, 1992, 2003, 2008;
some flooding (12 years)	1965, 1972, 1979, 1981, 1994, 1997, 2001, 2005, 2006, 2007, 2009, 2010;
no flooding (27 years)	1964, 1966, 1967, 1968, 1969, 1970, 1971, 1973*, 1975, 1976, 1977, 1980, 1982, 1983, 1984, 1987, 1988, 1990, 1991, 1993, 1995, 1996, 1998, 1999, 2000, 2002, 2004.

**Note: since there was no documentation on the 1973 breakup, it is reasonable to assume it was a non-flood year.*

Table B-2: Extracted or processed independent variables from the hydrometric data at HRHR.

Year	H_{OF}	D_{OR}	H_{OR}	D_{FC}	H_{FC}	t_i	D_i	***DECAY***
	m		*m*		*m*	*m*		
1964	2.63	26/04/1964	1.79	27/04/1964	3.51	0.58	17/04/1964	0
1965	2.54	07/04/1965	1.65	23/04/1965	3.96	0.78	09/03/1965	0
1966	1.94	09/04/1966	1.75	04/05/1966	3.44	0.80	06/04/1966	1
1967	1.70	01/05/1967	1.68	06/05/1967	2.26	0.63	12/04/1967	0
1968	1.70	09/04/1968	1.81	10/04/1968	3.51	0.74	19/03/1968	0
1969	1.83	11/04/1969	1.60	17/04/1969	2.03	0.62	08/04/1969	0
1970	2.36	23/04/1970	1.70	24/04/1970	2.12	0.61	13/04/1970	0
1971	1.66	18/04/1971	1.54	25/04/1971	1.86	0.81	15/04/1971	0
1972	1.55	25/04/1972	1.40	03/05/1972	1.91	0.55	25/04/1972	0
1973	1.62	NA	NA	NA	NA	0.66	10/04/1973	0
1974	2.18	NA	NA	NA	NA	0.62	09/04/1974	0
1975	2.46	NA	NA	NA	NA	0.67	10/04/1975	0
1976	2.15	15/04/1976	1.85	18/04/1976	2.38	0.43	13/04/1976	1
1977	3.38	12/04/1977	2.38	24/04/1977	5.12	1.15	04/04/1977	0
1978	2.83	23/04/1978	1.93	29/04/1978	2.47	0.81	26/04/1978	1
1979	2.67	26/04/1979	1.89	08/05/1979	2.99	0.81	14/04/1979	0
1980	2.50	NA	NA	NA	NA	0.83	10/04/1980	1
1981	1.89	27/04/1981	1.81	29/04/1981	2.24	0.78	22/04/1981	0
1982	1.35	25/04/1982	1.71	30/04/1982	2.00	0.83	15/04/1982	1
1983	1.83	21/04/1983	1.88	25/04/1983	2.50	0.77	24/03/1983	0
1984	2.01	16/04/1984	1.66	19/04/1984	2.18	0.45	18/04/1984	1
1985	3.06	17/04/1985	1.93	26/04/1985	3.17	0.88	19/04/1985	0
1986	3.14	24/04/1986	2.10	29/04/1986	3.68	0.83	02/04/1986	0
1987	2.28	15/04/1987	1.86	22/04/1987	2.38	0.66	15/04/1987	1
1988	2.61	13/04/1988	1.72	22/04/1988	3.25	0.69	07/04/1988	0
1989	2.81	24/04/1989	2.01	01/05/1989	2.91	0.70	07/04/1989	0

Year	H_{OF}	D_{OR}	H_{OR}	D_{FC}	H_{FC}	t_i	D_i	***DECAY***
	m		*m*		*m*	*m*		
1990	2.41	18/04/1990	2.02	24/04/1990	2.73	0.64	10/04/1990	1
1991	1.63	16/04/1991	1.82	21/04/1991	2.63	0.59	12/04/1991	1
1992	2.45	11/04/1992	2.44	24/04/1992	3.56	0.74	14/04/1992	0
1993	3.84	11/04/1993	2.12	21/04/1993	3.03	0.88	07/04/1993	1
1994	2.56	14/04/1994	2.21	21/04/1994	3.60	0.92	18/04/1994	0
1995	1.67	NA	NA	NA	NA	0.65	18/04/1995	0
1996	1.52	29/04/1996	1.70	30/04/1996	2.06	0.65	18/04/1996	1
1997	2.65	21/04/1997	2.04	28/04/1997	2.75	0.67	14/04/1997	0
1998	4.68	07/04/1998	2.23	17/04/1998	3.41	0.71	14/04/1998	1
1999	1.82	16/04/1999	1.75	22/04/1999	2.20	0.42	14/04/1999	1
2000	2.38	19/04/2000	2.03	27/04/2000	2.71	0.61	10/04/2000	1
2001	2.42	16/04/2001	1.75	29/04/2001	3.00	0.59	17/04/2001	1
2002	2.72	28/04/2002	2.00	10/05/2002	2.95	0.74	22/04/2002	0
2003	2.40	17/04/2003	2.04	24/04/2003	3.15	0.90	17/04/2003	1
2004	2.23	10/04/2004	1.92	28/04/2004	3.60	0.64	12/04/2004	1
2005	2.25	16/04/2005	1.94	22/04/2005	4.30	0.70	13/04/2005	1
2006	2.46	12/04/2006	1.88	23/04/2006	4.30	0.63	06/04/2006	1
2007	1.72	19/04/2007	1.92	24/04/2007	3.45	0.83	17/04/2007	1
2008	3.11	15/04/2008	2.03	03/05/2008	4.35	0.62	15/04/2008	1
2009	2.92	19/04/2009	1.97	30/04/2009	3.78	0.64	16/04/2009	0
2010	2.92	14/04/2010	2.14	21/04/2010	3.10	0.70	13/04/2010	1

Table B-3: Extracted dependent variables from the hydrometric data at HRHR.

Year	D_{Qp}	Q_P	D_{QM}	Q_{MB}	D_{HM}	H_{MB}	D_{cl}
		m^3/s		m^3/s		m	
1964	12/05/1964	708	08/05/1964	725	07/05/1964	8.32	10/05/1964
1965	02/05/1965	750	02/05/1965	750	02/05/1965	9.21	04/05/1965
1966	10/05/1966	620	10/05/1966	620	09/05/1966	5.43	12/05/1966
1967	23/05/1967	793	11/05/1967	900	10/05/1967	6.27	13/05/1967
1968	06/05/1968	518	04/05/1968	476	30/04/1968	7.95	04/05/1968
1969	07/05/1969	889	29/04/1969	796	26/04/1969	6.61	29/04/1969
1970	03/05/1970	374	03/05/1970	374	03/05/1970	7.34	07/05/1970
1971	01/05/1971	600	01/05/1971	600	01/05/1971	5.02	30/04/1971
1972	09/05/1972	1020	09/05/1972	1020	09/05/1972	7.16	10/05/1972
1973	10/05/1973	513	27/04/1973	650	28/04/1973	6.09	02/05/1973
1974	02/05/1974	1240	02/05/1974	1240	01/05/1974	8.40	04/05/1974
1975	30/04/1975	680	30/04/1975	680	01/05/1975	5.23	01/05/1975
1976	30/04/1976	685	26/04/1976	665	22/04/1976	6.15	27/04/1976
1977	06/05/1977	289	27/04/1977	530	27/04/1977	7.41	04/05/1977
1978	03/05/1978	818	03/05/1978	818	05/05/1978	7.28	07/05/1978
1979	21/05/1979	694	17/05/1979	643	11/05/1979	>7.297	17/05/1979
1980	28/04/1980	120	28/04/1980	120	28/04/1980	2.82	29/04/1980
1981	04/05/1981	790	04/05/1981	790	04/05/1981	7.40	09/05/1981
1982	20/05/1982	604	09/05/1982	657	09/05/1982	8.02	10/05/1982
1983	30/04/1983	550	30/04/1983	550	30/04/1983	6.54	04/05/1983
1984	28/04/1984	79	21/04/1984	172	21/04/1984	3.61	30/04/1984
1985	06/05/1985	1080	06/05/1985	1080	06/05/1985	9.61	09/05/1985
1986	13/05/1986	697	06/05/1986	720	06/05/1986	9.67	08/05/1986
1987	06/05/1987	766	27/04/1987	772	28/04/1987	8.41	01/05/1987
1988	12/05/1988	480	27/04/1988	640	27/04/1988	7.46	02/05/1988
1989	08/05/1989	888	05/05/1989	912	03/05/1989	10.54	06/05/1989

Year	D_{Qp}	Q_P	D_{QM}	Q_{MB}	D_{HM}	H_{MB}	D_{cl}
		m^3/s		m^3/s		m	
1990	28/04/1990	560	28/04/1990	560	27/04/1990	8.14	02/05/1990
1991	02/05/1991	438	27/04/1991	460	24/04/1991	7.29	01/05/1991
1992	08/05/1992	861	28/04/1992	900	28/04/1992	9.68	30/04/1992
1993	30/04/1993	159	30/04/1993	159	30/04/1993	5.00	06/05/1993
1994	29/04/1994	792	29/04/1994	792	28/04/1994	10.41	01/05/1994
1995	02/05/1995	340	02/05/1995	340	04/05/1995	7.34	07/05/1995
1996	08/05/1996	645	02/05/1996	200	02/05/1996	5.46	02/05/1996
1997	13/05/1997	635	04/05/1997	555	03/05/1997	8.46	04/05/1997
1998	22/04/1998	390	22/04/1998	390	21/04/1998	6.16	08/05/1998
1999	04/05/1999	190	26/04/1999	181	26/04/1999	3.66	>04/27/1999
2000	15/05/2000	278	01/05/2000	267	29/04/2000	5.61	>04/25/2000
2001	07/05/2001	430	07/05/2001	430	04/05/2001	8.45	>05/04/2001
2002	22/05/2002	562	22/05/2002	562	15/05/2002	8.44	22/05/2002
2003	02/05/2003	675	02/05/2003	675	30/04/2003	>8.158	02/05/2003
2004	06/05/2004	209	05/05/2004	193	01/05/2004	6.41	05/05/2004
2005	30/04/2005	758	28/04/2005	737	24/04/2005	6.65	28/04/2005
2006	01/05/2006	470	29/04/2006	455	25/04/2006	7.35	29/04/2006
2007	14/05/2007	824	29/04/2007	500	27/04/2007	7.69	29/04/2007
2008	10/05/2008	893	08/05/2008	870	05/05/2008	8.92	08/05/2008
2009	13/05/2009	952	07/05/2009	700	06/05/2009	7.25	07/05/2009
2010	01/05/2010	436	28/04/2010	412	25/04/2010	7.67	28/04/2010

Note: From 1985 to 1989, all the Qp and QMB are adjusted to 80% of the WSC pulished data by Jesek (1993), except the Qp for year 1986. Reference: Jasek, M. 1993. Hay River Flood Control: Hay River, N.W.T.. The Town of Hay River, N.W.T.

Table B-4: Long-lead time variables developed from the meteorological data at HRA.

Year	***API***	D_{OF}	$ADDF_W$	D_{OT}	D_{MO}	AP_W	***SNGOT***
	mm		*°C-day*			*mm*	*cm*
1964	185.7	26/10/1963	3199.8	18/04/1964	04/05/1964	NA[1]	58
1965	158.8	29/10/1964	3126.1	01/04/1965	17/04/1965	99.4	13
1966	104.8	29/10/1965	3173.5	26/03/1966	04/05/1966	148.6	97
1967	113.2	16/10/1966	3689.8	20/04/1967	05/05/1967	153.3	48
1968	78.2	29/10/1967	2674.5	03/04/1968	06/05/1968	110.4	25
1969	147.6	30/10/1968	3140.0	07/04/1969	29/04/1969	121.1	48
1970	86.0	18/10/1969	2778.3	09/04/1970	09/05/1970	126.4	33
1971	67.1	04/11/1970	3130.4	13/04/1971	21/04/1971	84.5	13
1972	74.3	30/10/1971	3533.9	24/04/1972	04/05/1972	125.0	28
1973	121.2	23/10/1972	2928.9	08/04/1973	26/04/1973	88.1	15
1974	164.8	29/10/1973	3497.9	07/04/1974	28/04/1974	135.2	86
1975	143.9	07/10/1974	2957.5	06/04/1975	22/04/1975	136.5	58
1976	125.9	22/10/1975	3213.5	02/04/1976	25/04/1976	146.1	48
1977	122.1	05/11/1976	2337.0	07/04/1977	19/04/1977	74.6	38
1978	57.8	31/10/1977	2921.3	08/04/1978	03/05/1978	59.6	39
1979	104.3	23/10/1978	3457.2	21/04/1979	17/05/1979	92.9	44
1980	88.0	29/10/1979	2150.3	26/03/1980	19/04/1980	51.2	33
1981	186.1	22/10/1980	2477.8	19/04/1981	06/05/1981	107.8	52
1982	113.3	18/10/1981	3219.4	07/04/1982	17/05/1982	89.7	28
1983	96.9	27/10/1982	3364.1	12/04/1983	09/05/1983	119.1	52
1984	136.7	05/11/1983	2592.7	27/03/1984	18/04/1984	78.1	32
1985	197.9	21/10/1984	3183.3	12/04/1985	05/05/1985	109.9	40
1986	148.2	14/10/1985	2954.0	15/04/1986	07/05/1986	150.2	43
1987	101.0	26/10/1986	2308.9	29/03/1987	27/04/1987	118.2	71
1988	140.1	03/11/1987	2438.1	10/04/1988	07/05/1988	96.7	51
1989	184.4	18/10/1988	2985.7	08/04/1989	27/04/1989	89.4	40
1990	84.9	26/10/1989	3012.9	27/03/1990	22/04/1990	130.3	59
1991	206.7	10/10/1990	3127.0	29/03/1991	05/05/1991	155.2	82
1992	214.0	13/10/1991	2955.5	19/04/1992	04/05/1992	130.2	60
1993	134.1	02/11/1992	2155.6	20/03/1993	15/04/1993	43.0	33
1994	108.8	24/10/1993	3188.4	28/04/1994	08/05/1994	141.0	63
1995	76.4	28/10/1994	2712.6	16/04/1995	09/05/1995	118.9	82
1996	49.4	21/10/1995	3105.7	05/04/1996	26/04/1996	61.7	50
1997	156.8	16/10/1996	3041.1	09/04/1997	24/04/1997	64.8	48
1998	191.4	04/10/1997	2277.2	29/03/1998	18/04/1998	72.5	29
1999	208.0	29/10/1998	2142.4	20/03/1999	13/04/1999	78.1	53

Year	***API***	D_{OF}	$ADDF_W$	D_{OT}	D_{MO}	AP_W	***SNGOT***
	mm		*°C-day*			*mm*	*cm*
2000	120.2	27/10/1999	2108.9	20/03/2000	19/04/2000	55.6	29
2001	148.7	24/10/2000	2473.0	08/04/2001	19/04/2001	111.7	23
2002	256.7	16/10/2001	2974.2	26/04/2002	18/05/2002	121.0	18
2003	166.8	10/10/2002	2536.7	03/04/2003	23/04/2003	82.0	22
2004	121.6	28/10/2003	2655.7	29/03/2004	12/04/2004	90.3	42
2005	62.5	14/10/2004	2719.5	28/03/2005	19/04/2005	115.8	22
2006	189.1	29/10/2005	1857.3	21/03/2006	14/04/2006	72.2	22
2007	139.4	26/10/2006	2601.0	22/03/2007	16/04/2007	116.2	34
2008	185.2	28/10/2007	2917.2	07/04/2008	02/05/2008	91.0	29
2009	185.3	18/10/2008	2897.2	09/04/2009	05/05/2009	148.2	47
2010	132.8	28/10/2009	2152.3	28/03/2010	19/04/2010	95.4	12

Note: At HRA, the SWE was estimated as one tenth of snowfall depth until Sep 1964 when Nipher gauge was installed. This is confirmed by checking the daily.

Table B-5: Short-lead time variables developed from the meteorological data at HRA.

Year	AS_S	AR_S	$ADDT_{-5}$	$ADDF_{-5}$	RN_{PB}	SN_{PB}
	mm	*mm*	*°C-day*	*°C-day*	*mm*	*cm*
1964	0.8	7.1	30.3	2.6	0.0	0.8
1965	5.6	1.3	96.8	30.1	1.3	12.4
1966	30.7	0.3	110.8	194.3	0.3	44.6
1967	0.0	5.8	93.5	0.0	0.0	0.0
1968	20.3	8.5	23.4	4.0	4.6	1.0
1969	20.0	14.8	72.4	0.0	0.8	1.8
1970	51.6	1.8	107.6	1.4	0.0	10.9
1971	7.1	0.0	124.5	0.3	0.0	7.1
1972	0.0	0.0	63.5	0.0	0.0	0.0
1973	3.8	1.8	NA	NA	NA	NA
1974	0.8	1.5	NA	NA	NA	NA
1975	1.8	12.0	NA	NA	NA	NA
1976	0.0	8.1	119.4	1.1	1.0	0.0
1977	3.6	0.2	125.0	0.0	0.0	3.6
1978	5.0	10.9	51.3	34.1	10.7	5.0
1979	2.4	6.8	45.5	39.5	2.0	2.1
1980	0.8	0.2	NA	NA	NA	NA
1981	4.4	12.6	35.5	0.7	12.6	4.4
1982	37.5	7.3	99.7	8.5	3.1	7.8
1983	0.4	2.0	79.3	2.7	2.0	0.0
1984	0.0	1.6	139.2	16.7	0.0	0.0
1985	12.8	19.4	50.7	10.1	1.9	10.6
1986	3.2	6.9	54.5	2.8	0.0	3.2
1987	10.1	0.8	109.5	34.5	0.2	10.1
1988	7.2	5.0	65.4	4.3	4.8	2.4
1989	8.6	3.0	146.5	35.7	0.0	8.6
1990	0.6	8.9	138.5	20.1	8.9	0.6
1991	7.6	9.8	99.5	4.0	9.8	7.6
1992	4.6	6.6	38.8	0.0	0.0	0.8
1993	3.8	7.4	134.1	18.7	7.4	4.2
1994	0.0	0.0	0.0	0.0	0.0	0.0
1995	0.8	1.2	NA	NA	NA	NA
1996	0.8	5.5	114.1	29.9	5.5	0.8
1997	1.2	24.7	125.5	8.5	5.9	1.2
1998	0.0	0.0	106.3	1.7	0.0	0.0
1999	8.6	1.3	156.5	60.4	0.0	9.2

Year	AS_S	AR_S	$ADDT_{-5}$	$ADDF_{-5}$	RN_{PB}	SN_{PB}
	mm	*mm*	*°C-day*	*°C-day*	*mm*	*cm*
2000	0.8	8.0	175.5	107.9	1.6	0.8
2001	0.4	1.2	110.0	7.8	1.2	1.1
2002	28.6	0.8	40.9	33.2	0.0	27.0
2003	14.8	11.1	116.3	9.5	8.5	16.0
2004	2.8	6.4	104.3	46.7	6.4	3.6
2005	11.0	1.6	147.0	8.4	1.2	9.4
2006	6.0	9.0	137.7	47.7	9.0	10.7
2007	5.2	36.0	141.8	71.7	2.8	7.6
2008	9.6	0.4	155.6	46.7	0.2	11.6
2009	0.0	11.4	101.7	3.5	11.4	0.4
2010	23.8	0.2	168.7	9.1	0.0	26.4

Table B-6: Long-lead variables developed from the meteorological data at HLA.

Year	***API***	D_{OF}	$ADDF_W$	D_{OT}	AP_W
	mm		*°C-day*		*mm*
1964	NA	NA	NA	NA	NA
1965	NA	NA	NA	NA	NA
1966	NA	NA	NA	NA	NA
1967	NA	NA	NA	NA	NA
1968	82.0	23/10/1967	2285.2	21/03/1968	120.4
1969	58.3	31/10/1968	2935.2	03/04/1969	102.5
1970	42.0	04/11/1969	2241.4	09/04/1970	104.1
1971	71.5	22/10/1970	2866.9	02/04/1971	76.7
1972	99.4	25/10/1971	3235.3	11/04/1972	164.4
1973	57.0	25/10/1972	2460.6	23/03/1973	142.0
1974	42.6	31/10/1973	3104.8	06/04/1974	181.0
1975	16.7	06/11/1974	2408.2	07/04/1975	106.9
1976	63.8	22/10/1975	2763.6	25/03/1976	144.3
1977	37.4	09/11/1976	1734.1	03/04/1977	51.6
1978	48.1	31/10/1977	2476.3	28/03/1978	85.0
1979	60.8	08/11/1978	2988.2	07/04/1979	102.1
1980	39.9	03/11/1979	2016.2	26/03/1980	58.7
1981	41.1	03/11/1980	1947.6	08/03/1981	100.5
1982	89.7	24/10/1981	2995.4	07/04/1982	84.6
1983	56.0	28/10/1982	2664.6	31/03/1983	128.1
1984	50.4	04/11/1983	2274.0	23/03/1984	66.7
1985	90.2	16/10/1984	2831.2	31/03/1985	133.4
1986	90.6	20/10/1985	2435.2	26/03/1986	105.2
1987	36.7	25/10/1986	2232.7	29/03/1987	179.4
1988	96.2	29/10/1987	2065.2	08/04/1988	114.5
1989	47.1	19/10/1988	2722.7	06/04/1989	183.9
1990	62.5	26/10/1989	2693.1	27/03/1990	139.1
1991	98.0	11/10/1990	2664.3	15/03/1991	190.0
1992	67.2	16/10/1991	2257.1	10/03/1992	148.7
1993	92.2	02/11/1992	1964.8	27/02/1993	53.4
1994	59.2	28/10/1993	2475.9	25/03/1994	109.5
1995	54.0	28/10/1994	2429.5	07/04/1995	89.4
1996	29.3	22/10/1995	3142.9	05/04/1996	142.7
1997	30.1	16/10/1996	2860.5	10/04/1997	100.0
1998	78.5	07/10/1997	2017.1	16/03/1998	72.4
1999	32.6	07/11/1998	2062.6	19/03/1999	61.6
2000	49.4	02/11/1999	1973.6	21/03/2000	63.9
2001	78.1	25/10/2000	2212.2	26/03/2001	83.3

Year	***API***	D_{OF}	$ADDF_W$	D_{OT}	AP_W
	mm		*°C-day*		*mm*
2002	82.2	17/10/2001	2593.1	10/04/2002	73.3
2003	45.8	14/10/2002	2268.0	06/04/2003	79.6
2004	61.1	28/10/2003	2343.4	28/03/2004	78.0
2005	60.0	15/10/2004	2422.5	27/03/2005	181.5
2006	30.3	31/10/2005	1714.8	21/03/2006	87.6
2007	32.8	28/10/2006	2422.5	22/03/2007	118.0
2008	59.8	04/11/2007	2447.8	06/04/2008	114.3
2009	93.0	26/10/2008	2631.1	27/03/2009	121.2
2010	66.4	29/10/2009	2007.5	28/03/2010	97.9

Table B-7: Short-lead variables developed from the meteorological data at HLA.

Year	$\boldsymbol{D_{MO}}$	$\boldsymbol{AS_S}$	$\boldsymbol{AR_S}$
		mm	*mm*
1964	NA	NA	NA
1965	NA	NA	NA
1966	NA	NA	NA
1967	NA	NA	NA
1968	4/6/1968	0.8	6.5
1969	4/17/1969	3.1	27.9
1970	4/18/1970	4.6	5.4
1971	4/16/1971	7.9	7.6
1972	4/29/1972	1.1	1.6
1973	4/21/1973	1.0	15.6
1974	4/15/1974	0.0	0.0
1975	4/16/1975	0.0	5.8
1976	4/11/1976	0.0	11.9
1977	4/10/1977	0.0	2.6
1978	4/18/1978	6.2	22.5
1979	5/7/1979	27.2	19.8
1980	4/4/1980	0.0	5.6
1981	4/22/1981	17.5	37.8
1982	4/14/1982	3.0	43.4
1983	4/24/1983	12.2	0.3
1984	4/7/1984	2.1	3.2
1985	4/26/1985	2.0	4.0
1986	4/15/1986	1.2	14.2
1987	4/24/1987	2.6	12.4
1988	4/16/1988	0.0	10.8
1989	4/29/1989	5.4	0.2
1990	4/18/1990	7.4	0.6
1991	4/21/1991	5.0	0.2
1992	4/21/1992	1.1	11.0
1993	3/26/1993	7.4	0.0
1994	4/11/1994	0.0	26.2
1995	4/21/1995	9.2	0.0
1996	4/25/1996	6.4	7.6
1997	4/23/1997	2.6	17.6
1998	4/6/1998	0.2	0.4
1999	4/13/1999	6.0	6.4
2000	4/17/2000	4.4	7.2
2001	4/19/2001	6.0	0.4

Year	D_{MO}	AS_S	AR_S
		mm	*mm*
2002	4/22/2002	4.8	1.3
2003	4/13/2003	0.0	21.8
2004	4/6/2004	0.0	7.2
2005	4/12/2005	0.8	7.4
2006	4/10/2006	0.0	12.6
2007	4/17/2007	14.2	24.2
2008	4/27/2008	11.9	4.6
2009	4/19/2009	2.8	12.0
2010	4/17/2010	8.5	14.4

Table B-8: Extracted variables from the hydrometric data at HRMR.

Year	H_{OF} *m*	D_{OR}	H_{OR} *m*	D_{Qp}	Q_P m^3/s
1964	NA	NA	NA	NA	NA
1965	NA	NA	NA	NA	NA
1966	NA	NA	NA	NA	NA
1967	NA	NA	NA	NA	NA
1968	NA	NA	NA	NA	NA
1969	NA	NA	NA	NA	NA
1970	NA	NA	NA	NA	NA
1971	NA	NA	NA	NA	NA
1972	NA	NA	NA	NA	NA
1973	NA	NA	NA	NA	NA
1974	NA	NA	NA	NA	NA
1975	4.10	18/04/1975	3.86	04/05/1975	202
1976	3.80	06/04/1976	3.84	28/04/1976	268
1977	5.15	09/04/1977	4.12	04/05/1977	200
1978	4.91	23/04/1978	4.09	05/05/1978	422
1979	4.35	26/04/1979	3.87	19/05/1979	492
1980	4.49	06/04/1980	3.83	23/04/1980	102
1981	3.60	23/04/1981	3.60	05/05/1981	563
1982	3.41	27/04/1982	3.69	18/05/1982	358
1983	3.63	17/04/1983	3.78	29/04/1983	300
1984	3.65	14/04/1984	3.64	26/04/1984	41.8
1985	4.80	17/04/1985	3.94	10/05/1985	496
1986	4.86	16/04/1986	3.79	14/05/1986	261
1987	4.13	16/04/1987	3.97	06/05/1987	341
1988	4.37	13/04/1988	3.99	12/05/1988	261
1989	4.79	21/04/1989	4.08	06/05/1989	631
1990	4.35	11/04/1990	4.06	28/04/1990	371
1991	3.52	17/04/1991	3.79	01/05/1991	221
1992	4.22	05/04/1992	4.43	07/05/1992	583
1993	5.27	02/04/1993	3.92	24/04/1993	87.8
1994	4.27	04/04/1994	4.03	29/04/1994	544
1995	3.67	23/04/1995	3.84	02/05/1995	175
1996	3.43	18/04/1996	3.86	05/05/1996	464
1997	4.66	22/04/1997	4.21	12/05/1997	507
1998	6.56	07/04/1998	4.34	19/04/1998	225
1999	3.71	17/04/1999	3.91	01/05/1999	147
2000	4.07	22/04/2000	4.08	13/05/2000	229
2001	4.34	20/04/2001	4.00	09/05/2001	182
2002	4.00	27/04/2002	3.86	21/05/2002	244

Year	H_{OF} m	D_{OR}	H_{OR} m	D_{Qp}	Q_P m^3/s
2003	4.04	16/04/2003	3.75	30/04/2003	480
2004	3.80	07/04/2004	3.84	05/05/2004	115
2005	4.17	07/04/2005	3.86	29/04/2005	518
2006	4.05	08/04/2006	3.90	30/04/2006	207
2007	3.64	15/04/2007	3.93	12/05/2007	629
2008	4.89	25/04/2008	4.37	10/05/2008	468
2009	4.63	14/04/2009	4.12	12/05/2009	441
2010	4.90	15/04/2010	4.31	29/04/2010	252

Table B-9. Late winter SWE from the snow course surveys at the Hay River basin.

Year	Upper basin *SWEsc*, mm		Lower basin *SWEsc*, mm	
	High Level	Assumption	Hay River	Swede Creek
1964				
1965				
1966				
1967				
1968				
1969				
1970				
1971				
1972				
1973				
1974				
1975				
1976				
1977				
1978				
1979				
1980				
1981				
1982			100	86
1983			122	95
1984			90	74
1985			111	119
1986	107	86	95	99
1987	128	124	97	78
1988	85	64	126	102
1989	146	152	67	67
1990	113	104	120	103
1991	135	131	94	85
1992	90	66	121	103
1993	27	0	51	36
1994	88	64	109	84
1995	58	52	121	99
1996	168	194	65	76
1997	108	114	74	85
1998	58	60	84	70
1999	70	61	72	69
2000	65	51	56	75

Year	Upper basin *SWEsc*, mm		Lower basin *SWEsc*, mm	
	High Level	Assumption	Hay River	Swede Creek
2001	80	79	104.1	104.1
2002	98	108	97	86.1
2003	93	75	90.5	80.5
2004	89	79	88.9	101.6
2005	150	116	111.8	134.6
2006	75	75	83.8	91.4
2007	123	117	129	88.9
2008	122	109	93.3	109.1
2009	121	124	141	143
2010	59	78	80	72

Table B-10: Extracted variables from the hydrometric data at CRHL.

Year	D_{Qp}	Q_P m^3/s
1964	NA	NA
1965	NA	NA
1966	NA	NA
1967	NA	NA
1968	NA	NA
1969	NA	NA
1970	25/04/1970	126
1971	28/04/1971	292
1972	07/05/1972	748
1973	04/05/1973	244
1974	29/04/1974	810
1975	03/05/1975	94.9
1976	26/04/1976	112
1977	01/05/1977	69.1
1978	02/05/1978	328
1979	17/05/1979	341
1980	19/04/1980	20
1981	04/05/1981	479
1982	16/05/1982	249
1983	27/04/1983	160
1984	24/04/1984	22.6
1985	08/05/1985	236
1986	15/05/1986	131
1987	05/05/1987	154
1988	09/05/1988	103
1989	04/05/1989	547
1990	26/04/1990	288
1991	29/04/1991	119
1992	04/05/1992	411
1993	24/04/1993	26.5
1994	26/04/1994	382
1995	30/04/1995	86.5
1996	03/05/1996	287
1997	10/05/1997	405
1998	20/04/1998	55
1999	29/04/1999	67.2
2000	11/05/2000	153
2001	10/05/2001	75
2002	19/05/2002	159

Year	D_{Qp}	Q_P m^3/s
2003	28/04/2003	337
2004	02/05/2004	72.5
2005	26/04/2005	409
2006	29/04/2006	74.8
2007	09/05/2007	625
2008	08/05/2008	267
2009	10/05/2009	230
2010	27/04/2010	84.8

Appendix C Extraction of peak snowmelt runoffs from the discharge hydrographs at the WSC gauges in the Hay River basin

This appendix shows all the available discharge hydrographs at the gauges of HRHR, HRMR and CRHL, and the extractions of the peak snowmelt runoffs for each gauge. These extracted variables were used in Chapter 4 as the output variables for the fuzzy logic models.

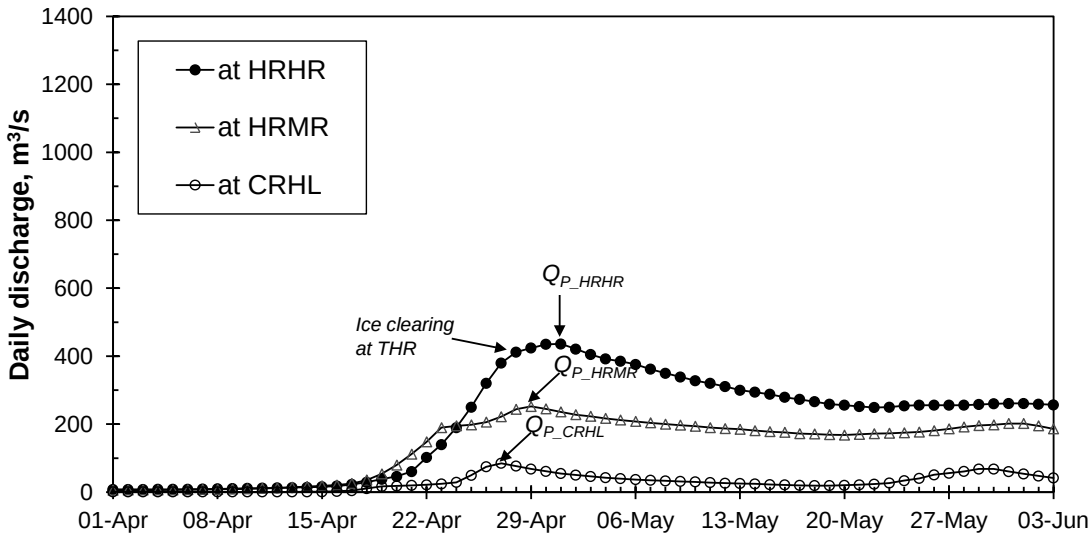

Figure C-1: Discharge hydrographs at the three Hay River WSC gauges in 2010.

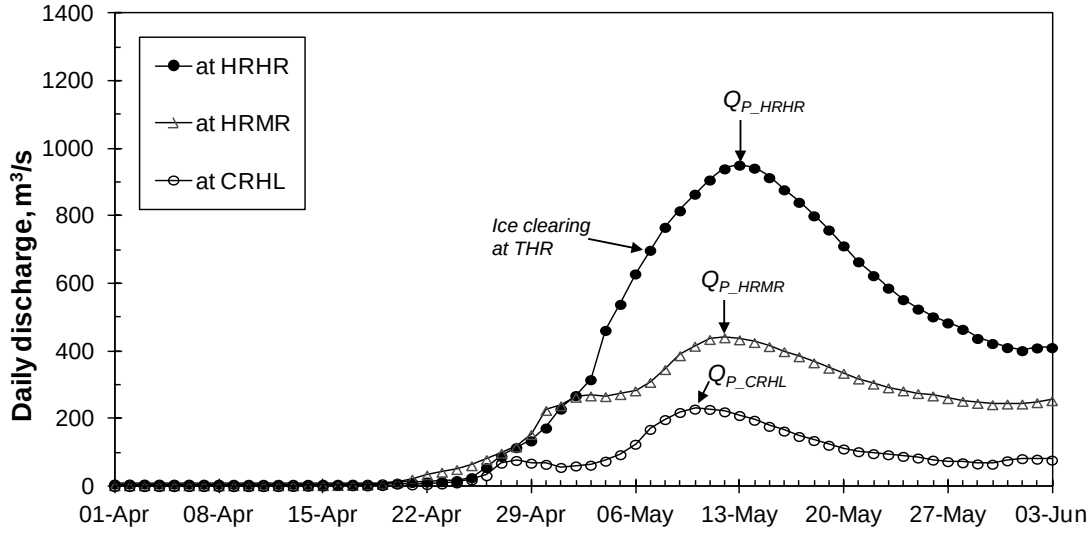

Figure C-2: Discharge hydrographs at the three Hay River WSC gauges in 2009.

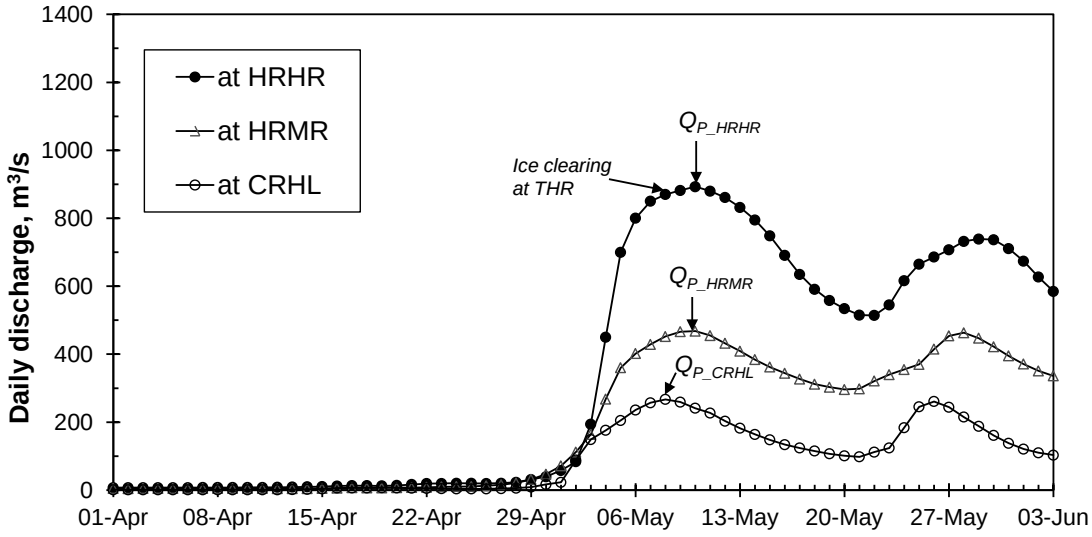

Figure C-3: Discharge hydrographs at the three Hay River WSC gauges in 2008.

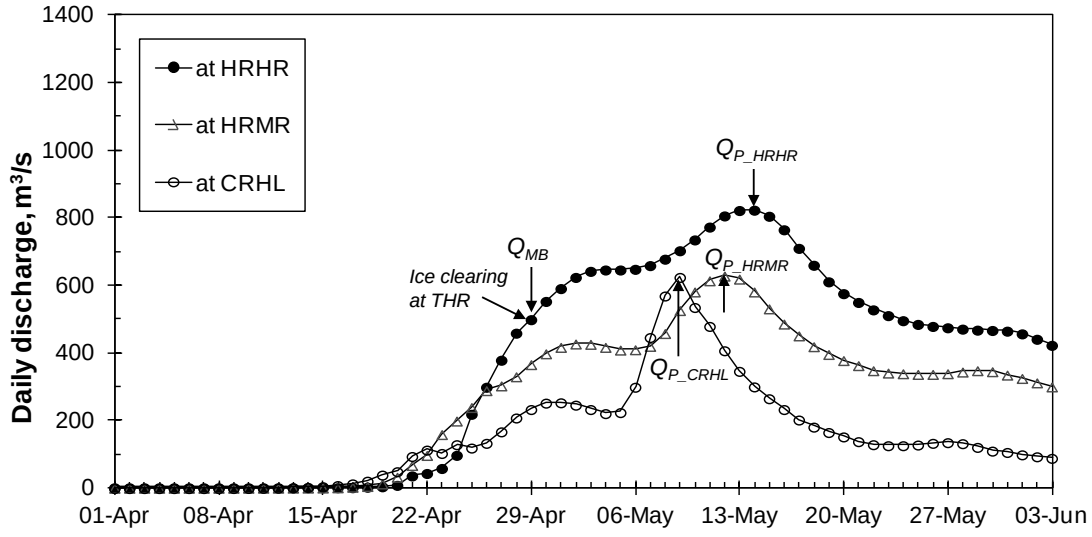

Figure C-4: Discharge hydrographs at the three Hay River WSC gauges in 2007.

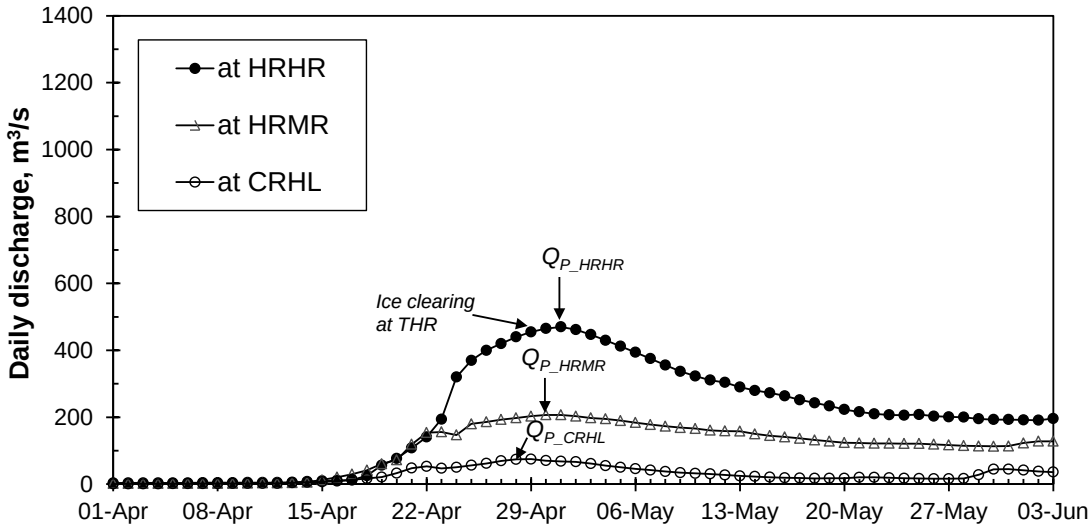

Figure C-5: Discharge hydrographs at the three Hay River WSC gauges in 2006.

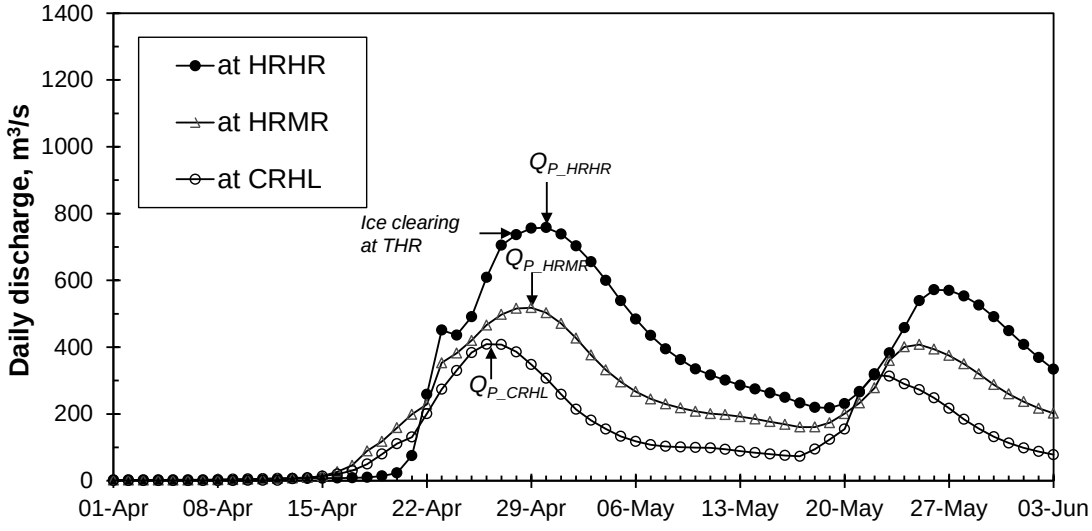

Figure C-6: Discharge hydrographs at the three Hay River WSC gauges in 2005.

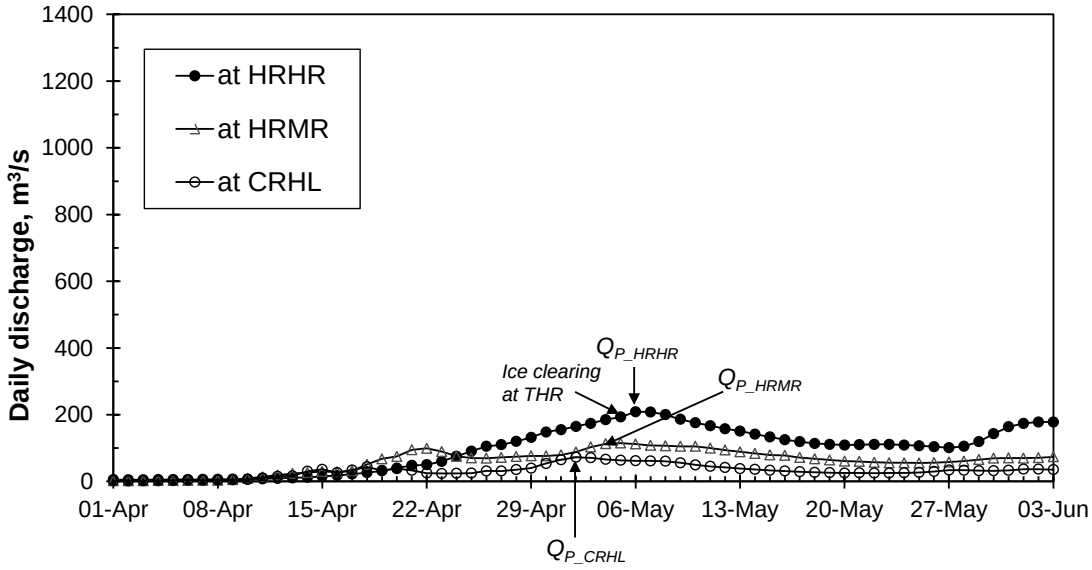

Figure C-7: Discharge hydrographs at the three Hay River WSC gauges in 2004.

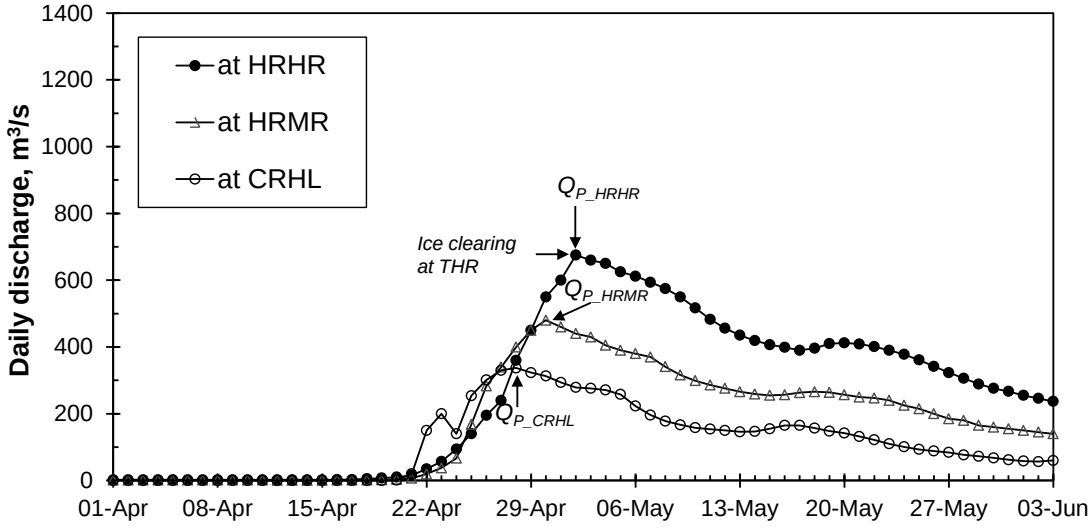

Figure C-8: Discharge hydrographs at the three Hay River WSC gauges in 2003.

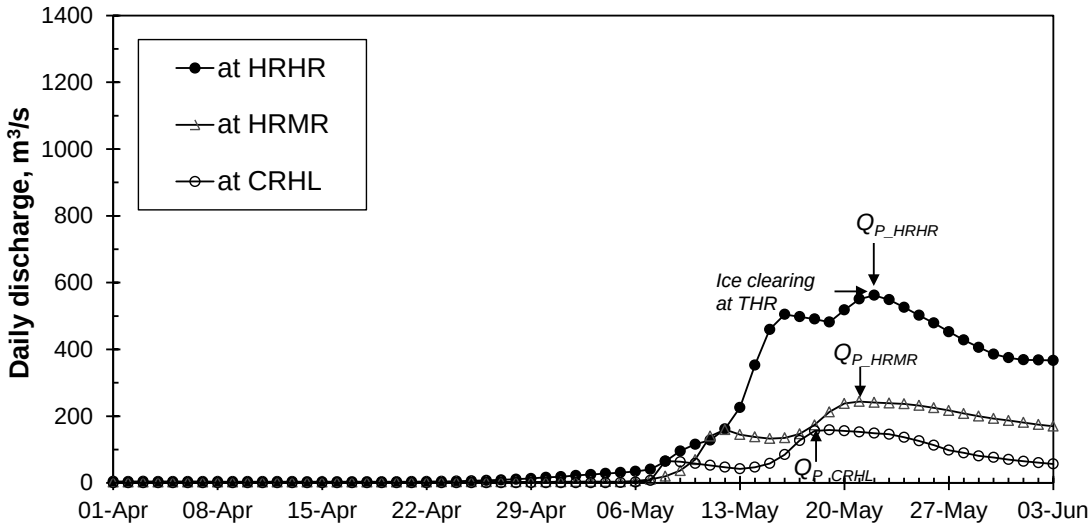

Figure C-9: Discharge hydrographs at the three Hay River WSC gauges in 2002.

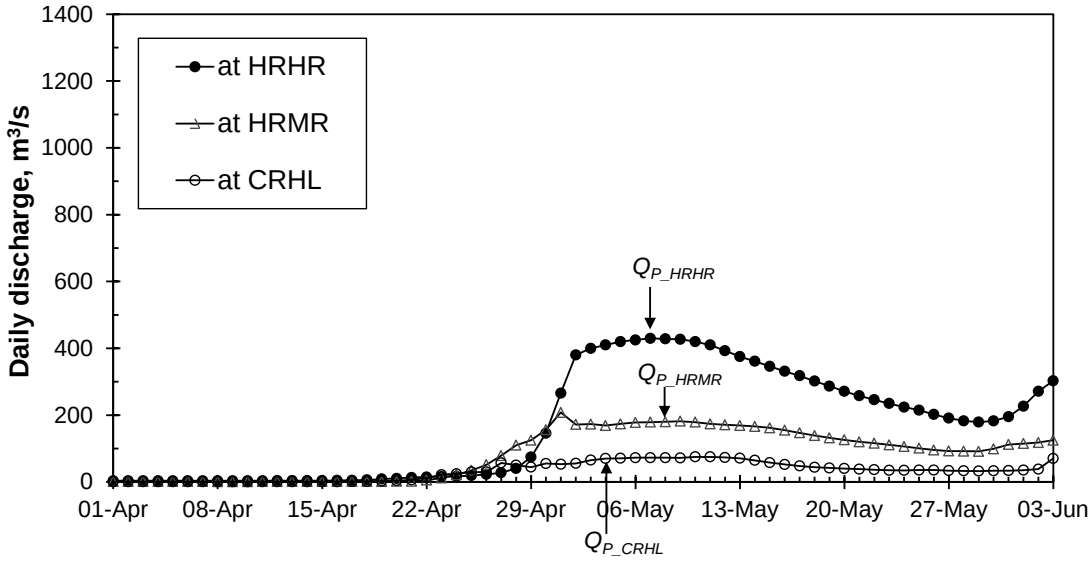

Figure C-10: Discharge hydrographs at the three Hay River WSC gauges in 2001.

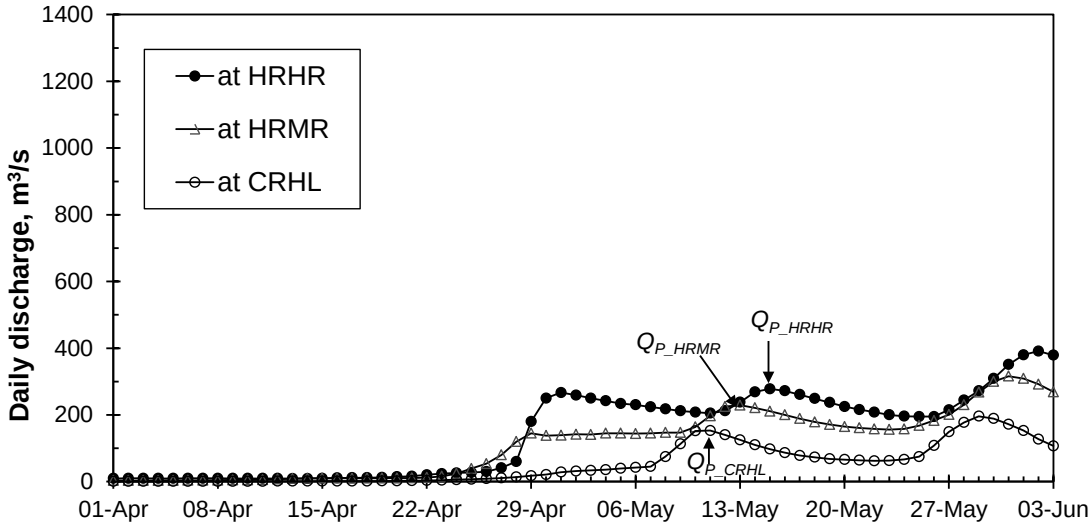

Figure C-11: Discharge hydrographs at the three Hay River WSC gauges in 2000.

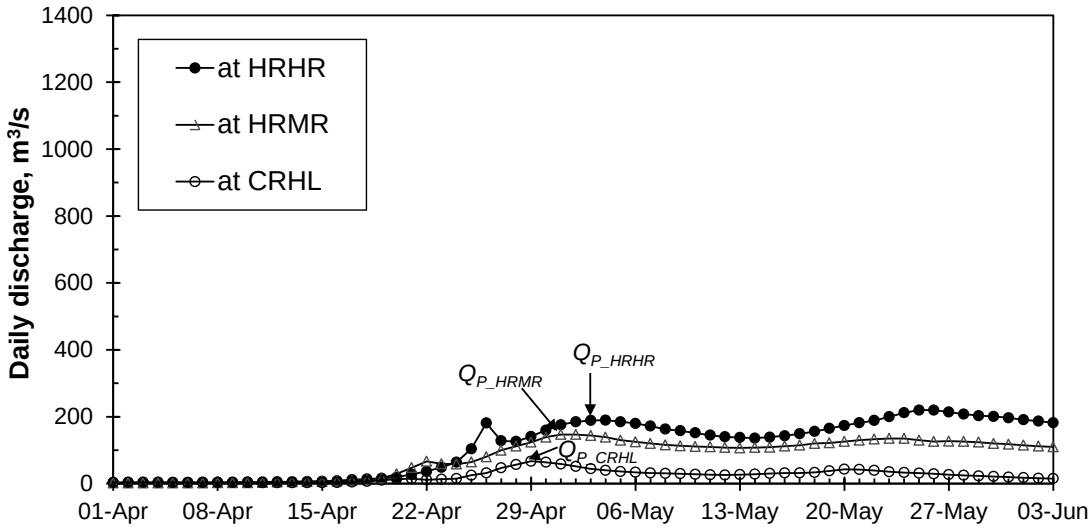

Figure C-12: Discharge hydrographs at the three Hay River WSC gauges in 1999.

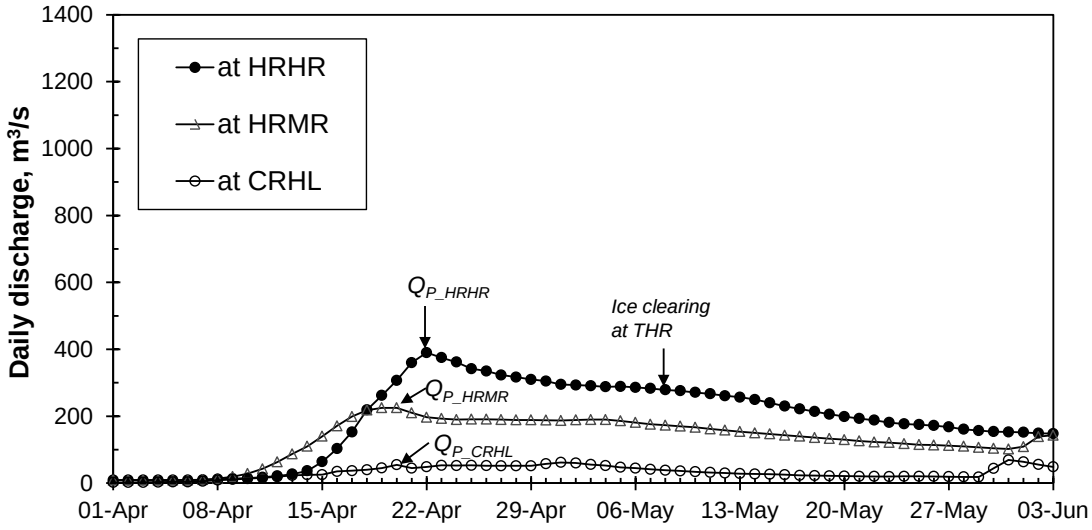

Figure C-13: Discharge hydrographs at the three Hay River WSC gauges in 1998.

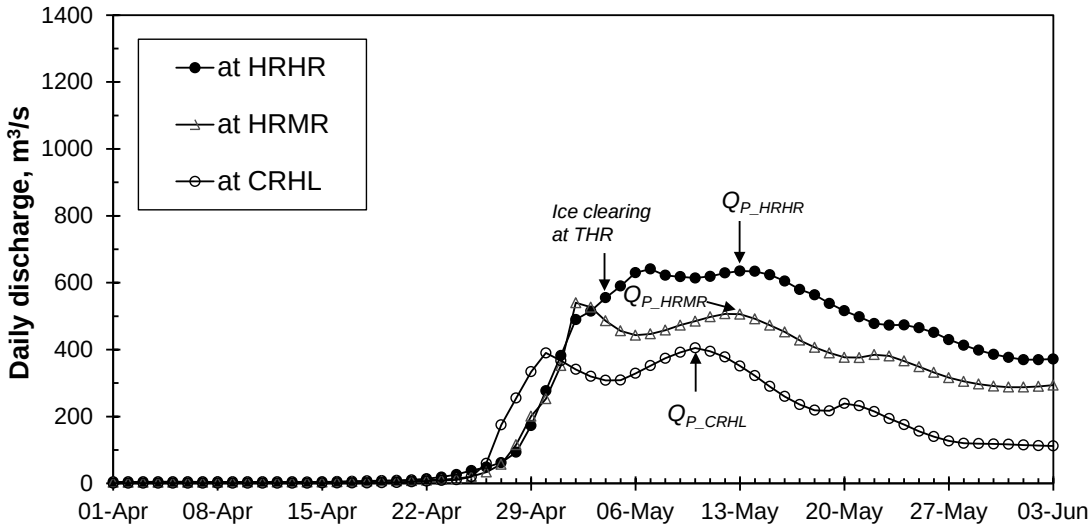

Figure C-14: Discharge hydrographs at the three Hay River WSC gauges in 1997.

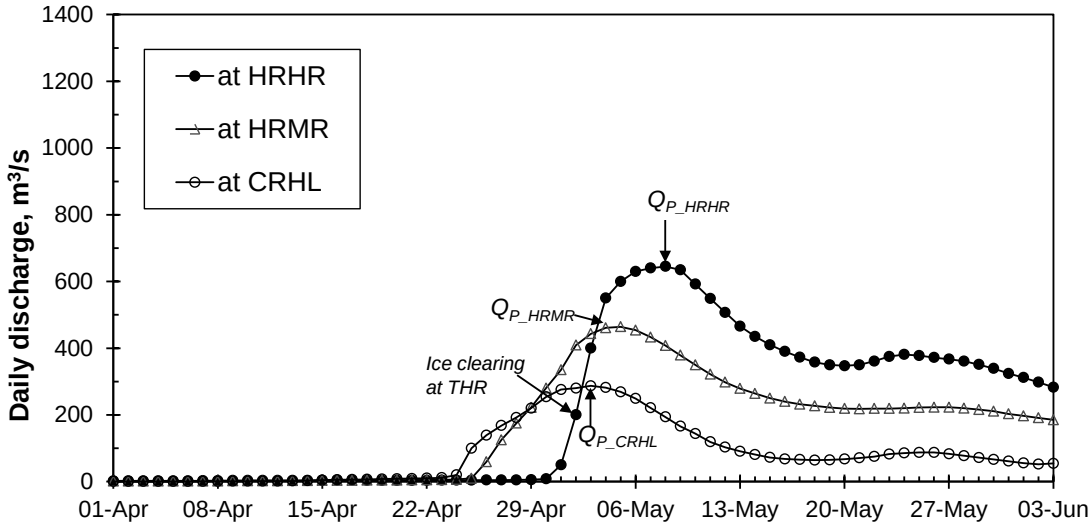

Figure C-15: Discharge hydrographs at the three Hay River WSC gauges in 1996.

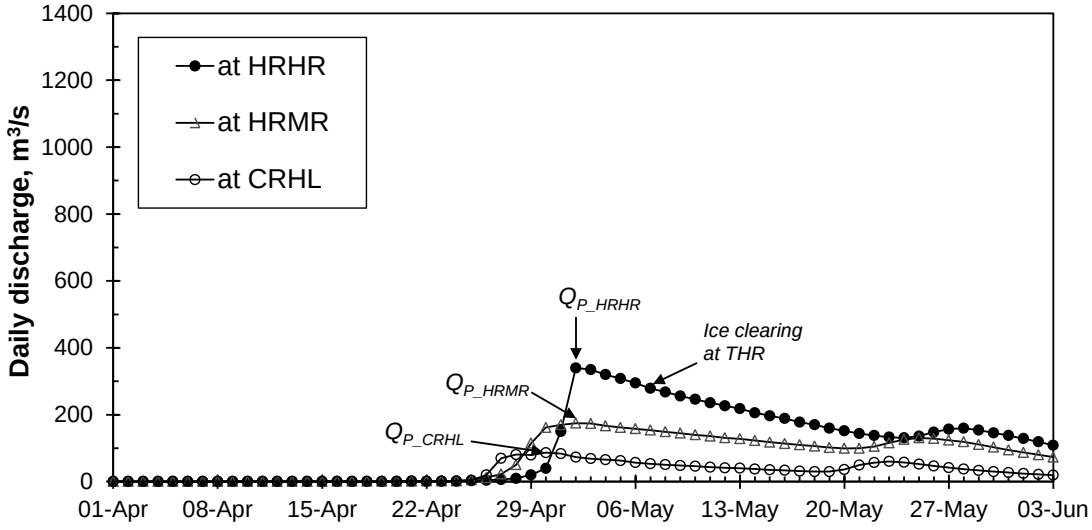

Figure C-16: Discharge hydrographs at the three Hay River WSC gauges in 1995.

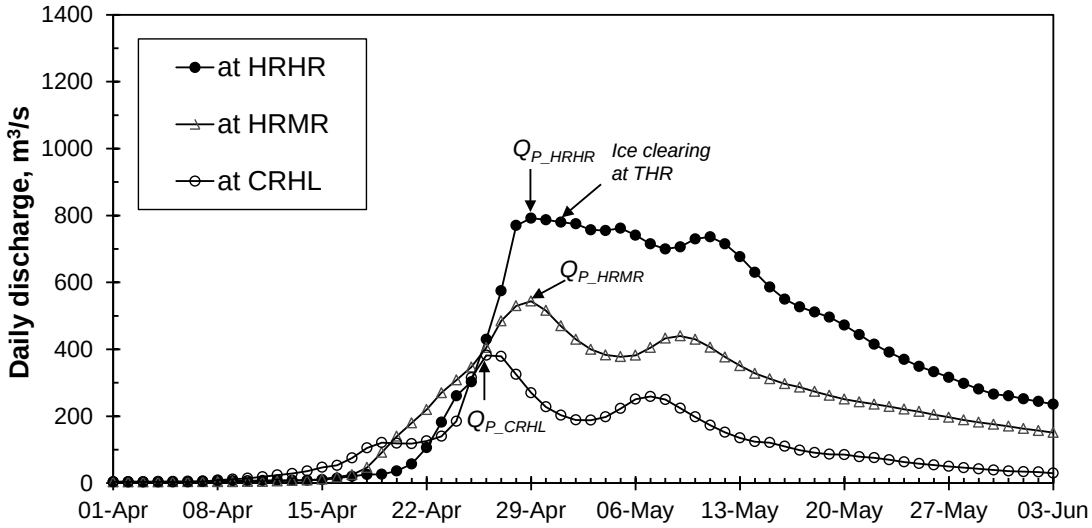

Figure C-17: Discharge hydrographs at the three Hay River WSC gauges in 1994.

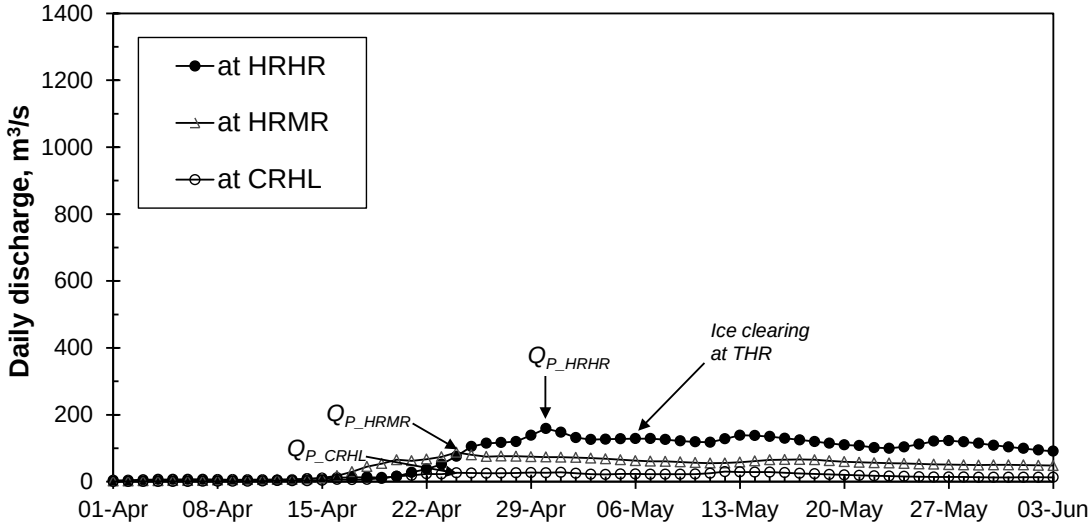

Figure C-18: Discharge hydrographs at the three Hay River WSC gauges in 1993.

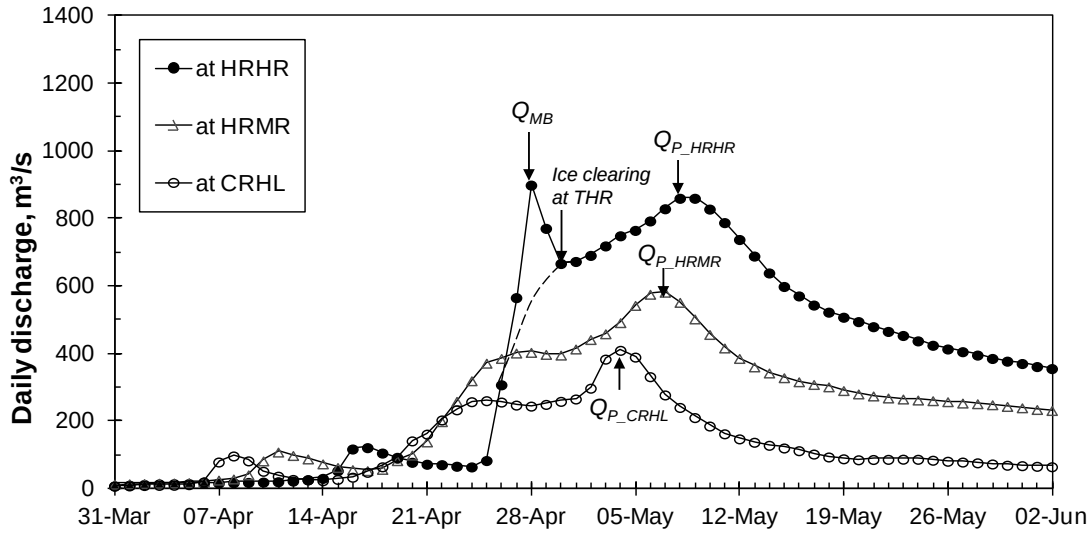

Figure C-19: Discharge hydrographs at the three Hay River WSC gauges in 1992.

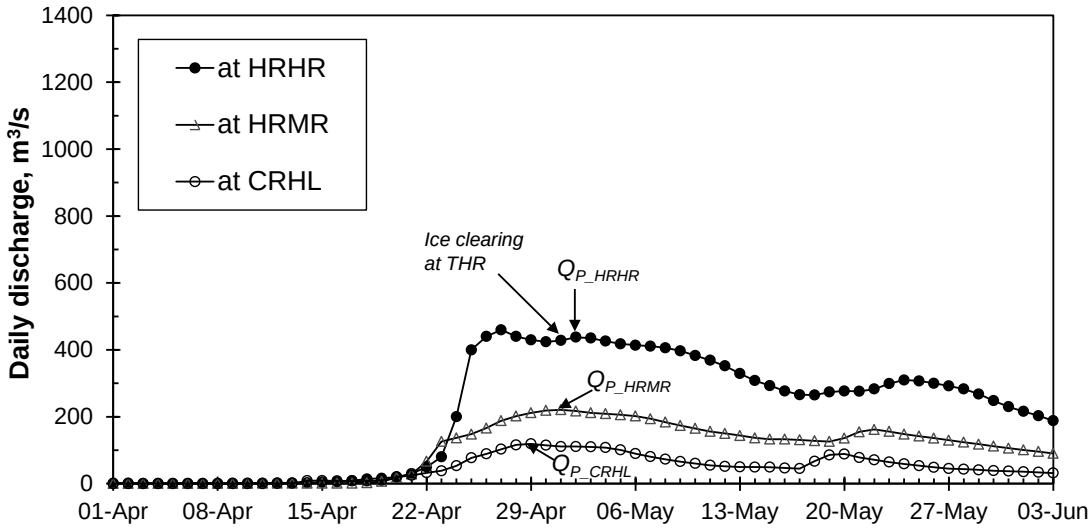

Figure C-20: Discharge hydrographs at the three Hay River WSC gauges in 1991.

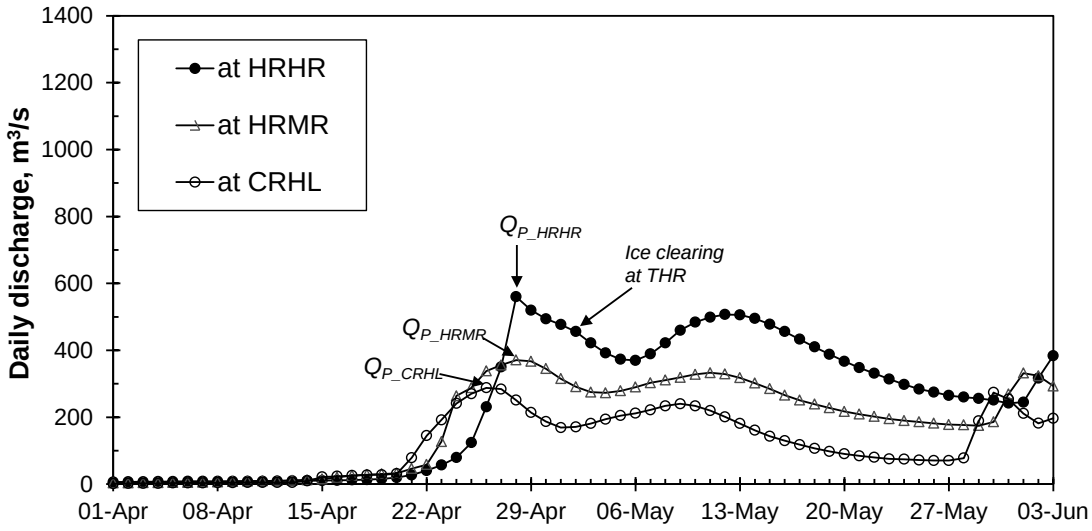

Figure C-21: Discharge hydrographs at the three Hay River WSC gauges in 1990.

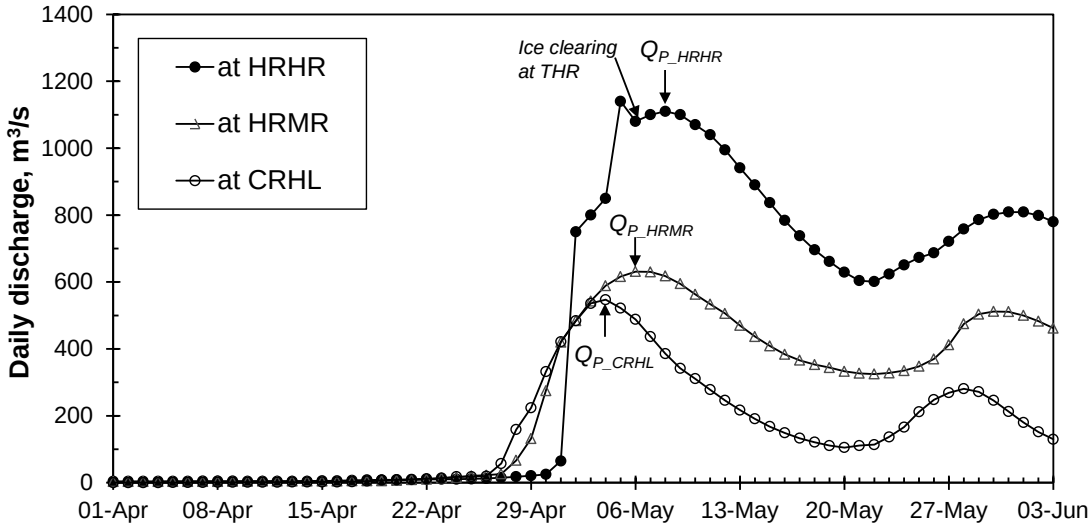

Figure C-22: Discharge hydrographs at the three Hay River WSC gauges in 1989.

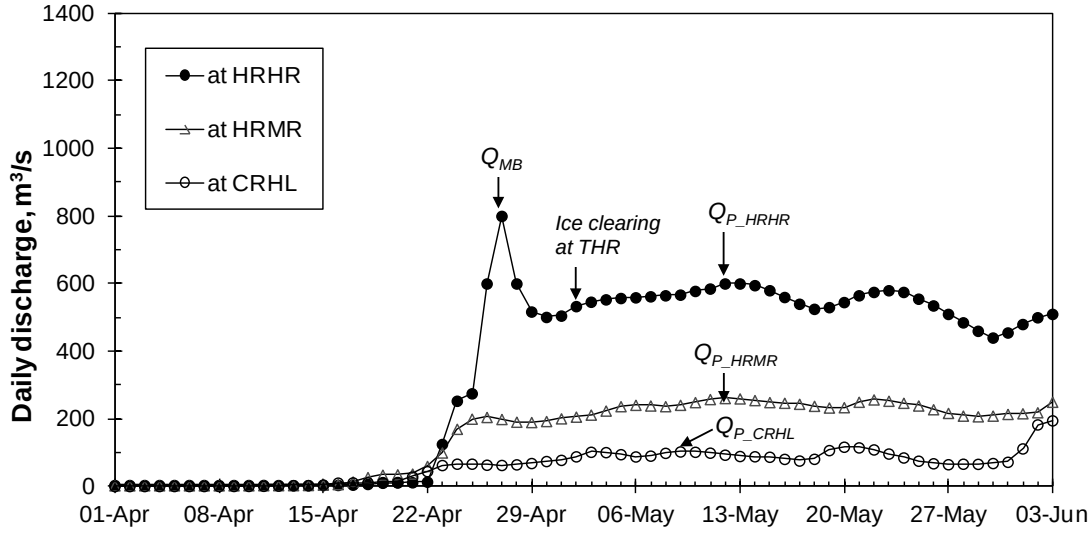

Figure C-23: Discharge hydrographs at the three Hay River WSC gauges in 1988.

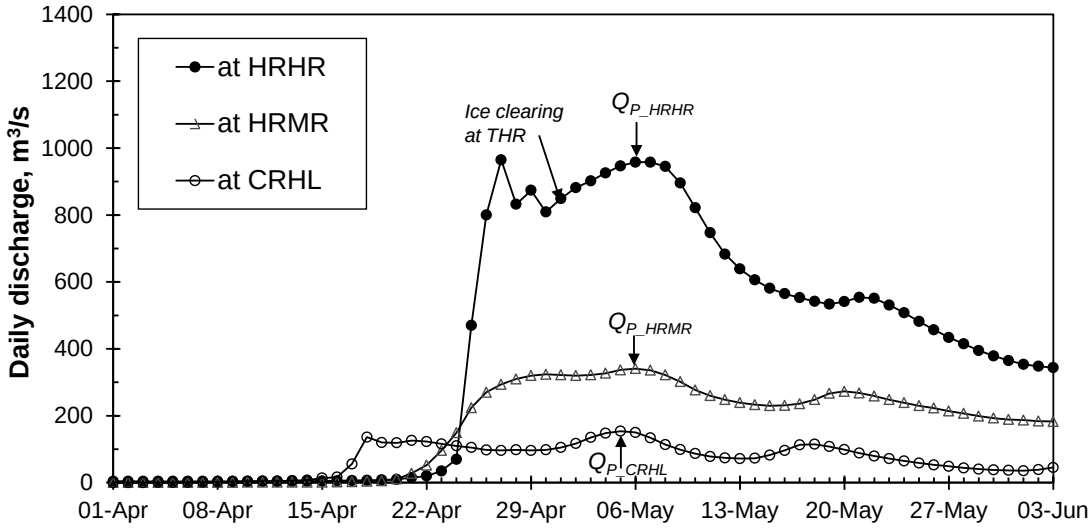

Figure C-24: Discharge hydrographs at the three Hay River WSC gauges in 1987.

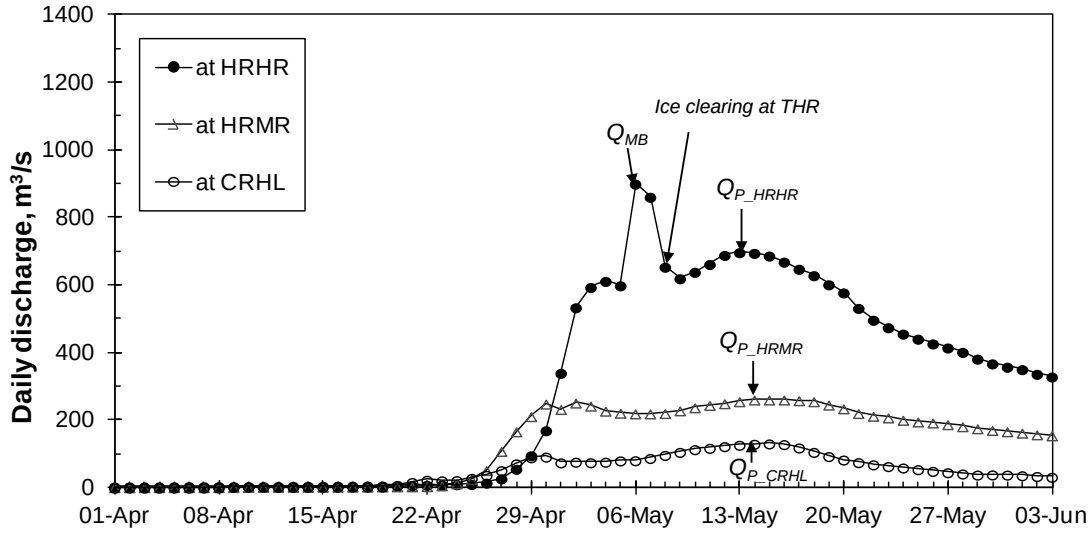

Figure C-25: Discharge hydrographs at the three Hay River WSC gauges in 1986.

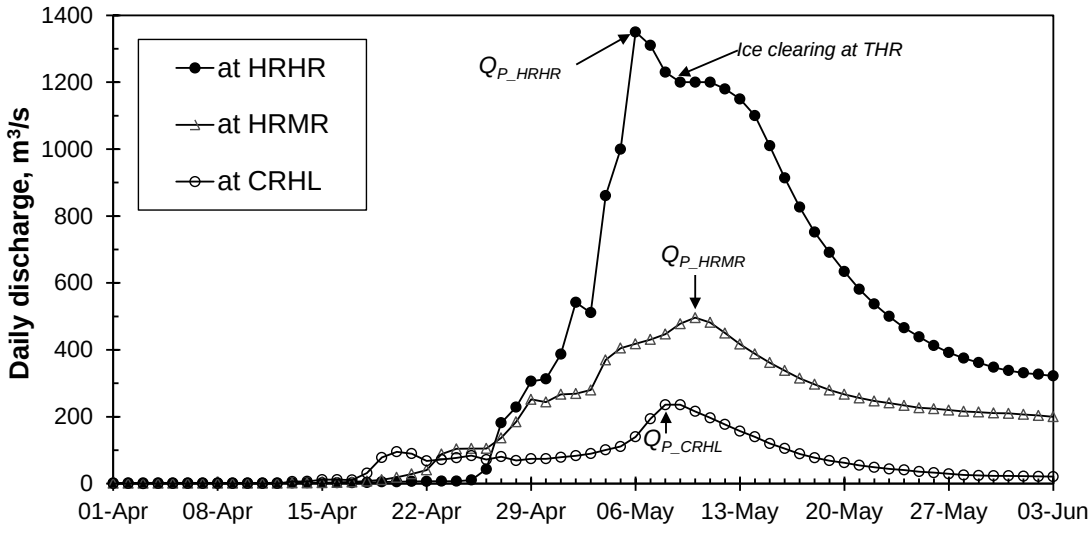

Figure C-26: Discharge hydrographs at the three Hay River WSC gauges in 1985.

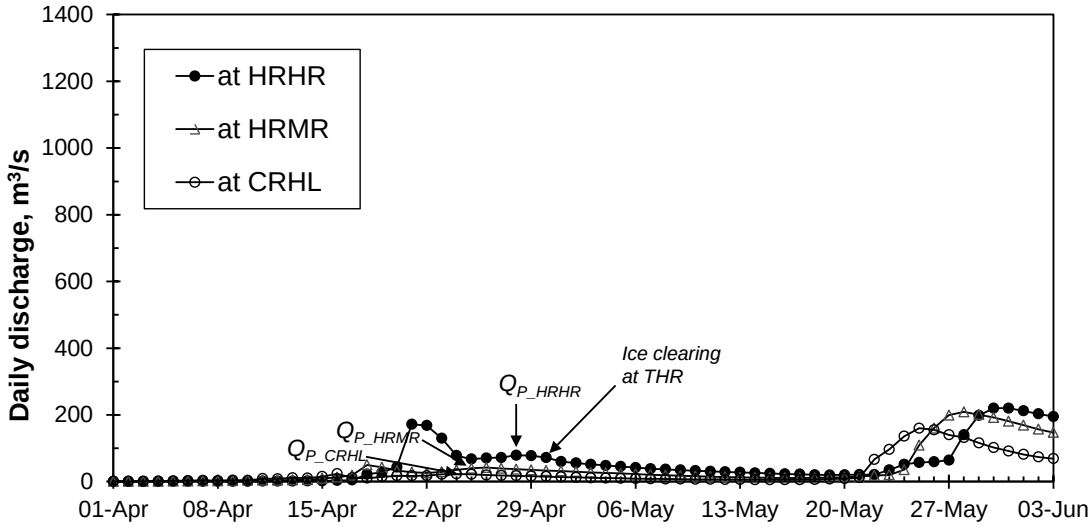

Figure C-27: Discharge hydrographs at the three Hay River WSC gauges in 1984.

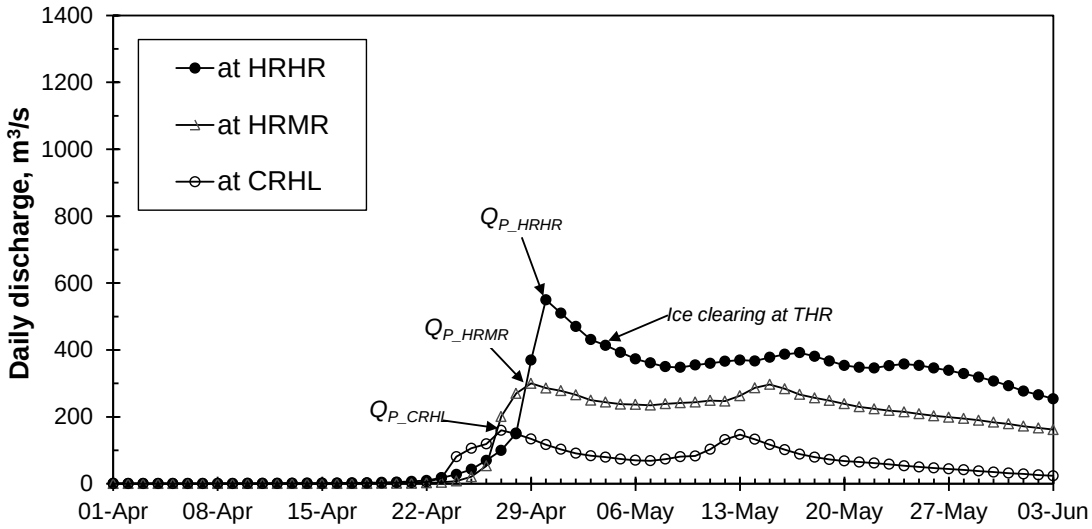

Figure C-28: Discharge hydrographs at the three Hay River WSC gauges in 1983.

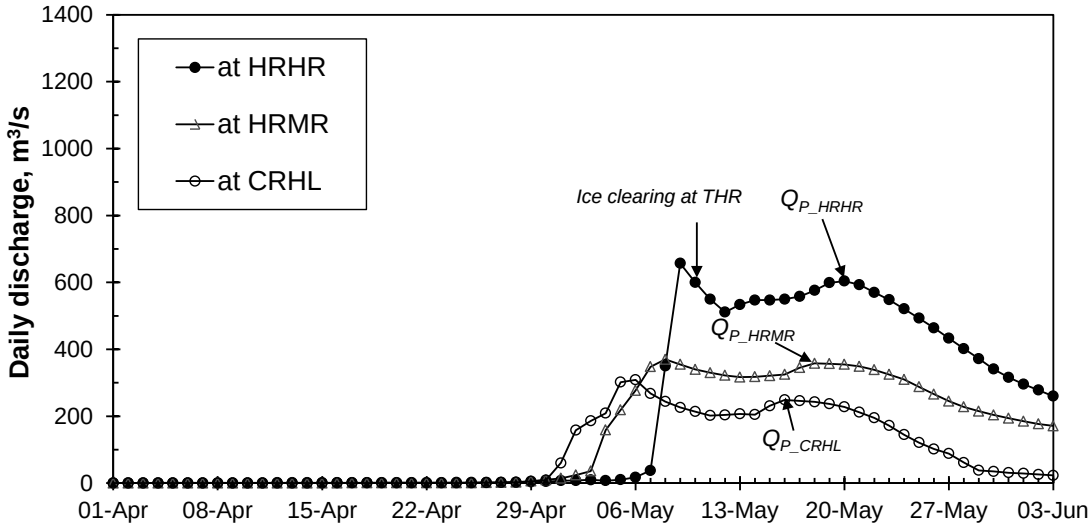

Figure C-29: Discharge hydrographs at the three Hay River WSC gauges in 1982.

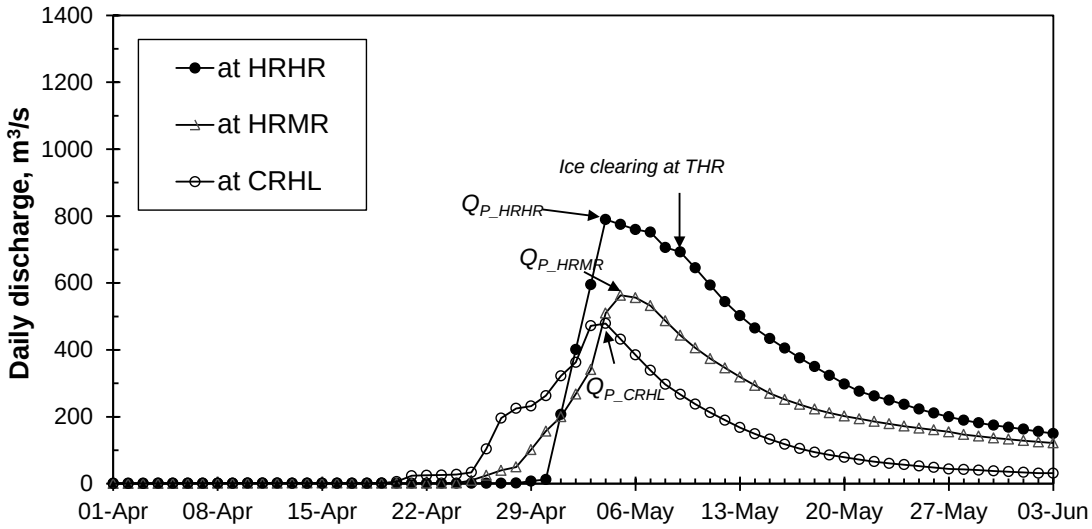

Figure C-30: Discharge hydrographs at the three Hay River WSC gauges in 1981.

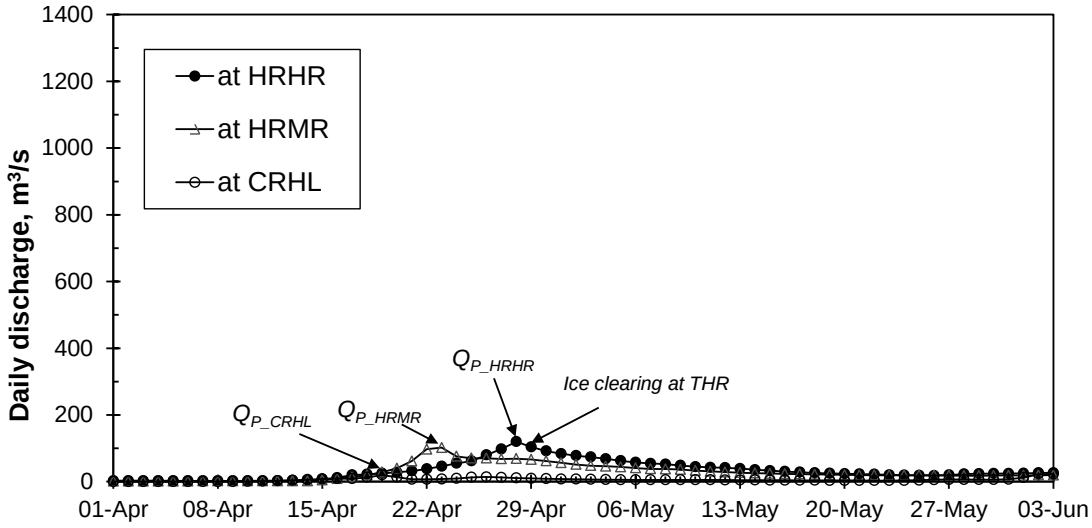

Figure C-31: Discharge hydrographs at the three Hay River WSC gauges in 1980.

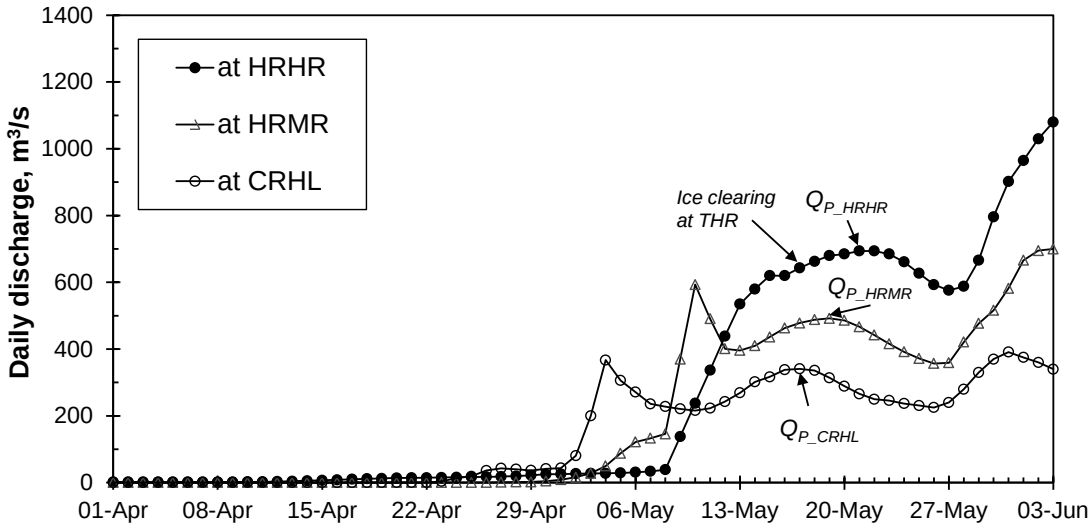

Figure C-32: Discharge hydrographs at the three Hay River WSC gauges in 1979.

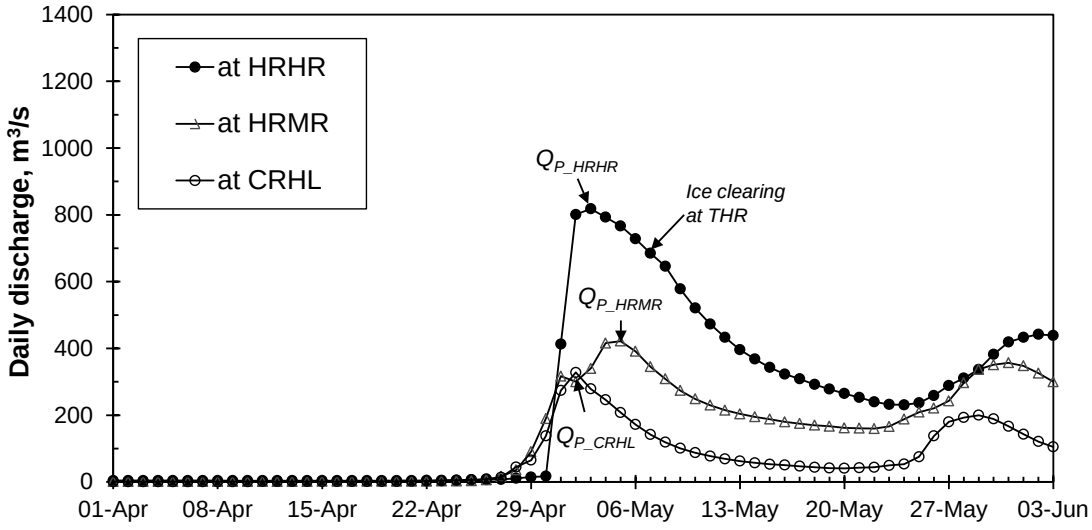

Figure C-33: Discharge hydrographs at the three Hay River WSC gauges in 1978.

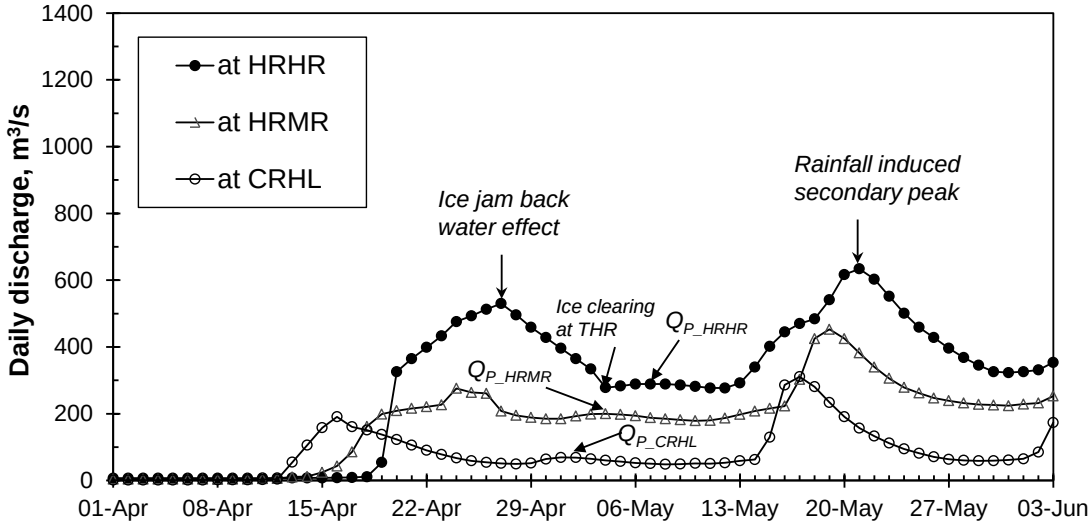

Figure C-34: Discharge hydrographs at the three Hay River WSC gauges in 1977.

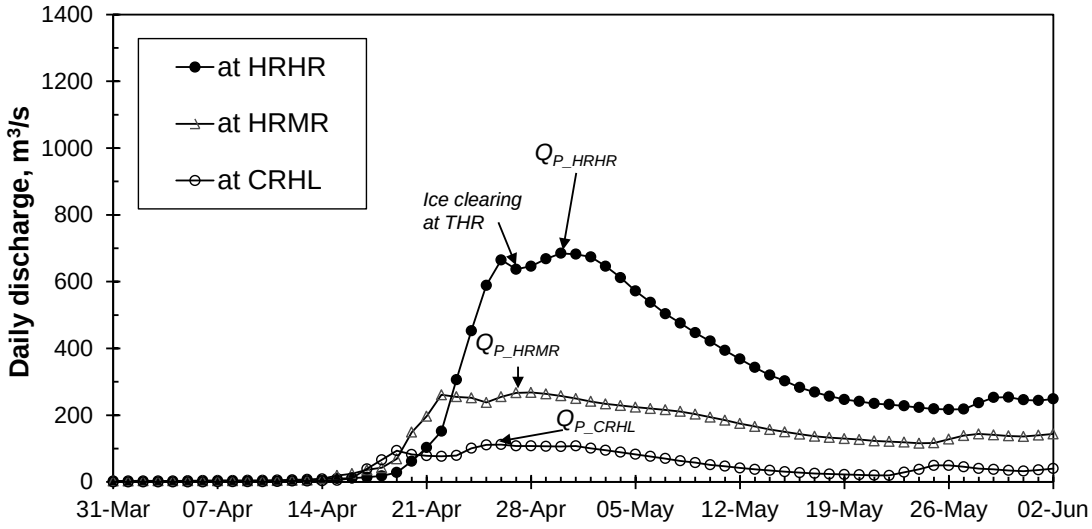

Figure C-35: Discharge hydrographs at the three Hay River WSC gauges in 1976.

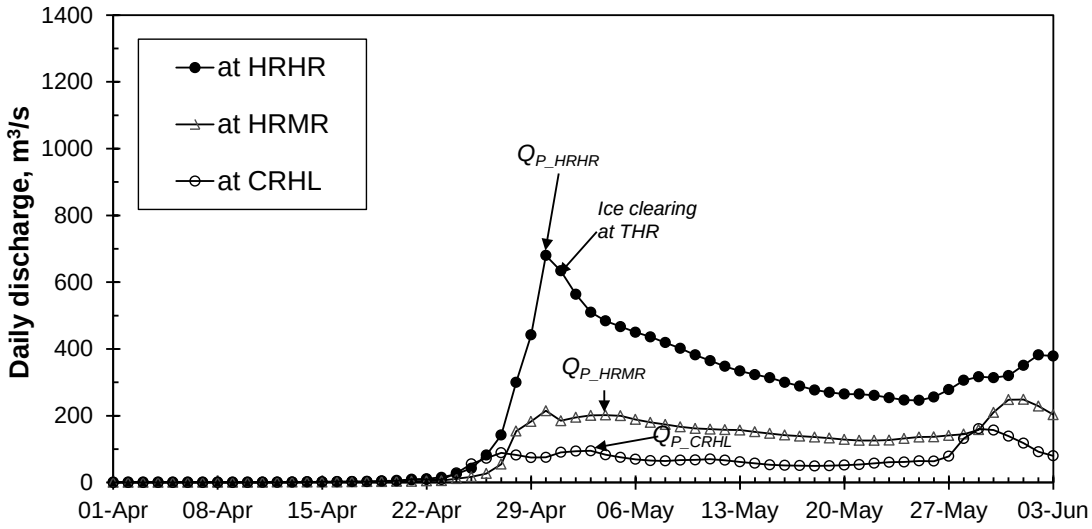

Figure C-36: Discharge hydrographs at the three Hay River WSC gauges in 1975.

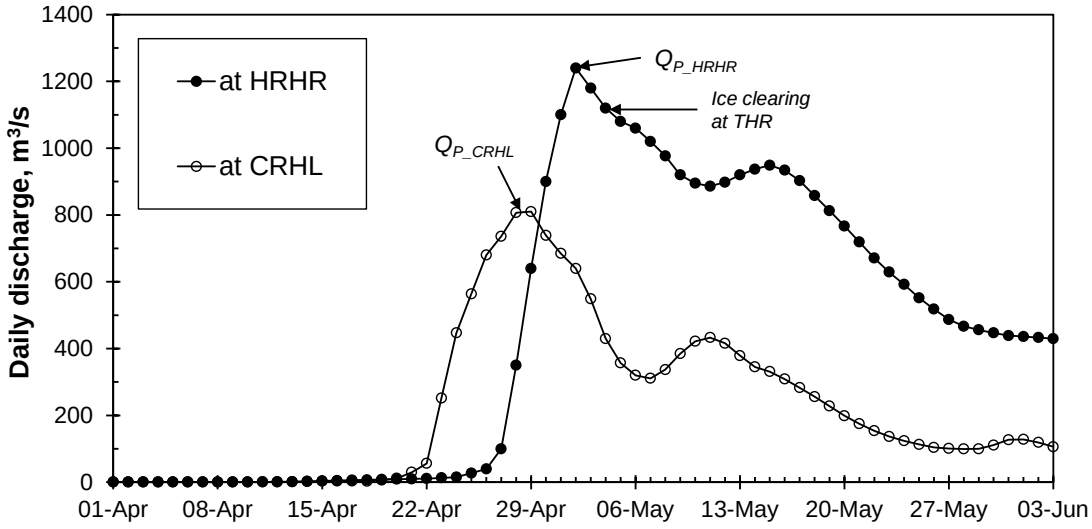

Figure C-37: Discharge hydrographs at the three Hay River WSC gauges in 1974.

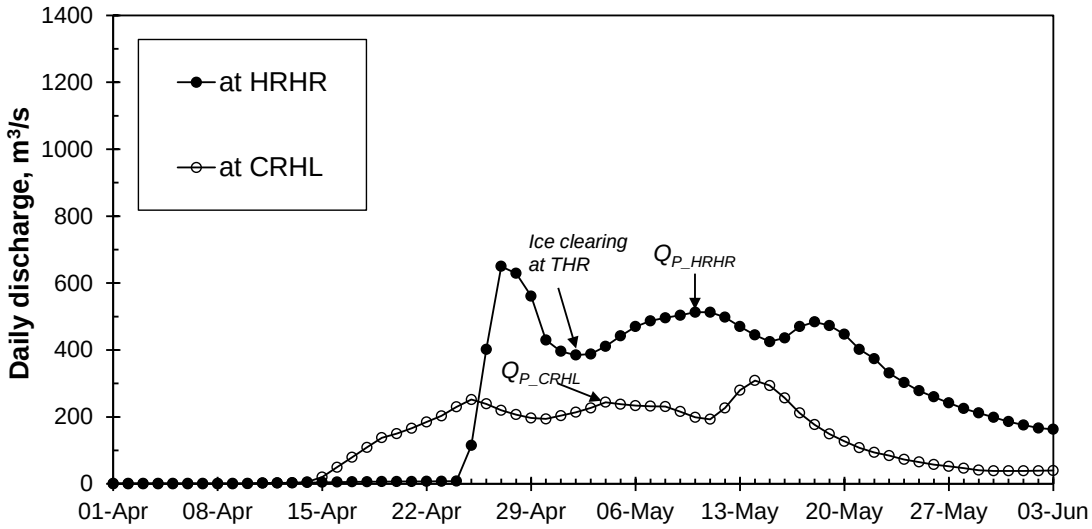

Figure C-38: Discharge hydrographs at the three Hay River WSC gauges in 1973.

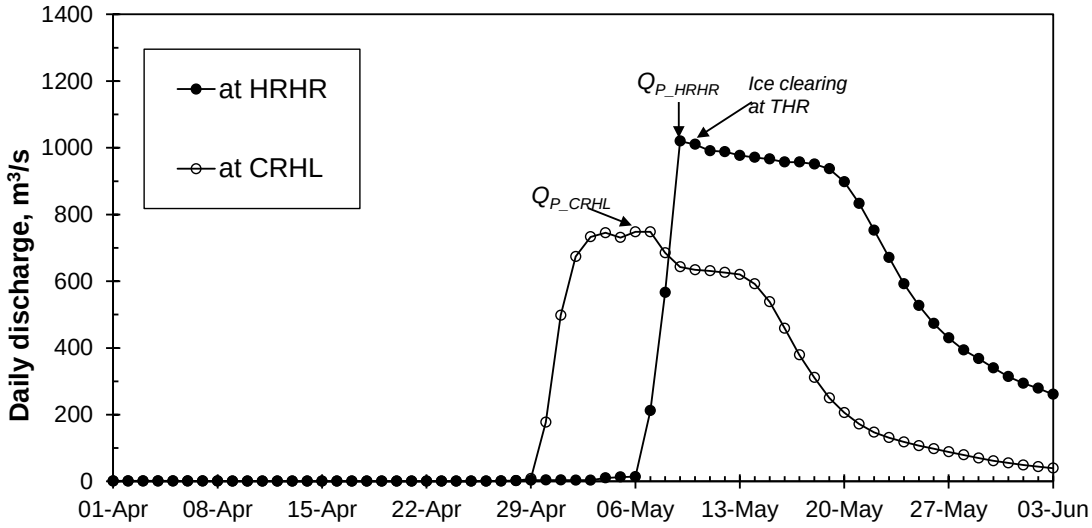

Figure C-39: Discharge hydrographs at the three Hay River WSC gauges in 1972.

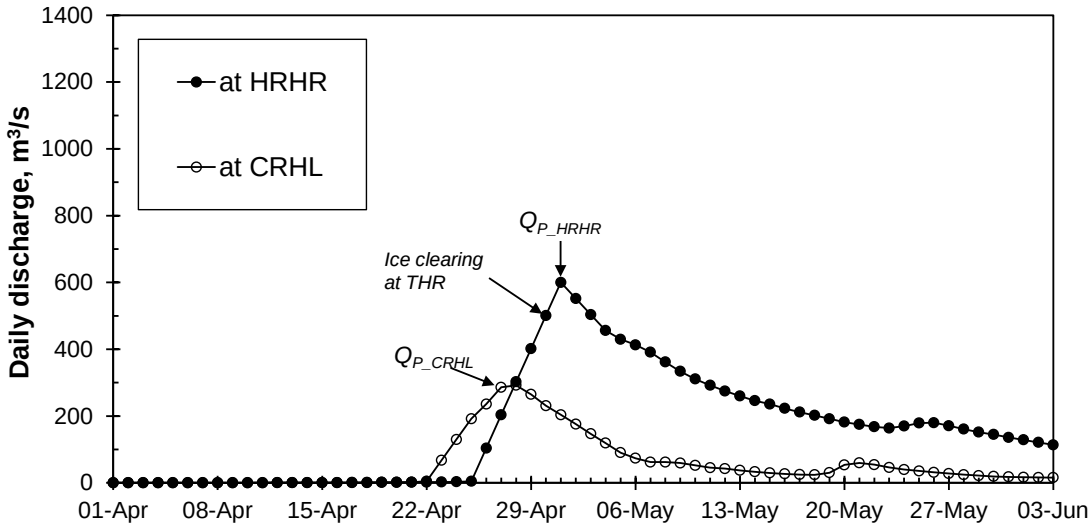

Figure C-40: Discharge hydrographs at the three Hay River WSC gauges in 1971.

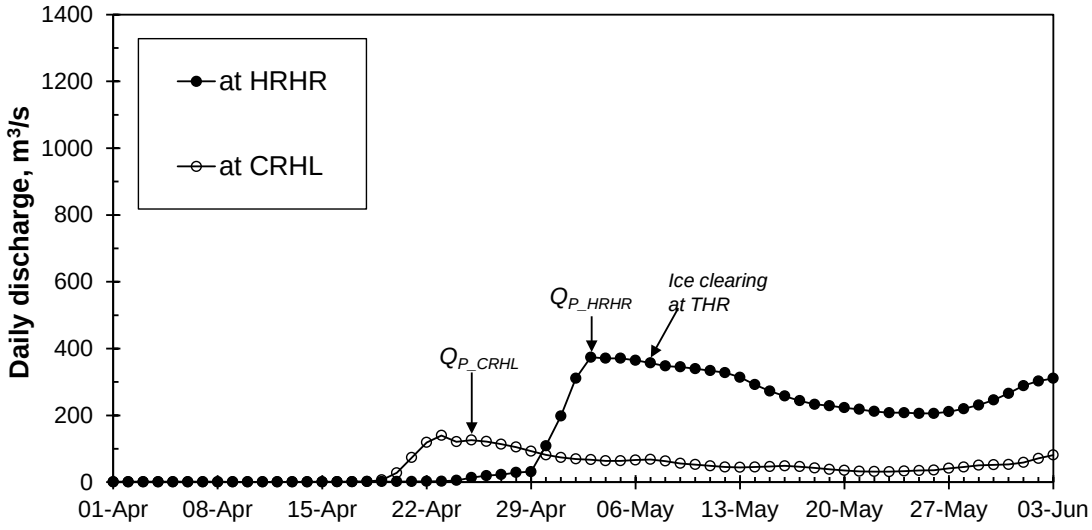

Figure C-41: Discharge hydrographs at the three Hay River WSC gauges in 1970.

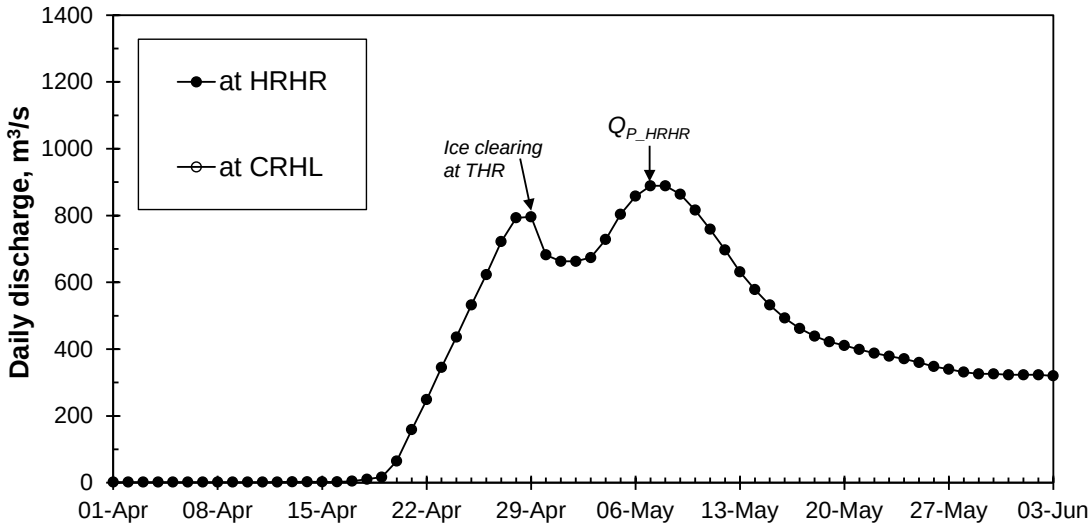

Figure C-42: Discharge hydrographs at the three Hay River WSC gauges in 1969.

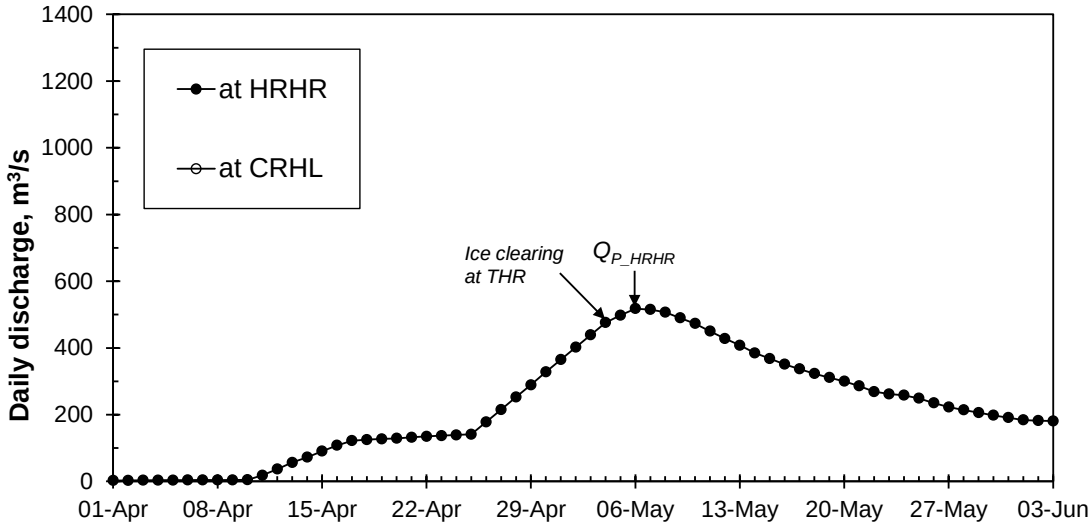

Figure C-43: Discharge hydrographs at the three Hay River WSC gauges in 1968.

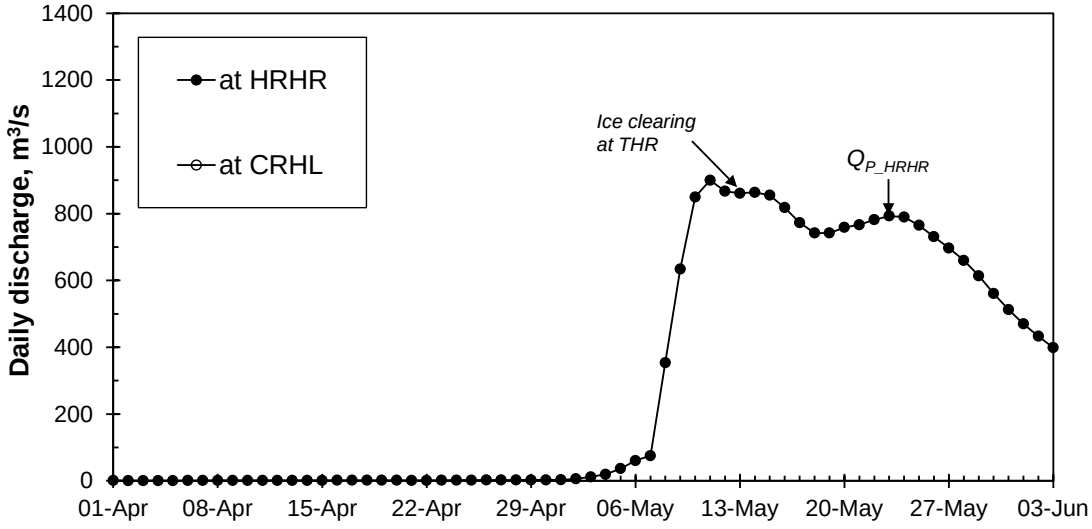

Figure C-44: Discharge hydrographs at the three Hay River WSC gauges in 1967.

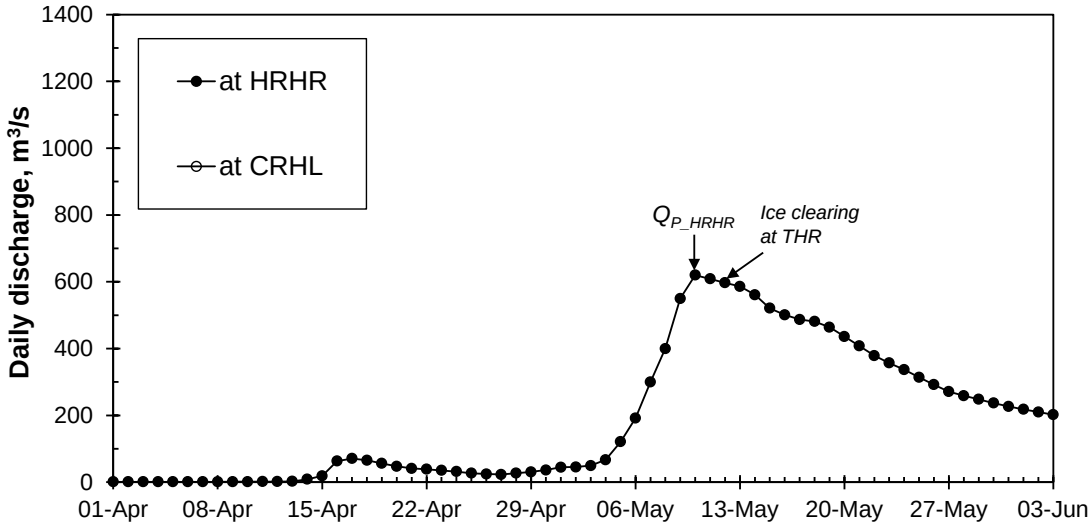

Figure C-45: Discharge hydrographs at the three Hay River WSC gauges in 1966.

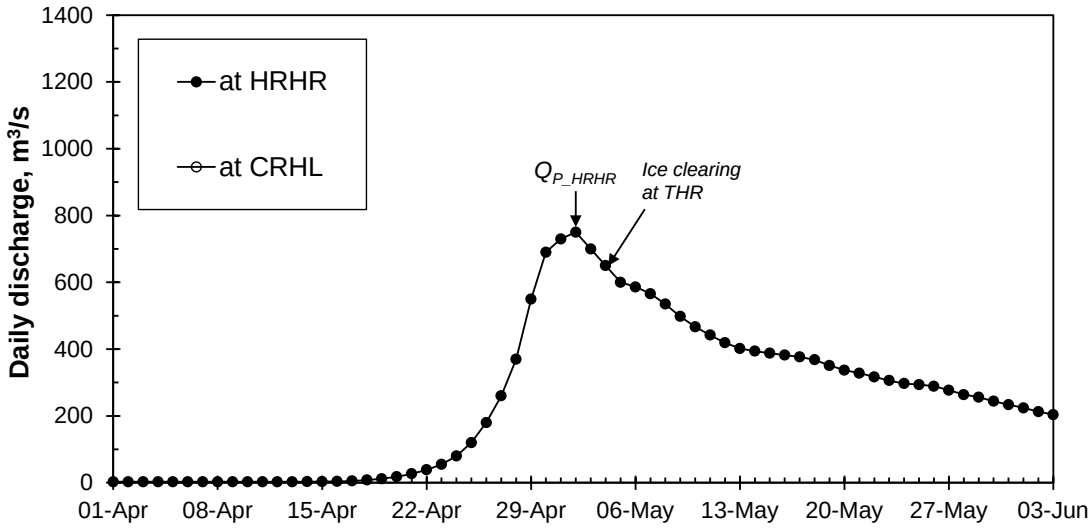

Figure C-46: Discharge hydrographs at the three Hay River WSC gauges in 1965.

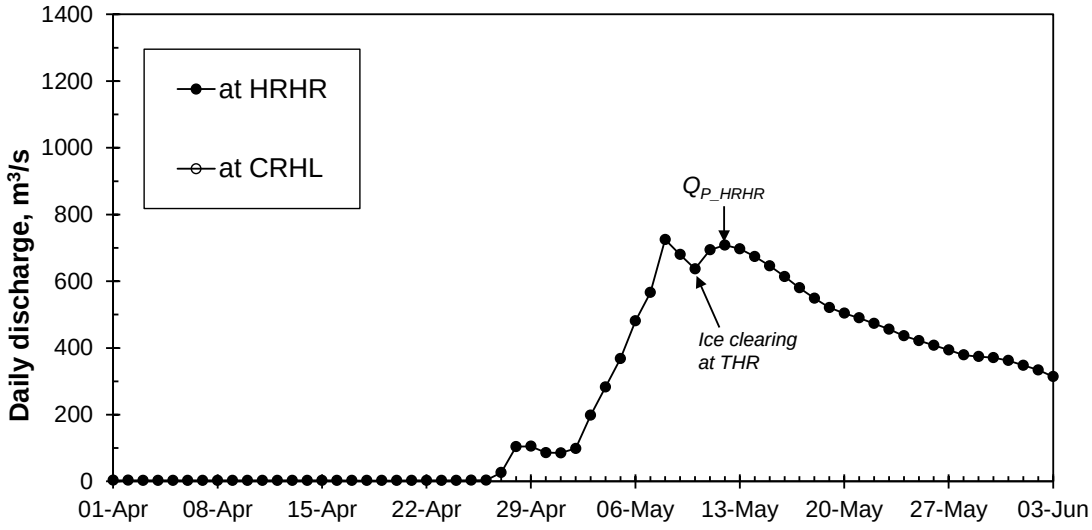

Figure C-47: Discharge hydrographs at the three Hay River WSC gauges in 1964.

Appendix D Forecasting the timing of breakup at the Town of Hay River, NWT

In northern regions, river ice breakup is an annual event that can present a significant threat to riverside communities. Water levels associated with ice jam events can rise several meters in just minutes; therefore, it is essential to have sufficient advance warning should evacuation become necessary. This study explores the potential for using readily available hydro-meteorological data from hydrometric gauges and climatic stations to develop a practicable forecasting model for breakup timing.

Artificial neural network (ANN) modelling is one of the most common data-driven techniques for solving complex non-linear problems which are not yet tractable through fully deterministic means (Maier *et. al.* 2010). In this study, the suitability of ANN modeling was tested to determine its potential to aid in forecasting the timing of breakup at the Town of Hay River, NWT, where breakup ice jam floods are a frequent occurrence. To achieve this, readily available hydro-meteorological data from within the Hay River basin were collated and processed to predict the date of breakup, D_B (i.e. the timing of the first push of ice) at the town site. Data for D_B were obtained from historical breakup reports and newspaper accounts (prior to 2003) and recent field work (from 2004 to 2011).

Operationally, the forecast would be conducted once each spring, on the date of the onset of breakup, D_{OB}, (taken as the date on which the rise of spring runoff commences based on the historical daily stage data). The breakup timing forecast would use both observed hydrometeorological data and short term weather forecasts as input. In this study, models for two alternative output variables were tested:

- ΔD_B: the number of days until breakup. In this case the model provides a direct forecast of the expected number of days between the onset of breakup (D_{OB}) and the first push at the town site (D_B).
- $ADDT_B$: the accumulated degree-days of thaw between the onset of breakup (D_{OB}) and the date of breakup (D_B). This provides an indirect prediction of breakup timing in terms of heat input to the ice cover required to initiate the breakup, with degree-days of thaw providing an index of this heat input.

The following variables were used as the input variables in these models:

- $ADDF_W$: the accumulated degree-days of freezing during the winter period, which starts from the onset of freezing degree-days (i.e. the first day of 5 consecutive days of subzero mean daily air temperatures) and ends at the onset of thawing degree-days (i.e. on the first of 5 consecutive days of air temperatures above -5°C). It is used as an index of late winter ice thickness and competence.

- AP_W: the accumulated snowfall during the winter period, in terms of snow water equivalent. It provides an index of the late winter snowpack in the basin, providing indication of the expected magnitude of spring runoff. It is also taken as an index of the snow coving the ice and insulating it against thermal deterioration. A high snowpack would be expected to delay the ice decay more than a low snowpack.

- RN_{PB}: the accumulated rainfall during the pre-breakup period (i.e. prior to D_{OB}). Rain can accelerate both snowmelt and ice cover decay, and thus the speed at which the breakup process can unfold.

- $ADDT_{PB}$: the accumulated degree-days of thaw during the pre-breakup period. It is taken as an index of the accumulated heat input to the ice cover which decreases ice thickness and/or ice strength during the pre-breakup period.

- $TDDF_{PB}$: the total degree-days of freezing during the pre-breakup period. It provides an indication of the potential impact of a cold spell after the onset of thaw, in terms of the potential for a delay in ice cover deterioration in the pre-breakup period.

An extended cold spell that occurs after the onset of breakup (i.e. after D_{OB}) would also be expected to delay breakup. However, given that this forecast would be conducted only once a year, on D_{OB}, such events in the record would not provide consistent calibration data. Therefore, with the caveat in mind that the model cannot account for the occurrence of a prolonged cold spell occurring *after*

the forecast, these events were excluded from the calibration set. This left a total of 34 years of record remaining in the data set. These data were split to develop the models: 7 (~20%) of these were reserved for validation and the remainder 27 (~80%) were used to calibrate the ANN model. The detailed approach used to calibrate the ANN model is similar to that employed by Zhao *et.al.* (2012). Two ANN models were developed for each of the two output variables (i.e. ΔD_B and $ADDT_B$). Also, two multiple linear regression (MLR) models were developed using the same data set to provide a comparison to the ANN models. The results of calibration and validation for all of these models are shown in Figure 1. For the output variable ΔD_B, the MLR_1 (Figure 1a) and ANN_1 (Figure 1b) models show very similar validation errors (mean errors of 5.3 days for MLR_1 and 5.5 days for ANN_2), although the ANN_1 exhibits a much better calibration result. For the other output variable, $ADDT_B$, the ANN_2 model (Figure 1d) shows much better results both for calibration and validation, compared to the MLR_2 model (Figure 1c). Also, when the validation results of the MLR_2 and ANN_2 models were evaluated using observed mean daily temperature data to determine to date of breakup, the mean errors were 2.4 days and 1.7 days, respectively. Thus the ANN_2 model had the lowest error of the four models. These results also suggest that the indirect variable $ADDT_B$ gives a better indication of breakup timing than the direct variable ΔD_B for this site.

In the next phase of this study, the effect of a cold spell following the onset of breakup will be further considered. As well, the significance of each input

variable to the output will be examined using the calibrated ANN models, so that the most important factors that control the onset of breakup can be identified.

References

Maier, H.R., Jain, A., Dandy, G.C., and Sudheer, K.P. 2010. Methods used for the development of neural networks for the prediction of water resource variables in river systems: Current status and future directions. Environmental Modelling & Software 25(8), 891-909.

Zhao, L., Hicks, F and Robinson Fayek, A. 2012. Applicability of multilayer feed-forward neural networks to model the onset of river breakup. Journal of Cold Regions Science and Technology, 70 (2012): 32-42.

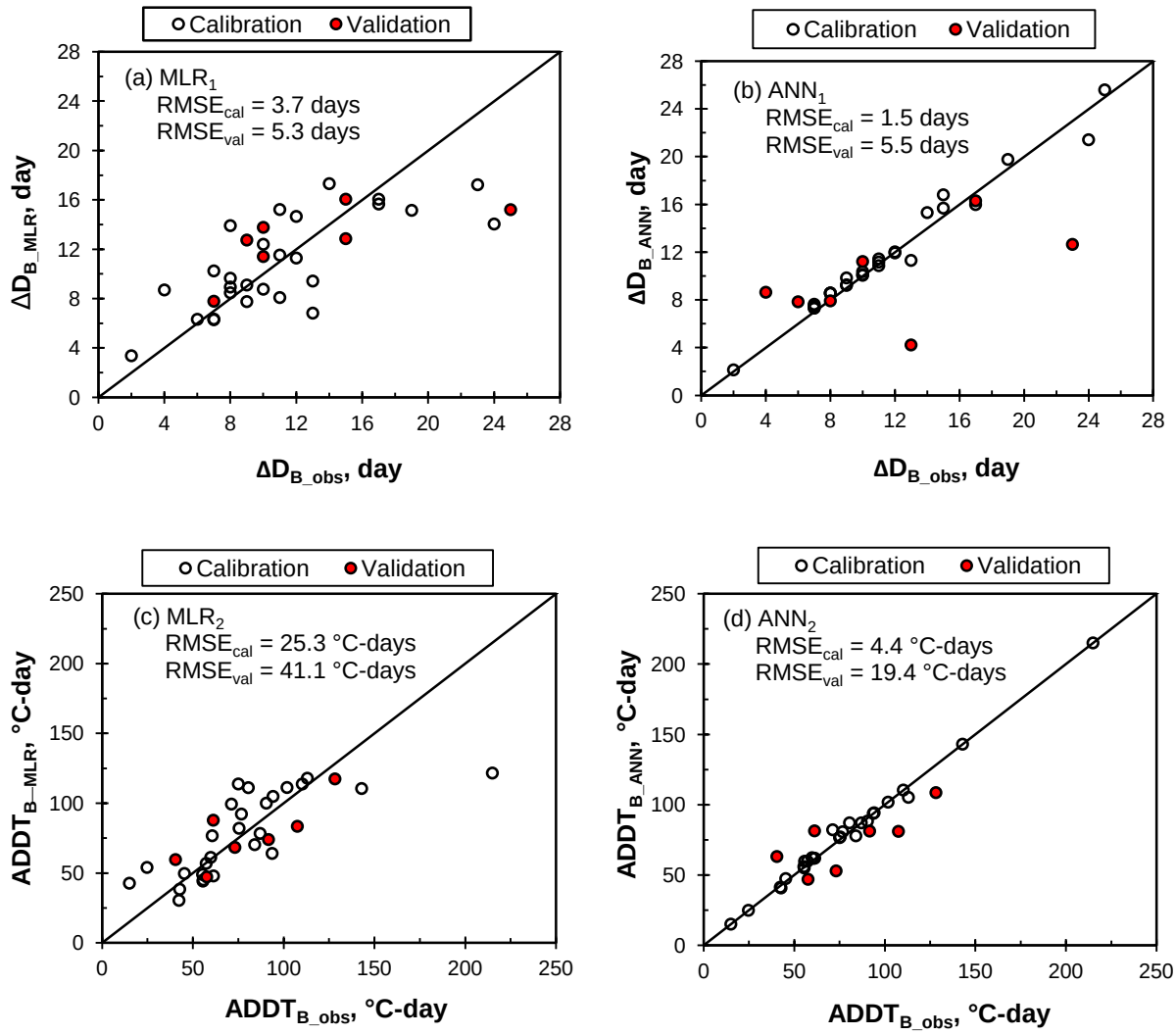

Figure D-1: Results of the calibration and validation of the four models. Note: $RMSE_{cal}$ and $RMSE_{val}$ indicate the root mean squared error of the calibration set and validation set. Sample size is 34 for MLR models development.